

VALIDATION AND INITIAL APPLICATIONS OF A MAGNETOMETER-FREE INERTIAL
SENSOR BASED MOTION CAPTURE SYSTEM FOR THE HUMAN LOWER BODY

Vom Fachbereich Sozialwissenschaften
der Technischen Universität Kaiserslautern
zur Verleihung des akademischen Grades
Doktor der Naturwissenschaften (Dr. rer. nat.)
genehmigte

Dissertation

vorgelegt von
Wolfgang Teufl

Tag der Disputation:	24. September 2020
Dekan:	Prof. Dr. Michael Fröhlich
Vorsitzende/r:	Prof. Dr. Thomas Schmidt
Gutachter/in:	1. Prof. Dr. Michael Fröhlich 2. Prof. Dr. Hermann Schwammeder

D 386

Kaiserslautern, April 2021

Danksagung

Ein prägender Lebensabschnitt geht zu Ende. Mein Promotionsverfahren an der TU Kaiserslautern ist nun abgeschlossen und so wird es Zeit, den an meiner Dissertation beteiligten Personen nochmals meinen herzlichsten Dank auszusprechen.

Zuallererst möchte ich mich bei meinem Doktorvater, Univ.-Prof. Dr. Michael Fröhlich, bedanken, der mir in seinem Fachbereich die Möglichkeit geboten hat mein Promotionsvorhaben in die Tat umzusetzen. Mit seinem Engagement und Know-How leitete er mich durch all die Höhen und Tiefen einer Promotion.

Weiterer Dank gilt meinen Kollegen aus der Arbeitsgruppe wearHEALTH am Fachbereich Informatik und allen voran deren Leitung, Frau Dr. Gabriele Bleser. Hier erhielt ich die fachliche und methodische Infrastruktur für meine Dissertation. Als Kollegen, Mentoren und Freunde unterstützten sie mich in den 4 Jahren, die ich mit ihnen zusammenarbeiten durfte.

Ein besonderer Dank geht hier auch an meine Kollegen aus der Sportwissenschaft, die mir auf Anfrage stets für einen fachlichen Austausch zur Verfügung standen.

Ebenfalls bedanken möchte ich mich bei meinem Zweitgutachter, Univ.-Prof. Dr. Hermann Schwameder, der sich die Zeit genommen hat meine Promotion zu begutachten und sich trotz schwieriger Zeiten auf den langen Weg von Salzburg nach Kaiserslautern gemacht hat, um meiner Disputation in persona beiwohnen zu können.

Schlussendlich möchte ich noch großen Dank an meine Familie richten. Hier möchte ich mich in aller Herzlichkeit bei meinen Eltern, Helga und Roland, bedanken. Ohne ihre Unterstützung wäre meine akademische Karriere nicht möglich gewesen. Ein ganz großer Dank gebührt auch meiner Lebensgefährtin, Nicole, die mir in der Schlussphase meiner Promotion bedingungslos zur Seite stand und mir stets den Rücken freigehalten hat.

Vielen herzlichen Dank!

Table of Contents

1	Introduction.....	1
1.1	Motivation	1
1.2	Research Question	1
1.3	Publications	2
1.4	Contributions	3
1.5	Outline.....	3
2	Background.....	5
2.1	Human Motion Capture	5
2.1.1	Gait Analysis	6
	Spatio-Temporal Parameters.....	6
	Joint Angles	7
2.1.2	Gait Classification.....	10
2.2	Inertial Measurement Units	11
2.2.1	Technical Background.....	11
	Drift Correction Approaches.....	12
2.2.2	Inertial Measurement Units and Gait Analysis	13
	Gait Event Detection and Spatio Temporal Parameters.....	13
	Joint Angles	15
2.2.3	Feedback Applications using MIMU / IMU.....	18
2.2.4	Composition of the present IMU system.....	20
	Hardware.....	20
	Sensor Placement	20
	Sensor Fusion Method	21
	Parameters	21
2.3	Validation approach.....	21
2.3.1	Reference System	22
2.3.2	System Synchronization.....	22
2.3.3	Subjects and Sample Size.....	23
2.3.4	Motion Tasks	23
2.3.5	Statistics.....	24

2.3.6	Reliability.....	25
3	Validation	26
3.1	Technical Validation of the Joint Angles.....	26
3.1.1	Journal Paper 1.....	26
	Summary.....	26
	Main Contributions	26
3.1.2	Journal Paper 2.....	49
	Summary.....	49
	Main Contributions	49
	Supplementary File of the Journal Paper 2	68
3.2	Validation of the Gait Event Detection and the Spatio-Temporal Parameters	73
3.2.1	Journal Paper 3.....	73
	Summary.....	73
	Main Contributions	73
4	Application and Extended Validation.....	94
4.1	Journal Paper 4.....	94
4.1.1	Summary.....	94
4.1.2	Main Contributions	94
4.2	Full Validation of the Joint Angles – Extended Results from JP 4	115
4.2.1	Procedure 1.....	115
4.2.2	Procedure 2.....	116
4.2.3	Procedure 3.....	118
4.2.4	Comparison of the three Procedures.....	121
5	Discussion.....	123
5.1	Discussion of the Additional Results	123
5.2	General Discussion	126
5.2.1	Magnetometer-free Tracking and Drift	126
5.2.2	Biomechanical Model.....	128
5.2.3	Sensor to Segment Calibration.....	129
5.2.4	Soft Tissue Artefacts	129
5.2.5	Classification Approach.....	130
5.2.6	Methodical Limitations and Critical Thoughts.....	130

5.3	Future Work	133
5.3.1	Full Body Kinematics	133
5.3.2	Automated I2S Calibration.....	133
5.3.3	Hardware	134
5.3.4	Machine Learning	134
5.3.5	Further Validation Steps.....	135
5.4	Outlook – the Future of Human Motion Capture	135
6	Conclusion.....	137
	Bibliography	138
	Scientific Curriculum Vitae	152

List of Abbreviations

AL	Anatomical landmarks
BA	Bland-Altman limits of agreement
CF	Coordinate frame
CI	Confidence interval
CMC	Coefficient of multiple correlations
HMC	Human motion capture
I2S	IMU to segment
IC	Initial contact
ICC	Intraclass correlation coefficient
IMU	Inertial measurement unit
JP	Journal paper
MAE	Mean absolute error
MIMU	Magnetic IMU
OMC	Optical motion capture
RB	Rigid Box
RMSE	Root mean squared error
ROM	Range of motion
ROME	Range of motion error
SD	Standard deviation
STA	Soft tissue artefact
STP	Spatio-temporal parameters
SVM	Support vector machine
TC	Terminal contact
THA	Total hip arthroplasty

1 Introduction

1.1 Motivation

3D human motion analysis has become an essential component in sport and medicine. No matter if injury screening, performance analysis or the evaluation of a rehabilitation progress, motion analysis systems play an important role in most of the rehabilitation or sports medical institutions. However, all of those institutions face the same question: Which systems are the right ones?

First, one has to decide which parameters he / she is interested in. There is a huge amount of features of the human motion that can be relevant depending on the question at hand. The most frequently analyzed features of the human motion are the kinematics, i.e. joint angles [1–4] and spatio-temporal parameters (STP) [2,3], the kinetics, i.e. ground reaction forces and based on those joint moments and loadings [2–4], and muscle activation [2,5,6].

Concerning the features of interest one has the choice between various systems that apparently all measure the same parameters, however, using different approaches. Beside the expense and usability two more factors should be overall decisive; the validity and reliability of the system. To the opinion of the author, it is essential to evaluate the validity and reliability of a system in comparison to an already validated reference prior to its widespread use.

Considering the measurement of 3D joint kinematics a new technology has spread among the movement scientists and attracts the attention of physicians and their like; Magnetic Inertial Measurement Unit (MIMU) systems and Inertial Measurement Unit (IMU) systems [7]. MIMU / IMU systems try to address the methodical disadvantages of the passive marker based optical motion capture (OMC) systems, which are considered the gold standard in the measurement of joint kinematics [8]. The use of OMC systems relies on expensive material, is spatially restricted, time consuming in the preparation as well as the post processing and requires expert knowledge. On the contrary MIMU / IMU systems are easily applied and can be used mobile and in-field.

However, MIMU / IMU systems bring along certain technical challenges and require an understanding of the methods used for the deduction of clinically interpretable parameters from the rather abstract sensor data, or at least a thorough validation of the new technology.

Miezial et al. [9,10] developed a new motion analysis system based on IMUs only, completely omitting magnetometer information, for the measurement of the lower body's joint kinematics and STP. This system aims at a widespread use in clinical settings as well as in a sports-related environment. A major interest of the developers is the application of the mentioned IMU system in orthopedic rehabilitation settings. In this context, it should be employed as the basis of a real-time feedback system that delivers information about the patient's gait pattern and its potential abnormalities and therefore works as a gait-training application.

It is desired to enable scientists as well as physicians, therapists, coaches and their like to use this system with the certainty of employing an accurate and well established system. Therefore, it is the aim of this thesis to thoroughly evaluate the validity and reliability of the 3D joint angles, the gait specific events, i.e. initial contact (IC) and terminal contact (TC), as well as the gait-specific STP, in the following just STP, measured by means of the above introduced IMU system. In this context it was further differentiated between three error sources, the tracking algorithm, the IMU to segment (I2S) calibration and the biomechanical model.

Further, it was the claim of this thesis to design an initial application of the discussed system. For this purpose the thesis focuses on a typical problem frequently addressed with motion capture systems, the classification of a pathological gait using machine learning approaches.

1.2 Research Question

Based on the above raised matters the following research questions are addressed in this thesis:

- Are the joint angles, in detail the hip, knee and ankle joint angle as well as the global pelvis motion in the sagittal, frontal and transversal plane, of gait as well as static and moderately dynamic motions measured by means of the above mentioned IMU system, consisting of a seven sensor set-up, comparable to the results of an OMC based approach?
- Are the STP and the gait-specific events IC and TC measured by means of the same IMU system comparable to the results of an OMC based approach?
- Are the joint angles and STP measured with constant accuracy independent of the measurement time, i.e. the test-retest reliability, and independent of the duration of the measurement, i.e. long-term stability?
- How is the difference between the OMC system and the IMU system distributed on different sources of error, i.e. the tracking algorithm, the I2S calibration and the biomechanical model?
- Is it possible to identify a certain group of patients incorporating certain features of the gait data measured by means of the described IMU system and employing a supervised machine learning algorithm?

1.3 Publications

The four journal papers (JP) (see Table 1) enclosed in this thesis address the questions raised in chapter 1.2.

JP 1 [11] is concerned with a technical evaluation of the IMU system within a homogeneous group of young and healthy subjects. Therefore, the 3D joint angles of the lower extremities during 6 minute walking were simultaneously recorded by means of the mentioned IMU system and an OMC system. The IMU system employed in this study still incorporated an OMC based I2S calibration as well as the biomechanical model defined by the markers attached to anatomical landmarks (AL).

JP 2 [12] extends the technical evaluation performed on the 3D joint angles of the gait in JP 1 to the 3D joint angles of physiotherapy and sport-specific movement tasks.

JP 3 [13] tackles the evaluation of the gait event detection and the estimation of the STP by means of the IMU system. For this the same gait recordings from JP 1 were used. However, in this study the IMU system incorporated a biomechanical model based on a human body model incorporating AL that is scaled according to anthropometric tables and an IMU based I2S calibration.

JP 4 [14] introduces the first application of the IMU system. The same version of the IMU system as described in JP 3 was employed to measure the 3D joint angles during gait within a group of patients after total hip arthroplasty (THA). Additionally, the gait data of the group of young and healthy subjects from JP 1, processed with the approach used in JP 3, was used in this study. Certain features from among the joint angles of the lower body were defined based on expert knowledge and recommendations from the literature. JP 4 evaluates the ability to classify a gait pattern based on these features as healthy or impaired, when they are employed to train a common machine learning classification algorithm.

Table 1. References of the journal papers included in the thesis.

Journal Paper 1	Teufl, W.; Miezal, M.; Taetz, B.; Fröhlich, M.; Bleser, G. Validity, Test-Retest Reliability and Long-Term Stability of Magnetometer Free Inertial Sensor Based 3D Joint Kinematics. <i>Sensors</i> 2018 , <i>18</i> , 1980, doi: 10.3390/s18071980 .
Journal Paper 2	Teufl, W.; Miezal, M.; Taetz, B.; Fröhlich, M.; Bleser, G. Validity of inertial sensor based 3D joint kinematics of static and dynamic sport and physiotherapy specific movements. <i>PLOS ONE</i> 2019 , <i>14</i> , e0213064, doi: 10.1371/journal.pone.0213064 .
Journal Paper 3	Teufl, W.; Lorenz, M.; Miezal, M.; Taetz, B.; Fröhlich, M.; Bleser, G. Towards Inertial Sensor Based Mobile Gait Analysis: Event-Detection and Spatio-Temporal Parameters.

Sensors **2018**, *19*, 38, doi:[10.3390/s19010038](https://doi.org/10.3390/s19010038).

Journal Paper 4 Teufl, W.; Taetz, B.; Miezal, M.; Lorenz; Pietschmann, J.; Jöllenbeck, T.; Fröhlich, M.; Bleser, G. Towards an Inertial Sensor-Based Wearable Feedback System for Patients after Total Hip Arthroplasty: Validity and Applicability for Gait Classification with Gait Kinematics-Based Features. *Sensors* **2019**, *19*, 5006, doi:[10.3390/s19225006](https://doi.org/10.3390/s19225006).

1.4 Contributions

The present thesis forms the foundation of a successful usage of a newly developed, mobile IMU system, omitting magnetometer information. The thesis evaluates in detail the validity and reliability of the lower limb joint angles, gait events and STP measured by means of the mentioned system and reveals the contribution of different sources of errors to the overall difference between the IMU system and the reference. Furthermore, it critically discusses the drawbacks and difficulties of measuring human motion by means of MIMU / IMU systems. In addition also the reference system, the OMC system, is critically viewed and its advantages and disadvantages are discussed.

In detail, the validity and reliability of the joint angles of the hip, knee and ankle as well as the 3D global motion of the pelvis during gait and static and moderately dynamic motion tasks are reported. Further, this thesis reveals the accuracy of the gait-event detection, IC and TC, as well as the accuracy of the STP. The validity is shown for two different populations, first, a homogeneous group of young and healthy subjects and, second, a heterogeneous group of patients after THA. This was done to examine the influence of the body physique and different motion patterns, common for pathological gait, on the accuracy of the IMU based joint angle estimation.

Further, the difference between the two systems is evaluated regarding its origin. Therefore three versions of the IMU processing procedure are considered, adding more OMC-independent information per processing stage. In Table 2 the different versions are described.

Table 2. Different ways of processing the IMU raw data.

Procedure 1	OMC based biomechanical model; OMC based I2S calibration; IMU based segment tracking
Procedure 2	OMC based biomechanical model; IMU based I2S calibration; IMU based segment tracking
Procedure 3	IMU based biomechanical model; IMU based I2S calibration; IMU based segment tracking

Finally, the thesis describes a first step towards the intended use of the IMU system by defining features from among the 3D gait kinematics that proved discriminative in the classification of impaired and non-impaired gait and therefore present useful trigger-parameters in a gait-training application.

1.5 Outline

The thesis is structured into four parts. First, a short description of the background of human motion capturing is given, with a closer look at the special case of gait analysis. Consequently, the gold standard system and reference in this thesis, the OMC system, is introduced. Then MIMU / IMU systems in general, their drawbacks and advantages, are described. Finally, the IMU system evaluated in this thesis is shortly introduced.

Second, the validation of the IMU system is treated in the JPs 1 – 3. The JPs are shortly introduced and then the original articles are displayed in full length including appendices but excluding supporting information online available, except for the JP 2. In this case, for the convenience of the reader, a protocol describing certain technical issues is attached.

Third, the JP 4 describes the application of the system in the problem of classifying impaired and non-impaired gait. The JP is again shortly introduced and then displayed in full length. Additionally, extended results from JP 4, not originally published, are included in this part presenting the validation results of the IMU based joint angles processed with Procedure 1 – 3 for the group of patients after THA and processed with Procedure 2 – 3 for the group of healthy subjects.

Fourth, besides the individual discussions of each separate JP the results are summed up and discussed in general. Further, this part focuses on limitations in the study design and future work. Finally, a holistic conclusion is drawn from the findings of this thesis.

2 Background

2.1 Human Motion Capture

Human motion capture (HMC) describes the application of systems based on different kinds of technical approaches to record the kinematics and kinetics of the human musculoskeletal system during different tasks in the 3D space [8]. In detail, information is collected on the pressure and forces produced by the human body and the thus induced joint loadings; the relative movement of the bony segments in the 3D space and therefore also the relative rotations between these segments, mostly expressed as joint angles; task specific motion events like initial and terminal ground contact; spatial and temporal information on certain movement sections; as well as the muscular activation.

The systems for measuring this information are plentiful. However, in every field of application there exists a so called gold standard reference. For example, ground reaction forces are typically measured using force plates. However, there are also alternative approaches based on MIMU / IMUs that try to reproduce the ground reaction forces using sensor data [15,16]. These alternative approaches, however, have to face up to the comparison with the gold standard systems to be scientifically accepted.

In the case of 3D joint angles the OMC systems are considered the reference when it comes to biomechanical analysis [7,8]. They are also used for the estimation of STP and deliver results comparable to pressure plates and force plates [17–19].

OMC systems are able to measure the position of retroreflective markers in 3D space with sub-millimeter precision [20]. However, it is a long way from sheer marker positions to the relative angles between segments. To define a segment, e.g. human bones, and its corresponding coordinate frame (CF) a minimum of three markers has to be non-collinearly aligned on it. There are different ways of how the markers are aligned on the human body, depending on the body part and the movement task one is interested in. These ways can be referred to as biomechanical marker protocols [21–24]. Although these marker protocols differ from each other they all try to fulfill standards designed for the reconstruction of human body segments. The Rizzoli marker set defined by Leardini et al. [21] follows the recommendations of Cappozzo et al. [25] for the definition of the segments of the lower body. In that protocol markers are attached onto the skin approximately over underlying AL. These AL are used for the segment definition as well as the segment tracking during motion. In comparison to that approach other protocols use a calibration wand or markers attached to relevant AL for a static segment definition. However, they then use so called marker clusters, a set of at least three markers attached to a rigid surface, for segment tracking during the movement task [22].

Based on the markers attached to AL according to a certain marker protocol, finally, a biomechanical model can be defined. The biomechanical model includes information about the segment lengths, joint centers and joint axes [26]. The definition of a biomechanical model prior to the kinematics estimation allows for the interpretation of the calculated angles between segments as anatomically relevant joint angles.

The segments are considered rigid. However, the HMC using OMC systems faces one big problem: markers cannot be placed directly on the AL. The muscles and skin, i.e. soft tissue, covering the bony structures prevent a direct approach. Therefore, the markers are prone to the relative movement of the soft tissue with respect to the underlying bone. This uncertainty in the estimation of the exact position of the AL introduces errors in the segment definition, the segment orientation estimation and finally in the calculation of the joint angles. This phenomenon is commonly referred to as soft tissue artefacts (STA) [27]. Depending on the differing physique of the subjects in question for motion analysis the impact of STA on the joint angles estimation can have differently grave effects.

A possible solution to better control the effect of STA during the segment tracking is to use, as mentioned above, marker clusters [27]. This approach is deemed to minimize the effect of STA on the distances between the markers attached to one segment since they are rigidly connected on the cluster. However, Leardini et al. [27] mentioned that there are also errors concerning the

inter-marker distances on a cluster due to systematical errors in the OMC system, although, as mentioned afore, they were proven to be in the region of sub-millimeters.

In summary, the quality of OMC based HMC depends on the marker set used, the marker placement, the approach for the segment CF definition, and finally the subject itself.

The applications of HMC are manifold. There are basically two huge areas for HMC, animation [28,29] and biomechanics [2,30,31]. In animation and the movie industry mainly active marker based OMC systems are used, whereas the field of biomechanics resorts to passive marker based OMC systems. The HMC in biomechanics has a long history [32]. However, the modern biomechanical HMC has its origin in the gait analysis.

2.1.1 Gait Analysis

The gait analysis has grown from the evaluation of children with cerebral palsy [33,34]. Thanks to experts like Richard Baker [35], James R. Gage [33], Perry and Burnfield [36] and in the German-speaking region Kirsten Götz-Neumann [37] the gait analysis has nowadays spread far over its original field of application into all kinds of different clinical areas. Typical applications are the early identification of neurological diseases [38,39], supporting or selecting surgical approaches [40,41], the evaluation of a rehabilitation progress [42,43] and many more.

Hereby, the gait analysis is mainly concerned with the evaluation of certain parameters during the so called gait cycle. The gait cycle is defined as the time from the IC of one lower limb to the consecutive IC of the ipsilateral limb. Further, the gait cycle is divided in relevant phases, which mainly differentiate between stance phase and swing phase [36] (see Figure 1).

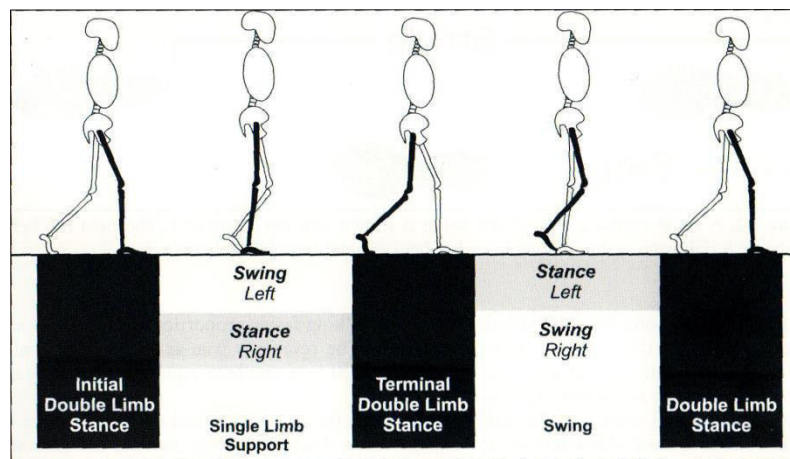


Figure 1. Presentation of the phases of one gait cycle. The stance phase equals approximately 60 % of the gait cycle. Accordingly, the swing phase equals 40 % of the gait cycle. Figure taken from Perry and Burnfield [36].

The commonly evaluated parameters in a gait analysis are kinetics like ground reaction forces and joint loadings [44,45] as well as kinematics, anatomical joint angles and STP [46–48]. As mentioned in chapter 1.1 OMC systems have established themselves as gold standard for the measurement of the latter two.

Spatio-Temporal Parameters

The STP are the typical parameters measured in a gait analysis and are commonly part of a standard clinical motion analysis [49]. The STP are comparably easy to measure using an OMC system. With, for example, only two markers, one on each calcaneus, it is possible to validly measure the IC of each leg [17]. This approach was used in the JP 1 to perform the segmentation of the joint angle waveforms to 100 % gait cycle based on the ICs estimated from the OMC data. In the JPs 3 and 4 this approach was extended and combined with the approach described in [50]. However, here the

virtual calcaneus markers of the biomechanical model of the IMU system were incorporated in this approach rather than the markers from the OMC system (refer to the JP 3 for details).

Based on the IC information it is possible to calculate STP like stride length, step length, step width, stride time, step time, cadence and speed (see Table 1 from JP 3). Adding two more markers on the head of the left and right Os metatarsale I and using the combined approach for gait event detection from the JP 3 enables the estimation of the TC as well and therefore the calculation of single limb support, double limb support, stance time and swing time.

In comparison to the OMC system only pressure and force plates allow the calculation of the same amount of information. The mobile version of pressure plates, instrumented insoles, do not incorporate spatial assignment and therefore allow only the direct assessment of temporal parameters [51–54]. Consequently, alternative systems, like MIMU / IMU based sensor networks are needed for a mobile, complex evaluation of the gait specific STP.

Joint Angles

The calculation of the 3D joint angles requires a far more complex set-up compared to the four marker set-up needed for STP estimation. A typical marker set for the measurement of the joint angles of the lower body, mentioned afore in chapter 2.1, is the Rizzoli marker set, consisting of a minimum of 28 markers, including calibration markers [21]. Compared to another common marker set, the Plug-in gait [22], the Rizzoli marker protocol does not depend on anthropometric measurements. Further, the Plug-in gait depends on a knee-alignment device for optimal estimation of the axis of rotation in the knee joint. On the other hand the Rizzoli marker protocol needs more markers and depends on the knowledge of different AL as well as the experience in palpating them.

As mentioned in chapter 2.1 the AL on one segment serve the definition of the segment's CF and its origin with respect to a global frame. In the following this is explained on the example of the creation of the segment shank following [25].

According to the Rizzoli marker protocol markers shall be attached to the following AL on the tibia and fibula, respectively [21]:

- Caput fibularis
- Tuberositas tibiae
- Malleolus lateralis
- Malleolus medialis

See Figure 2 for a schematic representation of the creation of the segment shank according to [25].

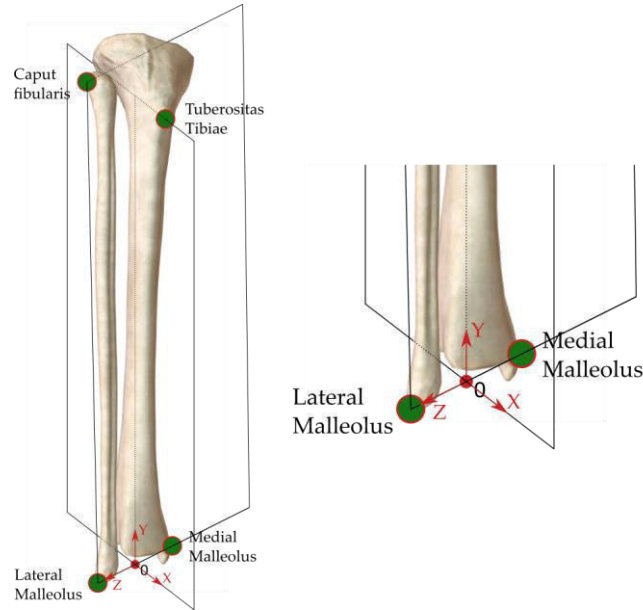


Figure 2. The origin of the coordinate frame of the segment shank (0) is defined as the midpoint between the line connecting the malleolus lateralis and the malleolus medialis. The longitudinal axis (y) is defined by the intersection of a quasi-frontal plane, defined by the malleolus lateralis, the malleolus medialis and the caput fibularis, and a quasi-sagittal plane, defined by the origin, the tuberositas tibiae and the orthogonality to the quasi-frontal plane. The medio-lateral axis (z) lies in the quasi-frontal plane. The posterior-anterior axis (x) is orthogonal to y and z.

After the construction of the segments the markers on the AL or marker clusters are used to reconstruct the orientation of the corresponding segment in a global frame. Consequently, angles between two adjacent segments can be calculated based on these orientations. Let R^{GT} be the orientation matrix of the segment thigh in the global frame and R^{GS} the orientation matrix of the segment shank in the global frame (see Figure 3).

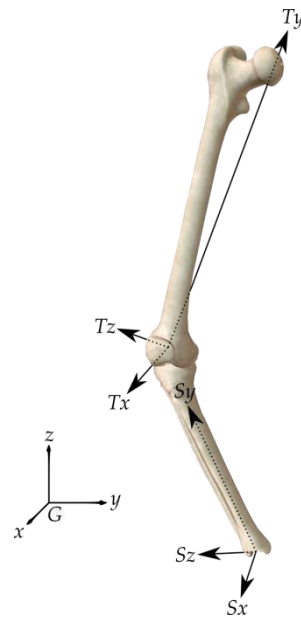


Figure 3. The segments shank and thigh with their defined coordinate frames S and T, respectively. G represents the global reference coordinate frame.

The relative rotation between the two segments can be calculated according to equation (1):

$$R^{TS} = (R^{GT})^T R^{GS} \quad (1)$$

The orientation matrix R^{TS} contains the information about the orientation of the shank relative to the thigh. However, to express that in clinically relevant terms it is necessary to extract from R^{TS} anatomically meaningful angles. Therefore the Euler angle or Cardan angle decomposition is used [55]. These approaches describe the complex information in the rotation matrix with three rotations around the spatial axes (x, y, z) according to a defined sequence. In this context, concerning Euler angle decomposition, the first and third rotation takes place around the same axis (see Figure 4). In the Cardan angle decomposition all three rotations are processed around the three different spatial axes.

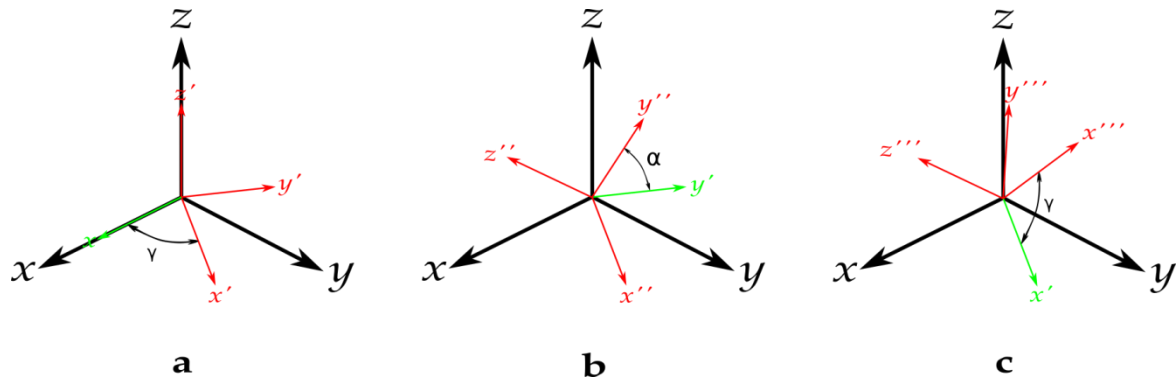


Figure 4. Shown is an example for the Euler angle sequence $z - x - z$. a: the coordinate system is rotated around the z axis. b: the new coordinate frame ($'$) is rotated around the x axis. c: the new coordinate frame ($''$) is rotated again around the z axis and results in the final coordinate frame ($'''$). γ represents the rotation around the z axis, α represents the rotation around the x axis.

In the example from Figure 3 an adequate sequence for the decomposition, that fits the anatomical properties in that example, would be the Cardan sequence $z - x - y$. Let the angles around z, x, y be γ, α, β , respectively. Accordingly:

$$R^{TS} = R_z^{TS}(\gamma)R_x^{TS}(\alpha)R_y^{TS}(\beta) \quad (2)$$

In this case, γ can be interpreted as flexion/extension, α as abduction/adduction and β as internal/external rotation (compare Figure 3).

The above mentioned approach for the segment definition represents an anatomical CF definition and therefore results in anatomically meaningful joint angles. The definition of a technical CF represents a less complex approach for the calculation of an angle between two segments. Here, the CF is constructed based on rigid marker clusters fixed to the segment (see Figure 5).

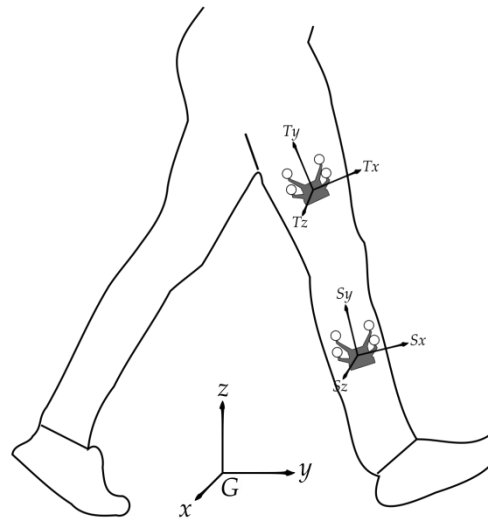


Figure 5. The segments thigh (T) and shank (S) are defined based on the corresponding rigid clusters equipped with four markers. G represents the global CF.

These marker clusters are considered bone, i.e. segment, embedded. As mentioned afore, a combination of both approaches can be used, i.e. the anatomical CF construction is based on AL and the segment tracking uses the rigid marker clusters.

The difference between the joint angle calculation based on a combination of clusters and markers attached to AL as well as the joint angle calculation based solely on markers attached to AL is highlighted in the JP 1 and 2.

2.1.2 Gait Classification

The classification of gait patterns based on the various parameters, recorded during gait analysis, using machine learning approaches is nowadays a widely discussed issue [56]. Gait classification is mainly employed to support the diagnosis or the clinical decision making in diseases like cerebral palsy [57,58], Parkinson [59–61], stroke [62–64] and others [65–67].

The instrumented gait analysis has the potential to deliver a huge amount of data and therefore a huge amount of possible features that can be employed for the training of a classification model. Therefore, data reduction and mainly feature selection are an essential part of machine learning [68]. One possibility is to employ such feature selection methods to automatically reduce the amount of data to a minimum of relevant parameters. The principal component analysis is one of the most common methods used for data reduction [69]. The principal component analysis is used to structure a large set of features by finding linear combinations of these features with maximum variance. The significance of each combination, the principal component, declines with increasing dimensionality. However, often the interpretability of the newly defined components decreases after the first two components [70].

A completely different approach to feature selection is the manual selection of adequate parameters that can be employed in a classification algorithm. It allows the researcher to design features based on expert knowledge and literature recommendations. Further, this approach may yield features that are better to understand for physicians and patients alike.

In the case of predefined features there are also ways to determine the importance, or the ranking, of the features involved. A common way to estimate the contribution of certain features to a classification model is the maximum relevance minimum redundancy algorithm [71].

Fact is that with the increasing number of wearables used in daily living the amount of data available for machine learning approaches increases in equal measure. Therefore, beside the quality of the data, the selection of the optimal features becomes ever more important. However, the data

amount increases not only in everyday living. Since the introduction of MIMU / IMU systems in HMC the recording of loads of clinical motion data has become far more simple.

2.2 *Inertial Measurement Units*

In the past 25 years the use of MIMU / IMUs in HMC has increased intensely [7]. Each year the sensor units get smaller, cheaper and more powerful. Therefore, of course the interest in MIMU / IMUs on behalf of researchers and potential users is still growing.

However, to be able to work with a technology it is essential to understand its composition and functionality to better gauge the chances and advantages as well as the potential drawbacks of its use.

2.2.1 Technical Background

A common IMU is composed of a three axes accelerometer, measuring linear acceleration along the three spatial axes, and a three axes gyroscope, measuring angular velocity around the three spatial axes. In the case of a MIMU also a magnetometer is included, providing a magnetic field measurement. To determine the orientation, velocity or position of an IMU the signals have to be integrated. For example, to derive the velocity, the acceleration has to be integrated. However, consider that the initial measurement is represented in the sensor CF. Further, the accelerometer also measures acceleration due to gravity, the latter pointing away from the geocenter. Therefore, the measured acceleration has to be represented in a global frame, where the gravity component can be subtracted. Consequently, one requires the knowledge about the sensor's orientation, which can be obtained by integrating the angular velocity. Therefore, the information of different sensors is fused. This approach of incorporating various sensors into an estimation problem is referred to as sensor fusion [72]. Kalman filters are typically employed for this purpose [73–75].

The resulting orientation of the MIMU / IMU is typically expressed in a quaternion [76]. An advantage of the quaternion-parametrization is, for example compared to the parametrization in Euler angles, that quaternions do not encounter singularities. However, the parametrization of rotations in quaternions are difficult to interpret geometrically. Therefore, to derive interpretable kinematics and to make the results comparable to other systems, in this case the kinematics of an OMC system, it is necessary to convert the quaternion rotations into Euler angles. This process incorporates again the Euler angle decomposition (compare chapter 2.1.1).

Despite a long period of research MIMU / IMUs face some important technical drawbacks. In this work only the two most essential are to be mentioned in foresight to the contributions of the described articles.

First, consider an IMU lying absolutely still on a surface. In this case, as mentioned before, the accelerometer measures the acceleration due to gravity. The gyroscope is considered to measure zero. However, due to technical restrictions the gyroscope as well as the remaining sensors can be afflicted with a bias. This bias can be for example influenced by changes in the temperature [77]. By integrating these biased sensor signal the measurement error accumulates. In the derived sensor orientation this bias is therefore interpreted as motion. In a graphical representation the sensor would therefore start to rotate around all three axes. That phenomenon is commonly referred to as drift.

However, in combination with the accelerometer the drift can be reduced. Incorporating the knowledge of the axis defined by gravity, the gyroscope induced drift can be removed from the two axes orthogonal to the gravity. Nevertheless, the orientation estimate will still drift around the gravity axis itself, commonly referred to as heading direction drift. A common solution is to incorporate the measurements of a magnetometer. Such MIMUs are now able to correct the drift in the heading direction by incorporating the knowledge of the magnetic field vector.

This introduces the second technical drawback of IMUs or rather MIMUs, magnetic disturbances. In an industrial environment the magnetic field can be disturbed by ferro-magnetic materials, steel, power lines, etc. Consequently, the assumption of a homogeneous magnetic field is

violated and therefore the magnetometer measurement cannot be used any longer for correction, causing again an offset in the measurement of the sensor orientation.

There is considerable work on the compensation for the MIMU / IMU drift [77–80] and the handling of magnetic disturbances [81–83]. For the latter a possibility is to estimate the MIMU / IMU orientation omitting all magnetometer information. In the literature various approaches exist concerning a purely accelerometer and gyroscope based orientation estimation [79,84–86]. Of course, in this case, other methods have to be found to compensate for the missing corrective information concerning the heading direction. Consider that the methods for drift correction depend on the number of IMUs available. With respect to the IMU system described in this thesis, only approaches concerning sensor networks with at least two sensors were considered.

Drift Correction Approaches

Dejnabadi et al. [87,88] tried to estimate the drift-free sagittal angle of the knee joint using one IMU on the thigh and shank, respectively and further introducing virtual sensors located at the joint center of rotation of the knee. These virtual sensors were defined by shifting the two physical sensors on the thigh and shank into the center of rotation between the two segments. Using the estimated accelerations of the virtual markers at the center of rotation they were able to deduce the orientation of these two virtual markers and calculate the angle between the virtual sensors, i.e. the angle between the segments (see Figure 6). Therefore, Dejnabadi et al. [87] extended an approach from Morris et al. [89] and Willemsen et al. [90] and calculated the angle between two segments without the need of integration. However, they needed the exact position of the physical sensors. Therefore, their model had to be individualized by anthropometric data and the sensor position was derived from photography.

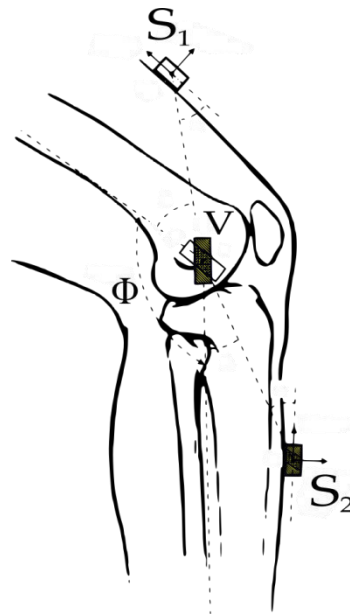


Figure 6. Physical sensor placement on the thigh (S_1) and shank (S_2) plus the corresponding virtual sensors (V) shifted to the center of rotation between the two segments. Φ represents the angle between the two virtual sensors in the sagittal plane, i.e. the knee flexion. Modified figure taken from Dejnabadi et al. [87].

A further common approach to drift correction is the detection of static phases in the sensor measurement where no, or a low, acceleration can be assumed, common in the stance phases of gait [77]. With a known gravity vector g the sensor acceleration I_a at the time of the static phase can be compared to I_g , the gravity expressed in the sensor frame. Consequently, any difference between I_a and I_g is interpreted as orientation drift [77,91]. However, this approach assumes phases of

minimum acceleration. That might be common in gait, whereas that might not be the case in highly dynamic movements.

Fasel et al. [78] developed a drift reduction method especially for the case of highly dynamic motions, e.g. alpine skiing. Their approach was based on the estimated accelerations of virtual sensors, located at a virtual joint of two adjacent segments. The distances between the real sensors on the proximal and distal segment, respectively, were derived using a numerical optimization approach. In comparison to Dejnabadi et al. [87] the approach of Fasel et al. [78] did not rely on anthropometric measurements and was further designed to cover all three dimensions.

Other approaches try to compensate for missing magnetometer information by combining the IMU measurements of all sensors included in the sensor network with a biomechanical model including biomechanical constraints [10,92]. In Miezal et al. [10] these biomechanical constraints are incorporated in an extended Kalman filter as measurement models and, e.g., prevent the connected segments from drifting apart in a physically impossible way.

The proposed methods all work only for multi-sensor set-ups and require additional information, e.g. distances between sensors and virtual sensors or biomechanical constraints. A recent review on lower limb kinematics estimation using MIMU / IMUs also summed up a few of the most common approaches used for drift compensation [93]

However, employing solutions like the ones mentioned above, MIMU / IMUs are nowadays widely applied in HMC and especially in gait analysis applications [7,94–98].

2.2.2 Inertial Measurement Units and Gait Analysis

MIMU / IMUs are employed in various fields of gait analysis to mainly gain information about the STP and the joint angles [96,98]. Further, there is initial research trying to estimate the ground reaction forces during gait based on MIMU / IMU data [15].

Gait Event Detection and Spatio Temporal Parameters

The estimation of gait events, IC and TC, and based on that the calculation of STP is the most common way of using MIMU / IMUs in gait analysis. Accordingly, Caldas et al. [96] and Petraglia et al. [98] included almost exclusively studies reporting the estimation of STP in their recent reviews on MIMU / IMUs in gait analysis. Consider, most of the studies concerned with MIMU / IMU based STP vary strongly in the number of parameters reported. That is because the complexity of the calculation of the parameters differs distinctively.

However, starting with the essential, first of all one has to define certain events or phases of the gait to deduce the STP. In the following only a few approaches to the gait event detection are described in more detail to gain an understanding of the different possibilities available.

Salarian et al. [99] estimated IC and TC based on a 1D gyroscope attached to the shank in a fashion to measure the rotational velocity around a medio-lateral axis. Here, a positive angular velocity was associated with the swing phase. Prior and after this phase a negative peak was evident. These peaks were associated with TC and IC, respectively (see. Figure 7).

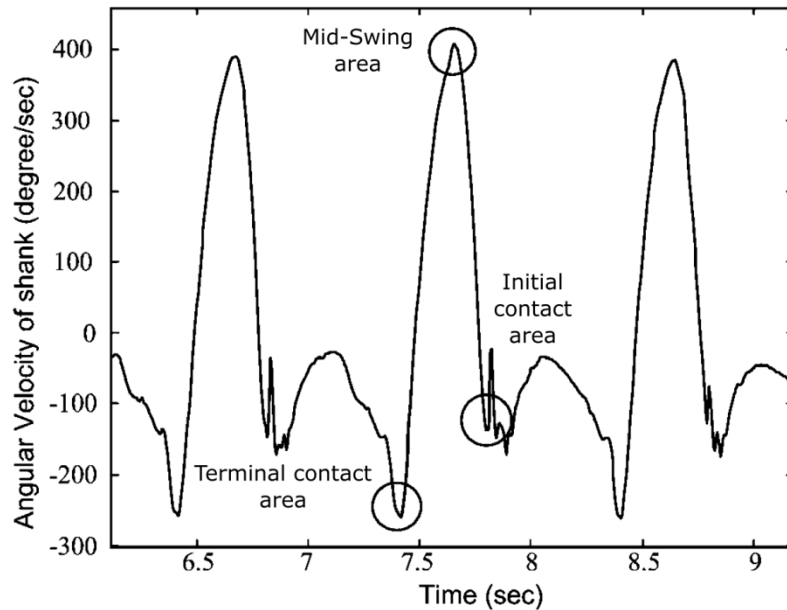


Figure 7. Gyroscope signal of a subject during walking. The 1D gyroscope was fixed to the shank in a manner to measure the angular velocity around a medio-lateral axis. The positive area of the medio-lateral angular velocity was associated with the swing phase. The negative peaks before and after that phase indicated the TC and IC, respectively. Modified figure taken from Salarian et al. [99].

Köse et al. [100] used an IMU mounted on the pelvis for the deduction of IC and TC. In detail they used the accelerometer measurements along the vertical axis and the medio-lateral axis. They further conducted a visual inspection of a few samples of the data comparing it with the gait events deduced from an OMC system. Using the information from the visual examination the events IC and TC could be estimated within certain areas.

Another approach for the detection of IC and TC is based on the initial identification of a period of highly probable swing and stance phase [101]. Here two MIMUs were mounted on the left and right shank just above the ankle joint. The phases of probable swing were identified based on the peaks of the medio-lateral angular velocity. The peaks were assumed to appear during the swing phase of the lower limb. The probable swing phase was defined as the period between the first and last crossing of a certain threshold, calculated from the maximum peak angular velocity [102]. Consequently, a period of probable swing meant a period of probable stance at the contralateral foot. The IC was then estimated as the minimum medio-lateral angular velocity in the phase between a swing period and a stance period, occurring just before an anterior-posterior acceleration peak. The TC was defined as the negative peak of the anterior-posterior acceleration appearing in the phase between a stance period and a swing period [102]. However, this approach might be susceptible to erroneous event detections in pathological gait patterns during which the foot is progressed forward without leaving the floor.

There are many more event detection approaches available based on the physical and geometrical evaluation of the MIMU / IMU signals [103–107]. Other approaches use also machine learning algorithms to deduce the gait events from MIMU / IMU data [108].

However, all these approaches have one thing in common. They rely on the information of two sensors. Despite the advantage of easy and quick applicability, the usage of only two MIUM / IMUs comes along with a few restrictions concerning the calculation of certain spatial parameters. It is rather straight forward to calculate parameters relying on the spatial information of one foot or one sensor, respectively. The stride length for example can be easily calculated by double-integrating the gravity-adjusted acceleration [105]. However, in the case of the step length or step width the spatial relation between two feet / sensors is needed. Since MIMU / IMUs do not directly measure position within a common global frame additional information and assumptions are necessary [100,103,109].

However, these approaches are specialized methods for the calculation of a certain parameter [100,103] or incorporate additional materials [109]. In contrast to that stand methods based on more

complex systems integrating a network of more than two sensors and incorporating biomechanical information and anthropometric measurements [10,110]. That means a spatial relation between the sensor and the actual human segment, the skeletal structure, is established, referred to as I2S calibration. A sensor network of more than one sensor per lower extremity, an I2S calibration and anthropometric information enable now not only the calculation of more complex STP but also the estimation of anatomically interpretable joint angles.

Joint Angles

Like with the OMC system it must be differentiated between technical angles and anatomically interpretable angles. Technical angles are those derived from the relative orientations of two MIMU / IMUs. To calculate these angles the orientation of one sensor has to be converted to the CF of the corresponding sensor. Consider these sensors attached to two adjacent human segments, assumed a rough known alignment is given, then the angles between these sensors can provide rudimentary information about a movement, neglecting all further anatomical and biomechanical conditions. In Figure 8 this approach is schematically depicted.

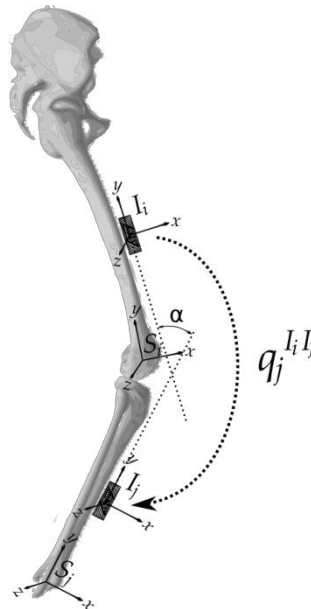


Figure 8. The sensor CF I_j is aligned with the sensor CF I_i . q_j represents the rotation quaternion of I_j to I_i , i.e. the relative rotation between I_i and I_j . The angle between both sensors' y-axes (α) is a technical angle and can be used, in this example, as an approximation to the anatomical flexion – extension angle between the segments S_i and S_j . Consider, this example presumes a rough manual alignment of the sensors' y axes with the longitudinal axes of the segments.

In contrast to that, the I2S calibration creates an alignment between the MIMU / IMU CF and the human segment CF to which the sensor is attached. That means the I2S calibration further determines the orientation of the sensor with respect to the corresponding segment after attaching the sensor to the segment in a random way. The theoretical idea of the I2S alignment is schematically depicted in Figure 9.

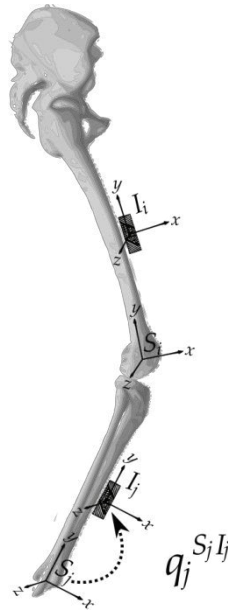


Figure 9. The sensor CF I_j is aligned with the segment CF S_j . q_j represents the rotation quaternion of I_j to S_j . If the same procedure is applied to I_i then the magnetic inertial measurement unit / inertial measurement unit (MIMU / IMU) orientations can be converted to segment orientations and anatomically meaningful joint angles can be derived from the relative orientations of connected segments.

There are various ways for the alignment of the MIMU / IMU CF with the anatomical CF of its corresponding segment [79,84,111–114]. The most common approaches are based on one or more known static poses [111,114,115], functional movements [79,84] or a combination of both [112]. Picerno et al. [113] proposed a calibration device equipped with an MIMU that was used to point on certain AL. However, this approach contradicts the MIMU / IMU system’s independency from expert knowledge and quick applicability.

One known static pose and a known alignment of one MIMU / IMU can be enough for the I2S calibration in the case of MIMUs. The knowledge of the gravity vector as well as the magnetic field vector are used to define the sensor’s CF [114]. In the absence of the magnetometer information more than one pose is needed. Here, the difference between the two gravity vectors from the different poses is used to build the CF [111].

In the case of functional movements the information of the angular velocity vector of two adjacent segments during a predefined motion is considered for anatomical CF construction [111].

To align a sensor CF to an anatomical, bone-embedded CF the knowledge of the latter is required. However, that imposes priorly measured or estimated biomechanical information, i.e. the position of certain AL. In [113], as mentioned above, a calibration wand incorporating a MIMU is used to point those AL out.

Another approach is based on anthropometric statistics [116–118]. In this case the segment lengths of a model are scaled based on a simple input, e.g. body height, and the statistical information from the mentioned tables. Further, one has to attach AL to these segments, e.g. by incorporating the information of a human body model derived from the survey of a cadaver [119].

However, this method relies strongly on the diversity of the collected data based on which the mentioned anthropometric statistics and the body model, which is scaled, were built and might therefore not be adequate for certain ethnical groups, underrepresented in the test data set, and for humans distinctly differing from the average. In [119], for example, the test data set consists of only one cadaver of a 85 year old male.

Considering these concerns alternative approaches are developed. A recent work of Taetz et al. [26] evaluates the creation of an individualized biomechanical model for the human lower body based on a single-view depth camera image. This method incorporates and extends approaches from Golyanik et al. [120] and Pishulin et al. [121]. The method is based on statistical human shape models

incorporating annotated AL derived from complete body scans [122], the S-SCAPE model. This model was refined by Pishulin et al. [121]. Using statistical shape fitting, these human body shape models are registered to the 3D point cloud derived from a depth camera image. The segment lengths and segment orientations as well as the joint centers are then calculated based on the annotated AL. The workflow of this approach is shown in Figure 10.

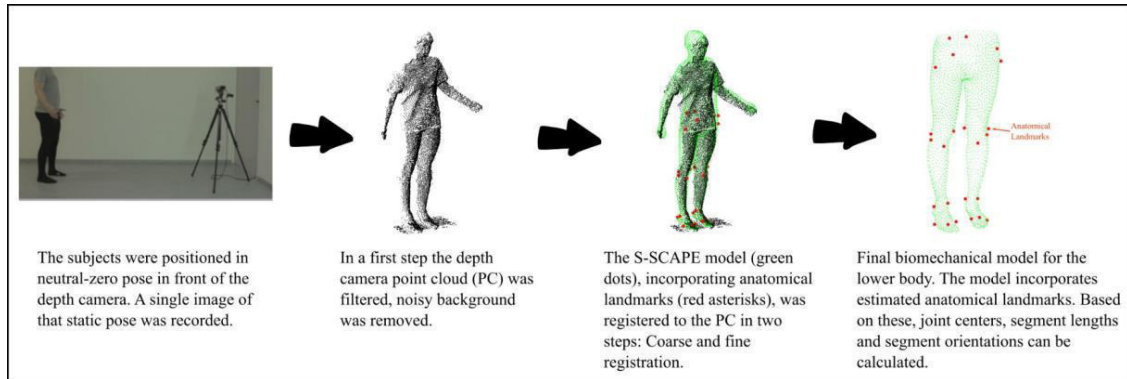


Figure 10. Workflow of the statistical shape fitting using a statistical human body model (green dots) incorporating annotated AL (red dots) and a depth camera based 3D point cloud (black dots). Figure taken from Taetz et al. [26].

With the preferred method for the creation of the biomechanical model and the so derived segment CF, segment lengths and joint centers, it is then possible to perform an I2S calibration. Afterwards the relative segment orientations and relative rotations between adjacent segments as well as meaningful Euler angles can be calculated in the same manner as described in chapter 2.1.1.

However, in the context of the I2S calibration, offsets are a further issue. As mentioned above the I2S calibration relies on known poses, e.g. the neutral-zero pose. This certain pose implies that the joint angles of hip, knee and ankle equal zero. However, in the case of human subjects, especially subjects suffering physical impairments, it is difficult if not impossible to take that position. In [123] this was examined within a group of healthy subjects and a group of patients after THA. It was shown that in certain joint angles the actual posture differs up to 15° from the assumed pose.

That difference in the assumed pose and the actual pose becomes noticeable in the MIMU / IMU based joint angles as static calibration offsets. Such static offsets are described in the JP 2. Figure 11 shows a static offset in the hip flexion during a squat motion task.

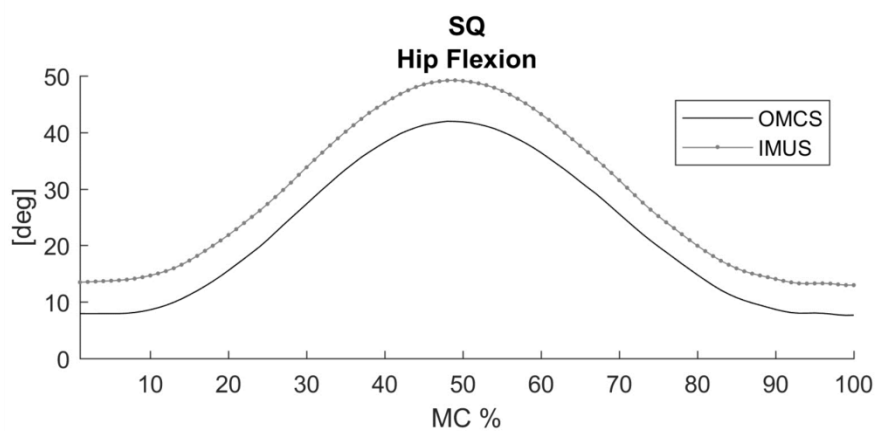


Figure 11. Figure from the supporting information of JP 2 [12]. Shown is the hip flexion of an exemplary subject during one squat (SQ) motion task. The x axis shows the motion cycle (MC) normalized to 100 percent. A static offset between the optical motion capture (OMC) system (solid line) and the IMU system (dashed line) was evident.

Beside calculating anatomically meaningful joint angles, incorporating the information of a detailed biomechanical model with respect to the lower body, allows for the calculation of the more complex STP mentioned above, e.g. step length, step width [13].

There is a lot of work in the literature that is concerned with the estimation of joint angles during gait and other activities using MIMU / IMU systems [79,84,112,124–134]. These studies differ widely concerning the application of the sensors, the processing of the data and the complexity of the parameters analyzed.

Despite an obvious amount of literature available, recent reviews about that topic considered mainly studies reporting the measurement of STP using MIMU / IMUs [96,98]. That underlines the suggestion that the measurement of simple STP in gait analysis using MIMU / IMUs is well established within the research community. However, it also shows that the evaluation of mobile sensor based systems estimating joint angles still lacks sufficient standardization and quality, therefore supporting the overall aim of this thesis to establish an IMU based system for complex 3D motion analysis of the lower body according to the highest research standards. Such a system would present promising opportunities for clinicians and researchers alike, e.g. in the real-time treatment of patients.

2.2.3 Feedback Applications using MIMU / IMU

The huge advantage that portable sensors have over camera based HMC systems is the possibility to use them in the subject's natural environment and perform a constant monitoring of the kinematic parameters over a longer time period. Further, the MIMU / IMUs grow smaller and more efficient, with respect to the frame rate and power consumption, by the day, therefore providing a system that minimally influences the movement of the subject. Recent developments in that area culminated in so called smart textiles in which the sensors vanish almost completely. In Figure 12 the smart pants of the Xenoma® Company are depicted.



Figure 12. The e-skin smart pants from Xenoma including a seven MIMU sensor network.¹

Various authors have developed feedback applications based on MIMU / IMU measurements using different feedback modalities [135–142]. In Hassan et al. [135] three MIMUs are used to measure the hip and knee joint kinematics of the unaffected limb of a hemiplegic patient as well as the motion of a cane used on the unaffected side. That information was employed to estimate the movement of the affected limb which is supported by a robot suit.

¹ <http://www.xenoma.com/>

In Karatsidis et al. [136] seven MIMUs are employed in combination with augmented reality glasses for the treatment of knee osteoarthritis patients. Here, the lower limb kinematics is used to calculate the foot progression angle and deliver visual feedback regarding this parameter via the glasses.

Seel et al. [137] and Valtin et al. [138] used IMUs in combination with functional electric stimulation to treat patients with drop foot.

Wang et al. [139] developed an exoskeleton to support the gait of paraplegic patients. In this case IMUs are used as a part of a complex system to control the motion and orientation of the lower limbs.

Pietschmann et al [142] employed IMUs to measure the sagittal hip joint angle in patients after THA and the knee joint angle in patients after total knee arthroplasty, respectively. The resulting joint angles were sonified and reported to the patient in real-time. The aim was to approximate the motion of the impaired and non-impaired side via sound and therefore increase the gait symmetry.

In Bell et al. [140] MIMUs are employed in a home-based rehabilitation program after knee injury. Here, the knee angle is estimated and visually represented to the patient.

A combination of 2 MIMUs and an exergame approach is introduced in [141,143]. Exergame describes a form of videogame that also provides the user with physical exercises. The idea here is to animate bedfast patients to perform the so called muscle-vein pump, i.e. alternating flexion / extension in the ankle joint, as a prevention of venous thrombosis. In this case the MIMUs are used to control if a certain range of motion (ROM) in the ankle is achieved. This achievement is then used to trigger the motion of a ball in an internet network operating system based game. See Figure 13 for a representation of that approach.



Figure 13. Set-up for the exergame “JumpBall”. Two MIMUs mounted on both feet are connected to an iPad (Apple, Inc.). The motion of the MIMUs triggers a jumping ball in the browser based application. Figure taken from [143].

Despite this amount of promising approaches only two are at a stage of development that allows for real-world application [140,141]. According to the author’s opinion one reason for that is the fact that the MIMU / IMU systems on the market lack sufficient accuracy, or at least the consistent proof of the latter, and proof of their effectiveness in health applications. That means that most of the evidence regarding the reliability and validity of MIMU / IMU systems states high error ranges. Besides developing systems with higher accuracy it is also of interest to find parameters that are less affected by the common error sources, e.g. calibration offsets. The JP 4 is concerned with that very problem.

2.2.4 Composition of the present IMU system

This chapter gives a brief introduction to the IMU system used in the present thesis. Detailed information can be found in the corresponding JPs.

Hardware

The sensors used in this study consisted of the wireless MTw Awinda MIMUs (Xsens Technologies BV, Enschede, The Netherlands). The detailed technical specification of the MIMUs can be viewed in Table 3. Figure 14 shows a single MTw Awinda MIMU.

Table 3. Specifications of the MTw Awinda MIMU

Sensor	Range
Accelerometer	$\pm 160 \text{ m/s}^2$
Gyroscope	$\pm 2000 \text{ deg/s}$
Magnetometer	$\pm 1.9 \text{ Gauss}$
Characteristics	
Wireless update rate	60 – 120 Hz*
Weight	16 g
Dimension	47 x 30 x 13 mm

* depends on the number of sensors



Figure 14. MTw Awinda MIMU (Xsens Technologies BV, Enschede, The Netherlands)

Sensor Placement

In the studies of the present thesis the sensors were placed on the segments of the lower body as follows:

- Pelvis: On the sacrum, between the left and right Spina iliaca posterior superior
- Left / Right thigh: on the lateral aspect approximately at two-thirds of the distance between the Trochanter major and the Epicondylus lateralis femoris
- Left / Right shank: on the lateral aspect approximately at 50 % of the distance between the Epicondylus lateralis femoris and the Malleolus lateralis.
- Left / Right foot: on the dorsum of the foot approximately atop the third and fourth Os metatarsale

In Figure 15 the sensor placement is schematically represented.



Figure 15. Placement of the MTw Awinda MIMUs on the segments of the lower body and the pelvis without the retroreflective markers of the OMC system.

Sensor Fusion Method

Despite the presence of a magnetometer in the sensors, in the present measurement approach only the accelerometer and gyroscope data was used. An iterated extended Kalman filter was employed to fuse the acceleration and gyroscope data and estimate the relative sensor orientation. The approach was enhanced with a global translation estimation incorporating ground contact estimation. The method was in detail described in [9,10]. In the appendix A of JP 1 the method was summarized for the convenience of the reader.

As mentioned above the IMU raw data was recorded using MTw Awinda MIMUs. The data was recorded in the Xsens MVN Biomech software 4.3.7 and reprocessed using the described sensor fusion algorithm, which was implemented in C++.

Parameters

Based on the reprocessed relative sensor orientations a wide range of parameters were extracted. Using the Euler angle decomposition anatomically meaningful angles between adjacent segments were derived from the relative sensor orientations. In detail, the joint angles of the hip, knee and ankle in the sagittal, frontal and transversal plane were calculated. Further, the global 3D pelvis motion was derived from the orientations of the sensor attached to the sacrum.

The human measurement model in the present system incorporates AL attached to the segments of the lower body. Consequently, the positions of these AL in the 3D space were derived from the IMU measurements. Consider, the validity of these positions was not evaluated in the present thesis.

Based on the incorporation of the AL the gait events IC and TC could be estimated using an extension of the approach from Zeni et al. [50] Using IC and TC as well as the knowledge about the position of the AL it was possible to calculate 12 STP (see Table 1 from JP 3).

2.3 Validation approach

The validation process of a HMC system demands a few essential components and steps, which are shortly described in this chapter.

2.3.1 Reference System

According to the information in chapter 2.1 the marker based OMC system was deemed the gold standard in HMC and therefore was chosen as reference system in the present approach. In detail the OptiTrack (NaturalPoint, Inc., Corvallis, OR, USA) system was employed. The system consisted of 12 Prime 13 cameras. The OMC data was recorded in the Motive software 1.10.0.

To reconstruct the movement of the lower body the Rizzoli marker set [21] was chosen. The Rizzoli marker set was preferred over alternative marker protocols since the reconstruction of the segments is based on AL and does not need anthropometric measurements or calibration tools.

The AL were palpated by a physical therapist / movement scientist with several years of experience in the area of HMC.

2.3.2 System Synchronization

An essential point for the validation is the synchronization between the compared systems. For this reason a hardware-synchronization was employed. using a standard 5 V transistor-transistor-logical signal. For the sake of comparison and to avoid additional interpolation, both systems shared the maximum frame rate of the Xsens set-up, 60 Hz.

It was further the aim of this study to reduce as much error sources as possible. For this reason special rigid boxes (RB) were designed to perfectly fit the Xsens MIMUs. Additionally, these RBs incorporated four additional retroreflective markers in a random alignment. See Figure 16 for an example of a RB with an inserted MIMU.

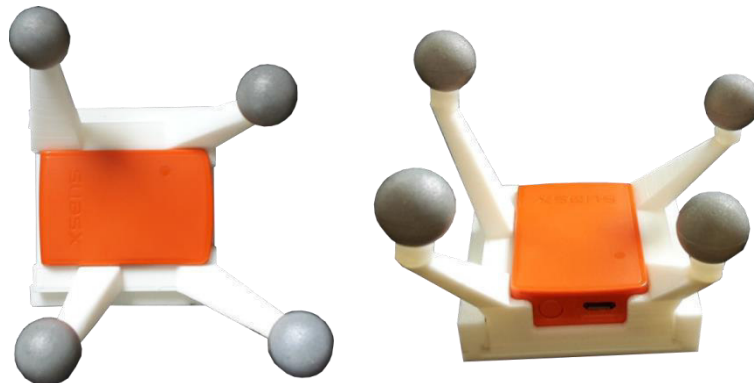


Figure 16. Rigid box (RB) with four randomly aligned retroreflective markers and an inserted MIMU

This design allowed minimizing differences between the OMC and the IMU system due to different STA. Therefore it was necessary to estimate the OMC based segment orientations using the information of the RBs' own markers instead of the markers attached to the AL. In fact, in the JP 1 and 2 both approaches were used independently for comparison.

Further, as mentioned above, in the JP 1 and 2 the I2S calibration incorporated OMC information. That means that the I2S alignment was deemed equal to the RB to segment alignment.

In more detail, the I2S alignments were obtained from the RB and the skin marker based segment positions and orientations. However, this is only possible, if the sensors and associated RBs share the same local CF or can be aligned via a rigid transformation between MIMU and RB. The procedure to estimate these rigid transformations (one relative orientation for each MIMU / RB pair, while the CF origins were assumed to coincide) from synchronized data sequences during motion (angular velocities) is sometimes referred to as hand eye calibration. For that purpose all RBs with their corresponding MIMUs inserted were mounted on a stick (see Figure 17) for a synchronized record. In that record, the stick with the attached RBs was randomly moved around all 3 spatial axes

for approximately 30 seconds. The estimation method was based on [144]. A detailed description of the hand-eye calibration can be found in the supplementary file of the JP 2, enclosed in this thesis.



Figure 17. The MIMUs inserted in the corresponding RBs necessary for the lower body motion analysis. The RBs are mounted on a rigid stick. The stick was moved around all three spatial axes during the record.

2.3.3 Subjects and Sample Size

The choice of the subjects and the sample size were in each case based on expert knowledge and experience of the recent literature. First, it was the aim to validate the IMU system on a homogenous group of subjects to exclude possible errors due to differences in age, height or weight. Therefore, the inclusion criteria for the first sample, referred to as “Healthy”, were an age between 18 and 30, and a BMI between 19 and 24. Further, subjects who suffered a recent orthopedic injury of the lower extremities were excluded. Also subjects with neurological or cardiovascular impairments were not considered.

For the second sample of the extended validation a group of individuals who represent one group for which the IMU system is actually intended was chosen: a group of patients after orthopedic surgery. The choice of patients after THA was based on the cooperation with the biomechanics institute of the Klinik Lindenplatz, Bad Sassendorf, Germany. Patients were included if they were able to walk at least for four minutes without crutches, cane, etc. They were included independently of the surgical approach or age. Only the BMI was restricted to < 40 .

An adequate sample size was required in both cases. The sample size was chosen based on related literature. The sample sizes in the regarding literature range from one subject [86] to 236 subjects [101]. However, the gross of the studies examined ten to 30 subjects [105,124,125,131]. Therefore, at least 20 subjects were deemed the appropriate number of participants for the validation of the present system. In both cases this number was accomplished.

2.3.4 Motion Tasks

Gait was deemed the main task of interest when considering a new HMC system since the gait analysis is, as mentioned in chapter 2.1.1, not only the best researched as well as the most important motion of the human kind, but also has gained a high relevancy in medical applications [2]. Further, it confronts IMU based systems with its most important technical issue: the drift in the heading direction during continues motions over a longer time period, without using magnetometer information. Of course, this problem has to be considered in every motion task. However, during indoor overground walking, violated magnetic field measurements might be more likely compared to static motions, e.g. squats, since in this case the MIMUs are exposed to the differing amount of ferromagnetic materials in the floor and the surrounding facilities. Consequently, to gain valid data a magnetic mapping of the measurement volume might be essential [145]. Therefore, it seems to be of high interest to prove the valid estimation of IMU based joint angles during indoor overground walking, omitting all magnetometer information.

Hence, it was not merely important to include gait in the validation protocol but rather a gait exceeding the standard extent of about ten gait cycles. As summed up in JP 1 there are only few

studies that examine the functionality of MIMU / IMU systems over a longer measurement time [79,130,146].

To close that gap in the validation of MIMU / IMU systems and to still maintain a relation to the clinical use the 6 minute walking test [147] was chosen for the evaluation.

However, despite the common gait analysis there are several more motion tasks that can contain important information about the musculoskeletal status of a human. Considering sports, injury prevention or rehabilitation, squats come to mind. The squat, particularly the single leg squat, provides information about the balance, core stability and the functionality of the leg axis [148–150]. The literature concerning complex 3D analysis of the lower extremities during a squat or single leg squat using MIMU / IMUs is at most rare. Al-Amri et al. [125] and Kianifar et al. [133] examine a squat task and single leg squat task, respectively, using more than two MIMU / IMUs.

Last but not least it was the aim of this thesis to provide proof that the present IMU system also delivers valid and reliable joint angles of the lower extremities during motions including higher accelerations and impacts. Considering these requirements a jumping task fits. It contains high accelerations and decelerations in the jumping and landing phases, respectively. In the present work the countermovement jump was chosen over comparable jumps like the squat jump or the drop jump because it can be separated into six different motion sections, including an accelerated downward motion, a breaking phase and an accelerated upward motion [151].

Further, the squat tasks and the countermovement jump produce higher ROMs in the joint angles of the lower body compared to the gait, which was another reason for considering these motions.

2.3.5 Statistics

The next important step is to choose adequate statistical measures for the comparison of two HMC systems. The statistical measures should be well approved and comparable to the corresponding literature. The following measures were the main ones used to evaluate the difference between the IMU system and the OMC system:

- Root Mean Squared Error (RMSE) and Mean Absolute Error (MAE)
 - In comparison to the mean error, employed in some validation studies, the RMSE and the MAE are not influenced by a mixture of negative and positive differences. In the case of the mean error negative as well as positive differences will lead to an average error around zero whereas the RMSE / MAE deliver a more trustworthy image of the error between two parameters. Concerning the RMSE and MAE, both are employed in related literature. However, Chai and Draxler [152] stated that the RMSE is to be preferred over the MAE when considering samples following a normal distribution, which was the case in the joint angle data of the JPs 1 to 4. Nevertheless in the case of scalar, time-specific, variables, i.e. ROM or STP, also the MAE was employed, mainly due to comparability to the related literature.
- Range of Motion Error (ROME)
 - The ROME was deemed essential for the evaluation of the IMU system since the accurate measurement of the ROM is an important tool in the clinical motion analysis [46,134,153,154]. The ROME equals in its calculation the mean absolute error. The ROM is calculated as the difference between the maximum and minimum of a joint angle waveform during one gait cycle. The ROME is the absolute difference between the ROM of the same joint angle of each HMC system.
- 95 % Confidence Interval (CI)
 - Besides the standard deviation also the 95 % CI of the RMSE and ROME were calculated. This was deemed of high interest since it delivers a better

understanding of the range of errors one has to expect in the different joint angles.

- Coefficient of Multiple Correlation (CMC)
 - The CMC was defined by Ferrari et al. [155]. They stated that the CMC takes into consideration offsets between the compared joint angle waveforms. Further, it takes into account the inter-gait cycle variability, typical for motion tasks. Therefore it was considered more adequate for the comparison of joint angle waveforms, compared to the Pearson correlation coefficient. Nevertheless, in the JP 4, the Pearson correlation coefficient was also employed for the comparison of scalar parameters, e.g. gait events or symmetry values.
- Bland-Altman Limits of Agreement (BA)
 - The calculation of BA [156] is a widespread method in the comparison of two measurement methods. Especially the graphical representation of the results of the BA analysis provides an overview of the agreement between two systems and to which limits the results can be trusted. Further, the BA plots show how an error develops if the amplitude of a parameter changes. See for an example Figure 18.

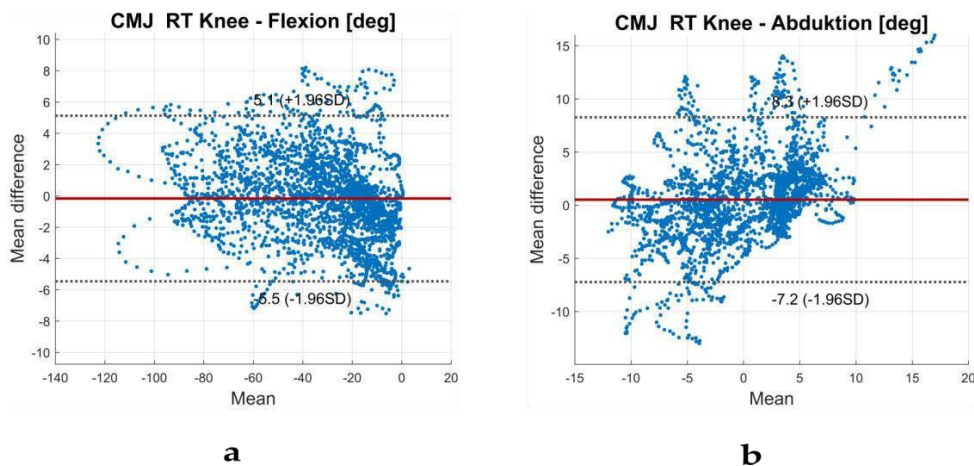


Figure 18. Shown are the BA analysis of the right knee flexion (a) and the right knee abduction (b) for 28 subjects during a countermovement jump. In this case the IMU based joint angle calculation was compared with the OMC system joint angle estimation based on the markers attached to AL rather than the rigid boxes. In (a) the error distribution remains constant with respect to the parameter's amplitude. In (b) the mean difference changes from negative values to positive values according to the parameters progression. Figure taken from JP 2 [12].

2.3.6 Reliability

There are different kinds of reliability that can be evaluated regarding a HMC system. Intra-tester or test-retest reliability describes the consistency of the data recorded by a single tester from one collection to the next. In contrast, inter-tester reliability assesses the correlation between the data recorded by two or more different testers using an identical measurement set-up.

It was not within the bounds of the present thesis to evaluate all kinds of reliability, therefore it was focused on the test-retest reliability [105,157,158]. The test-retest reliability was deemed important since in clinical settings recurrent measurements, performed by one tester, for example to evaluate a rehabilitation progress, are commonly used.

For the evaluation of the test-retest reliability a two way random effect model of the intraclass correlation coefficient (ICC) was calculated [159]. The relevant measurements were repeated twice, approximately one week apart, for this evaluation.

3 Validation

3.1 Technical Validation of the Joint Angles

3.1.1 Journal Paper 1

Summary

JP 1 covers the technical validation of the sensor-fusion algorithm used to estimate the relative IMU orientations and based on those the joint angles of the lower body as well as the global pelvis orientation during 6 minute walking of young and healthy subjects. Therefor in this work the IMU system relies on an I2S calibration based on data from the reference system, the OMC system. Also the biomechanical model derived from the marker information of the OMC system was incorporated for the IMU tracking. However, the segment tracking during the gait after the initialization via the OMC system is based purely on IMU data. This was done to isolate errors caused by the sensor-fusion algorithm from errors originating from the IMU based I2S calibration and a different biomechanical model.

Further, the results of the IMU based tracking are compared to two different variations of the OMC system. First, the OMC based segment orientations are estimated using markers attached to AL. Second, the OMC based segment orientations are estimated using the information of the RBs with the inserted IMUs. This was done to minimize the effect of STA on the difference between the orientations of the segments calculated for each system, respectively. The joint angles of the lower body were calculated incorporating the relative segment orientations based on the IMU system and the two versions of the OMC system, respectively. The results were compared according to chapter 2.3.5.

Further, the drift stability of the measured joint angles during the 6 minute walking was assessed. For this, the RMSE between the two systems was analyzed at three different sections of the total record via a linear regression.

For the evaluation of the test-retest reliability of the results the same test procedure was reproduced approximately seven days later.

It was the aim of this article to prove the validity, reliability and the long-term stability of the joint angles of the lower body, calculated based on the mentioned sensor-fusion algorithm, in comparison to a reference system during the most important activity of daily living and therefore the most discussed issue in the research of HMC, gait.

Main Contributions

- Magnetometer-free 3D IMU based joint angles of the lower body during gait
- Long-term drift stability of the joint angles estimation > 5 minutes
- Difference between two common ways of calculating OMC based segment orientations during gait



Article

Validity, Test-Retest Reliability and Long-Term Stability of Magnetometer Free Inertial Sensor Based 3D Joint Kinematics

Wolfgang Teufl ^{1,*}, Markus Miezal ¹, Bertram Taetz ¹, Michael Fröhlich ²  and Gabriele Bleser ¹

¹ Junior Research Group wearHEALTH, Technische Universität Kaiserslautern, Gottlieb-Daimler-Str. 48, 67663 Kaiserslautern, Germany; miezal@cs.uni-kl.de (M.M.); taetz@informatik.uni-kl.de (B.T.); bleser@informatik.uni-kl.de (G.B.)

² Department of Sports Science, Technische Universität Kaiserslautern, Erwin-Schrödinger-Str. 57, 67663 Kaiserslautern, Germany; michael.froehlich@sowi.uni-kl.de

* Correspondence: teufl@cs.uni-kl.de; Tel.: +49-631-205-3332

Received: 12 April 2018; Accepted: 7 June 2018; Published: 21 June 2018



Abstract: The present study investigates an algorithm for the calculation of 3D joint angles based on inertial measurement units (IMUs), omitting magnetometer data. Validity, test-retest reliability, and long-term stability are evaluated in reference to an optical motion capture (OMC) system. Twenty-eight healthy subjects performed a 6 min walk test. Three-dimensional joint kinematics of the lower extremity was recorded simultaneously by means of seven IMUs and an OptiTrack OMC system. To evaluate the performance, the root mean squared error (RMSE), mean range of motion error (ROME), coefficient of multiple correlations (CMC), Bland-Altman (BA) analysis, and intraclass correlation coefficient (ICC) were calculated. For all joints, the RMSE was lower than 2.40°, and the ROME was lower than 1.60°. The CMC revealed good to excellent waveform similarity. Reliability was moderate to excellent with ICC values of 0.52–0.99 for all joints. Error measures did not increase over time. When considering soft tissue artefacts, RMSE and ROME increased by an average of 2.2° ± 1.5° and 2.9° ± 1.7°. This study revealed an excellent correspondence of a magnetometer-free IMU system with an OMC system when excluding soft tissue artefacts.

Keywords: 3D joint kinematics; drift; inertial sensor; soft tissue; test-retest reliability; validity

1. Introduction

Marker-based optical motion capture (OMC) systems are commonly used in clinical movement analysis [1] and are therefore considered the gold standard. However, despite high resolutions and sub-millimeter accuracy, the application of OMC is expensive, time-consuming, and restricted to a laboratory environment. Therefore, body-worn inertial measurement units (IMUs) present a mobile alternative [1]. IMUs incorporate 3D accelerometers, 3D gyroscopes, and, typically, 3D magnetometers, measuring 3D linear acceleration, 3D angular velocity, and 3D magnetic field, respectively. Using sensor fusion algorithms, e.g., variations of the Kalman filter or optimization based methods [2], it is possible to estimate the IMUs' orientation in reference to a global coordinate system [3]. Combining more IMUs attached to linked body segments, it is possible to estimate the joint kinematics of the specified segments [1,4,5].

There are drawbacks concerning IMU systems that have to be addressed when measuring human motion. First, IMU-based orientation estimation suffers from drift due to the integration of noisy gyroscope measurements [6]. This is particularly challenging when omitting magnetometer data, which provide a global heading reference and can therefore be used to compensate for drift in the transversal plane [2].

Second, the incorporation of magnetometer measurements is typically based on the assumption of a homogeneous magnetic field, which is often violated [7]. There are efforts to develop methods for handling magnetic disturbances [8,9] or completely omit magnetometer data [4,10–12]. Concerning the latter, El-Gohary and McNames [11] present an unscented Kalman filter based approach for estimating the joint angles of a three segment kinematic chain using three IMUs. The kinematic model represents a human arm with stationary shoulder joint position but considers only two rotational degrees of freedom (DOFs) in each joint, including the shoulder, to match the DOFs of the industrial robot arm, which was used for validation in a 15-min trial. For drift reduction, they propose gyroscope and accelerometer bias estimation, limited joint ranges of motion, and zero velocity updates. Seel et al. [4] present a magnetometer-free method for calculating the angles around one dominant axis of one joint using two IMUs. In [4] they consider the knee and ankle flexion/extension angles during walking. The method was evaluated with one transfemoral amputee during repeated 10 m walking trials. Fasel et al. [12] focus on the validation of functional calibration and segment orientation estimation methods adapted for outdoor activities with highly dynamic movements. They recorded and analyzed 120 s of skiing on an indoor skiing carpet with nine IMUs on shanks, thighs, lower back, sternum, upper back, and head. They first estimate the orientation of each IMU separately from the acceleration and angular velocity measurements and then propose a drift correction method for adjacent segments using similar principles as in [4] (i.e., the acceleration vector in the joint position should be identical in the global frame, no matter from which IMU, preceding or following, it was predicted). The drift reduction method is detailed in [13]. The current study investigates a slightly modified version of a previously published sensor fusion algorithm for real-time lower body joint kinematics estimation with seven IMUs on pelvis, thighs, shanks, and feet [14]. In this study, the method was extended with accelerometer bias estimation as in [11], and magnetometer data was completely omitted. In contrast to [11], the method uses a so-called free segments biomechanical model (with six DOFs per segment), which was shown to outperform the kinematic chain model with respect to the influence of model calibration errors and the dependence on undisturbed magnetometer information on simulated and real data from one test person in [2]. In contrast to the magnetometer-free method in [4], the proposed method is not restricted to joint movements with one dominant axis of rotation. In contrast to [12], the segment kinematics are all estimated jointly by fusing the IMU measurements with information from the biomechanical model and environmental constraints (i.e., ground contacts), which results in a built-in drift reduction for the joint angles (cf. Sections 3.4 and 4.4). Moreover, in contrast to the previously mentioned methods, [14] also provides global segment position estimates, though this study focuses on the estimated orientations.

Researchers use simple IMU set ups to calculate spatio-temporal gait parameters [15,16]. However, the measurement of 3D joint angles based on IMUs is still subject to extensive development and lacks in adequate validity and reliability studies.

Various authors tried to fill this gap [17–20]. Robert-Lachaine et al. [17] examined a commercially available IMU system, capturing ergonomic lifting and carrying tasks over a time period of 32 min. Zhang and Novak [18] evaluated the IMU derived joint angles of ten subjects during gait. Ferrari et al. [19] compared IMU system based joint kinematics with OMC system derived joint kinematics during a ten meter walk using identical coordinate frames and rigid marker clusters. Al-Amri et al. [20] validated the IMU based joint kinematics of gait, squat, and a jumping task of 27 subjects. Nevertheless, most studies are expandable in terms of the measurement and evaluation protocol. Despite the long-time measurement, Robert-Lachaine et al. [17] did not report results of different time sections of their records. Bergamini et al. [21] examined the global drift of two IMUs attached to the wrist and sacrum during 180 s of level walking. They found a global drift, mainly in the transversal plane.

Other authors used coordinate frames inconsistent between IMU and OMC systems [12,18,20]. Kainz et al. [22] demonstrated the high impact of coordinate system differences on the accuracy of the

calculated joint kinematics. Hence, it was a special objective of this study to evaluate the pure technical error between the OMC and IMU system using consistent coordinate frames.

Further, the number of subjects examined rarely exceeds 10 [18,19]. Additionally, most of these studies used marker clusters rigidly fixed to the IMUs for optical joint angle calculation. Thus, both systems suffer from the same amount of soft tissue artefacts (STA), minimizing the error between the systems due to different positioning. Few studies used marker sets attached to anatomical landmarks for the validation rather than marker sets rigidly fixed to the IMUs, therefore taking into account errors due to STA [4,12,20,23]. Al-Amri et al. [20] mainly investigates the reliability of a commercial IMU system, but they did not report detailed results for the validity, especially concerning the frontal and transversal plane joint angles. Nüesch et al. [23] also evaluated a commercial IMU system delivering only sagittal plane joint angles. Seel et al. [4] highlighted the impact of STA on the joint angle data by comparing error measures of the human leg and the prosthesis of one transfemoral amputee. As mentioned above, they also focused on one dominant axis of rotation. In contrast, the present work highlights the amount of errors linked to STA for the complete 3D joint angles of the lower body.

The aim of this study was to fill the mentioned gaps concerning the study design and evaluate a previously published sensor fusion algorithm without using magnetometer information. The main target was to evaluate the validity and test-retest reliability of the estimated 3D joint kinematics. A second objective of the analysis was to examine drift in the estimated kinematics, when measuring over an extended time period (>1 min). Additionally, a specific concern was to highlight the effects of STA on IMU-derived data.

2. Materials and Methods

2.1. Subjects and Data Acquisition

Twenty-eight healthy subjects (15 females, 13 males; age 24 ± 2.70 years; 70 ± 12.70 kg and 1.76 ± 0.09 m in height) participated in the study. Each of the subjects performed two test sessions on two days (6.75 ± 2.26 days in between). A test session consisted of one static neutral zero position (n-pose) sequence and a 6 min walk test [24]. The study was approved by the ethical committee of the Technische Universität Kaiserslautern (TUK) and meets the criteria of the declaration of Helsinki. After receiving all relevant study information, the participants signed an informed consent to the study including a permission to publish data.

On both test days lower extremity 3D kinematics was simultaneously captured using twelve OptiTrack Prime 13 cameras (NaturalPoint, Inc., Corvallis, OR, USA) and seven XSens MTw Awinda (Xsens Technologies BV, Enschede, The Netherlands) IMUs.

IMUs were activated at least 20 min before measurement start. A static trial was performed before each subject was instrumented, with the sensors lying still for a period of at least 10 s, to estimate and subtract the gyroscope bias. These steps were conducted in accordance with the recommendations of Bergamini et al. [21].

Thirty-two retroreflective markers were attached to anatomical landmarks (AL) according to Leardini et al. [25] and the OptiTrack recommendations. Each IMU was secured in matched 3D printed boxes to which four markers were rigidly attached. These markers were used for unique identification in the optical point cloud as well as for orientation estimation. Using the OptiTrack Software, the origin of the boxes was moved to the center of the attached sensor casing. These box/sensor compounds were fixed to the body segments using straps and double-sided adhesive tape. IMUs were attached on the right and left dorsum of the foot approximately atop the base of metatarsal II-IV, on the right and left lateral aspect of the shank, due to better visibility, on the right and left lateral aspect of the lower third of the thigh and between the Spinae Iliacae Posteriores Superiores approximately atop the sacral base (Figure 1).



Figure 1. Instrumentation of one exemplary subject. Marker set and rigid marker clusters.

Inertial and optical data were simultaneously recorded at 60 Hz using XSens MVN Biomech (Version 4.3.7) and OptiTrack Motive (Version 1.10.0) which were hardware synchronized using a standard 5 V TTL signal. The alignment orientations between the IMUs and the rigid boxes were calculated using the method described in [7]. The biomechanical model according to Cappozzo et al. [26] and the IMU-to-segment calibrations were extracted from the OMC data of the n-pose sequence. The joint centers were also calculated from the OMC data during the n-pose sequence according to the definitions of Visual3D (C-Motion, Inc, Germantown, MD, USA), a widely used software tool for 3D biomechanics research. The first OMC frame of each walking sequence was used as initialization for the IMU-based kinematics estimation. Both systems used the same biomechanical model.

The inertial data was processed with an iterated extended Kalman filter (IEKF) approach based on [14] while omitting magnetometer information. The gyroscope biases were extracted from a static sequence (see above), while the accelerometer biases were estimated in the IEKF along with the kinematics estimation using the model described in [11,27]. The same sequence was processed twice: initially to obtain a converged estimate of the acceleration bias, which was then used as initial guess in the second run. The estimated segment orientations were used to derive relative joint orientations. These were decomposed into joint angles using Euler angle decomposition [28]. The sensor fusion method is detailed in Appendix A.

To minimize STA, the OMC-based joint angles were derived from marker clusters on the rigid boxes (condition 1). For secondary analyses the joint angles were calculated based on the markers attached to the anatomical landmarks (condition 2). Initial contact (IC) was detected based on the left and right heel marker [29]. Turning phases in the 6 min walk tests were omitted. In order to investigate drift behavior, 10 left and right steps (one trial) were identified at three sections, i.e., beginning (A), middle (B), and end (C) of the test. All joint angle curves were normalized to 100 percent gait cycle (GC).

2.2. Statistical Analysis

To evaluate the IMU system, the root mean squared error (RMSE) and range of motion error (ROME), as well as 95% confidence interval (CI) were calculated for hip, knee, ankle joint, and the global pelvis orientation per section per GC. Further, Bland-Altman analysis (BA) was conducted to evaluate the limits of agreement (LoA) between the mean joint angle waveforms over all 28 subjects for both systems, considering only the normalized GC of section A. The results of the BA analysis are presented in the form $0.0^{\circ}\text{--}0.0^{\circ} \pm 0.0^{\circ}\text{--}0.0^{\circ}$. The first two numbers indicate the minimum and maximum of the mean differences between the systems. The last two numbers indicate the minimum and maximum of the limits of agreement (95% CI) of the two systems. The coefficient of multiple

correlation (CMC) was calculated for each parameter per section per GC according to Ferrari et al. [30]. In [30] they showed that if a joint angle waveform reveals a similar ROM compared to the overall offset between the two signals, the CMC can become a complex number. If that happened in the current calculations for individual subjects, these results were not considered for further analysis. All these calculations were conducted for both, condition 1 and condition 2.

A paired *t*-test was performed to identify significant differences in the RMSE and ROME of the joint angles of all sections between condition 1 and condition 2. Alpha level was set a priori to 0.05. The Chi-square goodness-of-fit test was carried out to check for normal distribution in the data.

For the evaluation of the test-retest reliability, the intraclass correlation coefficient (ICC) for inter-day reliability was calculated for test day one and test day two for both systems for every joint and section according to McGraw and Wong [31]. CMC and ICC values were rated according to Koo and Li [32].

The global heading direction error of the pelvis in the transversal plane (pelvis rotation error) was examined at minute 0, 1, 2, 3, 4, 5, and 6. In addition, the RMSE and the ROME of the joint angles and pelvis flexion/obliquity were examined regarding potential linear trends over time. Therefore, lines were fitted via linear least squares regression to the RMSE and ROME values of each GC for the abovementioned angles and all test persons (Matlab function “fit” with “fittype = poly1”). The slopes of the fitted lines were computed and plotted to evaluate potential trends. Processing of the joint angles and statistics were conducted in Matlab 2015 (Mathworks Inc., Natick, MA, USA).

3. Results

3.1. Condition 1—Marker Clusters

RMSE and ROME for all parameters over all sections are shown in Table 1. RMSE and ROME between the two systems revealed mean values lower than 2.40° and lower than 1.60° respectively in all joints. The poorest outcome concerning the RMSE was evident in knee rotation (1.75° – 2.34°) and knee abduction for ROME (1.11° – 1.58°). Figure 2a exemplary shows the left (LT) ankle flexion of a representative subject.

Table 1. Mean root mean squared error (RMSE) and mean range of motion error (ROME) of condition 1 over all subjects \pm standard deviation (SD); brackets contain 95% confidence interval (CI). A, B, C indicate beginning, middle, and end of the 6 min walk test.

	RMSE (deg) \pm SD (95% CI)			ROME (deg) \pm SD (95% CI)		
	A	B	C	A	B	C
LT Hip—Abduction	1.05 \pm 0.42 (0.78–1.11)	1.14 \pm 0.55 (0.75–1.17)	1.06 \pm 0.45 (0.77–1.12)	0.54 \pm 0.21 (0.43–0.59)	0.57 \pm 0.29 (0.38–0.60)	0.57 \pm 0.27 (0.44–0.64)
LT Hip—Rotation	1.94 \pm 0.92 (1.49–2.20)	2.29 \pm 1.36 (1.85–2.91)	2.25 \pm 1.16 (1.80–2.70)	0.68 \pm 0.27 (0.53–0.74)	0.70 \pm 0.28 (0.55–0.77)	0.68 \pm 0.28 (0.56–0.75)
LT Hip—Flexion	1.02 \pm 0.35 (0.79–1.06)	0.99 \pm 0.29 (0.83–1.06)	1.00 \pm 0.32 (0.78–1.02)	0.93 \pm 0.36 (0.71–1.00)	0.89 \pm 0.36 (0.72–0.99)	0.85 \pm 0.37 (0.70–0.99)
LT Knee—Abduction	1.59 \pm 0.48 (1.22–1.59)	1.58 \pm 0.50 (1.26–1.65)	1.57 \pm 0.51 (1.31–1.71)	1.58 \pm 0.79 (1.20–1.81)	1.54 \pm 0.92 (0.97–1.68)	1.54 \pm 0.83 (1.09–1.73)
LT Knee—Rotation	2.34 \pm 1.08 (1.63–2.48)	2.34 \pm 1.16 (1.43–2.33)	2.27 \pm 1.10 (1.37–2.23)	1.09 \pm 0.32 (0.92–1.16)	1.09 \pm 0.39 (0.93–1.23)	1.16 \pm 0.41 (0.98–1.30)
LT Knee—Flexion	1.47 \pm 0.34 (1.25–1.51)	1.44 \pm 0.31 (1.29–1.53)	1.41 \pm 0.34 (1.17–1.44)	0.70 \pm 0.27 (0.57–0.78)	0.67 \pm 0.27 (0.51–0.72)	0.72 \pm 0.33 (0.60–0.86)
LT Ankle—Abduction	1.61 \pm 0.39 (1.42–1.73)	1.63 \pm 0.36 (1.50–1.78)	1.62 \pm 0.43 (1.35–1.68)	1.29 \pm 0.51 (0.96–1.35)	1.43 \pm 0.43 (1.29–1.62)	1.22 \pm 0.39 (0.97–1.27)
LT Ankle—Rotation	2.16 \pm 0.68 (1.80–2.33)	2.12 \pm 0.65 (1.70–2.21)	2.13 \pm 0.68 (1.69–2.19)	1.56 \pm 0.57 (1.18–1.63)	1.51 \pm 0.61 (1.13–1.59)	1.53 \pm 0.45 (1.35–1.69)
LT Ankle—Flexion	1.55 \pm 0.34 (1.46–1.72)	1.54 \pm 0.36 (1.41–1.69)	1.61 \pm 0.47 (1.35–1.72)	0.97 \pm 0.38 (0.73–1.03)	0.98 \pm 0.38 (0.73–1.02)	1.08 \pm 0.44 (0.85–1.19)
RT Hip—Abduction	1.09 \pm 0.54 (0.63–1.05)	1.09 \pm 0.55 (0.68–1.11)	1.12 \pm 0.54 (0.69–1.11)	0.56 \pm 0.22 (0.42–0.59)	0.55 \pm 0.26 (0.32–0.52)	0.53 \pm 0.25 (0.38–0.57)

Table 1. Cont.

	RMSE (deg) \pm SD (95% CI)			ROME (deg) \pm SD (95% CI)		
	A	B	C	A	B	C
RT Hip—Rotation	1.64 \pm 1.00 (1.00–1.77)	1.78 \pm 1.76 (0.68–2.04)	2.07 \pm 1.72 (0.92–2.25)	0.65 \pm 0.47 (0.40–0.76)	0.56 \pm 0.19 (0.46–0.60)	0.51 \pm 0.20 (0.42–0.57)
RT Hip—Flexion	0.98 \pm 0.51 (0.68–1.07)	0.89 \pm 0.30 (0.68–0.91)	0.86 \pm 0.28 (0.69–0.91)	0.98 \pm 1.26 (0.21–1.18)	0.73 \pm 0.40 (0.52–0.83)	0.69 \pm 0.43 (0.44–0.77)
RT Knee—Abduction	1.26 \pm 0.51 (0.90–1.30)	1.26 \pm 0.44 (1.08–1.43)	1.24 \pm 0.48 (0.90–1.27)	1.11 \pm 0.54 (0.79–1.21)	1.12 \pm 0.59 (0.77–1.23)	1.19 \pm 0.70 (0.69–1.23)
RT Knee—Rotation	1.75 \pm 0.63 (1.38–1.87)	1.91 \pm 0.72 (1.38–1.93)	1.93 \pm 0.84 (1.49–2.14)	1.03 \pm 0.57 (0.65–1.09)	0.90 \pm 0.42 (0.67–1.00)	1.00 \pm 0.45 (0.69–1.04)
RT Knee—Flexion	1.51 \pm 0.43 (1.31–1.64)	1.40 \pm 0.28 (1.28–1.50)	1.37 \pm 0.27 (1.26–1.47)	0.76 \pm 0.41 (0.43–0.75)	0.75 \pm 0.30 (0.56–0.79)	0.71 \pm 0.31 (0.47–0.71)
RT Ankle—Abduktion	1.33 \pm 0.35 (1.09–1.36)	1.27 \pm 0.33 (1.07–1.33)	1.30 \pm 0.29 (1.13–1.35)	1.02 \pm 0.48 (0.70–1.07)	1.08 \pm 0.49 (0.79–1.06)	0.97 \pm 0.35 (0.79–1.06)
RT Ankle—Rotation	1.52 \pm 0.41 (1.27–1.59)	1.56 \pm 0.46 (1.26–1.62)	1.63 \pm 0.51 (1.29–1.68)	1.27 \pm 0.57 (0.90–1.34)	1.18 \pm 0.48 (0.89–1.27)	1.18 \pm 0.48 (0.92–1.29)
RT Ankle—Flexion	1.60 \pm 0.36 (1.43–1.71)	1.60 \pm 0.38 (1.44–1.74)	1.60 \pm 0.42 (1.32–1.65)	1.02 \pm 0.37 (0.78–1.07)	0.97 \pm 0.38 (0.78–1.07)	0.91 \pm 0.38 (0.68–0.97)
Pelvis—Flexion	0.64 \pm 0.18 (0.55–0.69)	0.62 \pm 0.21 (0.52–0.68)	0.62 \pm 0.21 (0.51–0.67)	0.32 \pm 0.15 (0.22–0.34)	0.35 \pm 0.20 (0.25–0.40)	0.33 \pm 0.20 (0.25–0.41)
Pelvis—Obliquity	0.62 \pm 0.16 (0.57–0.69)	0.61 \pm 0.20 (0.51–0.67)	0.59 \pm 0.18 (0.47–0.61)	0.31 \pm 0.11 (0.23–0.32)	0.32 \pm 0.12 (0.24–0.33)	0.33 \pm 0.10 (0.28–0.36)
Pelvis—Rotation	x	x	x	0.42 \pm 0.15 (0.32–0.43)	0.47 \pm 0.22 (0.35–0.52)	0.51 \pm 0.29 (0.29–0.51)

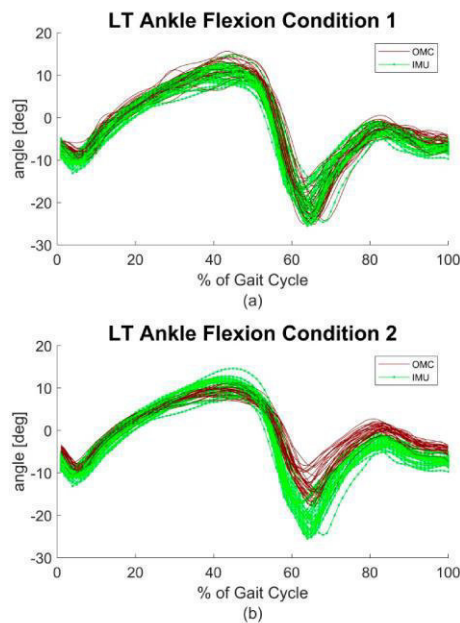


Figure 2. Left (LT) ankle flexion of a representative subject. Soft tissue artefacts (STA) error excluded (a) and included (b). At 60 to 100% Gait Cycle (GC) appears a typical offset between optical motion capture (OMC) and inertial measurement unit (IMU)-derived data.

BA analysis revealed mean differences between the systems of -0.6° – $0.6^{\circ} \pm 0.5^{\circ}$ – 1.3° for sagittal joint angles. The best outcome showed the global pelvis flexion with a bias $0.0^{\circ} \pm 0.3^{\circ}$. Frontal plane joint angles showed biases of -0.3° – $0.1^{\circ} \pm 0.3^{\circ}$ – 0.8° and transversal plane joint angles revealed biases of -0.9° – $1.4^{\circ} \pm 0.3^{\circ}$ – 0.7° . BA plots are shown in Appendix B (Figure A2 through Figure A4). Figure 3 (upper row) shows the BA diagrams for the most affected joint angles of every plane.

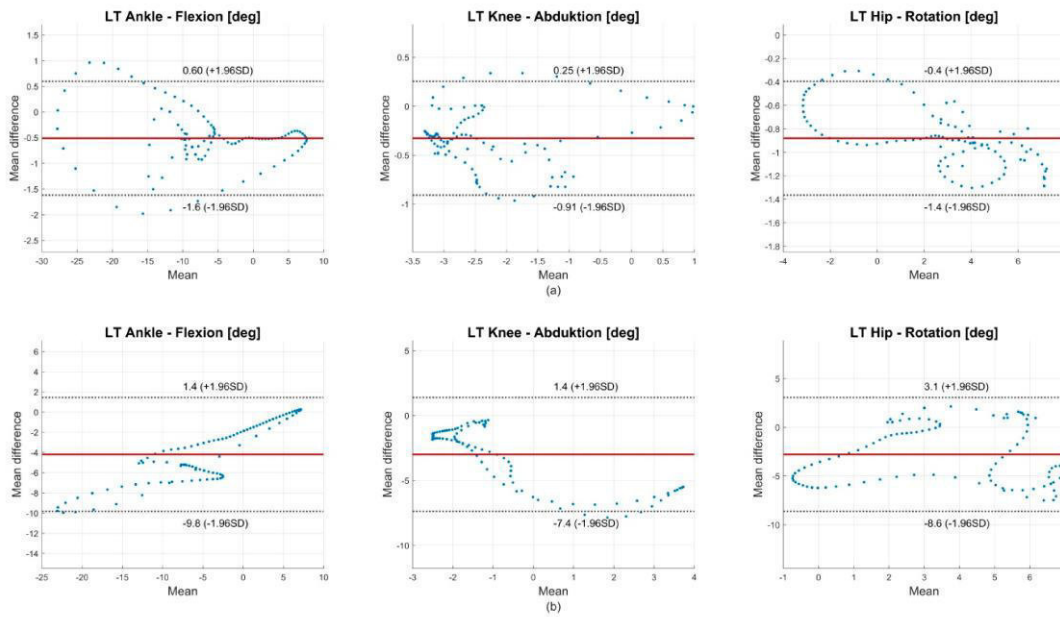


Figure 3. Bland-Altman (BA) diagrams for the most affected joint angles of every plane. The plots show the agreement between the 100% GC normalized joint angle waveforms of OMC and IMU system (averaged over all 28 participants). A normalized joint angle waveform contains 100 data points, which results in 100 data points in the BA diagrams. Upper row (a) shows condition 1, the lower row (b) condition 2. The solid line indicates the mean difference. The dashed lines indicate the limits of agreement (LoA) (95% CI of the mean difference).

The CMC showed very high waveform similarity for the joint angles in the sagittal plane with mean values ranging from 0.99 to 1. Concerning the frontal and transversal plane, the CMC showed slightly lower correspondence with mean values ranging from 0.88 to 0.99. All CMC values are mapped in the box-and-whisker-plot in Figure 4a.

3.2. Condition 2—Skin Markers

Most error measures showed results inferior to condition 1, when considering STA.

RMSE and ROME for all joint angles over all sections are shown in Table 2. RMSE showed values lower than 6.00° over all planes and joints. ROME showed values lower than 6.10° for hip, knee and pelvis in all planes, and ankle joint in transversal and frontal plane. However, the movement in the sagittal plane in the ankle joint revealed a ROME of up to 10.66° . Figure 2b exemplary shows the LT ankle flexion of a representative subject for condition 2.

Table 2. Mean RMSE and ROME of condition 2 over all subjects \pm SD; brackets contain 95% CI. A, B, C indicate beginning, middle and end of the 6 min walk test.

	RMSE (deg) \pm SD (95% CI)			ROME (deg) \pm SD (95% CI)		
	A	B	C	A	B	C
LT Hip—Abduction	2.57 \pm 0.88 (2.14–2.83)	2.69 \pm 1.05 (2.11–2.92)	2.69 \pm 1.03 (2.05–2.85)	4.91 \pm 2.14 (3.74–5.40)	4.85 \pm 2.24 (3.84–5.57)	4.94 \pm 2.14 (3.93–5.58)
LT Hip—Rotation	5.37 \pm 1.66 (4.36–5.64)	5.60 \pm 2.16 (4.52–6.20)	5.54 \pm 2.10 (4.37–6.00)	3.98 \pm 2.63 (2.48–4.52)	4.17 \pm 2.61 (3.27–5.29)	4.24 \pm 2.82 (3.12–5.31)
LT Hip—Flexion	3.53 \pm 3.37 (1.25–3.87)	3.64 \pm 3.47 (1.39–4.08)	3.67 \pm 3.53 (1.26–4.00)	1.67 \pm 1.22 (0.88–1.82)	1.42 \pm 0.94 (0.76–1.50)	1.42 \pm 0.96 (0.71–1.45)

Table 2. Cont.

	RMSE (deg) ± SD (95% CI)			ROME (deg) ± SD (95% CI)		
	A	B	C	A	B	C
LT Knee—Abduction	4.19 ± 1.15 (3.63–4.53)	4.14 ± 1.22 (3.53–4.48)	4.13 ± 1.20 (3.45–4.38)	2.89 ± 1.74 (1.83–3.18)	2.76 ± 1.93 (1.68–3.18)	2.85 ± 1.98 (1.83–3.37)
LT Knee—Rotation	4.56 ± 1.33 (3.80–4.83)	4.70 ± 1.40 (4.02–5.11)	4.72 ± 1.44 (4.02–5.13)	3.53 ± 2.08 (2.11–3.72)	3.78 ± 2.05 (2.43–4.02)	3.69 ± 2.33 (2.00–3.81)
LT Knee—Flexion	2.38 ± 0.63 (2.16–2.64)	2.38 ± 0.61 (2.03–2.50)	2.40 ± 0.64 (2.05–2.55)	1.48 ± 1.07 (0.78–1.62)	1.58 ± 1.15 (0.87–1.76)	1.59 ± 1.14 (0.95–1.84)
LT Ankle—Abduction	2.92 ± 1.31 (1.93–2.95)	3.01 ± 1.41 (1.97–3.06)	3.00 ± 1.37 (1.91–2.97)	2.49 ± 1.40 (1.80–2.88)	2.52 ± 1.61 (1.32–2.57)	2.53 ± 1.47 (1.54–2.68)
LT Ankle—Rotation	3.28 ± 1.32 (2.38–3.41)	3.41 ± 1.37 (2.84–3.91)	3.45 ± 1.32 (2.85–3.87)	4.74 ± 2.25 (3.90–5.65)	5.02 ± 2.52 (3.75–5.70)	4.94 ± 2.56 (3.59–5.57)
LT Ankle—Flexion	5.30 ± 1.56 (4.52–5.73)	5.42 ± 1.61 (4.55–5.79)	5.48 ± 1.65 (4.60–5.88)	10.07 ± 2.18 (8.94–10.63)	10.63 ± 2.50 (9.51–11.44)	10.66 ± 2.65 (9.62–11.68)
RT Hip—Abduction	2.58 ± 0.64 (2.35–2.85)	2.62 ± 0.63 (2.34–2.83)	2.63 ± 0.65 (2.47–2.98)	4.80 ± 1.44 (4.41–5.53)	4.71 ± 1.48 (4.15–5.30)	4.68 ± 1.53 (4.05–5.24)
RT Hip—Rotation	5.01 ± 1.37 (4.44–5.51)	4.97 ± 1.26 (4.20–5.18)	5.01 ± 1.07 (4.60–5.43)	3.01 ± 1.83 (1.77–3.19)	2.93 ± 1.54 (1.98–3.17)	3.12 ± 1.50 (2.15–3.31)
RT Hip—Flexion	3.57 ± 3.23 (1.27–3.77)	3.76 ± 3.34 (1.54–4.13)	3.83 ± 3.33 (1.61–4.19)	1.48 ± 0.62 (1.00–1.49)	1.52 ± 0.77 (1.00–1.59)	1.53 ± 0.86 (1.10–1.76)
RT Knee—Abduction	3.83 ± 1.72 (2.52–3.85)	3.79 ± 1.69 (2.53–3.84)	3.72 ± 1.68 (2.45–3.75)	3.16 ± 1.66 (2.07–3.35)	3.21 ± 1.77 (2.27–3.65)	3.21 ± 1.86 (2.22–3.66)
RT Knee—Rotation	4.41 ± 1.01 (3.76–4.54)	4.48 ± 1.06 (3.71–4.53)	4.54 ± 1.22 (3.71–4.66)	4.14 ± 2.13 (3.05–4.69)	4.09 ± 1.85 (3.02–4.46)	4.12 ± 2.10 (3.37–5.00)
RT Knee—Flexion	2.59 ± 0.90 (2.00–2.70)	2.66 ± 0.90 (2.00–2.70)	2.65 ± 1.01 (1.99–2.77)	1.76 ± 1.05 (0.97–1.78)	1.67 ± 1.07 (1.05–1.89)	1.58 ± 1.10 (0.86–1.71)
RT Ankle—Abduktion	2.90 ± 1.62 (1.90–3.16)	2.97 ± 1.88 (1.59–3.05)	2.99 ± 1.97 (1.52–3.05)	2.10 ± 1.03 (1.46–2.26)	2.25 ± 1.10 (1.60–2.45)	2.05 ± 1.34 (1.10–2.15)
RT Ankle—Rotation	3.46 ± 1.10 (2.76–3.61)	3.58 ± 1.22 (2.68–3.63)	3.74 ± 1.30 (2.83–3.84)	5.78 ± 1.88 (4.96–6.42)	6.01 ± 2.13 (5.26–6.91)	6.03 ± 2.09 (5.36–6.98)
RT Ankle—Flexion	4.49 ± 1.27 (4.03–5.02)	4.50 ± 1.19 (4.09–5.01)	4.45 ± 1.30 (4.16–5.17)	9.08 ± 2.95 (8.15–10.43)	9.52 ± 2.71 (8.34–10.44)	9.49 ± 2.63 (8.27–10.31)
Pelvis—Flexion	1.69 ± 0.76 (1.17–1.76)	1.77 ± 0.79 (1.26–1.87)	1.81 ± 0.82 (1.28–1.91)	1.91 ± 1.11 (1.49–2.35)	1.98 ± 1.29 (1.47–2.47)	2.07 ± 1.34 (1.33–2.37)
Pelvis—Obliquity	2.52 ± 2.83 (0.68–2.88)	2.60 ± 3.02 (0.49–2.83)	2.57 ± 3.00 (0.51–2.83)	1.02 ± 0.60 (0.56–1.02)	1.02 ± 0.68 (0.48–1.01)	0.96 ± 0.65 (0.54–1.05)
Pelvis—Rotation	x	x	x	1.40 ± 1.21 (0.51–1.44)	1.42 ± 1.26 (0.36–1.34)	1.38 ± 1.17 (0.55–1.45)

Concerning condition 2 BA analysis revealed mean differences inferior to condition 1. Sagittal joint angles showed biases of -4.2° – $2.2^{\circ} \pm 1.6^{\circ}$ – 5.6° . Frontal angles showed biases of -3.0° – $1.0^{\circ} \pm 0.8^{\circ}$ – 4.5° . Transversal angles showed biases of -2.8° – $2.4^{\circ} \pm 2.4^{\circ}$ – 5.8° . BA plots are shown in Appendix B (Figures A5 through A6). Figure 3 (lower row) shows the BA diagrams for the most affected joint angles of every plane.

CMC values in the sagittal plane were good to excellent with values ranging from 0.89 to 1. CMC values of the transversal and frontal plane showed moderate to good results ranging from 0.53 to 0.90. The hip joint in the transversal plane exhibited the poorest outcome (CMC = 0.53 – 0.67). All CMC values are mapped in the box-and-whisker-plot in Figure 4b.

The paired *t*-test revealed significant differences between condition 1 and condition 2 of the RMSE in all joint angles and sections. ROME showed significant differences between condition 1 and 2 in all joint angles and sections excepting the right hip flexion of section A ($p = 0.08$). For detailed results see Table 3.

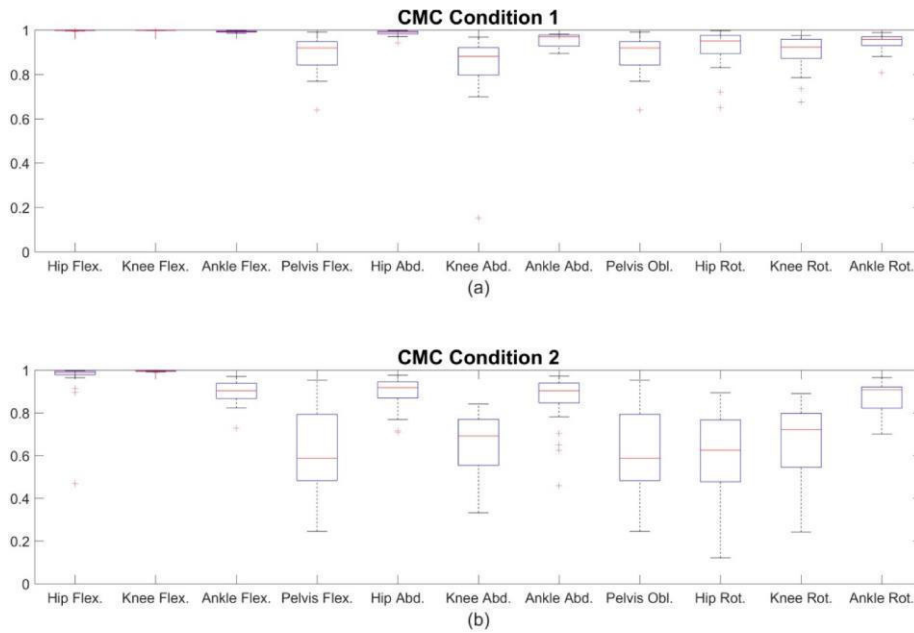


Figure 4. Mean coefficient of multiple correlation (CMC) values over all subjects of section A for condition 1 (a) and condition 2 (b). Exemplary only the joint angles of the left lower extremity are shown.

Table 3. Results of the paired *t*-test for RMSE and ROME of every joint and all three sections. Bold values indicate non-significant differences between condition 1 and condition 2.

	RMSE			ROME		
	A	B	C	A	B	C
	<i>p</i> -Value					
LT Hip—Abduction	<0.001	<0.001	<0.001	<0.001	<0.001	<0.001
LT Hip—Rotation	<0.001	<0.001	<0.001	<0.001	<0.001	<0.001
LT Hip—Flexion	<0.001	<0.001	<0.001	0.004	0.011	0.006
LT Knee—Abduction	<0.001	<0.001	<0.001	0.002	<0.001	0.005
LT Knee—Rotation	<0.001	<0.001	<0.001	<0.001	<0.001	<0.001
LT Knee—Flexion	<0.001	<0.001	<0.001	<0.001	<0.001	<0.001
LT Ankle—Abduction	<0.001	<0.001	<0.001	<0.001	0.001	<0.001
LT Ankle—Rotation	<0.001	<0.001	<0.001	<0.001	<0.001	<0.001
LT Ankle—Flexion	<0.001	<0.001	<0.001	<0.001	<0.001	<0.001
RT Hip—Abduction	<0.001	<0.001	<0.001	<0.001	<0.001	<0.001
RT Hip—Rotation	<0.001	<0.001	<0.001	<0.001	<0.001	<0.001
RT Hip—Flexion	<0.001	<0.001	<0.001	0.081	<0.001	<0.001
RT Knee—Abduction	<0.001	<0.001	<0.001	<0.001	<0.001	<0.001
RT Knee—Rotation	<0.001	<0.001	<0.001	<0.001	<0.001	<0.001
RT Knee—Flexion	<0.001	<0.001	<0.001	<0.001	<0.001	<0.001
RT Ankle—Abduction	<0.001	<0.001	<0.001	<0.001	<0.001	<0.001
RT Ankle—Rotation	<0.001	<0.001	<0.001	<0.001	<0.001	<0.001
RT Ankle—Flexion	<0.001	<0.001	<0.001	<0.001	<0.001	<0.001
Pelvis—Flexion	<0.001	<0.001	<0.001	<0.001	<0.001	<0.001
Pelvis—Obliquity	0.001	0.002	0.002	<0.001	<0.001	<0.001
Pelvis—Rotation	x	x	x	<0.001	<0.001	<0.001

3.3. Test-Retest Reliability

The ICC revealed moderate to excellent correlations over all joints in the frontal and transversal plane (0.52–0.93) and excellent values in the sagittal plane (0.94–0.99) (Table 4). The knee joint in the frontal and transversal plane, the pelvis in the frontal plane, and the hip joint in the transversal plane showed the lowest values (0.52–0.76). This tendency consented with the results from ICC calculation

of the optical system (0.63–0.83). However, overall ICC values of the OMC system (0.63–0.99) were higher compared to the IMU system.

Table 4. Mean intraclass correlation coefficient (ICC) values for the IMU system over all subjects \pm SD; brackets contain 95% CI. A, B, C indicate beginning, middle, and end of the 6 min walk test.

	ICC \pm SD (95% CI)		
	A	B	C
LT Hip—Abduction	0.92 \pm 0.07 (0.90–0.96)	0.91 \pm 0.07 (0.91–0.96)	0.92 \pm 0.06 (0.91–0.96)
LT Hip—Rotation	0.75 \pm 0.20 (0.70–0.86)	0.76 \pm 0.18 (0.73–0.87)	0.76 \pm 0.16 (0.72–0.84)
LT Hip—Flexion	0.98 \pm 0.01 (0.98–0.99)	0.99 \pm 0.01 (0.98–0.99)	0.99 \pm 0.01 (0.99–0.99)
LT Knee—Abduction	0.57 \pm 0.26 (0.53–0.73)	0.58 \pm 0.27 (0.54–0.75)	0.57 \pm 0.30 (0.52–0.75)
LT Knee—Rotation	0.69 \pm 0.13 (0.65–0.75)	0.71 \pm 0.13 (0.64–0.74)	0.71 \pm 0.12 (0.66–0.76)
LT Knee—Flexion	0.98 \pm 0.01 (0.97–0.98)	0.98 \pm 0.01 (0.98–0.99)	0.98 \pm 0.01 (0.98–0.99)
LT Ankle—Abduction	0.79 \pm 0.09 (0.75–0.81)	0.79 \pm 0.10 (0.77–0.84)	0.80 \pm 0.08 (0.78–0.84)
LT Ankle—Rotation	0.82 \pm 0.06 (0.81–0.86)	0.84 \pm 0.07 (0.82–0.88)	0.85 \pm 0.05 (0.85–0.89)
LT Ankle—Flexion	0.94 \pm 0.02 (0.94–0.96)	0.94 \pm 0.03 (0.94–0.96)	0.94 \pm 0.03 (0.94–0.96)
RT Hip—Abduction	0.93 \pm 0.05 (0.92–0.97)	0.92 \pm 0.06 (0.91–0.96)	0.91 \pm 0.07 (0.91–0.97)
RT Hip—Rotation	0.76 \pm 0.20 (0.75–0.90)	0.76 \pm 0.20 (0.74–0.90)	0.75 \pm 0.22 (0.75–0.92)
RT Hip—Flexion	0.99 \pm 0.01 (0.98–0.99)	0.98 \pm 0.01 (0.98–0.99)	0.98 \pm 0.01 (0.98–0.99)
RT Knee—Abduction	0.56 \pm 0.34 (0.56–0.83)	0.56 \pm 0.35 (0.57–0.84)	0.56 \pm 0.34 (0.52–0.78)
RT Knee—Rotation	0.69 \pm 0.14 (0.67–0.78)	0.69 \pm 0.14 (0.64–0.75)	0.68 \pm 0.16 (0.64–0.76)
RT Knee—Flexion	0.98 \pm 0.01 (0.98–0.99)	0.98 \pm 0.01 (0.98–0.99)	0.98 \pm 0.01 (0.98–0.99)
RT Ankle—Abduction	0.76 \pm 0.13 (0.75–0.85)	0.77 \pm 0.13 (0.76–0.86)	0.76 \pm 0.16 (0.75–0.87)
RT Ankle—Rotation	0.85 \pm 0.05 (0.83–0.87)	0.86 \pm 0.05 (0.85–0.89)	0.86 \pm 0.06 (0.84–0.88)
RT Ankle—Flexion	0.94 \pm 0.02 (0.94–0.95)	0.95 \pm 0.02 (0.94–0.96)	0.95 \pm 0.03 (0.93–0.96)
Pelvis—Flexion	0.90 \pm 0.06 (0.89–0.94)	0.90 \pm 0.07 (0.89–0.95)	0.90 \pm 0.08 (0.90–0.96)
Pelvis—Obliquity	0.52 \pm 0.19 (0.50–0.64)	0.52 \pm 0.20 (0.51–0.67)	0.52 \pm 0.23 (0.47–0.65)
Pelvis—Rotation	0.82 \pm 0.12 (0.82–0.91)	0.81 \pm 0.12 (0.79–0.88)	0.78 \pm 0.15 (0.79–0.91)

3.4. Drift

The global heading direction of the pelvis in the transversal plane (pelvis rotation) drifted linearly but not consistently between subjects ($45^\circ \pm 58^\circ$). Global heading errors after six minutes ranged from 0.21° up to 230° (Figure 5).

To analyze the drift in the joint angle data, changes in the RMSE and ROME of condition 2 over time were evaluated through linear least squares regression (line fitting). The slopes of the fitted lines of RMSE and ROME for all joint angles of the left side and global pelvis flexion and obliquity of all test persons are shown in Figures 6 and 7. Consistent positive slopes (i.e., increasing RMSE/ROME error values over time) would indicate a systematic drift over time. However, as visible in the figures, the slopes of both RMSE and ROME over time reside above as well as below zero, so that there is no clear trend over all test persons visible. Moreover, the slopes are in a range where the errors cannot be distinguished from noise given disturbing effects such as STA.

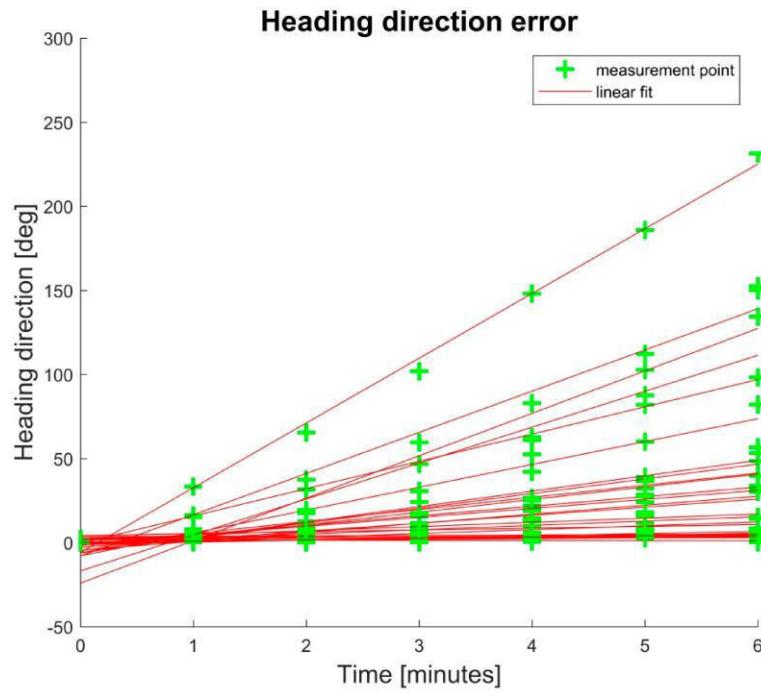


Figure 5. Error of the global pelvis rotation in the transversal plane at minute 0, 1, 2, 3, 4, 5, and 6 for all subjects. The drift in the global transversal plane showed a linear trend but no consistent dimension.

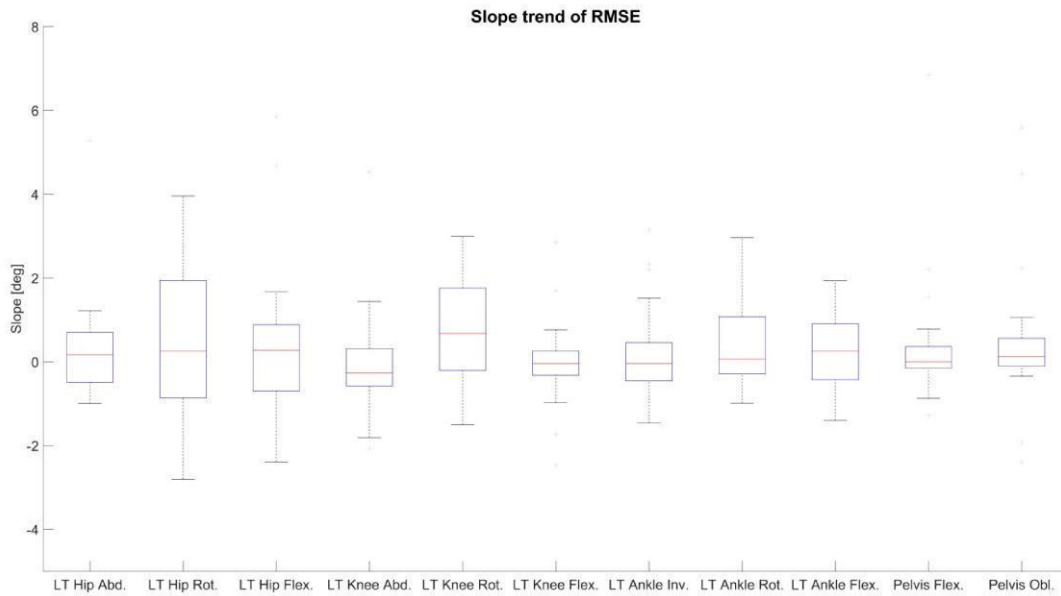


Figure 6. Evaluation of linear regression of RMSE for condition 2 over time exemplary for the left lower extremity and global pelvis angles in sagittal and frontal plane. On the vertical axis is the slope of the regression line in degree. Median slope values, quartiles, and whiskers are above and below zero indicating no increasing trend of RMSE over time.

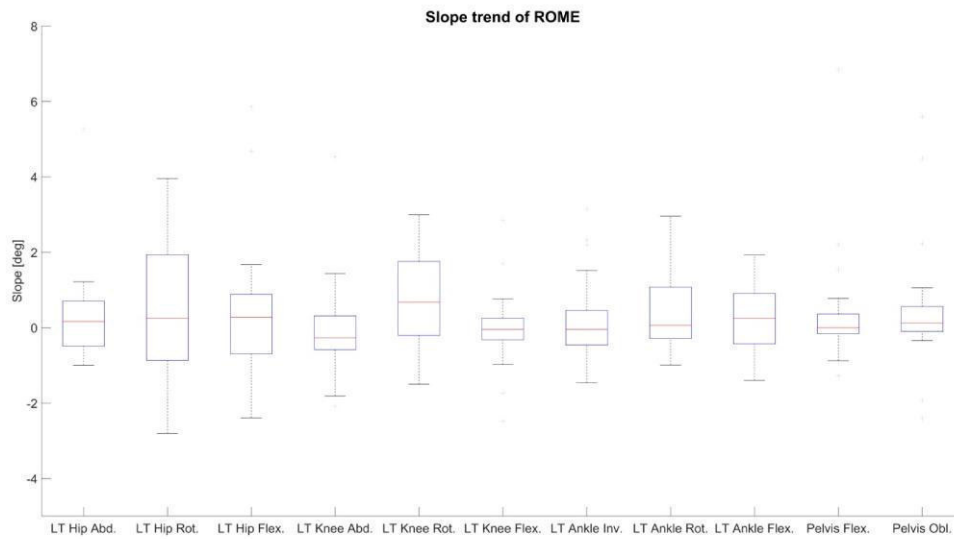


Figure 7. Evaluation of linear regression of ROME for condition 2 over time exemplary for the left lower extremity and global pelvis angles in sagittal and frontal plane. On the vertical axis is the slope of the regression line in degree. Median slope values, quartiles as well as whiskers are above and below zero indicating no increasing trend of ROME over time.

4. Discussion

This paper evaluated the performance of a sensor fusion algorithm for estimating 3D kinematics from gyroscope and accelerometer data.

4.1. Condition 1—Marker Clusters

RMSE in the present examination outperformed the results of Robert-Lachaine et al. [17] (1.90° – 7.30°). Ferrari et al. [19] showed similar results for their “Off” calculation (-2° – $+2^{\circ}$) and for ROME (0.60° – 1.50°).

The BA analysis revealed excellent agreement between the systems. Mean difference results were similar to the results of Robert-Lachaine et al. [17]. They consent with the present findings of the sagittal joint angles showing the best agreement and the transversal joint angles the poorest agreement between the two systems. However, the limits found by Robert-Lachaine et al. [17] ranged from 2.8° – 7.0° , compared to limits of 0.3° – 1.3° in the present findings.

CMC values showed excellent correspondence between the systems in the sagittal plane and good to excellent correspondence in the frontal and transversal plane. These findings are in accordance with Ferrari et al. [19] and outperform the results of Zhang et al. [18]. However, the former performed an offset correction to increase waveform similarity and did not consider transversal and frontal plane of the knee joint. Zhang et al. used different coordinate systems for joint angle calculation [18]. The findings of Robert-Lachaine et al. [17] showed better CMC values concerning knee rotation and abduction (0.91 and 0.97). For ankle joint rotation and abduction, they report their lowest CMC values (0.89 and 0.77). In this case, the current system achieved higher correspondence (0.96–0.98). However, Robert-Lachaine et al. [17] do not report whether these results are mean values over the entire time period of 32 min. Furthermore, Robert-Lachaine et al. [17] analyzed a complex combination of movements rather than a standardized motion.

CMC values were lowest for knee abduction (0.88–0.93). The majority of literature reports lowest CMC outcomes considering motion in the transversal and frontal planes [17–19]. However, during walking, movements in these planes show smaller ranges of motion compared to the sagittal plane. It has been shown that the CMC decreases as the amplitude of movement decreases [33]. This might

also explain the rather good results of Robert-Lachaine et al. concerning the CMC of the knee in frontal and transversal plane (0.91–0.97). In this study, subjects had to perform lifting and turning tasks which could have led to increased ROM in the mentioned planes.

4.2. Condition 2—Skin Markers

As mentioned, most values of errors increased. This consented with the findings of Seel et al. [4] who compared knee and ankle sagittal joint kinematics of the human leg and the transfemoral prosthesis of an above-knee amputee. They found the errors on the human leg four times higher than on the prosthesis. On average, RMSE and ROME increased by $2.20^\circ \pm 1.50^\circ$ and $2.90^\circ \pm 1.70^\circ$, respectively. Nüesch et al. [23] reported RMSE of the sagittal plane for hip, knee, and ankle joint (9.60° , 7.60° , 4.50°). The present system revealed better results concerning the sagittal plane for hip and knee (3.83° , 2.66°) and similar results for the ankle (5.48°). However, Nüesch et al. [23] conducted their examination on a treadmill, which could have affected IMU-derived data [14]. Fasel et al. [12] found in their evaluation of skiing similar hip abduction ROME ($-3.3^\circ \pm 4.1^\circ$), slightly higher knee abduction ROME ($4.2^\circ \pm 5.5^\circ$) and distinctively higher hip flexion ROME ($-10.7^\circ \pm 4.3^\circ$). Their findings concerning knee flexion, hip and knee rotation showed better results for ROME around -0.1° and 0.5° . However, note that Fasel et al. [12] investigated a different task, which limits comparability. Further, they conducted their examination on an indoor skiing carpet, comparable to a treadmill, therefore inviting the same considerations associated with Nüesch et al. [23]. Interestingly, ROME of the ankle joint flexion increased from 1.61° in condition 1 to 10.66° in condition 2. In the IMU system and when calculating joint angles based on marker clusters, the foot is assumed to be one rigid segment. However, the foot is a complex organization of bony segments [34]. Skin markers attached to anatomical landmarks on the foot are in fact placed on different segments rather than on one segment only. This might explain the differences in the ankle flexion between IMU and OMC system.

BA analysis also showed increased biases compared to condition 1. The ankle flexion was the most affected joint angle in the sagittal plane, the knee abduction the most affected joint angle in the frontal plane and the hip rotation the most affected joint angle in the transversal plane (Figure 3). CMC values decreased mostly for the transversal and frontal plane. This might be due to the increased uncertainty concerning CMC and smaller ranges of motion [33]. However, the ankle joint flexion still presents good to excellent values. Qualitative examination of the ankle flexion waveforms showed that there is an excellent match between waveforms of the IMU system and the OMC system at about 10 to 50% GC. However, at 60 to 100% GC an offset appeared (Figure 2b). This might explain the difference of ROM, but still similar shape of waveform and good CMC values. Al-Amri et al. [20] showed a similar shape of waveform for ankle flexion in their examination. No such differences were found between the IMU system and the OMC system based on the marker clusters (Figure 2a). Al-Amri et al. [20] examined in their recent study the validity of a commercial IMU system during one 8 m walk, taking into account errors due to STA. They found excellent CMC values concerning the sagittal plane of all three joints and the frontal plane of the hip joint but stated a poor outcome for the remaining joints in the frontal and transversal plane. However, they did not report exact values of the CMC for the frontal and transversal plane because results were complex numbers at times. In this study, CMC values for some subjects also resulted in complex numbers. On average, 3 out of 28 subjects per joint angle resulted in complex numbers. However, these subjects were ignored for the calculation of the mean CMC values shown in Figure 4. Nevertheless, concerning the findings of Al-Amri et al. [20], R^2 values indicated rather poor correlations for the joint angles in the transversal plane. That consents with the present results, showing moderate CMC values in the hip joint angle of the transversal plane (Figure 4b). Al-Amri et al. [20] used different biomechanical models for their analysis and stated possible uncertainties in the optical data due to the marker protocol. Further, Fiorentino et al. [35] showed that the 3D hip joint angles and ROM based on OMC systems are significantly influenced by STA.

4.3. Test-Retest Reliability

ICC values revealed moderate to excellent results for all joint angles. Knee abduction (0.56–0.58) and pelvis obliquity (0.52) showed the lowest test-retest correlation. These results are in accordance with Mills et al. [36]. However, the ICC calculation for the OMC system based on skin markers showed overall better outcome. This fact might be explained by expert marker placement. The IMUs were attached only approximately to the same spot on the segments. Furthermore, the IMUs were more prone to STA than the skin markers due to the rigid boxes and positioning focused on better visibility. These circumstances may have caused different amounts of errors on the two measurement days. For both systems, values of measures of reproducibility were not high. A possible explanation is the fact that inter-day variability of gait is considered higher than, for example, intra-day variability [36].

4.4. Drift

One difference of the current IMU system compared to the systems used in the referenced studies is the omission of the magnetometer information. Favre et al. [10] measured the 3D knee angle omitting magnetometer information and presented results with a mean error of 4.00° to 8.10° . They also introduced a functional calibration method to align the joint coordinate system. Note that the present evaluation relates to the sensor fusion algorithm, while the calibration, as mentioned in Section 2.1, was obtained from the OMC system. Thus, the results presented in this study can be considered free of calibration errors.

However, omitting global heading direction information (obtained through undisturbed magnetometer measurements) typically leads to drift [2,12]. In the present study, gait was measured for six minutes. Robert-Lachaine et al. [17] analyzed ergonomic tasks over a period of 32 min. However, they do not state results for different sections of their test procedure and thus give no hint as to whether drift appeared in the kinematic data or not.

Fasel et al. [12] measured skiing for 120 s. They reported errors in their joint angle results (based on individual per-IMU orientation estimates) due to drift and introduced methods for drift reduction [13] based on adjacent segments as a second processing stage (cf. Section 1). On the contrary, the present study revealed no systematic drift over all test persons, neither in the 3D joint angle data nor in the global pelvis flexion/obliquity. This is due to including biomechanical constraints in terms of connected segments and environmental constraints in terms of ground contacts directly into the estimation. However, Fasel et al. [13] reported that mainly highly flexed joint angles were affected from the drift. In their examination of skiing subjects reached distinctively higher peaks in hip and knee flexion compared to the present study.

Bergamini et al. [21] examined the drift in the orientation obtained from two inertial sensors mounted on wrist and pelvis during 180 s of gait. In the transversal plane, a drift of up to 40° was measured. In the sagittal plane and frontal plane, drift was smaller with values up to approximately 5° . The findings of Bergamini et al. [21] are comparable with this study's results for drift in the global heading direction estimate (investigated at the root segment, i.e., the pelvic rotation) measured at values of up to 230° . Note, inter-segment constraints do not provide corrective information concerning the global heading direction, which explains the linear drift observed. Consequently, the global pelvic rotation was neglected in the evaluation. However, the evaluation and interpretation of the ROM of the pelvic rotation and its reproducibility were independent of the drift.

5. Conclusions

The present algorithm for the calculation of 3D joint angles based on gyroscope and accelerometer data from seven IMUs mounted on the lower body shows good to excellent agreement when compared to a common OMC system and excluding STA. However, in this study, the influence of STA was shown. Especially the ankle joint was highly affected by these and further artefacts, e.g., a limited biomechanical model. Further research has to be conducted to better compensate these effects.

In terms of reliability, the results indicate that an OMC system combined with an experienced examiner delivers a better outcome, particularly for knee abduction and rotation and the ankle joint. Better placement of the shank sensor and smaller IMUs might improve overall reliability and sensitivity to STA.

Systematic drift was observed only in the global transversal plane angle (investigated at the root segment, i.e., the pelvis rotation). There was no systematic drift observed over all test persons in the other kinematic parameters. However, in clinical gait analysis the ROM per GC is the more essential criterion, which was also measured with satisfying accuracy for the pelvis rotation.

The current sensor fusion algorithm was not only shown to be comparable to other algorithms, but also tends to outperform most algorithms examined so far in terms of its accuracy while being magnetometer-independent. However, it has to be considered that this study focused on the evaluation of the sensor fusion algorithm, while the IMU-to-segment calibration, the biomechanical model and the initialization were obtained from the OMC system. Therefore, the next step consists of evaluating the validated sensor fusion method in a setup, where all information was obtained purely from the IMU system.

Nevertheless, this examination reveals promising results of a magnetometer-independent sensor fusion algorithm that showed no systematic drift in the joint angle data. Therefore, a stand-alone system incorporating this algorithm provides potential for applications in clinical gait analysis and further implementations.

Author Contributions: W.T. contributed to the development of the study conception, data acquisition, analysis and interpretation, manuscript drafting and revision. M.M. contributed to data acquisition, data processing, manuscript drafting. B.T. contributed to data analysis, manuscript drafting and revision. M.F. contributed to study conception, data interpretation, manuscript drafting and revision. G.B. contributed to study conception, data processing, data interpretation, manuscript drafting and revision.

Funding: This research was funded by Bundesministerium für Bildung und Forschung, grant numbers [16SV7115, 03IHS075B].

Conflicts of Interest: The authors declare no conflict of interest. The authors alone are responsible for the content and writing of this paper. The founding sponsors had no role in the design of the study; in the collection, analyses, or interpretation of data; in the writing of the manuscript, and in the decision to publish the results.

Appendix A

The here presented sensor fusion method for segment kinematics estimation is a slightly modified version of [14], which itself was based on [2]. Note that the contribution of [14] was the extension of the best performing extended Kalman filter (EKF)-based segment orientation estimation method of [2] with global translation estimation via ground contact estimation. For this study, the method of [14] was used while omitting magnetometer measurements (i.e., skipping measurement updates with the magnetometer data). Moreover, it was extended with online accelerometer bias estimation as proposed in [11,27] and by using an IEKF instead of an EKF [37]. For the reader's convenience, the resulting method is detailed in the following. For further information, please refer to the abovementioned publications.

Appendix A.1. Biomechanical Model

The biomechanical model is a stick-figure-like model with rigid segments. Each segment $S_i \in \mathbb{S}$ has an associated segment coordinate frame localized in the global position-less coordinate system G . The latter has z pointing up (opposing gravity). The global six DOF pose of the i -th segment is represented by the unit quaternion q^{GS} (denoting the orientation between G and S) and the position vector S^G (denoting the position of frame S in G). Furthermore, each segment S_i defines a set of points P^{S_i} which are represented in the segment coordinate system and are used for joint definitions: a joint $J_k \in \mathbb{J}$ defines which points from which segments are connected. Hence, a joint is a quadruple (i, k, j, l) , meaning that $p_k \in P^{S_i}$ is connected to $p_l \in P^{S_j}$ in the global frame. Additionally, each segment S_i

has an IMU I_i attached, with the rigid transformation $\{q^{SI}, I^S\}_i$. This transformation is referred to as IMU-to-segment (I2S) calibration. The full model of the lower body is depicted in Figure A1.

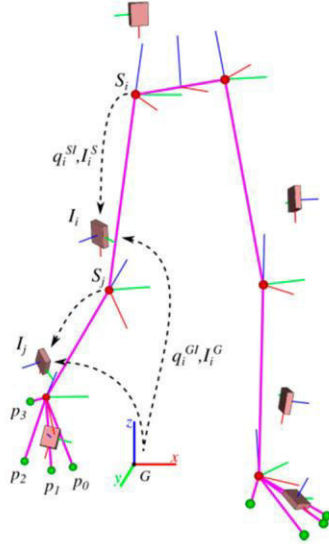


Figure A1. Biomechanical model of the lower body with segments (magenta lines), joint centers (red spheres), four ground contact points on each foot (green spheres), IMU placement, and involved coordinate frames. A technical coordinate system is associated to each IMU (I). The segment coordinate systems (S) are drawn at the proximal ends of the segments. The six DoF transformations, each in terms of an orientation (quaternion) q^{SI} and a translation I^S , between the IMU coordinate frames and the associated segment coordinate frames are called IMU-to-segment calibrations. The symbol G denotes the global coordinate system. The figure has been taken from [14].

Appendix A.2. Segment Kinematics Estimation Method

The goal is to estimate the segment kinematics by fusing information from the gyroscope and accelerometer measurements with assumptions from a motion model as well as from the biomechanical model. This is realized through an IEKF and an IMU-centered state-space model, i.e., the IMU kinematics are estimated and the segment kinematics are derived from these using the following equations:

$$q^{GS} = q^{GI} \odot q^{IS}$$

$$S^G = I^G - R(q^{GS})I^S,$$

where \odot denotes the quaternion multiplication, $R(\cdot)$ converts a quaternion to the corresponding rotation matrix and the I2S calibration is assumed known. Note, in [2], the IMU-centered state-space model outperformed the segment-centered state-space model for the considered tasks of magnetometer-free human motion tracking, which justifies this choice.

Hence, the state contains the following IMU-centered kinematic parameters of all n segments of the considered biomechanical model at time t :

$$x_t = \left(\left\{ q^{GI}, \omega_I^{GI}, I^G, \dot{I}^G, \ddot{I}^G, b^a \right\}_{i=0}^{n-1} \right)_t^T,$$

where q^{GI} is the orientation of the IMU wrt. the global frame, ω_I^{GI} is the rotational velocity of the IMU relative to the global frame, expressed in the IMU frame, I^G is the IMU position in the global

frame, and \dot{I}^G and \ddot{I}^G are the corresponding linear velocity and acceleration. The symbol b^a denotes the accelerometer bias, represented in the IMU frame.

The motion model (used in the IEKF time update) assumes constant angular velocity (with noise in angular acceleration), constant linear acceleration (with noise in jerk) and a random walk for the accelerometer bias. Hence, after T seconds, the prediction for the state variables is

$$x_{t+T} = \begin{bmatrix} q_{i,t}^{GI} \odot \exp\left(\frac{T}{2}\omega_{i,t}^{GI}\right) \\ \omega_{i,t}^{GI} + T\hat{\delta}_t^\omega \\ I_{i,t}^G + T\dot{I}_{i,t}^G + \frac{T^2}{2}\ddot{I}_{i,t}^G \\ \dot{I}_{i,t}^G + T\ddot{I}_{i,t}^G \\ \ddot{I}_{i,t}^G + T\hat{\delta}_t^a \\ b_{i,t}^a + \hat{\delta}_t^b \\ \vdots \end{bmatrix},$$

where $\exp(\cdot)$ is the quaternion exponential and $\hat{\delta}^\omega \sim \mathcal{N}(0, \hat{\Sigma}^\omega)$, $\hat{\delta}^a \sim \mathcal{N}(0, \hat{\Sigma}^a)$ and $\hat{\delta}^b \sim \mathcal{N}(0, \hat{\Sigma}^b)$ are Gaussian white process noises. The vertical dots indicate that these variables are given for each IMU $i \in \{0, \dots, n-1\}$.

The (implicitly formulated) measurement models for the inertial measurements, i.e., the acceleration $y_{i,t}^a$ and the rotational velocity $y_{i,t}^\omega$, are

$$0 = y_{i,t}^a - b_{i,t}^a - R(q_{i,t}^{GI})^T \left[\ddot{I}_{i,t}^G - g^G \right] - \delta_i^a,$$

and

$$0 = y_{i,t}^\omega - \omega_{i,t}^{GI} - \delta_i^\omega,$$

where $(\cdot)^T$ is the matrix transpose, g^G denotes acceleration due to gravity in the global system, and $\delta^a \sim \mathcal{N}(0, \Sigma^a)$ as well as $\delta^\omega \sim \mathcal{N}(0, \Sigma^\omega)$ are Gaussian white measurement noises.

Biomechanical model constraints, i.e., the fact that segments are connected at the joints, are also modeled as noisy measurements (hence, soft constraints), where the noises account for inaccuracies of the assumed biomechanical model. Let joint (i, k, j, l) connect point $p_k \in P^{S_i}$ with $p_l \in P^{S_j}$ in the global frame, the measurement model is

$$\begin{aligned} 0 &= p_k^G - p_l^G - \delta^p \\ 0 &= S_i^G + R(q_i^{GS})p_k^{S_i} - \left[S_j^G + R(q_j^{GS})p_l^{S_j} \right] - \delta^p \\ 0 &= S_i^G + R(q_i^{GI} \odot q_i^{IS})p_k^{S_i} - \left[S_j^G + R(q_j^{GI} \odot q_j^{IS})p_l^{S_j} \right] - \delta^p \\ 0 &= I_i^G + R(q_i^{GI} \odot q_i^{IS}) \left[p_k^{S_i} - I_i^S \right] - I_j^G - R(q_j^{GI} \odot q_j^{IS}) \left[p_l^{S_j} - I_j^S \right] - \delta^p, \end{aligned}$$

where $\delta^p \sim \mathcal{N}(0, \Sigma^p)$ denotes Gaussian white measurement noise.

Environmental constraints in terms of ground contacts are also incorporated into the estimation as noisy measurements. For this, in each time step, probabilistic ground contact estimations are carried out in parallel to the kinematics estimation for a set of potential ground contact points $P^c \subset \bigcup_{i=0}^{n-1} P^{S_i}$ (cf. Figure A1). For each of these points, ground contact probabilities are calculated, given the point height and velocity as obtained from the kinematics estimation. Let $p_k \in P^{S_i}$ and also $p_k \in P^c$, then

$$u_k = \left(p_k^G \right)_z = \left[I_i^G + R(q_i^{GI} \odot q_i^{IS}) \right] \left[p_k - I_i^S \right]_z$$

is the estimated global point height, and

$$y_k = \dot{I}_i^G + R(q_i^{GI})S(\omega_{I,i}^{GI}) \left[R(q_i^{IS}) (p_k - I_i^S) \right]$$

is the estimated global point velocity. Here, $S(\cdot)$ denotes the skew-symmetric matrix of a vector.

For information fusion, a binary discrete Bayes filter [38] is used for each potential contact point. Assuming the prediction being independent of the previous state, given a random variable $X_t = \{x_1 := \text{contact} \mid x_2 := \text{no contact}\}$ the Bayes filter simplifies to

$$p(X_t = x_1) = \eta p(X_{t-1} = x_1 | u_k) p(y_k | X_t = x_1),$$

with

$$\eta = (1 - p(X_{t-1} = x_1 | u_k) + 2p(y_k | X_t = x_1)p(X_{t-1} = x_1 | u_k) + p(y_k | X_t = x_1))^{-1}.$$

The probabilities are obtained as follows:

$$p(X_{t-1} = x_1 | u_k) = 1 - \text{sig}_{\{0.5, 0.9, 60, 0.05\}}(u_k),$$

for the prediction, and

$$p(y_k | X_t = x_1) = 1 - \text{sig}_{\{0.5, 0.95, 0.9, 0.7\}}(y_k),$$

as measurement using the sigmoid function

$$\text{sig}_{\{c, m, s, o\}}(x) = c + \frac{m}{2} \tanh(s(x - o)).$$

Here, the parameters for the sigmoid function were empirically determined. For each ground contact point, these probabilities are calculated in every time step. If the largest ground contact probability exceeds a threshold p_{th} , then two soft constraints (in terms of measurement updates) are applied to the corresponding point p_k inside the kinematics estimation filter: a zero-velocity update

$$0 = \dot{I}_i^G + R(q_i^{GI})S(\omega_{I,i}^{GI}) \left[R(q_i^{IS}) (p_k - I_i^S) \right] + \delta^{\dot{p}}$$

and, to prevent a drift in height, a zero-plane update

$$0 = \left[I_i^G + R(q_i^{GI} \odot q_i^{IS}) \right] [p_k - I_i^S]_z + \delta^z$$

with $\delta^{\dot{p}} \sim \mathcal{N}(0, \Sigma^{\dot{p}})$ and $\delta^z \sim \mathcal{N}(0, \Sigma^z)$ being Gaussian white measurement noises. If the threshold was not exceeded, a zero-plane update is applied to the lowest ground contact point only if this has a negative height. Otherwise no additional measurement update is conducted. Obviously, in the current state, the method assumes one plane. Table A1 contains all previously introduced noises and parameters.

Table A1. Noise and parameter settings for the presented kinematics estimation method.

Parameter	$\hat{\Sigma}^{\omega}$	$\hat{\Sigma}^a$	$\hat{\Sigma}^b$	Σ^{ω}	Σ^a	Σ^p	$\Sigma^{\dot{p}}$	Σ^z	p_{th}
Value	$10^5 \times I_{3 \times 3}$	$3 \times 10^5 \times I_{3 \times 3}$	$10^{-8} \times I_{3 \times 3}$	$10^{-3} \times I_{3 \times 3}$	$10^{-2} \times I_{3 \times 3}$	$10^{-4} \times I_{3 \times 3}$	$10^{-2} \times I_{3 \times 3}$	10^{-5}	0.7

Appendix B

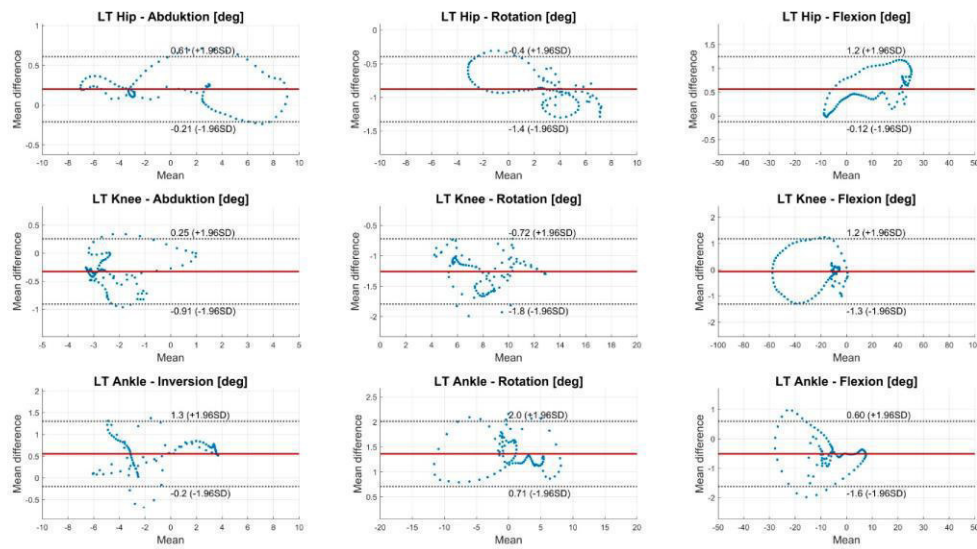


Figure A2. BA diagrams of 3D joint rotations of hip, knee and ankle of the left side for condition 1. The solid line indicates the mean difference. The dashed lines indicate the LoA (95% CI of the mean difference).

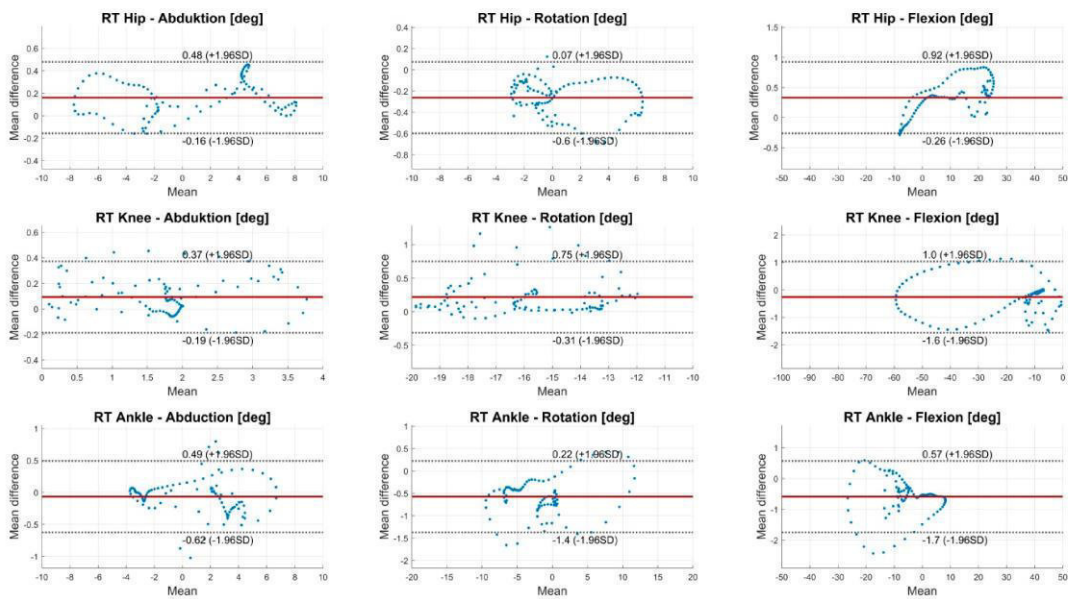


Figure A3. BA diagrams of 3D joint rotations of hip, knee and ankle of the right side for condition 1. The solid line indicates the mean difference. The dashed lines indicate the LoA (95% CI of the mean difference).

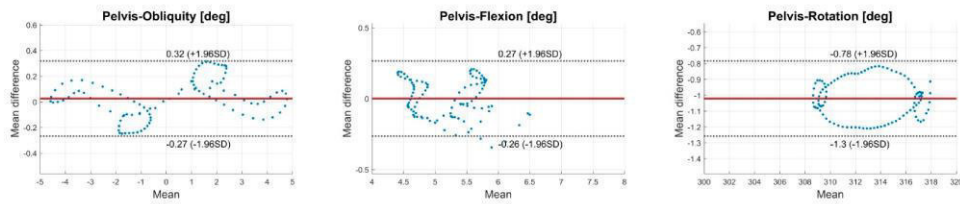


Figure A4. BA diagrams of 3D joint rotations of the pelvis for condition 1. The solid line indicates the mean difference. The dashed lines indicate the LoA (95% CI of the mean difference).

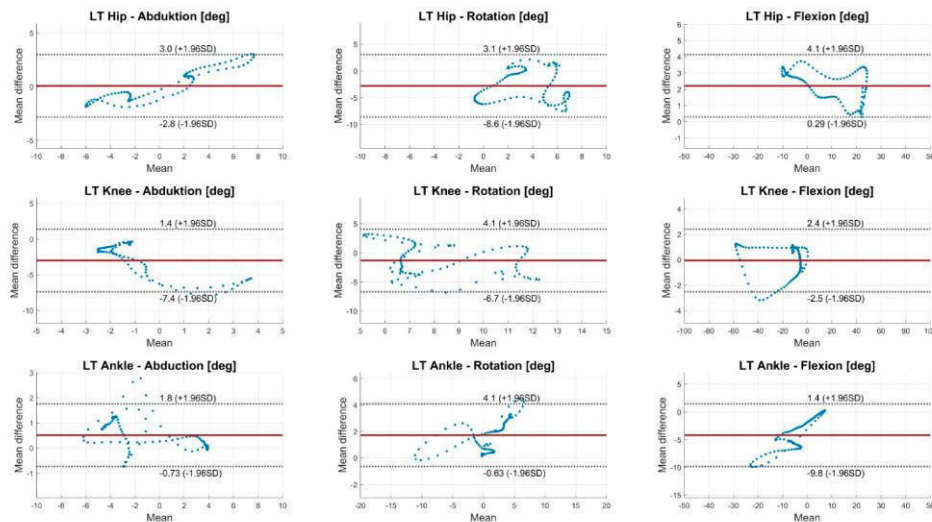


Figure A5. BA diagrams of 3D joint rotations of hip, knee, and ankle of the left side for condition 2. The solid line indicates the mean difference. The dashed lines indicate the LoA (95% CI of the mean difference).

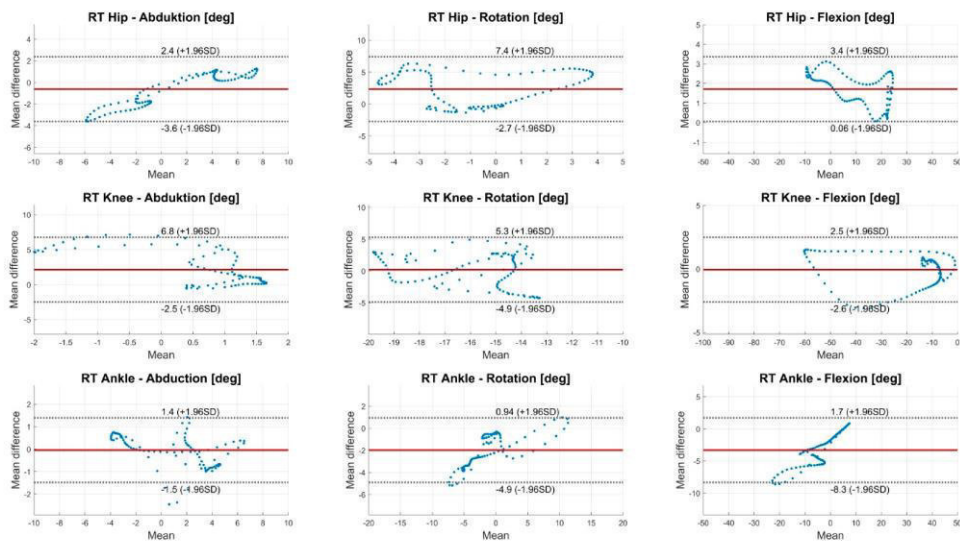


Figure A6. BA diagrams of 3D joint rotations of hip, knee, and ankle of the right side for condition 2. The solid line indicates the mean difference. The dashed lines indicate the LoA (95% CI of the mean difference).

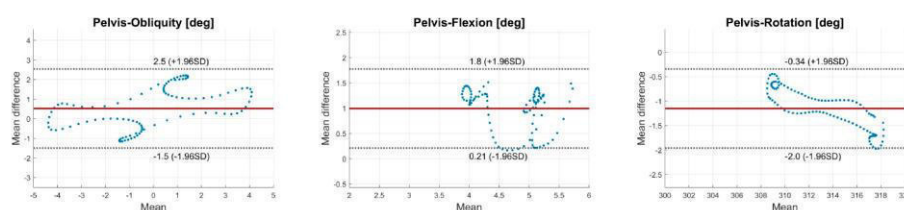


Figure A7. BA diagrams of 3D joint rotations of the pelvis for condition 2. The solid line indicates the mean difference. The dashed lines indicate the LoA (95% CI) of the mean difference.

References

- Picerno, P. 25 years of lower limb joint kinematics by using inertial and magnetic sensors: A review of methodological approaches. *Gait Posture* **2017**, *51*, 239–246. [[CrossRef](#)] [[PubMed](#)]
- Miezal, M.; Taetz, B.; Bleser, G. On Inertial Body Tracking in the Presence of Model Calibration Errors. *Sensors* **2016**, *16*, 1132. [[CrossRef](#)] [[PubMed](#)]
- Sabatini, A.M. Kalman-Filter-Based Orientation Determination Using Inertial/Magnetic Sensors: Observability Analysis and Performance Evaluation. *Sensors* **2011**, *11*, 9182–9206. [[CrossRef](#)] [[PubMed](#)]
- Seel, T.; Raisch, J.; Schauer, T. IMU-Based Joint Angle Measurement for Gait Analysis. *Sensors* **2014**, *14*, 6891–6909. [[CrossRef](#)] [[PubMed](#)]
- Filippeschi, A.; Schmitz, N.; Miezal, M.; Bleser, G.; Ruffaldi, E.; Stricker, D. Survey of Motion Tracking Methods Based on Inertial Sensors: A Focus on Upper Limb Human Motion. *Sensors* **2017**, *17*, 1257. [[CrossRef](#)] [[PubMed](#)]
- Xing, H.; Hou, B.; Lin, Z.; Guo, M. Modeling and Compensation of Random Drift of MEMS Gyroscopes Based on Least Squares Support Vector Machine Optimized by Chaotic Particle Swarm Optimization. *Sensors* **2017**, *17*, 2335. [[CrossRef](#)] [[PubMed](#)]
- De Vries, W.H.K.; Veeger, H.E.J.; Baten, C.T.M.; van der Helm, F.C.T. Magnetic distortion in motion labs, implications for validating inertial magnetic sensors. *Gait Posture* **2009**, *29*, 535–541. [[CrossRef](#)] [[PubMed](#)]
- Ligorio, G.; Sabatini, A. Dealing with Magnetic Disturbances in Human Motion Capture: A Survey of Techniques. *Micromachines* **2016**, *7*, 43. [[CrossRef](#)]
- Harada, T.; Mori, T.; Sato, T. Development of a Tiny Orientation Estimation Device to Operate under Motion and Magnetic Disturbance. *Int. J. Robot. Res.* **2007**, *26*, 547–559. [[CrossRef](#)]
- Favre, J.; Aissaoui, R.; Jolles, B.M.; de Guise, J.A.; Aminian, K. Functional calibration procedure for 3D knee joint angle description using inertial sensors. *J. Biomech.* **2009**, *42*, 2330–2335. [[CrossRef](#)] [[PubMed](#)]
- El-Gohary, M.; McNames, J. Human Joint Angle Estimation with Inertial Sensors and Validation with A Robot Arm. *IEEE Trans. Biomed. Eng.* **2015**, *62*, 1759–1767. [[CrossRef](#)] [[PubMed](#)]
- Fasel, B.; Spörri, J.; Schütz, P.; Lorenzetti, S.; Aminian, K. Validation of functional calibration and strap-down joint drift correction for computing 3D joint angles of knee, hip, and trunk in alpine skiing. *PLoS ONE* **2017**, *12*, e0181446. [[CrossRef](#)] [[PubMed](#)]
- Fasel, B.; Spörri, J.; Chardonnes, J.; Kroll, J.; Muller, E.; Aminian, K. Joint Inertial Sensor Orientation Drift Reduction for Highly Dynamic Movements. *IEEE J. Biomed. Health Inform.* **2017**. [[CrossRef](#)] [[PubMed](#)]
- Miezal, M.; Taetz, B.; Bleser, G. Real-time inertial lower body kinematics and ground contact estimation at anatomical foot points for agile human locomotion. In Proceedings of the 2017 IEEE International Conference on Robotics and Automation (ICRA), Singapore, 29 May–3 June 2017; pp. 3256–3263.
- Kluge, F.; Gaßner, H.; Hannink, J.; Pasluosta, C.; Klucken, J.; Eskofier, B.M. Towards Mobile Gait Analysis: Concurrent Validity and Test-Retest Reliability of an Inertial Measurement System for the Assessment of Spatio-Temporal Gait Parameters. *Sensors* **2017**, *17*, 1522. [[CrossRef](#)] [[PubMed](#)]
- Storm, F.A.; Buckley, C.J.; Mazzà, C. Gait event detection in laboratory and real life settings: Accuracy of ankle and waist sensor based methods. *Gait Posture* **2016**, *50*, 42–46. [[CrossRef](#)] [[PubMed](#)]
- Robert-Lachaine, X.; Mecheri, H.; Larue, C.; Plamondon, A. Validation of inertial measurement units with an optoelectronic system for whole-body motion analysis. *Med. Biol. Eng. Comput.* **2017**, *55*, 609–619. [[CrossRef](#)] [[PubMed](#)]

18. Zhang, J.-T.; Novak, A.C. Concurrent validation of Xsens and MVN measurement of lower limb joint angular kinematics. *Physiol. Meas.* **2013**, *34*. [[CrossRef](#)] [[PubMed](#)]
19. Ferrari, A.; Cutti, A.G.; Garofalo, P.; Raggi, M.; Heijboer, M.; Cappello, A.; Davalli, A. First in vivo assessment of “Outwalk”: A novel protocol for clinical gait analysis based on inertial and magnetic sensors. *Med. Biol. Eng. Comput.* **2010**, *48*, 1–15. [[CrossRef](#)] [[PubMed](#)]
20. Al-Amri, M.; Nicholas, K.; Button, K.; Sparkes, V.; Sheeran, L.; Davies, J.L. Inertial Measurement Units for Clinical Movement Analysis: Reliability and Concurrent Validity. *Sensors* **2018**, *18*, 719. [[CrossRef](#)] [[PubMed](#)]
21. Bergamini, E.; Ligorio, G.; Summa, A.; Vannozzi, G.; Cappozzo, A.; Sabatini, A.M. Estimating orientation using magnetic and inertial sensors and different sensor fusion approaches: Accuracy assessment in manual and locomotion tasks. *Sensors* **2014**, *14*, 18625–18649. [[CrossRef](#)] [[PubMed](#)]
22. Kainz, H.; Modenese, L.; Lloyd, D.G.; Maine, S.; Walsh, H.P.J.; Carty, C.P. Joint kinematic calculation based on clinical direct kinematic versus inverse kinematic gait models. *J. Biomech.* **2016**, *49*, 1658–1669. [[CrossRef](#)] [[PubMed](#)]
23. Nüesch, C.; Roos, E.; Pagenstert, G.; Mündermann, A. Measuring joint kinematics of treadmill walking and running: Comparison between an inertial sensor based system and a camera-based system. *J. Biomech.* **2017**, *57*, 32–38. [[CrossRef](#)] [[PubMed](#)]
24. Vreede, K.; Henriksson, J.; Borg, K.; Henriksson, M. Gait characteristics and influence of fatigue during the 6-min walk test in patients with post-polio syndrome. *J. Rehabil. Med.* **2013**, *45*, 924–928. [[CrossRef](#)] [[PubMed](#)]
25. Leardini, A.; Sawacha, Z.; Paolini, G.; Ingrosso, S.; Nativo, R.; Benedetti, M.G. A new anatomically based protocol for gait analysis in children. *Gait Posture* **2007**, *26*, 560–571. [[CrossRef](#)] [[PubMed](#)]
26. Cappozzo, A.; Catani, F.; Croce, U.D.; Leardini, A. Position and orientation in space of bones during movement: Anatomical frame definition and determination. *Clin. Biomech.* **1995**, *10*, 171–178. [[CrossRef](#)]
27. Bleser, G.; Stricker, D. Advanced tracking through efficient image processing and visual-inertial sensor fusion. In Proceedings of the 2008 IEEE Virtual Reality Conference, Reno, NE, USA, 8–12 March 2008; pp. 137–144.
28. Eie, M.; Wei, C.-S. Generalizations of Euler decomposition and their applications. *J. Number Theory* **2013**, *133*, 2475–2495. [[CrossRef](#)]
29. Banks, J.J.; Chang, W.-R.; Xu, X.; Chang, C.-C. Using horizontal heel displacement to identify heel strike instants in normal gait. *Gait Posture* **2015**, *42*, 101–103. [[CrossRef](#)] [[PubMed](#)]
30. Ferrari, A.; Cutti, A.G.; Cappello, A. A new formulation of the coefficient of multiple correlation to assess the similarity of waveforms measured synchronously by different motion analysis protocols. *Gait Posture* **2010**, *31*, 540–542. [[CrossRef](#)] [[PubMed](#)]
31. McGraw, K.; Wong, S.P. Forming Inferences about Some Intraclass Correlation Coefficients. *Psychol. Methods* **1996**, *1*, 30–46. [[CrossRef](#)]
32. Koo, T.K.; Li, M.Y. A Guideline of Selecting and Reporting Intraclass Correlation Coefficients for Reliability Research. *J. Chiropr. Med.* **2016**, *15*, 155–163. [[CrossRef](#)] [[PubMed](#)]
33. Roislien, J.; Skare, Ø.; Opheim, A.; Rennie, L. Evaluating the properties of the coefficient of multiple correlation (CMC) for kinematic gait data. *J. Biomech.* **2012**, *45*, 2014–2018. [[CrossRef](#)] [[PubMed](#)]
34. Leardini, A.; Benedetti, M.G.; Berti, L.; Bettinelli, D.; Nativo, R.; Giannini, S. Rear-foot, mid-foot and fore-foot motion during the stance phase of gait. *Gait Posture* **2007**, *25*, 453–462. [[CrossRef](#)] [[PubMed](#)]
35. Fiorentino, N.M.; Atkins, P.R.; Kutschke, M.J.; Goebel, J.M.; Foreman, K.B.; Anderson, A.E. Soft tissue artifact causes significant errors in the calculation of joint angles and range of motion at the hip. *Gait Posture* **2017**, *55*, 184–190. [[CrossRef](#)] [[PubMed](#)]
36. Mills, P.M.; Morrison, S.; Lloyd, D.G.; Barrett, R.S. Repeatability of 3D gait kinematics obtained from an electromagnetic tracking system during treadmill locomotion. *J. Biomech.* **2007**, *40*, 1504–1511. [[CrossRef](#)] [[PubMed](#)]
37. Kailath, T.; Sayed, A.H.; Hassibi, B. *Linear Estimation*; Prentice Hall: Upper Saddle River, NJ, USA, 2000; ISBN 978-0-13-022464-4.
38. Thrun, S.; Burgard, W.; Fox, D. *Probabilistic Robotics (Intelligent Robotics and Autonomous Agents)*; The MIT Press: Cambridge, MA, USA, 2005; ISBN 978-0-262-20162-9.



3.1.2 Journal Paper 2

Summary

JP 2 covers the technical validation of the sensor-fusion algorithm from JP 1 used to estimate the relative IMU orientations, and based on those the joint angles, of the lower body based on the IMU data during physiotherapeutic and sport specific motion tasks within a group of young and healthy subjects. The measurement set-up and the approach for the calculation of the segment orientations for each system were the same as in JP 1. It was the aim of this article to extend the validation and reliability evaluation of the IMU based joint angles during gait to motion tasks incorporating a higher ROM and higher accelerations. Therefore, a squat, a single-leg squat and a countermovement jump were chosen.

Main Contributions

- Magnetometer-free 3D IMU based joint angles of the lower body during squat, single-leg squat and countermovement jump
- Accuracy of the IMU based joint angles estimation during movements with a high ROM and high acceleration
- Difference between two common ways of calculating OMC based segment orientations during physiotherapeutic and sport specific motion tasks and critical discussion of OMC based HMC methods

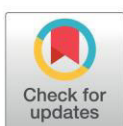
RESEARCH ARTICLE

Validity of inertial sensor based 3D joint kinematics of static and dynamic sport and physiotherapy specific movements

Wolfgang Teuffl^{1,2*}, Markus Miezal¹, Bertram Taetz¹, Michael Fröhlich², Gabriele Bleser¹

1 Department of Computer Science, Technische Universität Kaiserslautern, Kaiserslautern, Germany, **2** Department of Sport Science, Technische Universität Kaiserslautern, Kaiserslautern, Germany

* teuffl@cs.uni-kl.de


 OPEN ACCESS

Citation: Teuffl W, Miezal M, Taetz B, Fröhlich M, Bleser G (2019) Validity of inertial sensor based 3D joint kinematics of static and dynamic sport and physiotherapy specific movements. PLoS ONE 14 (2): e0213064. <https://doi.org/10.1371/journal.pone.0213064>

Editor: John Leicester Williams, University of Memphis, UNITED STATES

Received: August 13, 2018

Accepted: February 14, 2019

Published: February 28, 2019

Copyright: © 2019 Teuffl et al. This is an open access article distributed under the terms of the [Creative Commons Attribution License](https://creativecommons.org/licenses/by/4.0/), which permits unrestricted use, distribution, and reproduction in any medium, provided the original author and source are credited.

Data Availability Statement: All relevant data are within the manuscript and its Supporting Information files. A detailed description of the IMU to segment calibration method, the rigid transformation of IMU to rigid marker cluster, the initialization process and the joint angle calculation is accessible on protocols.io via the DOI [dx.doi.org/10.17504/protocols.io.vvye7fw](https://doi.org/10.17504/protocols.io.vvye7fw). The additional Bland-Altman plots of the hip, knee and ankle joint and pelvis global 3D motion of both evaluation methods is accessible on protocols.io under the DOI: [dx.doi.org/10.17504/protocols.io.sj4ecqw](https://doi.org/10.17504/protocols.io.sj4ecqw).

Abstract

3D joint kinematics can provide important information about the quality of movements. Optical motion capture systems (OMC) are considered the gold standard in motion analysis. However, in recent years, inertial measurement units (IMU) have become a promising alternative. The aim of this study was to validate IMU-based 3D joint kinematics of the lower extremities during different movements. Twenty-eight healthy subjects participated in this study. They performed bilateral squats (SQ), single-leg squats (SLS) and countermovement jumps (CMJ). The IMU kinematics was calculated using a recently-described sensor-fusion algorithm. A marker based OMC system served as a reference. Only the technical error based on algorithm performance was considered, incorporating OMC data for the calibration, initialization, and a biomechanical model. To evaluate the validity of IMU-based 3D joint kinematics, root mean squared error (RMSE), range of motion error (ROME), Bland-Altman (BA) analysis as well as the coefficient of multiple correlation (CMC) were calculated. The evaluation was twofold. First, the IMU data was compared to OMC data based on marker clusters; and, second based on skin markers attached to anatomical landmarks. The first evaluation revealed means for RMSE and ROME for all joints and tasks below 3°. The more dynamic task, CMJ, revealed error measures approximately 1° higher than the remaining tasks. Mean CMC values ranged from 0.77 to 1 over all joint angles and all tasks. The second evaluation showed an increase in the RMSE of 2.28°–2.58° on average for all joints and tasks. Hip flexion revealed the highest average RMSE in all tasks (4.87°–8.27°). The present study revealed a valid IMU-based approach for the measurement of 3D joint kinematics in functional movements of varying demands. The high validity of the results encourages further development and the extension of the present approach into clinical settings.

Funding: This work was performed by the interdisciplinary Junior Research Group wearHEALTH, funded by the Federal Ministry of Education and Research (BMBF), Grant numbers: 16SV7115 to GB, and 03IHS075B to GB. For more information, please visit the website www.wearhealth.org. The funders had no role in study design, data collection and analysis, decision to publish, or preparation of the manuscript.

Competing interests: The authors have declared that no competing interests exist.

1 Introduction

The assessment of functional movements has become an important part of physical therapy and the practice of sports medicine [1]. Functional movement, or fundamental movement, describes a kind of complex 3D movement along several joints and the incorporating muscle synergies. Three functional movements used for analysis in these professions are the bilateral squat (SQ) [2], the single-leg squat (SLS) [3,4], and the countermovement jump (CMJ) [5,6]. These functional movements can provide information about rehabilitation status or injury risks [7,8]. It is not only important to assess the movement performance (e.g., speed, repetitions, jump height, etc.), but also how the movement is executed. The joint kinematics recorded during functional movements can reveal information about the correctness of the movement. Optical motion capture systems (OMC) are commonly used to evaluate joint kinematics [9]. However, OMC systems do not always allow the subject to move in his/her accustomed environment. In this context, inertial measurement units (IMU) present a local independent alternative [10], and their use has been widely accepted. A single IMU has been used to examine the horizontal and vertical displacement of the pelvis during a CMJ [11], to evaluate kinetic data from three different jumping tasks [12], and to assess the performance of a CMJ [13]. The 3D joint kinematics of the hip and ankle, as well as the 1D joint kinematics of the knee during a SLS, were evaluated using a set of three IMU's attached to the pelvis, thigh and shank [7]. However, some of these studies only used one IMU and focused only on performance measures [11–13]. Others examined joint kinematics but did not compare their results to a reference system [7].

The accuracy of IMU-based joint kinematics, or spatio-temporal parameters, have been examined in several studies on gait analysis [14–18]. Despite the increasing application of IMU's the availability of validity studies regarding the measurement of 3D joint kinematics in functional movements is limited. Al-Amri et al. [14] examined the reliability and validity of SQ and vertical jumping 3D joint kinematics of the lower extremity. However, they failed to report detailed results concerning the validity of the transversal and frontal plane joint kinematics. Robert-Lachaine et al. [19] evaluated the accuracy of full body joint kinematics during ergonomic tasks. However, IMU's aim to be used in rehabilitation and sports medicine. The functional movements mentioned above differ from common gait inasmuch as they incorporate almost no global translation, usually demand higher ranges of motion (ROM) and, in the case of the CMJ, higher global accelerations. Thus, the validity of IMU-based 3D joint kinematics of slow and dynamic functional movements has to be further investigated.

A recently described sensor-fusion algorithm for the estimation of 3D IMU kinematics [20,21] revealed long-term stable results of the joint kinematics estimation of the lower extremities in a gait analysis [18]. These results proved to be unaffected by drift, despite omitting magnetometer information. Based on those results, the primary aim of this study was to evaluate the performance of this algorithm in estimating 3D joint kinematics in dynamic, clinically-relevant movements with high ROM. As in [18], this evaluation focuses on the technical differences between IMU- and OMC-based joint kinematics associated to algorithmic issues. Thus, the IMU initialization, calibration, and the biomechanical model were derived from the OMC system.

Like optical markers, IMU's are prone to artefacts caused by the displacement of the sensor and that of the underlying tissue with respect to the bone [22]. These artefacts are commonly referred to as soft tissue artefacts (STA). The effect of STA on OMC- and IMU-based joint kinematics [9,23–25] and possible compensation mechanisms [26–29] have been intensively examined in the recent literature. It was an objective of the present study to minimize the differences between the two systems associated to STA. Researchers use rigid marker clusters (RMC) affixed to the IMU for the calculation of OMC-based joint kinematics to achieve this goal [11,17,19]. The alternative calculation of OMC-based joint kinematics involves skin

markers attached to anatomical landmarks. Examinations have shown that the OMC-based joint kinematics derived from RMC are less susceptible to errors caused by STA than markers mounted on bony prominences [30]. However, both methods are commonly used in research as well as clinical settings. Furthermore, few studies have reported results that compare IMU joint kinematics with OMC joint kinematics based on skin markers attached to anatomical landmarks [14,16,31].

Therefore, the second aim of the study was to compare IMU-based joint kinematics with OMC-based joint kinematics derived from skin markers attached to anatomical landmarks instead of RMC.

2 Methods and materials

2.1 Subjects and data acquisition

Twenty-eight healthy subjects (15 females, 13 males; 24 ± 2.70 years; 70 ± 12.70 kg; 176 ± 9.00 cm) participated in the study. The subjects were recruited via e-mail, bulletins, and presentations in specific lectures at the local university. The study was approved by the local ethical committee of the Technische Universität Kaiserslautern (TUK) and meets the criteria of the declaration of Helsinki. After receiving all relevant study information, the participants signed an informed consent to the study including a permission to publish the data. A test session consisted of one static neutral zero position (n-pose) sequence [32]; three trials of five, right-legged SLS; three trials of five SQ; and, three trials of three CMJ. A SLS and SQ cycle was defined as the time from maximum knee extension to the next maximum knee extension. A CMJ cycle was defined as the time from the first downward movement of the pelvis marker until it reached the next static phase. Every SLS, SQ, and CMJ considered for evaluation was normalized to 100% movement cycle.

OMC lower extremity 3D joint kinematics was captured using OptiTrack Motive 1.10 (NaturalPoint, Inc., Oregon, USA). IMU raw data was recorded by means of seven Xsens MTw Awinda IMU and Xsens MVN Biomech software version 4.3.7 (Xsens Technologies BV, Enschede, Netherlands). Both systems were synchronized and recorded at 60 Hz.

All IMU's were activated 20 minutes prior to each test session and before the subjects were instrumented. Before testing, a static trial was conducted by laying all IMU's on the ground for about 10 seconds. These measurements were used to estimate and subtract the gyroscope bias according to [33].

Thirty-two retroreflective markers were attached to anatomical landmarks according to [34]. Six additional markers were applied following the OptiTrack recommendations. Each IMU was inserted into a matching 3D printed box equipped with four retroreflective markers (Fig 1). These boxes were attached to the body segments of the lower extremities using straps and double-sided adhesive tape. The IMU and RMC for the thigh and shank were placed according to recommendations by Manal et al. [35,36]. The IMU and RMC attached to the pelvic segment was placed on top of the sacrum according to Cutti et al. [37]. The IMU and RMC for the feet could only be placed on the dorsum of the foot due to their size and visibility. Schematic marker protocol and IMU placement are shown in Fig 2.

To exclude possible errors in the IMU-derived data based on different coordinate systems, calibration, or the initialization process, the biomechanical model [34] and IMU-to-segment calibrations were calculated based on the OMC data of the recorded n-pose sequence. Additionally, the initialization of the IMU-based kinematics estimation incorporated data from the OMC system.

The IMU raw data was processed with a sensor-fusion algorithm using an iterated extended Kalman Filter (EKF) approach based on [20] and enhanced with global translation estimation

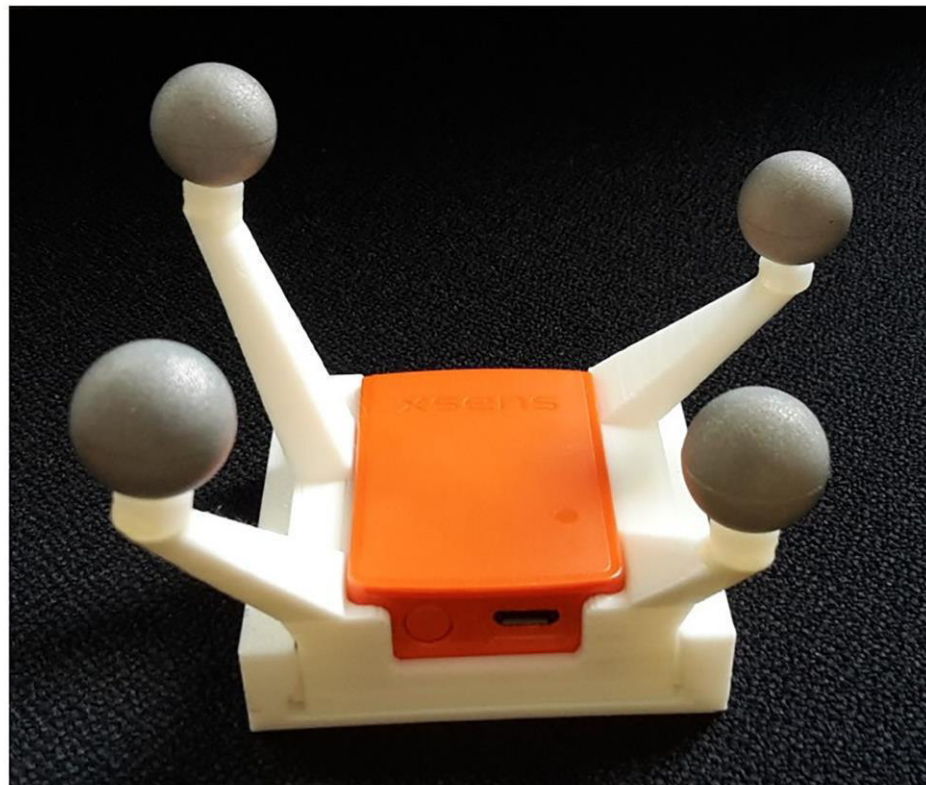


Fig 1. Sensor fixation. Inertial Measurement Unit (IMU) inserted into a matched, 3D-printed Rigid Marker Cluster (RMC).

<https://doi.org/10.1371/journal.pone.0213064.g001>

[21] that used only accelerometer and gyroscope data; magnetometer information was omitted. The complete algorithm is described in [18]. The same filter settings and tuning parameters that are described in [18] were used in this study. The estimated segment orientations were used to derive relative joint orientations. These were decomposed into joint angles using Euler angle decomposition [38]. The OMC joint angle data was calculated based on the RMC and the skin markers according to the recommendations by Visual 3D (C-Motion, Inc, Germantown, MD, USA). A more detailed description of the calibration, initialization and joint angle calculation can be found at [dx.doi.org/10.17504/protocols.io.vvye7fw](https://doi.org/10.17504/protocols.io.vvye7fw).

2.2 Statistical analysis

The analysis of the IMU system was twofold. First, the joint kinematics data from the IMU was compared to the OMC joint kinematics data based on the RMC, in order to minimize the error between the systems caused by different positioning of the IMU and markers respectively (RMC evaluation). In a secondary analysis, the IMU data was compared to the OMC data from the skin markers attached to anatomical landmarks (skin marker evaluation).

To determine the validity of the IMU system, the following statistical measures were calculated for each evaluation of the hip, knee, ankle joint, and global 3D pelvis orientations per



Fig 2. Marker protocol and IMU placement. Retroreflective markers attached to the anatomical landmarks and the RMC. IMU are not inserted in the RMC in this schematic picture.

<https://doi.org/10.1371/journal.pone.0213064.g002>

movement cycle: the root mean squared error (RMSE), the range of motion error (ROME), as well as 95% confidence interval (CI). A Bland-Altman (BA) analysis was conducted to evaluate the bias and limits of agreement between the OMC- and IMU-based joint kinematics according to [39]. For the BA analysis, the average of all movement cycles for each subject was used. This approach was deemed appropriate given that the mean of a similar number of movement cycles is usually examined in clinical measurements [40]. Further, the coefficient of multiple correlation (CMC) was calculated for each parameter per movement cycle according to [41]. CMC values were rated according to [42]. For further interpretation, the mean of the statistical measures of all subjects and movement cycles was calculated.

An ANOVA was conducted to identify significant differences in the RMSE between the three different functional movements. Additionally, the data from a previous study [18] that used the same approach for the calculation of IMU-based 3D joint kinematics during gait, was included in the comparison. The significance level was set to $\alpha = 0.05$. The Chi-square goodness-of-fit test was conducted to check for normal distribution in the data. A post hoc analysis revealed which groups differed in the case of significant p-values.

The changes in RMSE and ROME between the RMC evaluation and the skin marker evaluation were graphically represented.

The segmentation of the joint angles and all statistics were conducted in Matlab 2017 (Mathworks Inc.) using custom written scripts.

3 Results

3.1 RMC evaluation

RMSE and ROME of all joint angles for SQ, SLS and CMJ are shown in Table 1. For the readers convenience, Table 1 includes the RMSE of the gait data from [18]. S1–S3 Figs in the supporting information show the mean joint angle waveforms of one exemplary subject for all three tasks and all three planes.

The following considers only the results of the functional movements. The RMC evaluation of the IMU data revealed RMSE and ROME to be below 3° for all joints and all movements. The highest RMSE was evident in the frontal and transversal plane. The sagittal plane revealed a RMSE between 0.93° and 1.22° and a ROME between 0.60° – 1.29° for SQ and SLS. CMJ showed a higher RMSE and ROME than SQ and SLS with respect to the hip, knee, and ankle in the sagittal plane; values ranged from 1.44° – 2.48° RMSE and 1.32° – 2.19° ROME, respectively. The best outcome in the sagittal plane for all tasks was in global pelvis flexion (RMSE 0.70° – 1.03°). Concerning the joint angles in the frontal and transversal plane, SQ, SLS, and CMJ revealed similar RMSE's. However, ankle inversion and rotation were again highest in the CMJ task. ROME in the frontal and transversal plane was also higher in the CMJ task. The global pelvis obliquity and rotation showed the best results in the frontal and transversal plane with a RMSE below 1.00° and a ROME below 0.70° .

Table 2 shows the results of the ANOVA for the inter-task comparison of the RMSE. The most significant differences were found between the CMJ task and the remaining functional movements and Gait. No significant differences were found between SQ and SLS.

The CMC values were good to excellent for all joints in the SLS, SQ and CMJ tasks. The CMC values of the joint angles of the right lower extremity are plotted in Fig 3. The SQ task showed higher variances of CMC in the transversal plane as compared to SLS and CMJ tasks. SLS displayed higher uncertainties in the hip and knee rotations.

A BA analysis was conducted to evaluate the limits of agreement between the IMU and OMC data in all joint angles. The SQ data revealed biases from -1.10° – 1.20° and limits ranging from $\pm 1.07^\circ$ – $\pm 5.06^\circ$. The SLS data displayed biases from -1.10° – 1.36° and limits ranging from $\pm 0.96^\circ$ – $\pm 3.25^\circ$. In the CMJ data, biases ranged from -1.34° – 1.35° and limits were between $\pm 1.18^\circ$ – $\pm 4.48^\circ$. Exemplary BA diagrams of the right knee flexion and abduction for all tasks are shown in Fig 4.

3.2 Skin marker evaluation

The RMSE and ROME of all joint angles for SQ, SLS, and CMJ are shown in Table 3. S4–S6 Figs in the supporting information show the mean joint angle waveforms of one exemplary subject in all three tasks and for all three planes.

Table 1. Results of the RMC evaluation.

	RMSE [deg] ± SD (95% CI)				ROME [deg] ± SD (95% CI)		
	Gait [18]	SQ	SLS	CMJ	SQ	SLS	CMJ
LT Hip – Abduction	1.05 ± 0.42 (0.78–1.11)	1.70 ± 0.89 (1.12–1.81)	x	1.23 ± 0.43 (1.03–1.37)	1.72 ± 1.26 (0.83–1.80)	x	1.20 ± 0.57 (0.89–1.33)
LT Hip – Rotation	1.94 ± 0.92 (1.49–2.20)	2.28 ± 1.25 (1.65–2.62)	x	1.78 ± 0.78 (1.12–1.73)	1.19 ± 0.90 (0.50–1.20)	x	1.01 ± 0.38 (0.78–1.08)
LT Hip – Flexion	1.02 ± 0.35 (0.79–1.06)	1.17 ± 0.45 (0.94–1.29)	x	1.55 ± 0.31 (1.42–1.66)	0.89 ± 0.54 (0.55–0.97)	x	1.42 ± 0.81 (0.97–1.59)
LT Knee – Abduction	1.59 ± 0.48 (1.22–1.59)	2.06 ± 0.72 (1.62–2.18)	x	2.02 ± 0.68 (1.67–2.20)	1.49 ± 0.84 (0.84–1.50)	x	2.20 ± 1.13 (1.49–2.37)
LT Knee – Rotation	2.34 ± 1.08 (1.63–2.48)	2.66 ± 1.55 (1.71–2.91)	x	2.75 ± 0.97 (2.39–3.14)	1.59 ± 0.87 (0.98–1.66)	x	1.85 ± 0.86 (1.41–2.07)
LT Knee – Flexion	1.47 ± 0.34 (1.25–1.51)	1.10 ± 0.28 (0.93–1.15)	x	1.83 ± 0.46 (1.54–1.89)	1.29 ± 0.62 (1.03–1.51)	x	1.72 ± 1.00 (1.10–1.87)
LT Ankle – Inversion	1.61 ± 0.39 (1.42–1.73)	1.83 ± 0.74 (1.31–1.88)	x	2.46 ± 0.73 (1.98–2.55)	2.06 ± 1.30 (1.29–2.30)	x	2.43 ± 1.17 (1.82–2.73)
LT Ankle – Rotation	2.16 ± 0.68 (1.80–2.33)	2.01 ± 1.15 (1.50–2.39)	x	2.92 ± 0.94 (2.50–3.22)	0.91 ± 0.62 (0.51–0.99)	x	2.28 ± 0.83 (1.68–2.32)
LT Ankle – Flexion	1.55 ± 0.34 (1.46–1.72)	1.22 ± 0.51 (0.92–1.32)	x	2.48 ± 0.53 (2.29–2.71)	0.60 ± 0.23 (0.47–0.65)	x	2.11 ± 0.97 (1.60–2.35)
RT Hip – Abduction	1.09 ± 0.54 (0.63–1.05)	1.39 ± 0.80 (0.78–1.40)	1.26 ± 0.68 (0.78–1.30)	1.30 ± 0.61 (0.90–1.37)	1.29 ± 0.78 (0.74–1.34)	1.34 ± 0.87 (0.77–1.45)	1.14 ± 0.61 (0.73–1.21)
RT Hip – Rotation	1.64 ± 1.00 (1.00–1.77)	1.77 ± 1.05 (1.21–2.02)	2.11 ± 0.99 (1.51–2.28)	2.01 ± 1.07 (1.29–2.12)	1.03 ± 0.83 (0.38–1.02)	0.69 ± 0.38 (0.39–0.69)	1.05 ± 0.63 (0.79–1.28)
RT Hip – Flexion	0.98 ± 0.51 (0.68–1.07)	1.07 ± 0.30 (0.96–1.19)	1.01 ± 0.69 (0.60–1.13)	1.44 ± 0.35 (1.23–1.51)	0.82 ± 0.49 (0.51–0.88)	0.95 ± 0.84 (0.46–1.11)	1.32 ± 0.72 (0.95–1.51)
RT Knee – Abduction	1.26 ± 0.51 (0.90–1.30)	1.54 ± 0.75 (0.96–1.54)	1.49 ± 0.74 (1.18–1.76)	1.48 ± 0.51 (1.22–1.62)	1.40 ± 0.98 (0.68–1.44)	1.23 ± 0.96 (0.48–1.22)	1.33 ± 0.59 (0.97–1.43)
RT Knee – Rotation	1.75 ± 0.63 (1.38–1.87)	1.86 ± 1.28 (0.80–1.79)	2.06 ± 1.46 (1.30–2.44)	2.29 ± 1.14 (1.53–2.41)	0.94 ± 0.82 (0.36–0.99)	0.74 ± 0.36 (0.45–0.74)	1.46 ± 0.82 (0.97–1.60)
RT Knee – Flexion	1.51 ± 0.43 (1.31–1.64)	1.01 ± 0.27 (0.84–1.05)	1.03 ± 0.63 (0.62–1.10)	1.83 ± 0.38 (1.61–1.91)	1.13 ± 0.48 (0.99–1.37)	0.88 ± 0.54 (0.51–0.93)	1.80 ± 0.92 (1.02–1.73)
RT Ankle – Inversion	1.33 ± 0.35 (1.09–1.36)	1.18 ± 0.51 (0.85–1.24)	1.26 ± 0.71 (0.80–1.35)	1.77 ± 0.48 (1.42–1.79)	0.64 ± 0.37 (0.43–0.71)	0.77 ± 0.32 (0.63–0.88)	1.71 ± 0.65 (1.50–2.00)
RT Ankle – Rotation	1.52 ± 0.41 (1.27–1.59)	1.23 ± 0.61 (0.89–1.36)	1.22 ± 1.01 (0.58–1.39)	2.27 ± 0.83 (1.79–2.44)	0.84 ± 0.44 (0.60–0.93)	0.82 ± 0.58 (0.35–0.81)	1.78 ± 0.90 (1.30–2.00)
RT Ankle – Flexion	1.60 ± 0.36 (1.43–1.71)	0.93 ± 0.51 (0.55–0.95)	1.01 ± 0.47 (0.67–1.03)	2.41 ± 0.51 (2.20–2.59)	0.61 ± 0.24 (0.47–0.66)	0.72 ± 0.43 (0.44–0.78)	2.19 ± 1.17 (1.67–2.58)
Pelvis – Obliquity	0.64 ± 0.18 (0.55–0.69)	0.53 ± 0.37 (0.25–0.54)	0.60 ± 0.28 (0.39–0.61)	0.76 ± 0.27 (0.67–0.87)	0.36 ± 0.21 (0.21–0.37)	0.44 ± 0.26 (0.24–0.44)	0.62 ± 0.20 (0.54–0.70)
Pelvis – Flexion	0.62 ± 0.16 (0.57–0.69)	0.70 ± 0.28 (0.54–0.76)	0.71 ± 0.51 (0.38–0.78)	1.03 ± 0.28 (0.86–1.08)	0.45 ± 0.28 (0.26–0.47)	0.45 ± 0.27 (0.28–0.48)	1.24 ± 0.62 (0.86–1.35)
Pelvis – Rotation	X	0.88 ± 0.64 (0.45–0.95)	0.92 ± 0.46 (0.64–1.00)	0.84 ± 0.37 (0.56–0.85)	0.33 ± 0.13 (0.25–0.35)	0.44 ± 0.18 (0.30–0.44)	0.53 ± 0.23 (0.42–0.60)

Mean root mean squared error (RMSE) and mean range of motion error (ROME) of the rigid marker cluster (RMC) evaluation of all subjects ± standard deviation (SD); brackets contain 95% confidence interval (CI). Columns show the results for gait, bilateral squat (SQ), single-leg squat (SLS), and countermovement jump (CMJ).

<https://doi.org/10.1371/journal.pone.0213064.t001>

As compared to the RMC evaluation, RMSE increased by 2.28° for SLS, 2.35° (left) and 2.40° (right) for SQ, and 2.58° (left) and 2.55° (right) for CMJ on average for all joints. The most affected joint angle was the hip joint in the sagittal plane. Hip flexion showed a RMSE of 8.27° and 7.10° in SQ and CMJ, respectively. Hip flexion in the SLS revealed a RMSE of 4.87°. The ROME was also highest for hip flexion in all three tasks with values ranging from 5.22° up to 11.08°. Figs 5 and 6 show the differences in the RMSE and ROME between the two evaluation methods for the different tasks and joint angles.

The CMC primarily declined concerning the frontal and transversal plane. The CMC values of the joint angles of the right lower extremity are plotted in Fig 7. In the SLS task, CMC values for the mentioned planes were moderate to excellent. In the SQ and CMJ tasks, the CMC values were moderate to good. Overall, the CMC showed distinctively higher variances between the subjects in the transversal and frontal plane, which can be seen in the wide quartiles and whiskers in Fig 7.

The BA analysis in the skin marker evaluation revealed higher biases and limits in all tasks as compared to the RMC evaluation. SQ showed biases of -2.11° – 5.82° and limits of $\pm 3.09^{\circ}$ – $\pm 11.44^{\circ}$; SLS revealed biases of -1.45° – 2.89° and limits of $\pm 3.16^{\circ}$ – $\pm 9.55^{\circ}$; and, CMJ displayed biases of -3.54° – 4.45° and limits of $\pm 3.22^{\circ}$ – $\pm 12.47^{\circ}$. According to the BA analysis, the hip joint in the sagittal plane was again the most affected joint (biases 2.21° – 5.82° and limits $\pm 9.55^{\circ}$ – $\pm 12.47^{\circ}$ for all tasks). Exemplary BA diagrams of right knee flexion and abduction in all tasks are shown in Fig 8. The movements in the remaining sagittal joint angles, as well as the global pelvis rotation, were the least affected joints.

Table 2. Results of the ANOVA.

	RMSE					
	p-value					
	Gait vs SQ	Gait vs SLS	Gait vs CMJ	SQ vs SLS	SQ vs CMJ	SLS vs CMJ
LT Hip – Abduction	< 0.001	x	0.124	x	0.015	x
LT Hip – Rotation	0.255	x	0.475	x	0.078	x
LT Hip – Flexion	0.177	x	< 0.001	x	< 0.001	x
LT Knee – Abduction	0.007	x	0.009	x	0.859	x
LT Knee – Rotation	0.376	x	0.139	x	0.790	x
LT Knee – Flexion	< 0.001	x	0.002	x	< 0.001	x
LT Ankle – Inversion	0.173	x	< 0.001	x	0.003	x
LT Ankle – Rotation	0.553	x	0.001	x	0.002	x
LT Ankle – Flexion	0.006	x	< 0.001	x	< 0.001	x
RT Hip – Abduction	0.104	0.305	0.170	0.515	0.658	0.796
RT Hip – Rotation	0.634	0.079	0.189	0.211	0.407	0.696
RT Hip – Flexion	0.403	0.829	< 0.001	0.679	< 0.001	0.005
RT Knee – Abduction	0.122	0.198	0.121	0.812	0.752	0.969
RT Knee – Rotation	0.681	0.314	0.031	0.599	0.187	0.498
RT Knee – Flexion	< 0.001	0.002	0.004	0.885	< 0.001	< 0.001
RT Ankle – Inversion	0.200	0.666	< 0.001	0.597	< 0.001	0.003
RT Ankle – Rotation	0.038	0.162	< 0.001	0.987	< 0.001	< 0.001
RT Ankle – Flexion	< 0.001	< 0.001	< 0.001	0.567	< 0.001	< 0.001
Pelvis – Obliquity	0.193	0.544	0.043	0.470	0.011	0.030
Pelvis – Flexion	0.228	0.386	< 0.001	0.900	< 0.001	0.005
Pelvis – Rotation	x	x	x	0.815	0.788	0.518

P-values of the ANOVA for inter-task comparison of the RMSE. Rows show joint angles. Each column represents the comparison between two movements. Pelvis rotation was not compared between Gait and the remaining functional movements due to drift in the global pelvis rotation of the gait data (see [18])

<https://doi.org/10.1371/journal.pone.0213064.t002>

4 Discussion

The primary aim of this study was to validate the accuracy of a sensor-fusion algorithm used in calculating IMU-based 3D lower extremity joint kinematics of three typical functional movements as compared to OMC joint kinematics based on RMC. The secondary aim of the analysis was to determine the error between the IMU data and the OMC data based on skin markers.

4.1 RMC evaluation

The RMC evaluation of 3D joint kinematics based on the IMU data of the SQ, SLS, and CMJ tasks revealed excellent correspondence with the OMC data. However, it appeared that the CMJ task revealed the highest RMSE and ROME in the sagittal plane and in ankle inversion and rotation. These findings indicate that the IMU data was influenced by the high accelerations that can occur during the landing phase in a jumping task [43]. The IMU's used in this study employ an accelerometer with a maximum resolution of ± 16 g. A probable limitation was that the IMU recorded data with 60 Hz due to software restrictions.

The results of the ANOVA (Table 2) also revealed significantly higher RMSE in most joint angles for the CMJ (33/54) compared to the remaining tasks. The sagittal plane displayed most of the significant differences between the four tasks. That might be connected to the higher changes recorded in the ROM concerning this plane. These findings implicate that the

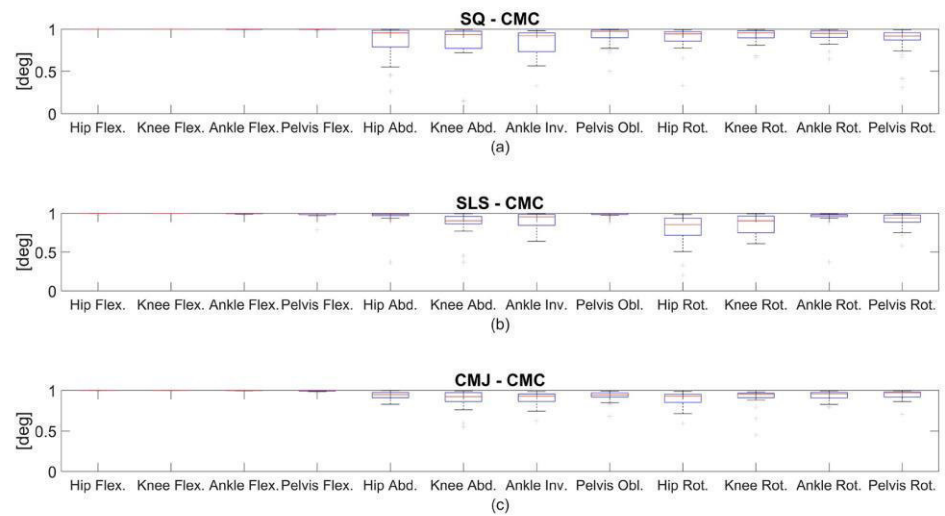


Fig 3. Coefficient of multiple correlation (CMC) of the RMC evaluation. CMC of the right lower extremity for all functional movements: (a) indicates SQ, (b) indicates SLS, and (c) indicates CMJ.

<https://doi.org/10.1371/journal.pone.0213064.g003>

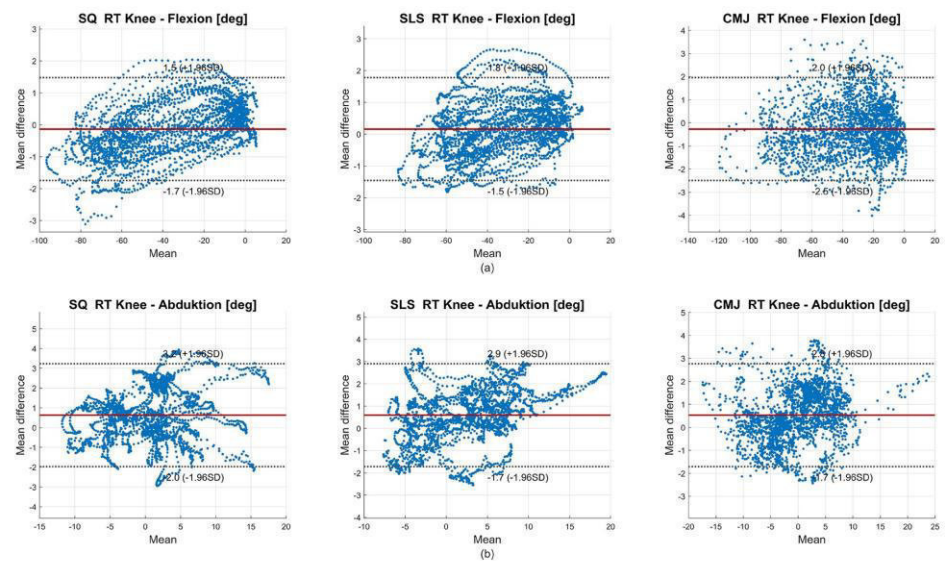


Fig 4. Bland-Altman (BA) diagrams of the right knee flexion (a) and abduction (b) for all subjects for the RMC evaluation. In (a), negative values on the x-axis indicate knee flexion. In (b), negative values on the x-axis indicate knee adduction. The solid line indicates the mean difference, dashed lines indicate $\pm 1.96 \times$ standard deviation (SD).

<https://doi.org/10.1371/journal.pone.0213064.g004>

Table 3. Results of the skin marker evaluation.

	RMSE [deg] ± SD (95% CI)			ROME [deg] ± SD (95% CI)		
	SQ	SLS	CMJ	SQ	SLS	CMJ
LT Hip – Abduction	3.26 ± 1.30 (2.88–3.89)	x	3.12 ± 1.56 (2.33–3.54)	3.45 ± 2.12 (2.05–3.70)	x	4.10 ± 2.76 (2.14–4.28)
LT Hip – Rotation	4.79 ± 2.40 (3.23–5.09)	x	5.26 ± 2.53 (3.86–5.82)	3.75 ± 3.15 (1.84–4.28)	x	3.12 ± 1.55 (1.98–3.18)
LT Hip – Flexion	8.27 ± 4.40 (5.42–8.84)	x	7.10 ± 3.60 (4.46–7.25)	11.08 ± 6.96 (6.66–12.05)	x	10.70 ± 6.64 (6.20–11.35)
LT Knee – Abduction	4.77 ± 2.40 (3.28–5.14)	x	4.11 ± 2.25 (2.66–4.41)	4.75 ± 3.44 (2.29–4.95)	x	3.49 ± 2.47 (2.06–3.97)
LT Knee – Rotation	4.09 ± 2.21 (2.50–4.22)	x	5.23 ± 2.36 (4.17–6.00)	3.89 ± 2.24 (2.95–4.69)	x	3.95 ± 2.08 (2.84–4.46)
LT Knee – Flexion	2.41 ± 1.82 (1.15–2.56)	x	2.84 ± 0.60 (2.59–3.05)	2.65 ± 2.39 (0.89–2.75)	x	3.43 ± 2.24 (1.84–3.58)
LT Ankle – Inversion	3.70 ± 2.07 (2.62–4.23)	x	5.00 ± 1.55 (4.31–5.51)	2.21 ± 1.58 (1.07–2.29)	x	4.47 ± 2.20 (3.51–5.22)
LT Ankle – Rotation	2.93 ± 1.82 (1.87–3.28)	x	4.27 ± 1.78 (3.46–4.84)	1.54 ± 1.00 (0.83–1.61)	x	3.04 ± 1.82 (1.62–3.03)
LT Ankle – Flexion	2.95 ± 1.42 (2.52–3.61)	x	5.32 ± 1.40 (4.80–5.89)	2.71 ± 1.68 (1.76–3.07)	x	6.23 ± 2.14 (5.54–7.20)
RT Hip – Abduction	2.69 ± 1.39 (2.14–3.22)	2.74 ± 1.66 (1.52–2.81)	2.71 ± 1.34 (1.80–2.84)	3.24 ± 2.31 (1.92–3.71)	2.05 ± 1.42 (0.84–1.94)	3.41 ± 2.39 (1.62–3.47)
RT Hip – Rotation	5.05 ± 2.77 (3.42–5.57)	5.18 ± 2.95 (3.38–5.67)	5.44 ± 3.15 (2.83–5.52)	3.83 ± 2.45 (2.93–4.83)	3.48 ± 2.06 (2.10–3.69)	3.32 ± 1.81 (2.25–3.66)
RT Hip – Flexion	7.67 ± 4.38 (5.08–8.48)	4.87 ± 3.06 (3.04–5.41)	7.11 ± 3.80 (4.79–7.74)	9.95 ± 7.47 (5.35–11.14)	5.22 ± 3.92 (2.59–5.63)	10.28 ± 6.77 (5.54–10.79)
RT Knee – Abduction	4.43 ± 2.88 (2.56–4.79)	4.77 ± 2.61 (3.08–5.11)	4.04 ± 2.18 (2.44–4.12)	5.38 ± 4.67 (1.68–5.30)	4.02 ± 3.99 (0.97–4.07)	4.45 ± 4.56 (1.60–5.13)
RT Knee – Rotation	4.08 ± 1.68 (3.05–4.35)	4.27 ± 2.64 (2.84–4.89)	5.08 ± 2.49 (3.49–5.42)	3.41 ± 2.22 (2.14–3.86)	3.42 ± 2.09 (2.38–4.00)	4.34 ± 1.86 (3.13–4.58)
RT Knee – Flexion	2.47 ± 1.33 (1.71–2.73)	2.81 ± 1.68 (1.55–2.86)	3.14 ± 1.05 (2.51–3.32)	2.86 ± 2.17 (1.63–3.31)	2.51 ± 1.74 (1.19–2.54)	3.35 ± 2.13 (1.90–3.55)
RT Ankle – Inversion	3.39 ± 1.85 (2.12–3.56)	3.58 ± 2.14 (1.92–3.58)	4.99 ± 2.01 (3.74–5.30)	2.17 ± 1.60 (1.23–2.47)	2.81 ± 1.66 (1.69–2.98)	4.32 ± 1.86 (3.21–4.65)
RT Ankle – Rotation	2.60 ± 1.45 (1.82–2.95)	3.41 ± 2.26 (1.90–3.65)	4.29 ± 2.16 (3.43–5.10)	1.56 ± 1.41 (0.31–1.40)	1.85 ± 1.11 (1.11–1.97)	3.46 ± 2.40 (1.83–3.69)
RT Ankle – Flexion	2.47 ± 1.26 (1.78–2.76)	2.81 ± 1.60 (1.61–2.85)	4.40 ± 1.42 (3.86–4.96)	2.56 ± 1.59 (2.13–3.36)	1.71 ± 1.08 (0.98–1.82)	5.33 ± 2.73 (3.49–5.61)
Pelvis – Obliquity	1.48 ± 1.02 (0.79–1.58)	1.76 ± 1.00 (1.24–2.02)	1.70 ± 0.97 (1.18–1.93)	1.22 ± 0.72 (0.70–1.26)	1.91 ± 1.44 (0.90–2.02)	1.76 ± 1.09 (1.19–2.04)
Pelvis – Flexion	4.93 ± 3.22 (2.86–5.36)	3.78 ± 2.65 (1.59–3.65)	5.35 ± 2.86 (3.42–5.64)	6.57 ± 5.11 (3.10–7.06)	3.25 ± 2.18 (1.85–3.54)	7.90 ± 5.15 (4.63–8.62)
Pelvis – Rotation	1.59 ± 1.09 (0.86–1.70)	2.12 ± 0.93 (1.75–2.48)	1.77 ± 0.97 (1.14–1.89)	0.82 ± 0.55 (0.50–0.93)	1.03 ± 0.64 (0.68–1.18)	0.95 ± 0.48 (0.66–1.03)

Mean RMSE and mean ROME of the skin marker evaluation of all subjects ± standard deviation (SD); brackets contain 95% confidence interval (CI). Columns show results for SQ, SLS, and CMJ tasks.

<https://doi.org/10.1371/journal.pone.0213064.t003>

accuracy of the measurement of joint kinematics depends on the amplitude of the movement. Significant differences were also found between Gait and SQ (7/20) as well as Gait and SLS (2/11). No significant differences were found between the SQ and SLS. However, when considering Table 1, it must be noted that the differences between tasks are in the range of the variability of the reference system itself. Thewlis et al. [44] compared two OMC systems and found differences ranging from 0.3°–3.9° over all joint angles of the LE.

There are few studies which have examined the joint kinematics of comparable tasks using an IMU system and that excluded the uncertainties based on different magnitudes of STA using RMC [19,45]. Robert-Lachaine et al. [19] validated a commercial IMU system against an OMC system in ergonomic lifting and turning tasks, which are comparable to squatting. Their results revealed a RMSE between 1.90°–7.30° and CMC values from 0.77–1.00. The present study showed RMSE from 0.33°–2.92° and CMC values from 0.77–1.00 over all tasks.

In the present study, the pelvic joint kinematics was assessed as the orientation of the pelvis segment with respect to the global coordinate system. The pelvic angle's RMSE and ROME outperformed the remaining joint angles. Lebel et al. [45] previously examined the validity of IMU orientation during a timed up-and-go test. They reported a RMSE for the global pelvis orientation for different motion sections of 1.00° (sit-to-stand), 2.20° (walk), and 1.70° (turn). The sit-to-stand movement can be viewed as a squat like motion. In this case, the present study revealed a slightly better RMSE for the global pelvic angle (0.53°–0.88°) than had been reported.

BA analysis revealed good agreement between the OMC and IMU system. However, that the definition of acceptable limits strongly depends on the requirements of the individual application should be considered [46]. In Fig 4 knee flexion and abduction are depicted. In the

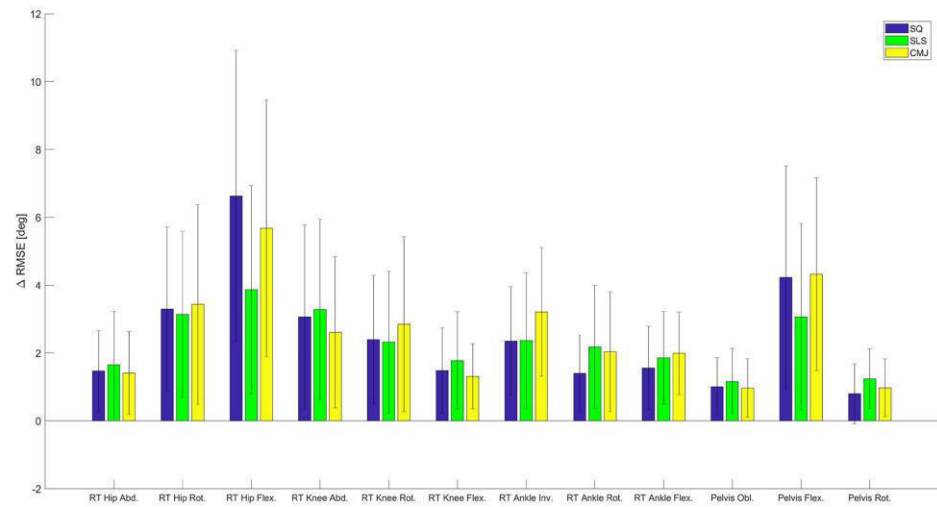


Fig 5. RMSE change. The mean difference in RMSE between the RMC evaluation and the skin marker evaluation in all three tasks for all joints (\pm SD).

<https://doi.org/10.1371/journal.pone.0213064.g005>

SQ right knee flexion, the IMU data tended to underestimate the flexion, and conversely tended to overestimate the extension. Similar findings were revealed in the SLS right knee abduction. In this case, knee adduction tended to be underestimated, and knee abduction tended to be overestimated. However, the ROM should be unaffected by an offset, assuming that it is constant. This is important considering the value of ROM measurements in the

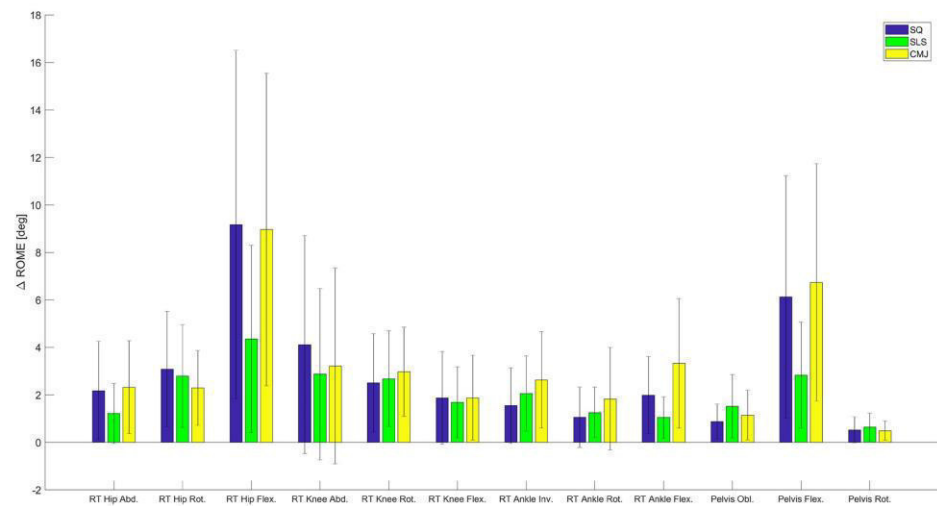


Fig 6. ROME change. The mean difference in ROME between the RMC evaluation and the skin marker evaluation in all three tasks for all joints (\pm SD).

<https://doi.org/10.1371/journal.pone.0213064.g006>

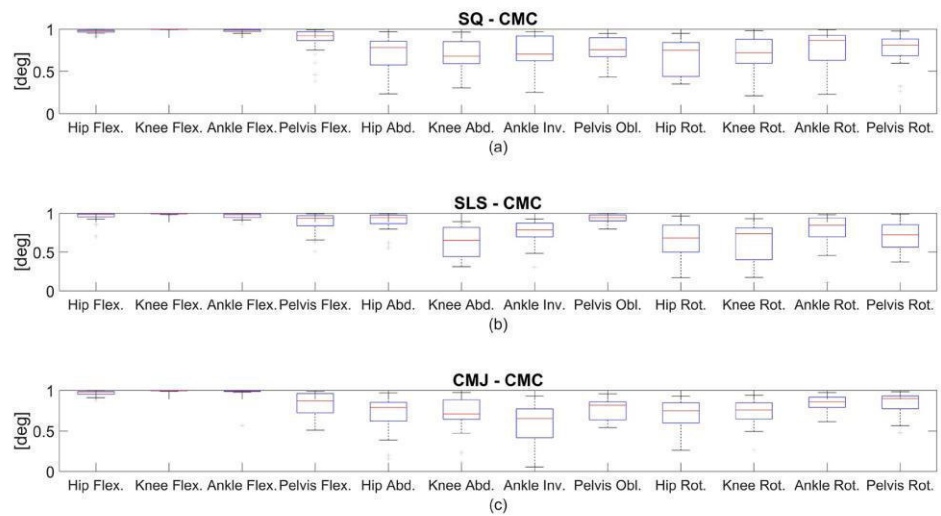


Fig 7. CMC in the skin marker evaluation. CMC of the right lower extremity for all functional movements: (a) indicates SQ, (b) indicates SLS, and (c) indicates CMJ.

<https://doi.org/10.1371/journal.pone.0213064.g007>

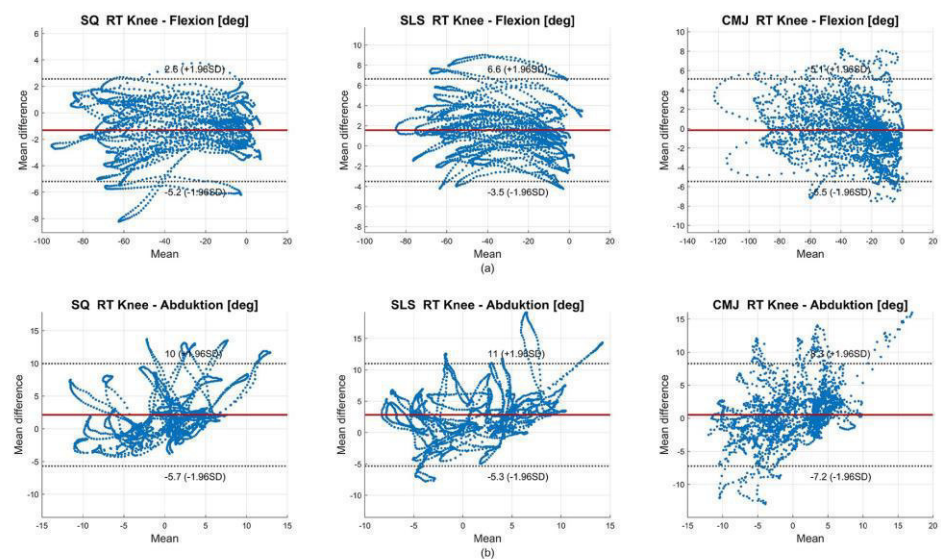


Fig 8. BA diagrams of the right knee flexion (a) and abduction (b) for all subjects in the skin marker evaluation. In (a), negative values on the x-axis indicate knee flexion. In (b), negative values on the x-axis indicate knee adduction. The solid line indicates the mean difference, dashed lines indicate $\pm 1.96 \cdot$ standard deviation (SD).

<https://doi.org/10.1371/journal.pone.0213064.g008>

clinical evaluation of rehabilitation progresses, for example [47]. The remaining knee joint angles seemed equally distributed within their limits.

4.2 Skin marker evaluation

The secondary validation of the IMU data revealed results distinctively inferior to the RMC evaluation. RMSE and ROME increased on average by approximately 2° to 3° for all tasks. The increase of the statistical error measures between the two evaluation methods was mainly associated to different effects of STA on the two systems due to the unrelated positioning of the skin markers and the IMU on the segments.

The BA analysis showed wider limits but only slightly higher mean differences. As shown in Fig 8, the data points of right knee flexion in all tasks seemed equally distributed between the limits. However, right knee abduction in all tasks tended to be overestimated by the IMU data, whereas the knee adduction tended to be underestimated.

In the skin marker evaluation, the hip flexion joint angle revealed the highest errors in the SQ and CMJ tasks. These findings are comparable to the results shown by Al-Amri et al. [14]. They found deviations of the maximum sagittal joint angle of the hip between IMU and OMC systems in the SQ and jumping tasks of approximately above 20°. However, Al-Amri et al. [14] found a static offset in their kinematic data, especially in hip flexion as well as knee and ankle rotation. An offset in the hip flexion occurred in the present study as well (S4 Fig). This might explain the rather poor results concerning the RMSE. However, CMC of the hip flexion revealed excellent correlations.

The relatively good results of the knee joint angles indicated that the offset concerning the hip sagittal joint angle did not originate from the IMU attached to the thigh. However, it appeared that the pelvis' global sagittal angle also exhibited an offset, which directly influences the hip joint angle. However, the RMC evaluation showed no offset between the OMC and IMU data. Furthermore, the RMSE and ROME of the hip flexion in the SLS task revealed lower values compared to the SQ and CMJ tasks. Examination showed that the pelvis flexion ROM of the SLS was approximately 7.84° smaller than in the SQ task. In this case, it could have been that the skin marker based OMC system was more influenced by STA than the IMU data because markers attached to the left and right Spina Iliaca Anterior Superior were more prone to STA during increased pelvis and hip flexion. Fiorentino et al. [48] previously showed that the hip joint angle of the OMC systems based on skin markers is significantly influenced by STA, using dual fluoroscopy as a reference. They stated that the ROM of the skin marker based measurement was reduced compared to dual fluoroscopy. This is consistent with the present findings. The ROM of the hip flexion of the RMC-based OMC joint kinematics calculation was approximately 8° higher than in the skin marker based calculation, concerning the SQ task. However, the IMU based ROM calculation of the hip flexion showed similar values compared to the RMC alternative. As mentioned above, the RMC based joint kinematics calculation was shown to reveal results more immune to STA compared to joint kinematics for markers attached to anatomical landmarks [30]. Thus, the RMC calculation was considered the gold standard reference in this study. It should be considered that the susceptibility to STA of the RMC depends on their positioning on the regarding segments. However, the primary evaluation of this study focused on the performance of the sensor-fusion algorithm. In this case, accuracy should not have been sensitive to variations in the IMU placement since IMU and RMC were rigidly connected. However, future studies should investigate the effects of different IMU placement on the accuracy of 3D joint kinematics.

The RMC evaluation revealed differences between the tasks regarding the RMSE and ROME of the sagittal plane joint angle. However, in the skin marker evaluation, the hip flexion RMSE

and ROME of the SQ task for the left lower extremity were higher than in the CMJ task. This could again be due to the above-mentioned susceptibility of the hip joint angle based on four markers to STA. However, differences in the error measures were around 1° between the tasks.

There are few studies that have examined the validity of IMU-derived 3D joint kinematics of dynamic tasks. Fasel et al. [31] analyzed the validity of IMU data during indoor skiing. However, their examination was performed on an indoor skiing carpet operator, thus ignoring global locomotion. They found ROME for hip and knee joint angles of 10.7° and 0.1° in the sagittal plane, 3.3° and 4.2° in the frontal plane, and 0.5° and 0.0° in the transversal plane. Thus, their results are more accurate concerning the transversal plane and the sagittal plane of the knee joint. Interestingly, the ROME regarding the hip flexion was similarly high compared to that of the present study. However, both studies differ concerning the method for joint kinematics estimation. While both studies used only gyroscope and accelerometer data for IMU joint kinematics estimation, Fasel et al. [31] also introduced a functional calibration method and initialized segment orientation using a strap down integration and joint drift reduction according to Fasel et al. [49]. In contrast, the present study obtained the calibration and segment orientation initialization of the OMC system, excluding errors regarding these issues.

5 Conclusion

In conclusion, the examined sensor-fusion algorithm for the calculation of IMU-based joint kinematics showed excellent correspondence with an OMC system in all three functional movements, when considering the technical error. The most dynamic task, the CMJ, showed slightly higher values for RMSE (below 3°), and ROME (below 2.5°), given a limited measurement rate of 60 Hz.

For skin markers, which are influenced by different STA compared to the IMU, the error measures increased mostly concerning the hip joint angle in the sagittal plane. However, it should be kept in mind that the reference system itself suffers from STA and uncertainties due to marker positioning. The findings mentioned above indicate that in certain cases, compared to OMC joint kinematics based on skin markers, IMU data could deliver more confident results. However, these suggestions need to be confirmed by conducting validation studies using dual fluoroscopy or comparable systems as a reference [50]. Additionally, further studies are necessary to add stepwise IMU information to the joint kinematics calculation (i.e., an IMU-to-segment calibration, initialization from IMU data and a biomechanical model based on anthropometric tables). It is critical to separate the magnitude of error associated with each of these issues. Nevertheless, the present examination revealed results that encourage the continued research and development of an IMU system aimed at applications in rehabilitative and sports medical contexts.

Supporting information

S1 Fig. Mean sagittal plane right joint angle waveforms. Joint angle waveforms of the sagittal plane of the rigid marker cluster (RMC) evaluation of one exemplary subject. Solid lines show the joint angles of the optical motion capture system (OMC), and dashed lines show the joint angles of the inertial measurement system (IMU).

(TIF)

S2 Fig. Mean frontal plane right joint angle waveforms. Joint angle waveforms of the frontal plane of the RMC evaluation of one exemplary subject. Solid lines show the joint angles of the OMC, and dashed lines show the joint angles of the IMU.

(TIF)

S3 Fig. Mean transversal plane right joint angle waveforms. Joint angle waveforms of the transversal plane of the RMC evaluation of one exemplary subject. Solid lines show the joint angles of the OMC, and dashed lines show the joint angles of the IMU.
(TIF)

S4 Fig. Mean sagittal plane right joint angle waveforms. Joint angle waveforms of the sagittal plane of the skin marker evaluation of one exemplary subject. Solid lines show the joint angles of the OMC, and dashed lines show the joint angles of the IMU.
(TIF)

S5 Fig. Mean frontal plane right joint angle waveforms. Joint angle waveforms of the frontal plane of the skin marker evaluation of one exemplary subject. Solid lines show the joint angles of the OMC, and dashed lines show the joint angles of the IMU.
(TIF)

S6 Fig. Mean transversal plane right joint angle waveforms. Joint angle waveforms of the transversal plane of the skin marker evaluation of one exemplary subject. Solid lines show the joint angles of the OMC, and dashed lines show the joint angles of the IMU.
(TIF)

Acknowledgments

The authors would like to thank Gregor Zolynski for constructing and crafting the 3D printed boxes for the inertial measurement units.

This work was performed by the Interdisciplinary Junior Research Group wearHEALTH, funded by the BMBF (16SV7115, 03IHS075B). For more information, please visit the website www.wearhealth.org.

Author Contributions

Conceptualization: Wolfgang Teufl, Bertram Taetz, Michael Fröhlich, Gabriele Bleser.

Data curation: Wolfgang Teufl, Markus Miezal, Bertram Taetz, Gabriele Bleser.

Formal analysis: Wolfgang Teufl, Gabriele Bleser.

Investigation: Gabriele Bleser.

Project administration: Wolfgang Teufl, Michael Fröhlich, Gabriele Bleser.

Software: Markus Miezal, Gabriele Bleser.

Supervision: Michael Fröhlich, Gabriele Bleser.

Writing – original draft: Wolfgang Teufl.

Writing – review & editing: Wolfgang Teufl, Markus Miezal, Michael Fröhlich, Gabriele Bleser.

References

1. Cook G, Burton L, Hoogenboom BJ, Voight M. FUNCTIONAL MOVEMENT SCREENING: THE USE OF FUNDAMENTAL MOVEMENTS AS AN ASSESSMENT OF FUNCTION—PART 1. *Int J Sports Phys Ther.* 2014; 9: 396–409. PMID: [24944860](https://pubmed.ncbi.nlm.nih.gov/24944860/)
2. Brauner T, Wearing S, Rämisch E, Zilliber M, Horstmann T. Can Measures of Limb Loading and Dynamic Stability During the Squat Maneuver Provide an Index of Early Functional Recovery After Unilateral Total Hip Arthroplasty? *Arch Phys Med Rehabil.* 2014; 95: 1946–1953. <https://doi.org/10.1016/j.apmr.2014.06.003> PMID: [24953251](https://pubmed.ncbi.nlm.nih.gov/24953251/)

3. de Baldon RM, Piva SR, Scattoni Silva R, Serrão FV. Evaluating Eccentric Hip Torque and Trunk Endurance as Mediators of Changes in Lower Limb and Trunk Kinematics in Response to Functional Stabilization Training in Women With Patellofemoral Pain. *Am J Sports Med.* 2015; 43: 1485–1493. <https://doi.org/10.1177/0363546515574690> PMID: 25790834
4. Weeks BK, Carty CP, Horan SA. Kinematic predictors of single-leg squat performance: a comparison of experienced physiotherapists and student physiotherapists. *BMC Musculoskelet Disord.* 2012; 13: 207. <https://doi.org/10.1186/1471-2474-13-207> PMID: 23098061
5. Gathercole R, Sporer B, Stellingwerff T, Sleivert G. Alternative Countermovement-Jump Analysis to Quantify Acute Neuromuscular Fatigue. *Int J Sports Physiol Perform.* 2015; 10: 84–92. <https://doi.org/10.1123/ijspp.2013-0413> PMID: 24912201
6. Menzel H-J, Chagas MH, Szmuchrowski LA, Araujo SRS, de Andrade AGP, de Jesus-Moraleida FR. Analysis of Lower Limb Asymmetries by Isokinetic and Vertical Jump Tests in Soccer Players: J Strength Cond Res. 2013; 27: 1370–1377. <https://doi.org/10.1519/JSC.0b013e318265a3c8> PMID: 22796999
7. Kianifar R, Lee A, Raina S, Kulic D. Automated Assessment of Dynamic Knee Valgus and Risk of Knee Injury During the Single Leg Squat. *IEEE J Transl Eng Health Med.* 2017; 5: 1–13. <https://doi.org/10.1109/JTEHM.2017.2736559> PMID: 29204327
8. McPherson AL, Dowling B, Tubbs TG, Paci JM. Sagittal plane kinematic differences between dominant and non-dominant legs in unilateral and bilateral jump landings. *Phys Ther Sport.* 2016; 22: 54–60. <https://doi.org/10.1016/j.ptsp.2016.04.001> PMID: 27583649
9. Leardini A, Chiari L, Croce UD, Cappozzo A. Human movement analysis using stereophotogrammetry. *Gait Posture.* 2005; 21: 212–225. <https://doi.org/10.1016/j.gaitpost.2004.05.002> PMID: 15639400
10. Picerno P. 25 years of lower limb joint kinematics by using inertial and magnetic sensors: A review of methodological approaches. *Gait Posture.* 2017; 51: 239–246. <https://doi.org/10.1016/j.gaitpost.2016.11.008> PMID: 27833057
11. McGinnis RS, Cain SM, Davidson SP, Vitali RV, Perkins NC, McLean SG. Quantifying the effects of load carriage and fatigue under load on sacral kinematics during countermovement vertical jump with IMU-based method. *Sports Eng.* 2016; 19: 21–34. <https://doi.org/10.1007/s12283-015-0185-3>
12. Setuain I, Martinikorena J, Gonzalez-Izal M, Martinez-Ramirez A, Gómez M, Alfaro-Adrián J, et al. Vertical jumping biomechanical evaluation through the use of an inertial sensor-based technology. *J Sports Sci.* 2015; 34: 843–851. <https://doi.org/10.1080/02640414.2015.1075057> PMID: 26256752
13. Picerno P, Camomilla V, Capranica L. Countermovement jump performance assessment using a wearable 3D inertial measurement unit. *J Sports Sci.* 2011; 29: 139–146. <https://doi.org/10.1080/02640414.2010.523089> PMID: 21120742
14. Al-Amri M, Nicholas K, Button K, Sparkes V, Sheeran L, Davies JL. Inertial Measurement Units for Clinical Movement Analysis: Reliability and Concurrent Validity. *Sensors.* 2018; 18: 719. <https://doi.org/10.3390/s18030719> PMID: 29495600
15. Kluge F, Gaßner H, Hannink J, Pasluosta C, Klucken J, Eskofier BM. Towards Mobile Gait Analysis: Concurrent Validity and Test-Retest Reliability of an Inertial Measurement System for the Assessment of Spatio-Temporal Gait Parameters. *Sensors.* 2017; 17. <https://doi.org/10.3390/s17071522> PMID: 28657587
16. Nüesch C, Roos E, Pagenstert G, Mündermann A. Measuring joint kinematics of treadmill walking and running: Comparison between an inertial sensor based system and a camera-based system. *J Biomech.* 2017; 57: 32–38. <https://doi.org/10.1016/j.jbiomech.2017.03.015> PMID: 28366438
17. Zhang J-T, Novak AC. Concurrent validation of Xsens and MVN measurement of lower limb joint angular kinematics. *Physiol Meas.* 2013; 34.
18. Teufel W, Miezal M, Taetz B, Fröhlich M, Bleser G. Validity, Test-Retest Reliability and Long-Term Stability of Magnetometer Free Inertial Sensor Based 3D Joint Kinematics. *Sensors.* 2018; 18: 1980. <https://doi.org/10.3390/s18071980> PMID: 29933568
19. Robert-Lachaine X, Mecheri H, Larue C, Plamondon A. Validation of inertial measurement units with an optoelectronic system for whole-body motion analysis. *Med Biol Eng Comput.* 2017; 55: 609–619. <https://doi.org/10.1007/s11517-016-1537-2> PMID: 27379397
20. Miezal M, Taetz B, Bleser G. On Inertial Body Tracking in the Presence of Model Calibration Errors. *Sensors.* 2016; 16: 1132. <https://doi.org/10.3390/s16071132> PMID: 27455266
21. Miezal M, Taetz B, Bleser G. Real-time inertial lower body kinematics and ground contact estimation at anatomical foot points for agile human locomotion. 2017 IEEE International Conference on Robotics and Automation (ICRA). 2017. pp. 3256–3263.

22. Benoit DL, Damsgaard M, Andersen MS. Surface marker cluster translation, rotation, scaling and deformation: Their contribution to soft tissue artefact and impact on knee joint kinematics. *J Biomech.* 2015; 48: 2124–2129. <https://doi.org/10.1016/j.jbiomech.2015.02.050> PMID: 25935684
23. Forner-Cordero A, Mateu-Arce M, Forner-Cordero I, Alcántara E, Moreno JC, Pons JL. Study of the motion artefacts of skin-mounted inertial sensors under different attachment conditions. *Physiol Meas.* 2008; 29: N21–N31. PMID: 18401071
24. Fiorentino NM, Atkins PR, Kutschke MJ, Goebel JM, Foreman KB, Anderson AE. Soft tissue artifact causes significant errors in the calculation of joint angles and range of motion at the hip. *Gait Posture.* 2017; 55: 184–190. <https://doi.org/10.1016/j.gaitpost.2017.03.033> PMID: 28475981
25. Barré A, Jolles BM, Theumann N, Aminian K. Soft tissue artifact distribution on lower limbs during treadmill gait: Influence of skin markers' location on cluster design. *J Biomech.* 2015; 48: 1965–1971. <https://doi.org/10.1016/j.jbiomech.2015.04.007> PMID: 25920897
26. Bonnet V, Richard V, Camomilla V, Venture G, Cappozzo A, Dumas R. Joint kinematics estimation using a multi-body kinematics optimisation and an extended Kalman filter, and embedding a soft tissue artefact model. *J Biomech.* 2017; 62: 148–155. <https://doi.org/10.1016/j.jbiomech.2017.04.033> PMID: 28551098
27. Cockcroft J, Louw Q, Baker R. Proximal placement of lateral thigh skin markers reduces soft tissue artefact during normal gait using the Conventional Gait Model. *Comput Methods Biomech Biomed Engin.* 2016; 19: 1497–1504. <https://doi.org/10.1080/10255842.2016.1157865> PMID: 26929983
28. Dumas R, Cheze L. Soft tissue artifact compensation by linear 3D interpolation and approximation methods. *J Biomech.* 2009; 42: 2214–2217. <https://doi.org/10.1016/j.jbiomech.2009.06.006> PMID: 19640540
29. Cappello A, Stagni R, Fantozzi S, Leardini A. Soft tissue artifact compensation in knee kinematics by double anatomical landmark calibration: performance of a novel method during selected motor tasks. *IEEE Trans Biomed Eng.* 2005; 52: 992–998. <https://doi.org/10.1109/TBME.2005.846728> PMID: 15977729
30. Angeloni C, Cappozzo A, Catani F, Leardini A. Quantification of relative displacement of skin- and plate-mounted markers with respect to bones. *J Biomech.* 1993;26.
31. Fasel B, Spörri J, Schütz P, Lorenzetti S, Aminian K. Validation of functional calibration and strap-down joint drift correction for computing 3D joint angles of knee, hip, and trunk in alpine skiing. *PLOS ONE.* 2017; 12: e0181446. <https://doi.org/10.1371/journal.pone.0181446> PMID: 28746383
32. Robert-Lachaine X, Mecheri H, Larue C, Plamondon A. Accuracy and repeatability of single-pose calibration of inertial measurement units for whole-body motion analysis. *Gait Posture.* 2017; 54: 80–86. <https://doi.org/10.1016/j.gaitpost.2017.02.029> PMID: 28279850
33. Bergamini E, Ligorio G, Summa A, Vannozzi G, Cappozzo A, Sabatini AM. Estimating orientation using magnetic and inertial sensors and different sensor fusion approaches: accuracy assessment in manual and locomotion tasks. *Sensors.* 2014; 14: 18625–18649. <https://doi.org/10.3390/s141018625> PMID: 25302810
34. Leardini A, Sawacha Z, Paolini G, Ingrosso S, Nativo R, Benedetti MG. A new anatomically based protocol for gait analysis in children. *Gait Posture.* 2007; 26: 560–571. <https://doi.org/10.1016/j.gaitpost.2006.12.018> PMID: 17291764
35. Manal K, McClay I, Stanhope S, Richards J, Galinat B. Comparison of surface mounted markers and attachment methods in estimating tibial rotations during walking: an in vivo study. *Gait Posture.* 2000; 11: 38–45. [https://doi.org/10.1016/S0966-6362\(99\)00042-9](https://doi.org/10.1016/S0966-6362(99)00042-9) PMID: 10664484
36. Manal K, McClay I, Richards J, Galinat B, Stanhope S. Knee moment profiles during walking: errors due to soft tissue movement of the shank and the influence of the reference coordinate system. *Gait Posture.* 2002; 15: 10–17. [https://doi.org/10.1016/S0966-6362\(01\)00174-6](https://doi.org/10.1016/S0966-6362(01)00174-6) PMID: 11809576
37. Cutti AG, Ferrari A, Garofalo P, Raggi M, Cappello A, Ferrari A. 'Outwalk': a protocol for clinical gait analysis based on inertial and magnetic sensors. *Med Biol Eng Comput.* 2009; 48: 17–25. <https://doi.org/10.1007/s11517-009-0545-x> PMID: 19911214
38. Eie M, Wei C-S. Generalizations of Euler decomposition and their applications. *J Number Theory.* 2013; 133: 2475–2495. <https://doi.org/10.1016/j.jnt.2013.01.010>
39. Bland JM, Altman DG. Measuring agreement in method comparison studies. *Stat Methods Med Res.* 1999; 8: 135–160. <https://doi.org/10.1177/096228029900800204> PMID: 10501650
40. Bland JM, Altman DG. Agreement Between Methods of Measurement with Multiple Observations Per Individual. *J Biopharm Stat.* 2007; 17: 571–582. <https://doi.org/10.1080/10543400701329422> PMID: 17613642

41. Ferrari A, Cutti AG, Cappello A. A new formulation of the coefficient of multiple correlation to assess the similarity of waveforms measured synchronously by different motion analysis protocols. *Gait Posture*. 2010; 31: 540–542. <https://doi.org/10.1016/j.gaitpost.2010.02.009> PMID: 20303272
42. Koo TK, Li MY. A Guideline of Selecting and Reporting Intraclass Correlation Coefficients for Reliability Research. *J Chiropr Med*. 2016; 15: 155–163. <https://doi.org/10.1016/j.jcm.2016.02.012> PMID: 27330520
43. Elvin NG, Elvin AA, Arnoczky SP. Correlation between ground reaction force and tibial acceleration in vertical jumping. *J Appl Biomech*. 2007; 23: 180–189. PMID: 18089915
44. Thewlis D, Bishop C, Daniell N, Paul G. Next-generation low-cost motion capture systems can provide comparable spatial accuracy to high-end systems. *J Appl Biomech*. 2013; 29: 112–117. PMID: 22813783
45. Lebel K, Boissy P, Nguyen H, Duval C. Inertial measurement systems for segments and joints kinematics assessment: towards an understanding of the variations in sensors accuracy. *Biomed Eng OnLine*. 2017; 16. <https://doi.org/10.1186/s12938-017-0347-6> PMID: 28506273
46. Giavarina D. Understanding Bland Altman analysis. *Biochem Medica*. 2015; 25: 141–151. <https://doi.org/10.11613/BM.2015.015> PMID: 26110027
47. Davis KE, Ritter MA, Berend ME, Meding JB. The Importance of Range of Motion after Total Hip Arthroplasty. *Clin Orthop*. 2007; 5.
48. Fiorentino NM, Atkins PR, Kutschke MJ, Goebel JM, Foreman KB, Anderson AE. Soft tissue artifact causes significant errors in the calculation of joint angles and range of motion at the hip. *Gait Posture*. 2017; 55: 184–190. <https://doi.org/10.1016/j.gaitpost.2017.03.033> PMID: 28475981
49. Fasel B, Sporri J, Chardonnes J, Kroll J, Muller E, Aminian K. Joint Inertial Sensor Orientation Drift Reduction for Highly Dynamic Movements. *IEEE J Biomed Health Inform*. 2017; 1–1. <https://doi.org/10.1109/jbhi.2017.2659758> PMID: 28141537
50. Peters A, Galna B, Sangeux M, Morris M, Baker R. Quantification of soft tissue artifact in lower limb human motion analysis: A systematic review. *Gait Posture*. 2010; 31: 1–8. <https://doi.org/10.1016/j.gaitpost.2009.09.004> PMID: 19853455

Supplementary File of the Journal Paper 2

Joint angle calculation from optical markers and IMUs attached to the lower body

The purpose of this protocol was to clarify the derivation of joint angles from both inertial measurement units (IMU system) and an optical motion capture (OMC) system as used in the article “Validity of inertial sensor based 3D joint kinematics of static and dynamic sport and physiotherapy specific movements”.

Notation

In this protocol, a rotation from coordinate frame B to frame A was denoted R^{AB} , where $(R^{AB})^T = R^{BA}$ was the inverse rotation. Rotations were parametrized as quaternions; e.g. q^{AB} was the quaternion representation of R^{AB} . The vector B^A denoted the location of the origin of coordinate frame B given in A . The vector p_i^A denoted the i^{th} point in coordinate frame A .

Physical setup

The physical setup is shown in Figure 1. Retroreflective markers were placed on a participant according to the protocol provided in Leardini et al. [1]. The segment coordinate systems (S) were created from the tracked 3D marker positions (NaturalPoint OptiTrack, 12 cameras) according to Cappozzo et al. [2]. For each segment S_i , the 3D positions of the associated markers and joint centers were denoted $p_i^{S_i} \in P^{S_i}$ (Figure 1 “Points in coordinate frame S_i ”). Each IMU was rigidly mounted in a 3D printed casing with four retroreflective markers attached to it (Figure 2). The markers were combined to rigid bodies using the OMC system and the positions B^G and orientations q^{GB} of the associated coordinate systems B with respect to the reference frame G were provided by the OMC system along with the single marker positions. Note, G was defined through the initial OMC system calibration and it was leveled so that z^G opposes gravity. Hence, G denotes both the OMC and the IMU reference frame. IMU measurements were provided in coordinate system I , which was assumed in the physical location of the accelerometer triad. Note, the marker rigid body coordinate systems were constructed so that their origins coincide with the origins of the associated IMU coordinate frames.

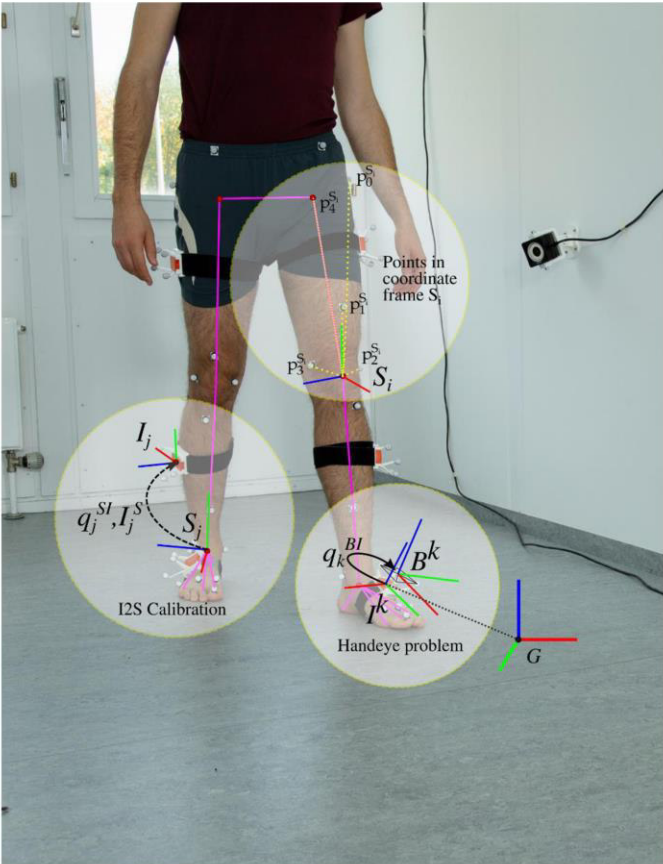


Figure 1: Coordinate systems and biomechanical model.

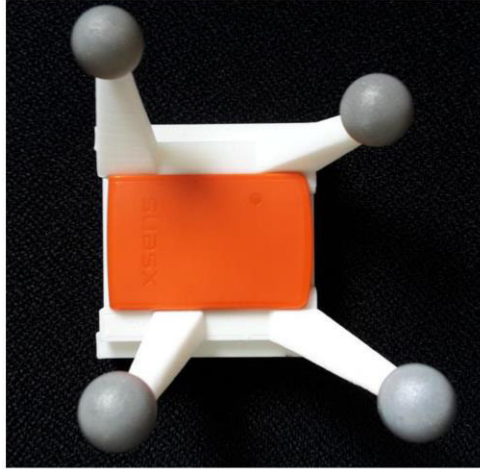


Figure 2: Inertial measurement unit inserted in 3D printed casing with four retroreflective markers

Segment pose estimation from OMC data

Let $S_{i,t}^G, q_{i,t}^{GS}$ be the sought global position and orientation of segment i at time t . This transformation was defined through a set of $n \geq 3$ linearly independent 3D point correspondences, i.e. the marker positions in the local segment coordinate frame $\{p_{1:n}^{S_i}\}$ and their observed positions in $G \{p_{i,j,t}^G\}$ as provided by the OMC system (Figure 1). The complete trajectory of segment i (i.e. the pose of each frame $t = 1..m$) was then obtained by minimizing:

$$\{S_{i,t}^G, q_{i,t}^{GS}\}_{t=1}^m = \underset{\{S_{i,t}^G, q_{i,t}^{GS}\}_{t=1}^m}{\operatorname{argmin}} \sum_{t=1}^m \operatorname{err}(S_{i,t})$$

with:

$$\operatorname{err}(S_{i,t}) = \sum_{j=1}^n \left\| S_{i,t}^G + R_{i,t}^{GS} p_j^{S_i} - p_{i,j,t}^G \right\|_2$$

When calculating this for each segment independently, the segments will likely not stay connected at the joints during the estimated movement. To enforce this, joint constraints were added to the optimization problem. As stated above, joint centers were, just like skin markers, defined as points in the local segment coordinate frames. A joint was defined as a four tuple of indices $J = \{i, j, k, l\}$ carrying the information that $p_j^{S_i}$ and $p_l^{S_k}$ should be connected in the global frame G . If $J_p = \{i, j, k, l\}$ is the p^{th} joint in the biomechanical model, the joint center distance at time t was:

$$\operatorname{err}(J_{p,t}) = \left\| p_{i,j,t}^G - p_{k,l,t}^G \right\|_2 = \left\| S_{i,t}^G + R_{i,t}^{GS} p_j^{S_i} - S_{k,t}^G + R_{k,t}^{GS} p_l^{S_k} \right\|_2$$

The resulting constrained optimization problem for deriving the movement of the complete biomechanical model including s segments connected through k joints at m frames was:

$$\{S_{i,t}^G, q_{i,t}^{GS}\}_{i=1,t=1}^{s,m} = \operatorname{argmin}_{\{S_{i,t}^G, q_{i,t}^{GS}\}_{i=1,t=1}^{s,m}} \sum_{t=1}^m \left(\sum_{j=1}^s \operatorname{err}(S_{j,t}) + \lambda \sum_{p=1}^k \operatorname{err}(J_{p,t}) \right)$$

where λ was a weight parameter to adjust the influence of the joint constraints. The above described calculations follow the definitions of Visual3D (C-Motion, Inc, Germantown, MD, USA), a widely used software tool for 3D biomechanics research. Choosing $\lambda = 0.01$ showed the best correspondence to segment poses obtained from Visual3D.

Handeye estimation

In this protocol, the handeye problem refers to the problem of calculating the rigid transformations between I and B for each IMU/rigid body pair. This was required for being able to relate the IMU measurements to the OMC rigid body data (Figure 1 “Handeye problem”). It was subsequently used for obtaining the IMU-to-segment (I2S) calibrations from the OMC data as well as for initializing the sensor fusion method for segment pose estimation from the IMU measurements. Since the origins of I and B coincided (as mentioned above), this came down to calculating the orientations q^{BI} for each IMU/rigid body pair. This was done based on a synchronized sequence of angular velocities ω^I measured by the IMUs and angular velocities ω^B derived from the marker rigid body orientations (first derivative), with $\omega^B = q^{BI}\omega^I$, according to the method proposed in Chardonnes et al. [3]. The data sequence was obtained by mounting the casings containing the IMUs on a bar and rotating the bar in all directions in the tracking volume.

I2S Calibration

The IMU-to-segment (I2S) calibration refers to the relative orientation q^{SI} between the IMU and the segment it is attached to (Figure 1 “I2S Calibration”). In order to exclude errors due to pose based or functional calibration methods, in this protocol, the I2S calibration was extracted from a static neutral pose sequence by exploiting the OMC data and the above described handeye orientation. The I2S orientation was:

$$R^{SI} = R^{SG}R^{GB}R^{BI}$$

where R^{SG} was the OMC segment orientation, R^{GB} was the OMC rigid body orientation and R^{BI} was the handeye orientation. Note, the indices are omitted since every segment was assumed to have one IMU attached to it. The I2S position was:

$$I^S = B^S = R^{SG}(B^G - S^G)$$

where B^G was the global rigid body position and S^G was the global segment position. In this protocol, the calibration was assumed to be fix. Thus, OMC based global segment orientations could be either obtained using the skin markers and the optimization based method described above, or they could be deduced from the rigid body orientations using:

$$R^{GS} = R^{GB}R^{BI}R^{IS}$$

Segment pose estimation from IMU data

The sensor fusion method for estimating the segment poses from IMU data assuming known I2S calibrations and known initial IMU poses was completely described in Teufl et al. [4]. As for the I2S calibrations, in this protocol, the initial IMU poses were obtained from the OMC data and the above described handeye transformation.

Joint angle decomposition

A joint orientation was here defined as the relative orientation between the connected segments; e.g. the right hip orientation was:

$$q_{RightHip}^{SS} = q_{Pelvis}^{SG} \odot q_{RightUpperLeg}^{GS}$$

where the global segment orientations were obtained using one of the methods above (OMC skin markers, OMC rigid bodies, IMU). The joint angles were then obtained by decomposing the relative joint orientations according to the coordinate system definitions in Cappozzo et al. [2] and the decomposition order proposed in Visual3D, i.e. flexion (θ_z) followed by abduction (θ_x) followed by internal rotation (θ_y). The Euler angle decomposition is taken from [5].

References

1. Leardini A, Sawacha Z, Paolini G, Ingrosso S, Nativo R, Benedetti MG. A new anatomically based protocol for gait analysis in children. *Gait Posture*. 2007;26: 560–571. doi:10.1016/j.gaitpost.2006.12.018
2. Cappozzo A, Catani F, Croce UD, Leardini A. Position and orientation in space of bones during movement: anatomical frame definition and determination. *Clin Biomech*. 1995;10: 171–178. doi:10.1016/0268-0033(95)91394-t
3. Chardonens J, Favre J, Aminian K. An effortless procedure to align the local frame of an inertial measurement unit to the local frame of another motion capture system. *J Biomech*. 2012;45: 2297–2300. doi:10.1016/j.jbiomech.2012.06.009
4. Teufl W, Miezal M, Taetz B, Fröhlich M, Bleser G. Validity, Test-Retest Reliability and Long-Term Stability of Magnetometer Free Inertial Sensor Based 3D Joint Kinematics. *Sensors*. 2018;18: 1980. doi:10.3390/s18071980
5. Eie M, Wei C-S. Generalizations of Euler decomposition and their applications. *J Number Theory*. 2013;133: 2475–2495. doi:10.1016/j.jnt.2013.01.010

3.2 *Validation of the Gait Event Detection and the Spatio-Temporal Parameters*

3.2.1 Journal Paper 3

Summary

The JP 3 is concerned with the IMU based estimation of gait-specific events, IC and TC, as well as the calculation of a wide range of STP within a group of young and healthy subjects. The approach, described in that article, implies a successful joint kinematics estimation, comparable to JP 1 and 2, as well as the knowledge of a biomechanical model incorporating AL. This allows for the calculation of a huge set of parameters, including more complex spatial parameters like step width or swing width. However, that implies a set-up incorporating seven IMUs.

In this JP the joint kinematics estimation incorporates purely IMU data (Procedure 3), introducing an IMU based I2S calibration and a biomechanical model based on anthropometric tables. Therefore, the IMU system for STP estimation presented in this article can be considered a stand-alone system.

In this work the validity and reliability of the kinematics based gait event estimation and STP calculation is compared with the OMC system.

Main Contributions

- Kinematics of the lower body calculated using only inertial data, pose based I2S calibration and a biomechanical model based on anthropometric tables
- IC and TC estimation using a kinematics based approach
- Calculation of twelve STP including step length, step width and swing width



Article

Towards Inertial Sensor Based Mobile Gait Analysis: Event-Detection and Spatio-Temporal Parameters

Wolfgang Teufl ^{1,2,*} , Michael Lorenz ¹, Markus Miezal ¹, Bertram Taetz ¹, Michael Fröhlich ² 
and Gabriele Bleser ¹ 

¹ Junior Research Group wearHEALTH, Technische Universität Kaiserslautern, Gottlieb-Daimler-Str. 48, 67663 Kaiserslautern, Germany; lorenz@cs.uni-kl.de (M.L.); miezal@cs.uni-kl.de (M.M.); taetz@informatik.uni-kl.de (B.T.); bleser@informatik.uni-kl.de (G.B.)

² Department of Sports Science, Technische Universität Kaiserslautern, Erwin-Schrödinger-Str. 57, 67663 Kaiserslautern, Germany; michael.froehlich@sowi.uni-kl.de

* Correspondence: teufl@cs.uni-kl.de; Tel.: +49-631-205-3332

Received: 24 October 2018; Accepted: 19 December 2018; Published: 22 December 2018



Abstract: The aim of this study was to assess the validity and test-retest reliability of an inertial measurement unit (IMU) system for gait analysis. Twenty-four healthy subjects conducted a 6-min walking test and were instrumented with seven IMUs and retroreflective markers. A kinematic approach was used to estimate the initial and terminal contact events in real-time. Based on these events twelve spatio-temporal parameters (STP) were calculated. A marker based optical motion capture (OMC) system provided the reference. Event-detection rate was about 99%. Detection offset was below 0.017 s. Relative root mean square error (RMSE) ranged from 0.90% to 4.40% for most parameters. However, the parameters that require spatial information of both feet showed higher errors. Step length showed a relative RMSE of 6.69%. Step width and swing width revealed the highest relative RMSE (34.34% and 35.20%). Test-retest results ranged from 0.67 to 0.92, except for the step width (0.25). Summarizing, it appears that the parameters describing the lateral distance between the feet need further improvement. However, the results of the validity and reliability of the IMU system encourage its validation in clinical settings as well as further research.

Keywords: accelerometer; gyroscope; inertial measurement unit; ambulatory motion analysis; gait parameters; wearable sensors

1. Introduction

Gait analysis is an important tool in the evaluation of operative procedures [1,2], rehabilitation progress [3], or the assessment of the motor status in neurologically impaired patients [4,5]. There are various parameters that are of interest such as joint kinematics (JK), spatio-temporal parameters (STP), joint forces, pressure distributions, and muscle activities. There are also various systems for the measurement/estimation of the above mentioned variables. However, most systems are specialized on the measurement of a subset of these parameters. Few systems can cover a wide range of parameters. For the measurement of 3D JK and STP it is common to use a marker based optical motion capture (OMC) system in combination with force or pressure plates [6,7]. However, OMC systems tend to be expensive, laboratory-bound and their usage tends to be time consuming and needs expert knowledge. The introduction of inertial measurement units (IMU) and magnetic inertial measurement units (MIMU) in the motion analysis [8,9] presented the research community with a wide range of possibilities in the assessment of gait.

IMU/MIMU systems are used to calculate 3D JK in different settings [10–12] and IMU/MIMU derived STP are increasingly discussed in recent literature [13,14]. Caldas et al. [14] reported that

event-detection, initial contact (IC) and terminal contact (TC), and its robustness and delay are important factors when calculating STP, especially in real-time applications. They further state that an IC accuracy of only 90% could be achieved when using only a gyroscope. However, detection accuracy was improved when additionally incorporating accelerometer data. Seel et al. [15] and Müller et al. [16] introduced an online gait phase detection algorithm with automatic adaptation to gait velocity changes based on one foot/shoe-mounted IMU. The mounting orientation on the foot is arbitrary. They also tested their algorithm with healthy people as well as with transfemoral amputees with a leg prosthesis and stroke patients.

There are already numerous IMU/MIMU systems based on one or two sensors [4,15–18]. However, these systems deliver mostly STP that incorporate the spatial information of one foot, stride length, stride time, stance time, or swing time. Parameters that depend on the spatial relation of both feet, e.g., step length and step width, are more complex to calculate and therefore there is a paucity of literature on this problem [18–21].

Takeda et al. [20] developed the IMU based system “H-Gait”. A kinematic approach based on seven IMUs which is able to deliver 3D JK and STP including step length and step width. However, in the validation of “H-Gait” [22] only sagittal angles and temporal parameters are mentioned. Köse et al. [19] used a single IMU attached to the sacrum to calculate left and right step length. However, this approach was specialized on the estimation of step length and step duration only. Cimolin et al. [23] also installed a single IMU on the lower back of 18 normal and obese subjects for the estimation of stride and step length. The step length was calculated based on an inverted pendulum model. However, Cimolin et al. [23] did not report results for the step length. Bertuletti et al. [21] developed a device consisting of an infrared time of flight proximity sensor and an MIMU to measure the distance between the feet at swing-through. This approach was validated with a mechanical pendulum and a small sample of one human subject. However, this apparatus needs a rather complex set-up procedure.

In general, there are few validated systems that deliver 3D joint kinematics and STP [22–25]. One commercial MIMU system, consisting of two or seven MIMUs offers the possibility of measuring a collection of STP as well as the sagittal joint angles of hip, knee, and ankle. This system was validated by Nüesch et al. [24] and Donath et al. [25,26].

The intention of the authors is the development of an IMU system for complex 3D gait analysis, delivering full 3D JK of the lower limbs and pelvis and a wide range of STP including parameters that depend on the spatial information of one as well as both feet. In addition, the present system features real-time event-detection and kinematic estimation, which is relevant in different applications; e.g., it provides the possibility of online feedback coupled to specific gait events/phases and related kinematic parameters for supporting gait interventions in clinical settings, see [27] for a review. Shull et al. [28] provided real-time vibrotactile feedback on multiple kinematic parameters (foot progression angle, tibia angle, trunk sway) measured through an OMC system to support gait retraining for knee osteoarthritis patients. In [29], vibrotactile feedback was coupled to gait events measured through insoles for supporting stroke patients in improving their gait symmetry. Crea et al. [30] restored the somatosensory feedback of special gait events in transfemoral amputees via vibrating elements on the thigh. These were controlled through the detection of gait events via pressure insoles. Another application concerns the real-time control of neuroprostheses as proposed, e.g., in Seel et al. [31] and Valtin et al. [32]. They developed a tool for foot eversion/inversion control and selective muscle activation in patients with drop foot. Their approach was based on the IMU derived kinematics of the foot. All of these applications require accurate and real-time estimation/detection of kinematic parameters and/or gait events.

A validation of the 3D JK calculated based on an initial version of the system used in this study was recently published [33]. Therefore, it is the continuative aim of this study to validate the accuracy of IMU based event-detection and STP, both calculated using a kinematic model approach.

A test session consisted of one 6-min walk test. Prior to the main test a variation of the two-step-calibration poses described by Palermo et al. [35] was conducted. The participants had to maintain a slightly inclined standing position for several seconds and then stand in a neutral zero position for another several seconds (Figure 2). The underlying assumptions are: in the neutral zero pose, all segments are aligned with gravity, the feet are parallel and pointing forward in the sagittal plane, i.e., they are neither outward nor inward rotated. Moreover, it is assumed that between the two poses every segment and IMU is rotated around the frontal body axis only, while the amounts of rotation can differ between segments. Subjects then were asked to walk along a straight line of about 5 m. On both ends of the line, the subjects had about 1 m additional space to turn sharply and then walk the line straight back again. The areas including the turning phases were omitted for the evaluation.

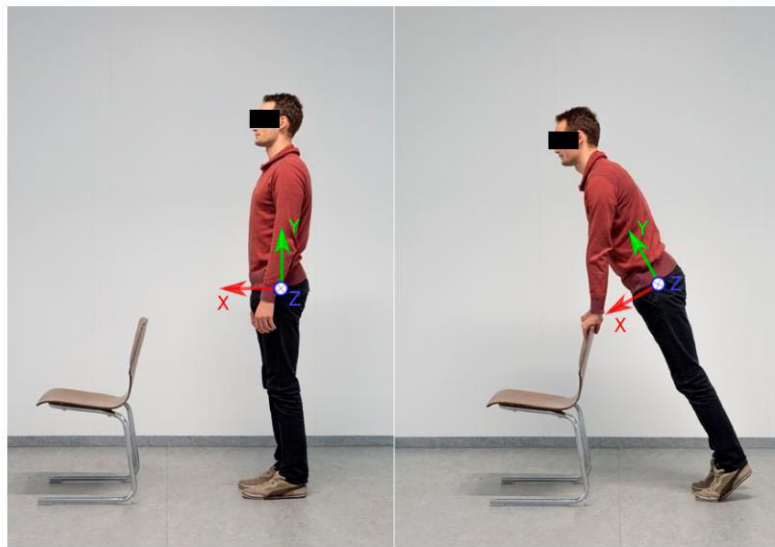


Figure 2. Demonstration of the two-step-calibration process. On the left side the subject is standing in neutral zero position. On the right side, the subject is slightly inclined forward, so that every lower body segment is rotated only around the z-axis shown in the figure (frontal body axis).

IMU and OMC data were hardware-synchronized, using a standard 5V transistor-transistor-logic signal, and recorded at 60 Hz using Xsens MVN Biomech (Version 4.3.7, Xsens Technologies BV, Enschede, The Netherlands) and OptiTrack Motive (Version 1.10.0, NaturalPoint, Inc., Corvallis, OR, USA).

The sensor-fusion method for obtaining the 6 degrees of freedom segment kinematics from the IMU data is summarized in [33] and based on [36,37]. Note, the segment kinematics serve as basis for the gait event-detection as well as for calculating the STP. The magnetometer-free kinematics estimation method fuses gyroscope and accelerometer measurements with assumptions from a per-segment motion model, biomechanical model constraints and environmental constraints in an iterated extended Kalman filter framework. For this, the state contains IMU-centered kinematics (global position, velocity, acceleration, orientation, angular velocity) of all seven lower body segments, which are all jointly estimated. These are related to the segment kinematics via the IMU-to-segment calibrations, which are assumed known and rigid. Note, the resulting coupled estimation of the complete lower body movement was already shown to provide drift-free joint kinematics estimates even without using magnetometer information in [33]. The biomechanical constraints model the fact that the body segments are connected at the joints. For this, the segment lengths are assumed known. The joints are all modeled with 3 degrees of freedom. The environmental constraints consist of estimated ground contacts at virtual foot contact points suggesting zero height and zero velocity pseudo measurements, since a level ground is currently assumed (Figure 3). The probabilistic ground contact estimation

method is carried out in parallel to the kinematics estimation for a set of potential ground contact points as shown in Figure 3, without making any assumptions concerning the type of movement (see [37] for more details). Hence, the segment kinematics estimation method as well as the calculation of the spatio-temporal parameters given the events are generally applicable, while only the chosen event-detection method is specific for gait. Compared to the description in [33], only the noise settings of the connected segments, the zero height and the zero velocity pseudo measurements were changed ($\Sigma^p = 10^{-8} \times I_{3 \times 3}$, $\Sigma^{\dot{p}} = 10^{-4} \times I_{3 \times 3}$, $\Sigma^z = 5 \times 10^6$). Note that the virtual contact points of the IMU system represent the marker positions in the OMC system projected on the foot soles [37] (Figure 1). The DP1 marker was omitted for the foot model in the IMU system, since no inertial information is available to estimate the orientations of the proximal and distal phalanges.

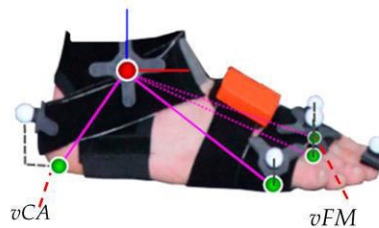


Figure 3. Foot model with optical markers and the four projected virtual contact points (green spheres) used for both the six degrees of freedom segment kinematics estimation and the IMU based gait event-detection. The virtual CA (vCA) marker and the virtual FM (vFM) marker, which were used for the event-detection in the IMU system, are denoted. The figure has been taken from [37].

In [33], the biomechanical model (including the segment lengths), the IMU-to-segment calibrations and the tracking initialization were extracted from the OMC data. In the present study, the biomechanical model was obtained from the Twente Lower Extremity Model (TLEM) 2.0 dataset [38] which was scaled based on the subject's gender and height using anthropometric tables [39]. The IMU-to-segment orientations were obtained from the above mentioned calibration poses according to [35] and the tracking process was initialized from inertial data only by assuming a neutral zero position. The IMU-to-segment positions were assumed fixed in the kinematic model. The assumed positions along the segments coincide with the description of the actual IMU positioning at the beginning of Section 2.1. The distances out of the segments were all assumed with 3 cm to roughly account for the tissue lying between bones and sensor origins. More specifically, the pelvis IMU position was assumed at 3 cm along the negative x -axis (see Figure 1), the IMUs attached to thighs and shanks were assumed at 3 cm along the positive (left) or negative (right) y -axis (pointing laterally, see [33]), and the IMUs attached to the feet were assumed at 3 cm along the positive z -axis (see Figure 3).

The real-time detection of IC and TC events, as mentioned above, uses a kinematics based algorithm. It is a modification of the coordinate-based treadmill algorithm described in Zeni et al. [40] for over-ground walking. The general idea of the base algorithm is that the IC corresponds to the heel having maximal distance to the pelvis center in walking direction, while the TC corresponds to the toe having maximal distance to the pelvis center against the walking direction. In the present study, this algorithm was applied to both the OMC data (optical markers on pelvis and feet) and the IMU data (estimated pelvis pose and virtual foot markers in the biomechanical model). Note, an offline version was used for deriving the events from the OMC data, while an online version was developed for obtaining real-time event-detections. The required modifications (compared to [40]) for over-ground walking and real-time detection are described in the following.

First of all, the walking direction, which changed with each turn in the present study (in contrast to the treadmill walking in [40]), was extracted from the captured data by filtering the estimated x -axis of the pelvis segment. The latter is a three dimensional unit vector lying in the sagittal plane and pointing in anterior direction for both the biomechanical model used to process the OMC and the IMU data (see Figure 1). The filtering was applied to compensate for small internal and external

rotations which naturally appear around the direction of movement during walking. It was based on an autoregressive model of first order (AR 1). After each filtering operation the axis was renormalized to unit length. In the offline version (for extracting the events from the OMC data), the filter was used in a zero-lag manner to avoid the introduction of a delay.

To obtain the IC and TC events, the relative positions of the respective real or virtual foot markers with respect to the sacrum were computed. These distances were then projected onto the estimated walking direction using the dot product. As in the original algorithm, the gait events were then extracted by finding the peaks of the projected distances. The maxima in the projected distances y_{IC} between the CA marker positions and the pelvis center positions defined the ICs and the minima in the projected distances y_{TC} between the DP1 marker positions (for the OMC data) or the FM marker positions (for the IMU data) and the pelvis center positions defined the TCs. An exemplary course of the projected distances y_{IC} for both systems with filtered and unfiltered x -axis is illustrated in Figure 4.

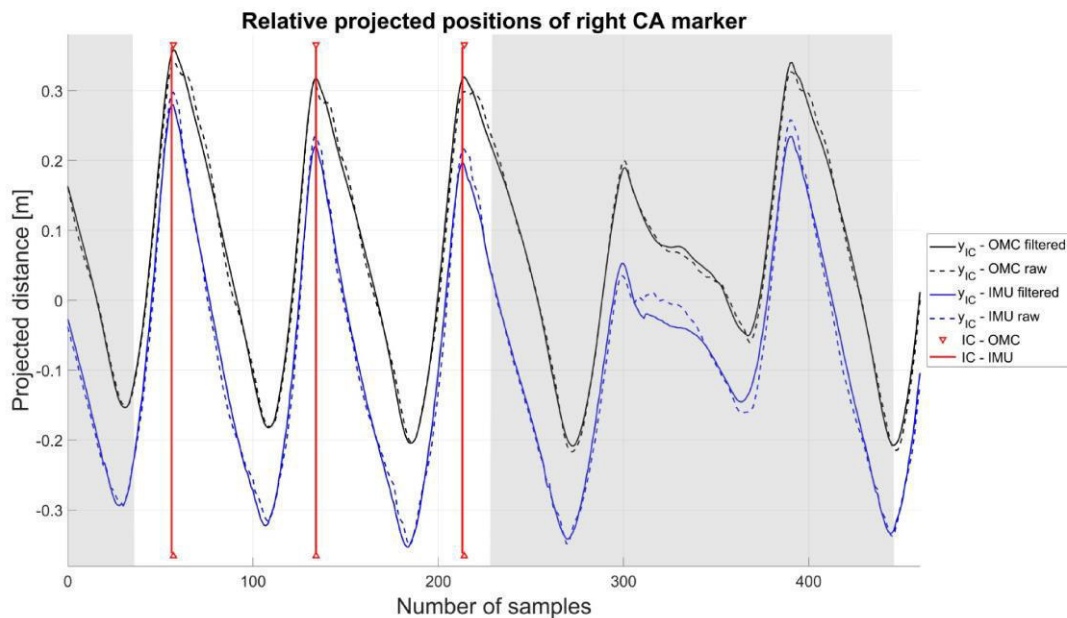


Figure 4. The shadowed areas indicate the turning phases. The offset between the OMC and IMU system originates in the different positions of the virtual and real heel marker as well as the different positions of the pelvis center.

In the offline version, the Matlab function *findpeaks* was used and the median of the complete sequence was used as a threshold for the minimal peak height.

In the online version, the extrema were detected as zero-crossings of differences of subsequent values of the projected distances y_{event} with $event \in \{IC, TC\}$. Instead of using the median as threshold for peak detection, the online version validates each found peak using the following conditions:

1. At the found peak, $y_{IC} > 0$ or $y_{TC} < 0$, i.e., the IC occurs in anterior and the TC in posterior direction.
2. After an event has been detected, a subsequent event of the same type cannot occur within a given amount of time (0.42 s in our experiments).
3. In addition to the previous temporal condition and in order to increase the robustness of the algorithm to false positive detections, a spatial condition based on the distance between two subsequent events has to be fulfilled. The absolute value of the projected distances between the current event and the last event $|y_{event} - y_{lastevent}|$ can be interpreted as the distance between the marker

positions associated to IC and TC or vice versa with respect to the pelvis segment center. We assume this distance to be $|y_{event} - y_{lastevent}| > h_{min,event}$, where $h_{min,event}$ indicates a threshold.

For the update of the threshold, we again use a filter based on a AR 1 model to compensate for greater fluctuations of the distances over time. After a valid event-detection the threshold is updated according to $h_{min,event} = (3 h_{previous,min,event} + 1 \bar{h}_{min,event}) / 4$. Here $h_{previous,min,event}$ denotes the threshold of the previous event and the value $\bar{h}_{min,event}$ is computed as $\bar{h}_{min,event} = a |y_{event} - y_{lastevent}|$. To ensure that also smaller strides are detected after several bigger strides, the scaling factor $a \in]0, 1]$ was introduced. In our setting it was chosen to be 0.7. The threshold was initialized with 1.2 times the foot size. Note, these parameters were empirically determined during pilot experiments and then used for the present study. The pilot experiments showed that the detection is not sensitive to the exact choice of the parameters.

Based on the detected events and estimated real/virtual foot marker positions, the STP parameters described in Table 1 were calculated and the combined average of both lower limbs was considered for evaluation.

Table 1. Description of the spatio-temporal parameters (STP).

Parameter	Description
Step Length (m) *	Distance between the CA marker positions of the left and right foot projected on the ground at two consecutive contralateral ICs
Stride Length (m)	Distance between the CA marker positions of one foot projected on the ground at two consecutive ipsilateral ICs
Step Width (m) *	Orthogonal distance between the line of the CA marker positions of one foot projected on the ground at two consecutive ipsilateral ICs and the CA marker position of the contralateral foot at the contralateral IC
Swing Width (m) *	Minimal distance between both CA markers during the swing phase
Step Time (s)	Period between two consecutive ICs of the left and right foot
Stride Time (s)	Period between two consecutive ICs of the ipsilateral foot
Cadence (steps/min)	60 divided by step time
Single Limb Support (s)	Period between contralateral TC and contralateral IC
Double Limb Support (s)	Stride time minus Single limb support
Stance Time (s)	Period between IC and TC of one foot
Swing Time (s)	Period between TC and IC of one foot
Speed (m/s)	Stride length divided by Stride time [4]

An asterisk * marks the STP that require the spatial information of both feet for the calculation.

2.2. Statistical Analysis

To evaluate the performance of the event-detection algorithm all erroneous detections of the IMU system were captured (surplus and missing events compared to the OMC system) and the relative error compared to the OMC system was calculated. Further, the average detection offset (time difference between events in the IMU and OMC system) for all subjects was calculated for IC and TC. Therefore, the detection offsets over all subjects were averaged and converted from frames per second (fps) to seconds according to the data acquisition frame rate of 60 Hz. Additionally, the detection offset of IC and TC was graphically represented.

To validate the results of the STP the mean error, the root mean square error (RMSE) plus 95% confidence interval (CI), the relative RMSE and Bland-Altman (BA) analysis were calculated. In the present evaluation the left and right side were combined.

The chi-square goodness-of-fit test was used to check for normal distribution in the data. Consequently, a paired sample t-test or the non-parametric Wilcoxon rank sum test was calculated to

find significant differences in the STP between the IMU and OMC system. The critical p -value was set to $\alpha = 0.05$.

To evaluate the test-retest reliability of the STP the intraclass correlation coefficient (ICC) was estimated. In this study a two way random effect model was used to calculate the reliability of the average of two measurements according to McGraw and Wong [41]. ICC values below 0.40 were rated poor, values between 0.41 and 0.59 fair, between 0.60 and 0.74 good and above 0.74 excellent [42].

All statistics, the calculation of the events from the OMC data and the calculation of the STP were conducted in Matlab 2017 (Mathworks Inc., Natick, MA, USA). The real-time event-detection from IMU based kinematics data was implemented in C++.

3. Results

3.1. Validity

In the following, the results of the left and right lower leg were combined for the evaluation. Differences between sides were below 0.006 m in the spatial parameters and below 0.004 s in the temporal parameters. The difference in the cadence of left and right side was 0.48 steps/min.

A total of 13,415 events were detected by the OMC system, IC, and TC combined. The detection error of the IMU system was below 1.2%. The detection offset was below 0.017 s. A detailed description of the results can be found in Table 2 and Figure 5.

Table 2. Event-detection results for Test 1. The total of detected events, number of erroneous detections, false-positives and false negatives, percentage error and the offset between optical (OMC) and inertial measurement unit (IMU) system plus standard deviation (SD) are shown.

Test 1	Total	Total Errors	False-Positive	False-Negative	% Error	Offset (SD) (s)
IC	6619	1	1	0	0.02	0.008 (0.007)
TC	6796	80	44	36	1.17	0.016 (0.010)

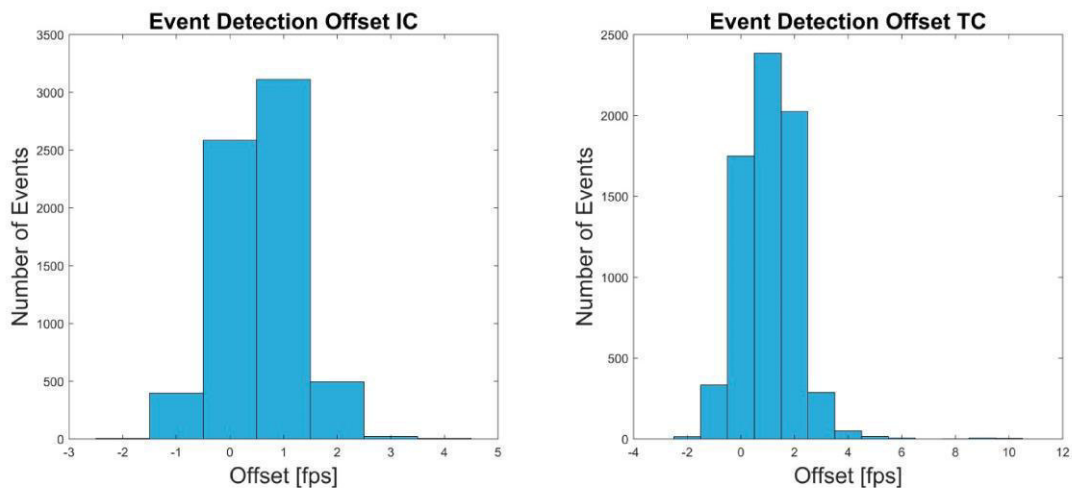


Figure 5. The Offset in frames per second (fps) between OMC and IMU system for the IC and TC events of test 1 are shown.

Mean OMC and IMU values of the different STP as well as the p-values of the significance test, the mean error, the RMSE \pm SD and 95% CI, relative RMSE and BA bias are shown in Table 3. Low errors and high agreement were observed over all parameters. Relative errors were below 7% with exception of the step width and swing width. The step width displayed a relative RMSE of 34.34%. The swing width revealed a relative RMSE of 35.20%. These values correspond to a RMSE of 0.03 m. The average step width as well as swing width measured at 0.09 m in the OMC and 0.10 m and 0.08 m in the IMU system, respectively. Further, the STP dependent on the spatial information of left and right CA or DP1/FM marker showed higher relative RMSE compared to the remaining parameters.

Table 3. Summary of the results of all STP. The mean parameters plus SD, p-values, mean error, root mean square error (RMSE) (95% confidence interval (CI)), relative RMSE and bias (SD) are shown. Bold *p* values indicate significant differences between the systems ($p < 0.05$).

	OMC	IMU	<i>p</i> Value	Mean Error	RMSE	Relative RMSE (%)	Bias
Step Length (m)	0.61 \pm 0.06	0.62 \pm 0.07	<0.05	0.006	0.04 (0.03–0.04)	6.69	0.006 (0.08)
Stride Length (m)	1.21 \pm 0.12	1.22 \pm 0.12	0.39	0.005	0.04 (0.03–0.04)	2.98	0.005 (0.07)
Step Width (m)	0.09 \pm 0.03	0.10 \pm 0.03	<0.05	0.008	0.03 (0.02–0.03)	34.34	0.008 (0.06)
Swing Width (m)	0.09 \pm 0.02	0.08 \pm 0.03	<0.05	−0.008	0.03 (0.02–0.03)	35.20	−0.008 (0.06)
Step Time (s)	0.60 \pm 0.06	0.60 \pm 0.06	0.33	0.002	0.02 (0.01–0.02)	2.94	0.002 (0.03)
Stride Time (s)	1.20 \pm 0.11	1.20 \pm 0.11	0.63	0.002	0.01 (0.01–0.01)	0.90	0.002 (0.02)
Cadence (steps/min)	101.09 \pm 10.02	100.79 \pm 9.76	0.33	−0.296	3.10 (2.23–2.87)	3.07	−0.296 (6.05)
Single Limb Support (s)	0.39 \pm 0.03	0.40 \pm 0.03	<0.05	0.008	0.02 (0.01–0.02)	4.26	0.008 (0.03)
Double Limb Support (s)	0.81 \pm 0.09	0.80 \pm 0.09	<0.05	−0.006	0.02 (0.02–0.02)	2.32	−0.006 (0.04)
Stance Time (s)	0.80 \pm 0.09	0.80 \pm 0.09	<0.05	−0.008	0.02 (0.01–0.02)	2.10	−0.008 (0.03)
Swing Time (s)	0.39 \pm 0.03	0.40 \pm 0.03	<0.05	0.010	0.02 (0.01–0.02)	4.40	0.010 (0.03)
Speed (m/s)	1.03 \pm 0.14	1.03 \pm 0.15	0.57	0.003	0.03 (0.02–0.03)	2.72	0.003 (0.05)

The BA analysis showed high agreement between the IMU system and the reference system for most of the parameters. Step width and swing width showed low biases but rather wide limits compared to the dimension of the actual parameter value. Figure 6 shows exemplary BA diagrams for step width and swing width. Additional BA diagrams (Figures A1–A10) can be found in Appendix A.

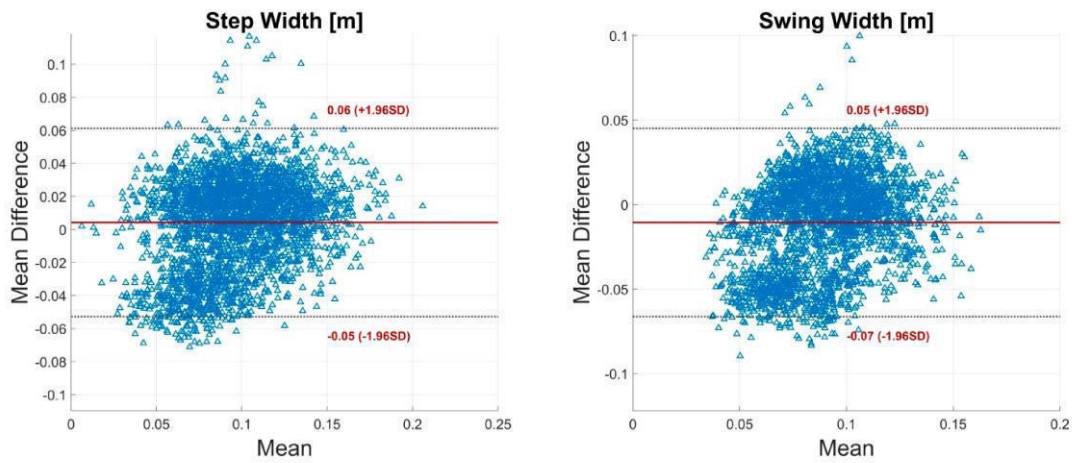


Figure 6. Bland-Altman (BA) plots for step width and swing width. Each plot contains all calculated data points of one parameter of all subjects. The solid line indicates the mean difference. The dashed lines indicate the limits of agreement (LoA) (95% CI of the mean difference).

3.2. Test-Retest Reliability

The event-detection of the retest revealed slightly more erroneous detections in both IC and TC. However, percentage error was below 1.60%. Detection offsets did not differ from Test 1. For details see Table 4 and Figure 7.

Table 4. Event-detection results for the retest. The total of detected events, number of erroneous detections, false positives and false negatives, percentage error and the offset between OMC and IMU system plus SD are shown.

Retest	Total	Total Errors	False-Positive	False-Negative	% Error	Offset (SD) (s)
IC	6802	15	7	8	0.22	0.007 (0.008)
TC	6780	105	58	47	1.55	0.015 (0.010)

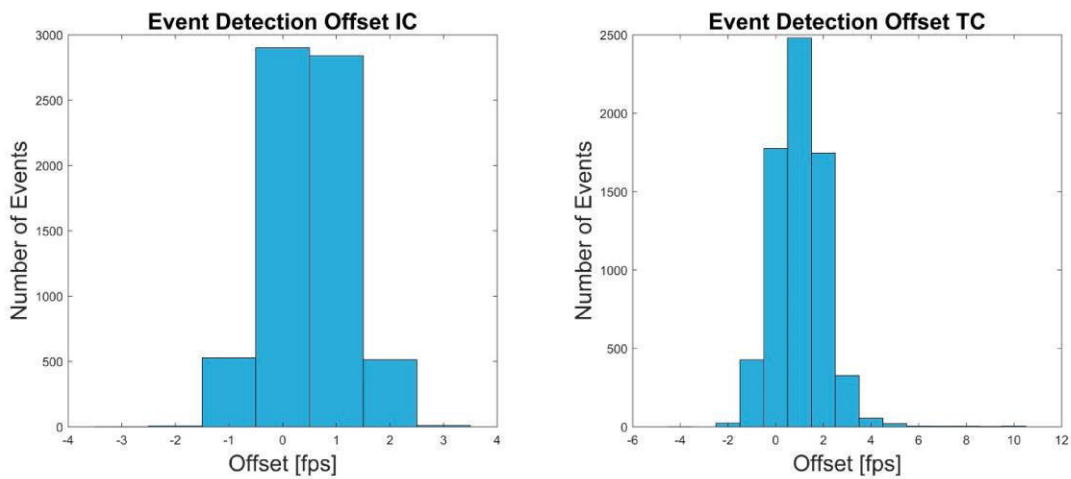


Figure 7. The Offset in frames per second (fps) between OMC and IMU system for the events IC and TC of retest are shown.

The ICC revealed excellent test-retest correlations for all parameters except swing time, step width, swing width and step length. Step width was rated poor (0.25). Step length, swing width, and swing time were rated good (0.67, 0.69, and 0.73). The ICC calculation for the OMC system showed good to excellent values over all parameters (>0.67). All ICC values for the IMU and OMC system are shown in Table 5.

Table 5. Summary of the results of the calculation of the intraclass correlation coefficient for the OMC and IMU system, respectively.

Parameter	ICC OMC	ICC IMU
Step Length (m)	0.88	0.67
Stride Length (m)	0.87	0.88
Step Width (m)	0.67	0.25
Swing Width (m)	0.90	0.69
Step Time (s)	0.87	0.87
Stride Time (m)	0.92	0.91
Cadence (steps/min)	0.87	0.87
Single Limb Support (m)	0.82	0.85
Double Limb Support (m)	0.89	0.90
Stance Time (s)	0.92	0.92
Swing Time (s)	0.81	0.73
Speed (m/s)	0.91	0.92

4. Discussion

4.1. Validity

The present evaluation of events and STP obtained from a real-time IMU based kinematic model approach revealed high validity compared to the reference system. The event-detection algorithm used in this study was designed for a kinematic approach in overground and treadmill walking. The algorithm was validated in Zeni et al. [40]. Therefore, it was considered a valid approach for the detection of IC and TC and was employed in this study rather than an alternative approach [43].

The detection rate of the event-detection was about 99% for IC and TC. Further, the detection offset was below 0.010 s for IC and below 0.017 s for TC. Storm et al. [44] found a similar detection offset for IC but a higher error for TC (0.051 s). Bertoli et al. [4] found a detection offset of -0.009 s to 0.009 s for IC and TC. However, their detection approach partly requires offline calculations.

Müller et al. [16] found a mean delay for TC of approximately 0.1 s and approximately 0.05 s for IC. However, consider that their recording frequency was restricted to 50 Hz. Further, they used a different algorithm for the event-detection in the reference system. However, Müller et al. [16] and Seel et al. [15] showed that their system does not depend on the knowledge of an accurate IMU-to-segment calibration, since mostly accelerometer and gyroscope measurement norms are considered for the detection of the gait phase transitions. Moreover, the rotation of the global coordinate system, which is required for obtaining the IMU velocity through integration of the acceleration measurements as basis for toe off detection, is dynamically determined as the rotation of the IMU at foot rest.

A limitation of the study was that the IMU based kinematic model did not provide a virtual marker on DP1. Therefore, the virtual marker FM was used for TC detection. This might have led to an increased detection offset between OMC and IMU system. Consider, the position of the CA marker of the IMU system was projected on the sole whereas the CA marker of the OMC system was located on the dorsal aspect of the calcaneus (Figure 3). Another drawback of the study was that the IMU-to-segment positions were assumed fixed rather than, e.g., estimated from IMU data. Therefore, differences between the assumed IMU positions in the model and the true positions on the segments could have appeared. The effect of these deviations on the estimated IMU orientations was examined for slow and fast movements in [36]. For example, a simulation study in [36] showed that a deviation of about 10 cm along the segment could lead to a mean angular error of up to

approximately 5° in fast movements when not using magnetometer information (up to about 6.5° for 10 cm out of segment deviations). However, there is work in progress to develop pose-independent and movement-independent calibration methods estimating not only the IMU-to-segment orientations but also the IMU-to-segment positions [45,46].

The temporal parameters and those that are dependent on the spatial information of one foot showed the lowest relative RMSE. Stride time revealed the lowest relative error, 0.90% (RMSE 0.01 s), for all parameters. These results are comparable to Kluge et al. [18] who found similar results for stride time. They examined a commercial IMU system consisting of two IMUs attached to the lateral aspect of the heels. Their results were compared to a marker-less OMC system. They further presented results for stance time (5.40%, RMSE 0.04 s), swing time (8.20%, RMSE 0.04 s), stride length (3.60%, RMSE 0.05 m), and speed (3.60%, RMSE 0.04 m/s). For all these parameters the present system revealed better results. Consider that the subjects in the study of Kluge et al. [18] displayed a higher overall stride length (~ 1.45 m) and a slightly lower stride time (~ 1.13 s).

Bertoli et al. [4] investigated a large sample of subjects (236) across different clinics and states of impairment. They used two MIMUs attached above both ankles and a pressure mat as a reference system. Further, they used an algorithm, assumed to be partially offline, based on the identification of trusted swing and stance phases of the lower limbs for the event-detection according to Trojaniello et al. [47]. They found rather good results concerning the validity of the temporal parameters and the stride length. The mean error of the stride length measured from -0.001 m to -0.014 m for the healthy group across the different clinics. Stride time, swing time, step time and stance time were all below 0.025 s. Therefore, they present similar results concerning the temporal parameters compared to the present study.

As addressed in the introduction Donath et al. [25] validated the STP of a commercial MIMU system combining the measurement of 1D (sagittal) JK and STP. They calculated RMSE for stride length (0.06 m), stride time (0.04 s), speed (0.08 m/s) and cadence (0.09 steps/min). The present system revealed better results concerning the stride length (0.04 m), stride time (0.01 s) and speed (0.03 m/s). However, the cadence showed a distinctively higher RMSE (3.10 steps/min). It is not clear how the cadence was estimated in the system used by Donath et al. [25]. In the present study, the cadence was calculated incorporating the step time (see Table 1).

As mentioned above there are few studies that measured IMU based spatial parameters dependent on the position information of both feet. Cimolin et al. [23] used one IMU attached to the pelvis to measure STP. They delivered a theoretical approach for the measurement of the step length, based on leg length and an inverted pendulum gait model. However, they omitted the results of the calculation.

Köse et al. [19] used a similar setting and came up with a special approach for the calculation of the step length. They assumed that the pelvic displacement along the line of progression between an ipsilateral IC and a contralateral IC equals the step length. They found promising results with a mean error of 0.009 m compared to an OMC system. The present study revealed a mean difference of 0.006 m. However, Köse et al. [19] examined a small sample size of 9 subjects and used a partial-offline calculation.

It was a special challenge of the present work to calculate the parameter step width. The step width was described as the most sensitive parameter for gait categorization in older adults [48]. Further, step width is an important evaluation parameter concerning cerebellar ataxic gait [49]. Ilg et al. [50] found a significant correlation of step width with the International Cooperative Ataxia Rating Scale. Stolze et al. [49] found that step width altered about 7 cm between a healthy and a cerebellar impaired population. The BA analysis of the present study revealed a bias of ± 0.06 m regarding the step width (Figure 6). These results indicate that the differentiation between healthy and impaired subjects would be challenging with the current system. Thus, the measurement of the step width has to be further improved. It might have been that imprecisions in the segment length scaling and the neutral zero position led to increased errors in the step width. The integration of an individualized biomechanical model and a pose-independent calibration might improve these results.

To the knowledge of the authors, there are no studies that report step width measurement based on IMUs that use the same definition of the parameter as presented in this work. Müller et al. [51] tried to measure step width using a Kinect sensor. Their BA analysis revealed a bias of -0.015 m (left) and 0.027 m (right) and limits of ± 0.076 m (left) and ± 0.127 m (right). The present findings showed a slightly lower bias and similar limits compared to the left side of their results.

In the present study, the term swing width in relation to gait was introduced. The authors deemed it necessary to clearly separate step width and swing width, as both measures can deliver independent information about pathological gait. Step width delivers mainly information about the increase or decrease of the base of support. Whereas the swing width might be able to identify a circumduction [52], a common gait abnormality. Awada et al. [53] measured the circumduction of nine post-stroke patients using an OMC system and force plates and defined the severity of the gait impairment as the maximum lateral displacement of the center of gravity between stance and swing phase. As mentioned in Table 1, in the present study the swing width was defined as the minimal distance of the CA markers during the swing phase. Considering this assumption, it might appear in pathological gait that the anterior-posterior distance of the CA markers is smaller compared to the lateral distance, in the case of increased circumduction and decreased step length. Therefore, it might be beneficial to redefine the parameter swing width as the orthogonal distance between the line consisting of the CA marker of the standing foot and the line of progression, and the CA marker of the swinging foot.

However, there is little literature about the measurement of inter-foot distance during the swing phase of gait based on IMUs. Shiotani and Watanabe [54] examined a system using seven IMUs attached to the lower extremities based on Watanabe and Saito [55] for the measurement of circumduction during gait. They calculated the 3D loci vector of the thigh segments and graphically interpreted the circumduction behavior of 12 healthy subjects. However, they did not state quantitative results.

Bertuletti et al. [21] described an approach using a device consisting of an IMU and an infrared time of flight proximity sensor for the measurement of the step width. However, they actually measured the parameter that corresponds to the present definition of swing width. They validated the approach during the gait of one healthy subject. Their results were slightly better compared to the present findings of swing width, revealing a mean error of 0.005 m. However, the results of Bertuletti et al. [21] depend on a rather complex device including a large plastic plate target affixed to the opposite foot. Further, an optical calibration of the geometries of the sensor and its corresponding target is necessary.

4.2. Test-Retest Reliability

The calculation of the ICC revealed good to excellent test-retest reliability for all STP except for step width and swing width. Kluge et al. [18] and Donath et al. [25] found similar correlations in their calculated parameters. However, as mentioned afore, these authors described only a few STP.

The ICC values for step width and swing width were rated poor (0.25) and good (0.69), respectively. However, in the OMC system the test-retest reliability of these parameters was distinctively higher (0.67 and 0.90). Further, the step length revealed a lower ICC value (0.67) compared to the OMC system (0.88) and also the ICC value of the swing time was lower in the IMU system (0.73) compared to the OMC system (0.81). It seems not to be a coincidence that the STP that depend on the spatial information of both feet showed the lowest correlations concerning the test-retest reliability. It is likely that these parameters were most influenced by deviations in the neutral zero position calibration of Test 1 and the Retest, e.g., altered hip abduction or hip rotation. Robert-Lachaine et al. [56] examined the difference of self-placed and passively-placed neutral zero positions. They found an offset in the segment longitudinal axes for the lower limbs of about 5° to 10° between self-placement and passive-placement. In the present study, the neutral zero position was explained to the subjects but self-placed. There was no further passive correction of the poses, but verbal in exceptional cases.

However, such deviations could not influence the measurements of the OMC system. This might explain the lower reliability concerning these STP in the IMU system.

5. Conclusions

In summary, the present study revealed valid results of an IMU system for 3D gait analysis delivering a wide range of clinically relevant parameters. Further, the real-time event-detection algorithm defined IC and TC with an error rate below 1.6% and an offset below 0.017 s. However, consider that in this study only young and healthy subjects participated. Therefore, the findings of this study apply only to normal gait. Future studies must show the validity and reliability of this approach in less standardized environments and examining subjects with gait impairment. Further, there is work in progress to introduce pose-independent and movement-independent calibration methods [45,46]. This could further improve the validity and reliability of STP like step width, swing width and step length. Additionally, the significance and the definition of acceptable resolutions concerning the step width and swing width have to be further discussed and examined in a clinical context.

Author Contributions: W.T. contributed to the development of the study conception, data acquisition, analysis and interpretation, manuscript drafting, and revision. M.L. contributed to data processing, manuscript drafting. M.M. contributed to data acquisition, data processing, manuscript drafting. B.T. contributed to data analysis, manuscript drafting and revision. M.F. contributed to study conception, data interpretation, manuscript drafting and revision. G.B. contributed to study conception, data processing, data interpretation, manuscript drafting and revision.

Acknowledgments: This work was performed by the Interdisciplinary Junior Research Group wearHEALTH, funded by the BMBF (16SV7115, 03IHS075B). For more information, please visit the website: www.wearhealth.org.

Conflicts of Interest: The authors declare no conflict of interest. The authors alone are responsible for the content and writing of this paper. The founding sponsors had no role in the design of the study; in the collection, analyses, or interpretation of data; in the writing of the manuscript, and in the decision to publish the results.

Ethical Statements: All subjects gave their informed consent for inclusion before they participated in the study. The study was conducted in accordance with the Declaration of Helsinki, and the protocol was approved by the Ethics Committee of Technische Universität Kaiserslautern.

Appendix A

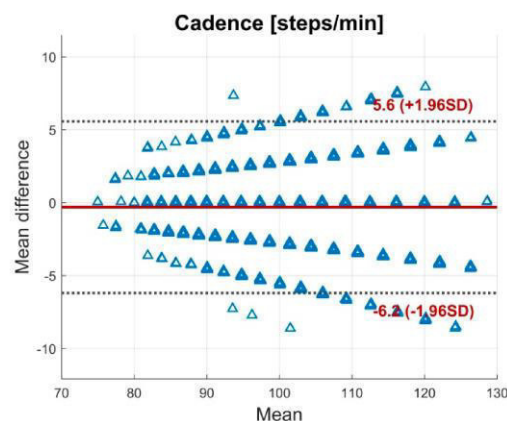


Figure A1. BA plot for the cadence. The plot contains all calculated data points of all subjects. The solid line indicates the mean difference. The dashed lines indicate the LoA (95% CI of the mean difference).

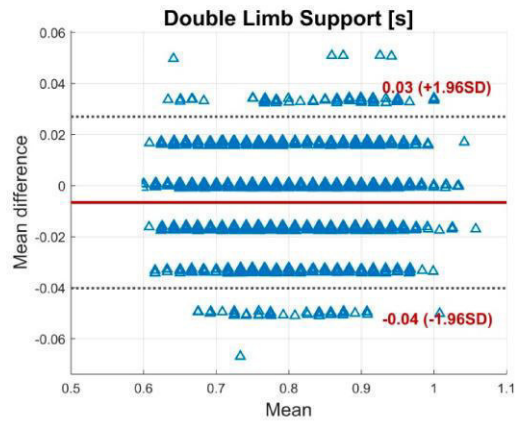


Figure A2. BA plot for the double limb support. The plot contains all calculated data points of all subjects. The solid line indicates the mean difference. The dashed lines indicate the LoA (95% CI of the mean difference).

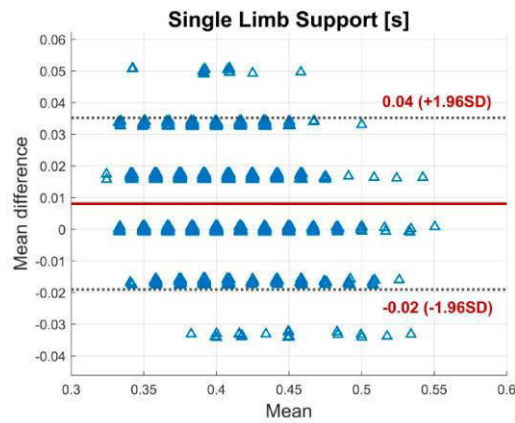


Figure A3. BA plot for the single limb support. The plot contains all calculated data points of all subjects. The solid line indicates the mean difference. The dashed lines indicate the LoA (95% CI of the mean difference).

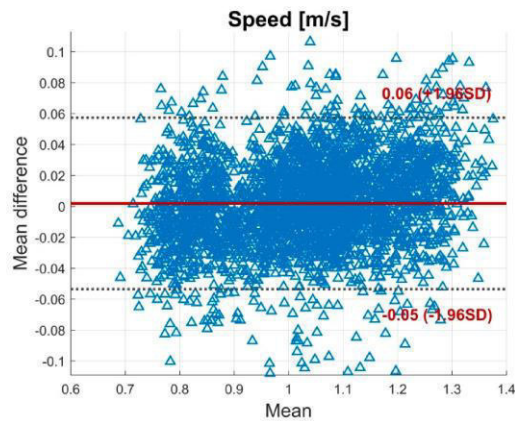


Figure A4. BA plot for the speed. The plot contains all calculated data points of all subjects. The solid line indicates the mean difference. The dashed lines indicate the LoA (95% CI of the mean difference).

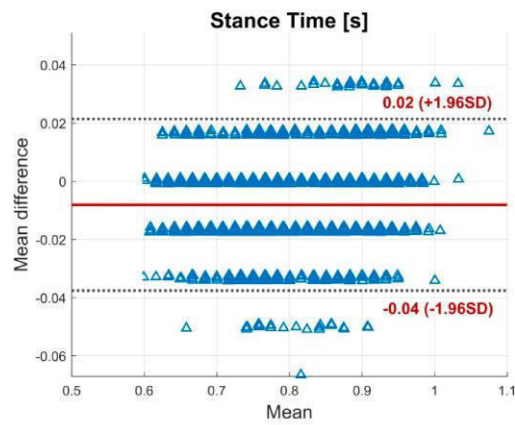


Figure A5. BA plot for the stance time. The plot contains all calculated data points of all subjects. The solid line indicates the mean difference. The dashed lines indicate the LoA (95% CI of the mean difference).

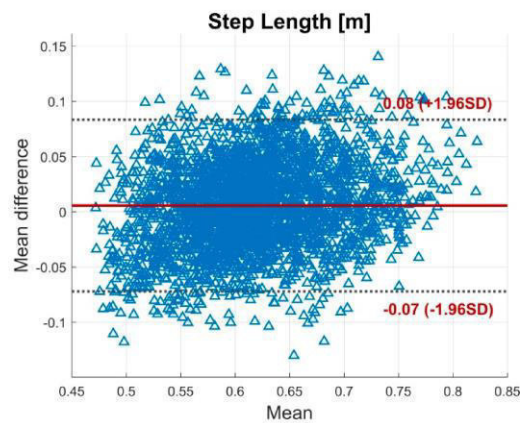


Figure A6. BA plot for the step length. The plot contains all calculated data points of all subjects. The solid line indicates the mean difference. The dashed lines indicate the LoA (95% CI of the mean difference).

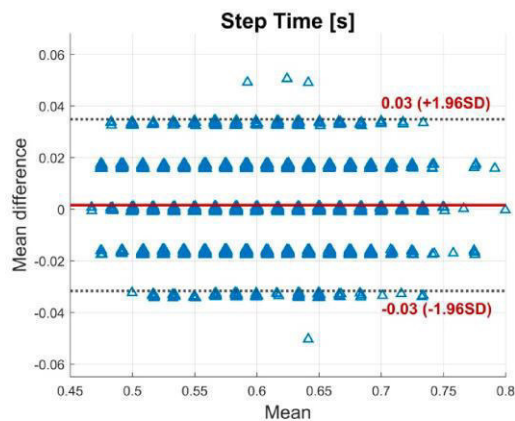


Figure A7. BA plot for the step time. The plot contains all calculated data points of all subjects. The solid line indicates the mean difference. The dashed lines indicate the LoA (95% CI of the mean difference).

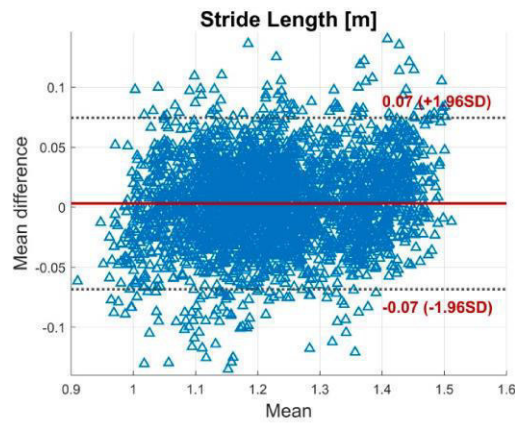


Figure A8. BA plot for the stride length. The plot contains all calculated data points of all subjects. The solid line indicates the mean difference. The dashed lines indicate the LoA (95% CI of the mean difference).

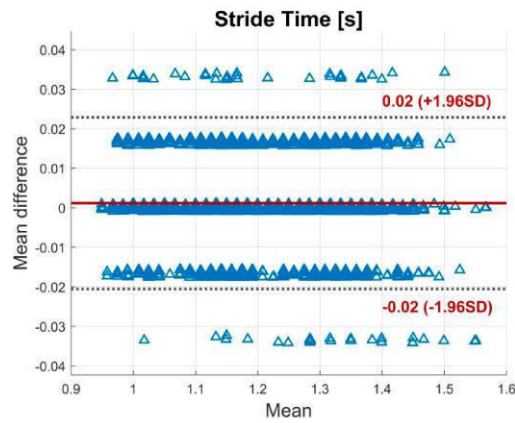


Figure A9. BA plot for the stride time. The plot contains all calculated data points of all subjects. The solid line indicates the mean difference. The dashed lines indicate the LoA (95% CI of the mean difference).

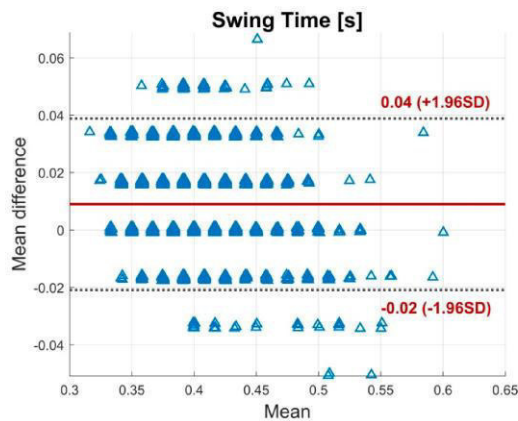


Figure A10. BA plot for the swing time. The plot contains all calculated data points of all subjects. The solid line indicates the mean difference. The dashed lines indicate the LoA (95% CI of the mean difference).

References

1. Loske, S.; Nüesch, C.; Byrnes, K.S.; Fiebig, O.; Schären, S.; Mündermann, A.; Netzer, C. Decompression surgery improves gait quality in patients with symptomatic lumbar spinal stenosis. *Spine J.* **2018**, *18*, 2195–2204. [CrossRef] [PubMed]
2. Zomar, B.O.; Bryant, D.; Hunter, S.; Howard, J.L.; Vasarhelyi, E.M.; Lanting, B.A. A randomised trial comparing spatio-temporal gait parameters after total hip arthroplasty between the direct anterior and direct lateral surgical approaches. *HIP Int.* **2018**, *28*, 478–484. [CrossRef] [PubMed]
3. Steultjens, M.P.M.; Dekker, J.; van Baar, M.E.; Oostendorp, R.A.B.; Bijlsma, J.W.J. Range of joint motion and disability in patients with osteoarthritis of the knee or hip. *Rheumatology* **2000**, *39*, 955–961. [CrossRef] [PubMed]
4. Bertoli, M.; Cereatti, A.; Trojaniello, D.; Avanzino, L.; Pelosin, E.; Del Din, S.; Rochester, L.; Ginis, P.; Bekkers, E.M.J.; Mirelman, A.; et al. Estimation of spatio-temporal parameters of gait from magneto-inertial measurement units: Multicenter validation among Parkinson, mildly cognitively impaired and healthy older adults. *Biomed. Eng. OnLine* **2018**, *17*, 58. [CrossRef] [PubMed]
5. Pau, M.; Corona, F.; Pili, R.; Casula, C.; Guicciardi, M.; Cossu, G.; Murgia, M. Quantitative assessment of gait parameters in people with Parkinson's disease in laboratory and clinical setting: Are the measures interchangeable? *Neurol. Int.* **2018**, *10*, 7729. [CrossRef] [PubMed]
6. Leijendekkers, R.A.; Marra, M.A.; Kolk, S.; van Bon, G.; Schreurs, B.W.; Weerdesteyn, V.; Verdonschot, N. Gait symmetry and hip strength in women with developmental dysplasia following hip arthroplasty compared to healthy subjects: A cross-sectional study. *PLoS ONE* **2018**, *13*, e0193487. [CrossRef] [PubMed]
7. Radzak, K.N.; Putnam, A.M.; Tamura, K.; Hetzler, R.K.; Stickley, C.D. Asymmetry between lower limbs during rested and fatigued state running gait in healthy individuals. *Gait Posture* **2017**, *51*, 268–274. [CrossRef] [PubMed]
8. Picerno, P. 25 years of lower limb joint kinematics by using inertial and magnetic sensors: A review of methodological approaches. *Gait Posture* **2017**, *51*, 239–246. [CrossRef] [PubMed]
9. Camomilla, V.; Bergamini, E.; Fantozzi, S.; Vannozzi, G.; Camomilla, V.; Bergamini, E.; Fantozzi, S.; Vannozzi, G. Trends Supporting the In-Field Use of Wearable Inertial Sensors for Sport Performance Evaluation: A Systematic Review. *Sensors* **2018**, *18*, 873. [CrossRef] [PubMed]
10. Kianifar, R.; Lee, A.; Raina, S.; Kulic, D. Classification of Squat Quality with Inertial Measurement Units in the Single Leg Squat Mobility Test. In Proceedings of the 2016 38th Annual International Conference of the IEEE Engineering in Medicine and Biology Society (EMBC), Orlando, FL, USA, 16–20 August 2016.
11. Robert-Lachaine, X.; Mecheri, H.; Larue, C.; Plamondon, A. Validation of inertial measurement units with an optoelectronic system for whole-body motion analysis. *Med. Biol. Eng. Comput.* **2017**, *55*, 609–619. [CrossRef]
12. Al-Amri, M.; Nicholas, K.; Button, K.; Sparkes, V.; Sheeran, L.; Davies, J.L. Inertial Measurement Units for Clinical Movement Analysis: Reliability and Concurrent Validity. *Sensors* **2018**, *18*, 719. [CrossRef] [PubMed]
13. Chen, S.; Lach, J.; Lo, B.; Yang, G.Z. Toward Pervasive Gait Analysis With Wearable Sensors: A Systematic Review. *IEEE J. Biomed. Health Inform.* **2016**, *20*, 1521–1537. [CrossRef] [PubMed]
14. Caldas, R.; Mundt, M.; Potthast, W.; Buarque de Lima Neto, F.; Markert, B. A systematic review of gait analysis methods based on inertial sensors and adaptive algorithms. *Gait Posture* **2017**, *57*, 204–210. [CrossRef] [PubMed]
15. Seel, T.; Cermeño Escobar, V.; Raisch, J.; Schauer, T. Online Gait Phase Detection with Automatic Adaption to Gait Velocity Changes Using Accelerometers and Gyroscopes. *Biomed. Tech.* **2014**, *59*, S795–S798.
16. Müller, P.; Seel, T.; Schauer, T. Experimental Evaluation of a Novel Inertial Sensor Based Realtime Gait Phase Detection Algorithm. Available online: https://www.control.tu-berlin.de/wiki/images/5/5e/Mueller_TAR2015.pdf (accessed on 26 November 2018).
17. Schwesig, R.; Leuchte, S.; Fischer, D.; Ullmann, R.; Kluttig, A. Inertial sensor based reference gait data for healthy subjects. *Gait Posture* **2011**, *33*, 673–678. [CrossRef] [PubMed]
18. Kluge, F.; Gaßner, H.; Hannink, J.; Pasluosta, C.; Klucken, J.; Eskofier, B.M. Towards Mobile Gait Analysis: Concurrent Validity and Test-Retest Reliability of an Inertial Measurement System for the Assessment of Spatio-Temporal Gait Parameters. *Sensors* **2017**, *17*, 1522. [CrossRef] [PubMed]
19. Köse, A.; Cereatti, A.; Della Croce, U. Bilateral step length estimation using a single inertial measurement unit attached to the pelvis. *J. NeuroEng. Rehabil.* **2012**, *9*, 9. [CrossRef] [PubMed]

20. Takeda, R.; Lisco, G.; Fujisawa, T.; Gastaldi, L.; Tohyama, H.; Tadano, S. Drift Removal for Improving the Accuracy of Gait Parameters Using Wearable Sensor Systems. *Sensors* **2014**, *14*, 23230–23247. [[CrossRef](#)]
21. Bertuletti, S.; Cereatti, A.; Comotti, D.; Caldara, M.; Della Croce, U. Static and Dynamic Accuracy of an Innovative Miniaturized Wearable Platform for Short Range Distance Measurements for Human Movement Applications. *Sensors* **2017**, *17*, 1492. [[CrossRef](#)]
22. Agostini, V.; Gastaldi, L.; Rosso, V.; Knaflitz, M.; Tadano, S. A Wearable Magneto-Inertial System for Gait Analysis (H-Gait): Validation on Normal Weight and Overweight/Obese Young Healthy Adults. *Sensors* **2017**, *17*, 2406. [[CrossRef](#)]
23. Cimolin, V.; Capodaglio, P.; Cau, N.; Galli, M.; Santovito, C.; Patrizi, A.; Tringali, G.; Sartorio, A. Computation of spatio-temporal parameters in level walking using a single inertial system in lean and obese adolescents. *Biomed. Eng. Biomed. Tech.* **2017**, *62*. [[CrossRef](#)] [[PubMed](#)]
24. Nüesch, C.; Roos, E.; Pagenstert, G.; Mündermann, A. Measuring joint kinematics of treadmill walking and running: Comparison between an inertial sensor based system and a camera-based system. *J. Biomech.* **2017**, *57*, 32–38. [[CrossRef](#)] [[PubMed](#)]
25. Donath, L.; Faude, O.; Lichtenstein, E.; Nüesch, C.; Mündermann, A. Validity and reliability of a portable gait analysis system for measuring spatiotemporal gait characteristics: Comparison to an instrumented treadmill. *J. Neuroeng. Rehabil.* **2016**, *13*, 6. [[CrossRef](#)] [[PubMed](#)]
26. Donath, L.; Faude, O.; Lichtenstein, E.; Pagenstert, G.; Nüesch, C.; Mündermann, A. Mobile inertial sensor based gait analysis: Validity and reliability of spatiotemporal gait characteristics in healthy seniors. *Gait Posture* **2016**, *49*, 371–374. [[CrossRef](#)] [[PubMed](#)]
27. Shull, P.B.; Jirattigalachote, W.; Hunt, M.A.; Cutkosky, M.R.; Delp, S.L. Quantified self and human movement: A review on the clinical impact of wearable sensing and feedback for gait analysis and intervention. *Gait Posture* **2014**, *40*, 11–19. [[CrossRef](#)] [[PubMed](#)]
28. Shull, P.B.; Lurie, K.L.; Cutkosky, M.R.; Besier, T.F. Training multi-parameter gaits to reduce the knee adduction moment with data-driven models and haptic feedback. *J. Biomech.* **2011**, *44*, 1605–1609. [[CrossRef](#)] [[PubMed](#)]
29. Afzal, M.R.; Oh, M.-K.; Lee, C.-H.; Park, Y.S.; Yoon, J. A Portable Gait Asymmetry Rehabilitation System for Individuals with Stroke Using a Vibrotactile Feedback. *BioMed Res. Int.* **2015**, *2015*, 375638. [[CrossRef](#)]
30. Crea, S.; Cipriani, C.; Donati, M.; Carrozza, M.C.; Vitiello, N. Providing Time-Discrete Gait Information by Wearable Feedback Apparatus for Lower-Limb Amputees: Usability and Functional Validation. *IEEE Trans. Neural Syst. Rehabil. Eng.* **2015**, *23*, 250–257. [[CrossRef](#)]
31. Seel, T.; Laidig, D.; Valtin, M.; Werner, C.; Raisch, J.; Schauer, T. Feedback control of foot eversion in the adaptive peroneal stimulator. In Proceedings of the 22nd Mediterranean Conference on Control and Automation, Palermo, Italy, 16–19 June 2014; pp. 1482–1487.
32. Valtin, M.; Seel, T.; Raisch, J.; Schauer, T. Iterative learning control of drop foot stimulation with array electrodes for selective muscle activation. In Proceedings of the 19th World Congress The International Federation of Automatic Control, Cape Town, South Africa, 24–29 August 2014.
33. Teufl, W.; Miezal, M.; Taetz, B.; Fröhlich, M.; Bleser, G. Validity, Test-Retest Reliability and Long-Term Stability of Magnetometer Free Inertial Sensor Based 3D Joint Kinematics. *Sensors* **2018**, *18*, 1980. [[CrossRef](#)]
34. Leardini, A.; Sawacha, Z.; Paolini, G.; Ingrassio, S.; Nativio, R.; Benedetti, M.G. A new anatomically based protocol for gait analysis in children. *Gait Posture* **2007**, *26*, 560–571. [[CrossRef](#)]
35. Palermo, E.; Rossi, S.; Marini, F.; Patanè, F.; Cappa, P. Experimental evaluation of accuracy and repeatability of a novel body-to-sensor calibration procedure for inertial sensor-based gait analysis. *Measurement* **2014**, *52*, 145–155. [[CrossRef](#)]
36. Miezal, M.; Taetz, B.; Bleser, G. On Inertial Body Tracking in the Presence of Model Calibration Errors. *Sensors* **2016**, *16*, 1132. [[CrossRef](#)] [[PubMed](#)]
37. Miezal, M.; Taetz, B.; Bleser, G. Real-time inertial lower body kinematics and ground contact estimation at anatomical foot points for agile human locomotion. In Proceedings of the 2017 IEEE International Conference on Robotics and Automation (ICRA), Singapore, 29 May– 3 June 2017; pp. 3256–3263.
38. Carbone, V.; Fluit, R.; Pellikaan, P.; van der Krogt, M.M.; Janssen, D.; Damsgaard, M.; Vigneron, L.; Feilkas, T.; Koopman, H.F.J.M.; Verdonschot, N. TLEM 2.0—A comprehensive musculoskeletal geometry dataset for subject-specific modeling of lower extremity. *J. Biomech.* **2015**, *48*, 734–741. [[CrossRef](#)] [[PubMed](#)]

39. Dreyfuss, H. *The Measure of Man: Human Factors in Design*; Whitney Library of Design: New York, NY, USA, 1967; ISBN 978-0-8230-7370-2.
40. Zeni, J.; Richards, J.; Higginson, J.S. Two simple methods for determining gait events during treadmill and overground walking using kinematic data. *Gait Posture* **2008**, *27*, 710–714. [[CrossRef](#)] [[PubMed](#)]
41. McGraw, K.; Wong, S.P. Forming Inferences About Some Intraclass Correlation Coefficients. *Psychol. Methods* **1996**, *1*, 30–46. [[CrossRef](#)]
42. Cicchetti, D.V. Guidelines, criteria, and rules of thumb for evaluating normed and standardized assessment instruments in psychology. *Psychol. Assess.* **1994**, *6*, 284–290. [[CrossRef](#)]
43. Banks, J.J.; Chang, W.-R.; Xu, X.; Chang, C.-C. Using horizontal heel displacement to identify heel strike instants in normal gait. *Gait Posture* **2015**, *42*, 101–103. [[CrossRef](#)]
44. Storm, F.A.; Buckley, C.J.; Mazzà, C. Gait event-detection in laboratory and real life settings: Accuracy of ankle and waist sensor based methods. *Gait Posture* **2016**, *50*, 42–46. [[CrossRef](#)]
45. Taetz, B.; Bleser, G.; Miezal, M. Towards self-calibrating inertial body motion capture. In Proceedings of the Information Fusion (FUSION), In Proceedings of 2016 19th International Conference on Information Fusion (FUSION), Heidelberg, Germany, 5–8 July 2016; pp. 1751–1759.
46. Seel, T.; Raisch, J.; Schauer, T. IMU-Based Joint Angle Measurement for Gait Analysis. *Sensors* **2014**, *14*, 6891–6909. [[CrossRef](#)]
47. Trojaniello, D.; Cereatti, A.; Pelosin, E.; Avanzino, L.; Mirelman, A.; Hausdorff, J.M.; Della Croce, U. Estimation of step-by-step spatio-temporal parameters of normal and impaired gait using shank-mounted magneto-inertial sensors: Application to elderly, hemiparetic, parkinsonian and choreic gait. *J. Neuroeng. Rehabil.* **2014**, *11*, 152. [[CrossRef](#)]
48. Beauchet, O.; Allali, G.; Annweiler, C.; Bridenbaugh, S.; Assal, F.; Kressig, R.W.; Herrmann, F.R. Gait Variability among Healthy Adults: Low and High Stride-to-Stride Variability Are Both a Reflection of Gait Stability. *Gerontology* **2009**, *55*, 702–706. [[CrossRef](#)] [[PubMed](#)]
49. Stolze, H. Typical features of cerebellar ataxic gait. *J. Neurol. Neurosurg. Psychiatry* **2002**, *73*, 310–312. [[CrossRef](#)]
50. Ilg, W.; Golla, H.; Thier, P.; Giese, M.A. Specific influences of cerebellar dysfunctions on gait. *Brain* **2007**, *130*, 786–798. [[CrossRef](#)] [[PubMed](#)]
51. Müller, B.; Ilg, W.; Giese, M.A.; Ludolph, N. Validation of enhanced kinect sensor based motion capturing for gait assessment. *PLoS ONE* **2017**, *12*, e0175813. [[CrossRef](#)] [[PubMed](#)]
52. Shorter, K.A.; Wu, A.; Kuo, A.D. The high cost of swing leg circumduction during human walking. *Gait Posture* **2017**, *54*, 265–270. [[CrossRef](#)] [[PubMed](#)]
53. Awad, L.N.; Bae, J.; Kudzia, P.; Long, A.; Hendron, K.; Holt, K.G.; O'Donnell, K.; Ellis, T.D.; Walsh, C.J. Reducing Circumduction and Hip Hiking During Hemiparetic Walking Through Targeted Assistance of the Paretic Limb Using a Soft Robotic Exosuit. *Am. J. Phys. Med. Rehabil.* **2017**, *96*, S157–S164. [[CrossRef](#)] [[PubMed](#)]
54. Shiotani, M.; Watanabe, T. A preliminary study on evaluation of circumduction movement during gait with wireless inertial sensors. In Proceedings of the 2014 36th Annual International Conference of the IEEE Engineering in Medicine and Biology Society, Chicago, IL, USA, 26–30 August 2014; pp. 5828–5831.
55. Watanabe, T.; Saito, H. Tests of wireless wearable sensor system in joint angle measurement of lower limbs. In Proceedings of the 2011 Annual International Conference of the IEEE Engineering in Medicine and Biology Society, Boston, MA, USA, 30 August–3 September 2011; pp. 5469–5472.
56. Robert-Lachaine, X.; Mecheri, H.; Larue, C.; Plamondon, A. Accuracy and repeatability of single-pose calibration of inertial measurement units for whole-body motion analysis. *Gait Posture* **2017**, *54*, 80–86. [[CrossRef](#)]



4 Application and Extended Validation

4.1 *Journal Paper 4*

4.1.1 Summary

The JP 4 extends the validation results of the JPs 1, 2 and 3 to a new group of, heterogeneous, subjects. These subjects represent one target group of the IMU system, a group of patients after THA, introducing a wider range of different body physiques and consequently different motion patterns. Further, this article introduces the first kind of application of the described IMU system, the classification of healthy and impaired gait based on certain features from the IMU based joint angles of the lower body. The relevant joint angles were calculated in the same manner as in JP 3 (following Procedure 3), using the stand-alone IMU system. Further, in this JP only the relevant features, rather than all 3D joint angles and all STP, were validated and published. For the complete validation of all 3D joint angles refer to chapter 4.2.

4.1.2 Main Contributions

- Validation of symmetry values and the ROM of the hip and pelvis joint angles as well as certain STP based on IMU data within a group of patients after THA
- Gait classification using IMU based features and a support vector machine (SVM)
- Feature selection based on expert knowledge and literature recommendations
- Comparison of gait classification based on STP and joint angles, respectively
- Comparison of the SVM model based on IMU data and OMC data, respectively
- Feature importance calculation



Article

Towards an Inertial Sensor-Based Wearable Feedback System for Patients after Total Hip Arthroplasty: Validity and Applicability for Gait Classification with Gait Kinematics-Based Features

Wolfgang Teufl ^{1,2,*} , Bertram Taetz ¹ , Markus Miezal ¹, Michael Lorenz ¹,
Juliane Pietschmann ³, Thomas Jöllenbeck ³, Michael Fröhlich ²  and Gabriele Bleser ¹ 

¹ Junior Research Group wearHEALTH, Technische Universität Kaiserslautern, Gottlieb-Daimler-Str. 48, 67663 Kaiserslautern, Germany; taetz@cs.uni-kl.de (B.T.); miezal@cs.uni-kl.de (M.M.); lorenz@cs.uni-kl.de (M.L.); bleser@cs.uni-kl.de (G.B.)

² Department of Sports Science, Technische Universität Kaiserslautern, Erwin-Schrödinger-Str. 57, 67663 Kaiserslautern, Germany; michael.froehlich@sowi.uni-kl.de

³ Institut für Biomechanik, Klinik Lindenplatz, Weslerner Str. 29, 59505 Bad Sassendorf, Germany; Juliane.Pietschmann@klinik-lindenplatz.de (J.P.); Thomas.Joellenbeck@klinik-lindenplatz.de (T.J.)

* Correspondence: teufl@cs.uni-kl.de; Tel.: +49 631 205-3332

Received: 24 October 2019; Accepted: 14 November 2019; Published: 16 November 2019



Abstract: Patients after total hip arthroplasty (THA) suffer from lingering musculoskeletal restrictions. Three-dimensional (3D) gait analysis in combination with machine-learning approaches is used to detect these impairments. In this work, features from the 3D gait kinematics, spatio-temporal parameters (Set 1) and joint angles (Set 2), of an inertial sensor (IMU) system are proposed as an input for a support vector machine (SVM) model, to differentiate impaired and non-impaired gait. The features were divided into two subsets. The IMU-based features were validated against an optical motion capture (OMC) system by means of 20 patients after THA and a healthy control group of 24 subjects. Then the SVM model was trained on both subsets. The validation of the IMU system-based kinematic features revealed root mean squared errors in the joint kinematics from 0.24° to 1.25°. The validity of the spatio-temporal gait parameters (STP) revealed a similarly high accuracy. The SVM models based on IMU data showed an accuracy of 87.2% (Set 1) and 97.0% (Set 2). The current work presents valid IMU-based features, employed in an SVM model for the classification of the gait of patients after THA and a healthy control. The study reveals that the features of Set 2 are more significant concerning the classification problem. The present IMU system proves its potential to provide accurate features for the incorporation in a mobile gait-feedback system for patients after THA.

Keywords: 3D gait analysis; inertial measurement unit; joint kinematics; machine learning; osteoarthritis; range of motion; rehabilitation; spatio-temporal parameters; support vector machine

1. Introduction

Hip osteoarthritis describes a degenerative process of the cartilage at the hip joint. Pain and immobility are the common consequences leading to changed gait patterns in the affected subjects. Total hip arthroplasty (THA) is considered the most promising option once conservative therapies are exhausted [1]. However, gait abnormalities, such as asymmetries in the kinematics between implanted and non-implanted hip joints, persist even after successful THA and the consecutive rehabilitation process [2]. The literature reveals persisting changes of the joint angle kinematics of the implanted

limb: rather, a higher posterior tilt of the pelvis during stance phase, an increased pelvic drop towards the non-implanted side while loading the implanted side, an increased hip internal rotation and hip adduction as well as a decreased hip extension peak and a reduced hip range of motion (ROM) in the sagittal plane [2–6]. According to Queen et al. [6], these asymmetries persist up to one year after the THA and they recommend a continuative physical therapy to eliminate these deviations.

Spatio-temporal gait parameters (STP) like stride length, gait velocity, etc. are further considered valuable parameters for the assessment of the outcome of THA [7–9]. Several studies reported a continuative reduction of stride length, step length and gait speed compared to able-bodied controls [10–12].

Persisting gait deviations can increase the risk of falls and interfere with the quality of life [3]. Gargiulo et al. [13] identified generalized rehabilitation methods instead of a patient specific rehabilitation process as one of the main problems.

Three-dimensional (3D) movement analysis has proven to be a useful tool for assessing the individual rehabilitation process and for comparing pre and post-operative gait in patients after THA [1,2,13,14]. Marker-based optical motion capture (OMC) systems are commonly used for gait analysis [15]. However, OMC systems cover only a limited capture volume and are not applicable in the subject's natural environment. In the last few decades, inertial measurement unit (IMU) systems have been intensively developed [16] to address these restrictions of the common measurement systems. The 3D joint angles as well as the STP of IMU systems were evaluated in different studies [17–28].

To be of use in a clinical background, Laroche et al. [1] pointed out that 3D gait analysis must prove its ability to discriminate impaired and non-impaired gait. For that reason, various studies used different machine-learning (ML) approaches to classify the gait of different populations [1,29–33].

One common method concerning a classification problem is the support vector machine (SVM). The basic theory of the SVM in a classification problem including two data sets is to find the hyperplane that best separates the two groups. If a linear separation cannot be found on the input data, the data can be transformed into a higher dimensional (feature) space, using different kinds of kernel functions, like a linear, polynomial or radial basis function (RBF) kernel. Subsequently, the separation can be searched in feature space [34].

A SVM has been used for the differentiation of impaired and non-impaired gait [1,29–31,35]. Figueiredo et al. [29] reported that the SVM is a reliable classifier of human gait based on high-dimensional data, especially for offline walking recognition.

Lau et al. [35], who used an SVM to classify the gait of patients after a stroke with drop foot employing two IMUs on shank and foot, suggested a Gaussian RBF kernel for individual gait classification problems.

Begg et al. [30] examined the gait of young and old subjects and employed an SVM with different kernel methods trained on 2D video analysis based features to differentiate their gait patterns. The SVM classifier incorporating a linear or polynomial kernel and different numbers of features reached an area under the curve (AUC) of 0.63 to 0.83. The SVM classifier employing an RBF kernel and different numbers of features reached an AUC of 0.75 to 0.95.

Laroche et al. [1] used a SVM with linear kernel to differentiate between the gait of patients with hip osteoarthritis and healthy controls based on 12 OMC-based joint angle trajectories. They reported an accuracy of their model of approximately 88%.

However, there is a lack of studies that try to differentiate between the IMU-based 3D joint kinematics of healthy subjects and those of patients after THA. Furthermore, for that purpose, no commonly acknowledged and biomechanically interpretable features, which can also be used to provide feedback, have been defined yet.

Hence, it was the aim of this study to employ a ML algorithm to classify the gait of healthy subjects and subjects after THA based on features selected from IMU-based kinematics. Therefore, a previously reported method was used [36] to calculate purely IMU-driven gait kinematics, STP as well as joint angles.

The IMU system in question is based on gyroscope and accelerometer data and incorporates an algorithm based on an iterated extended Kalman filter approach [37,38]. That system was validated against an OMC system in previous studies among a population of young and healthy subjects [36,39,40]. The 3D joint kinematics of the lower body was evaluated during the gait and physiotherapy specific movements in [39,40]. However, only the pure technical performance of the algorithm was evaluated, relying on an OMC-based calibration, initialization, and biomechanical model.

The event detection of initial contact and terminal contact [36] and, based on that, the estimation of the STP, were evaluated using the same algorithm as in [39,40], however, adding an IMU-based calibration, an IMU-based initialization as well as a biomechanical model based on scaling according to anthropometric tables, thereby introducing an autarkic system.

Most of the ML-related articles chose their features either automatically from raw input data or from employing statistical features or other input transformations, combined with a dimensionality reduction and/or a feature selection approach; this often renders interpretability of the employed features a hard task. In the present article, however, it was the aim to introduce meaningful features that are intuitive to physicians and patients alike. Therefore, in this study the features were chosen based on the literature and expert knowledge and then calculated from among the IMU-based kinematics.

Additionally, the features in question are validated against an OMC system, thus supporting the potential usefulness of the present system in a clinical context. Furthermore, the same ML algorithm trained on IMU data is in turn trained on OMC data, to indicate the independency of the selected features from the measurement system.

2. Materials and Methods

2.1. Feature Selection

In the present study the calculated features were chosen based on the literature [2–6,8–11,41] and the experience of movement scientists and physical therapists within the research group.

Pietschmann et al. [41] showed that the sagittal hip joint angle, measured by means of IMUs, is an essential measure in patients after THA for providing acoustic feedback during treadmill-based gait training. The sagittal hip joint angle was further described as an important measure in patients with THA by several other authors [2,4–6,10,11]. Gait speed [4,8,10], maximum hip extension [2,5,6,10], maximum hip flexion [3], pelvis transversal as well as sagittal [2] and frontal [42,43] ROM, stride length [10], stride time and cadence [9] were identified as further measures of interest regarding patients after THA.

The parameters mentioned above refer to a comparison of the operated side to a healthy control as well as to the contralateral limb, i.e., as symmetry value. This was one reason for choosing the difference between operated and non-operated limb, regarding the joint kinematic-based features, if possible. However, another reason for doing so was to reduce the transfer of errors from the measurement system, e.g., calibration offsets, into the selected features. Symmetry values and the ROM are considered independent of static offsets [40].

The features defined above were then separated into two sets. First, features which are easy to measure with common gait analysis tools, e.g., two IMUs or insoles and are, therefore, widely used in the assessment of gait, i.e., STP (Set 1). Second, features which are more complex to calculate and rely on the estimation of relative segment orientations, i.e., joint kinematics (Set 2).

The defined features are summarized in Table 1.

The features in Set 1 and Set 2, respectively, were investigated regarding their correlation within the corresponding set. Therefore, the Pearson correlation coefficient (r) was calculated.

Both feature sets combined were further investigated regarding the feature importance, independently of the actual SVM classification approach. The feature importance was evaluated using a minimum redundancy maximum relevance (MRMR) algorithm [44].

Table 1. Description of the two feature sets used for training the support vector machine (SVM) model.

Set 1	Definition
Stride Length [m]	Distance between the calcaneus positions of one foot projected on the ground at two consecutive ipsilateral initial contacts (IC)
Stride time [s]	Period between two consecutive ICs of the ipsilateral foot
Cadence [steps/min]	60 divided by the time from the IC of the ipsilateral foot to the IC of the contralateral foot
Speed [m/s]	Stride length divided by Stride time
Set 2	
Hip range of motion (ROM) symmetry [deg]	Difference between left and right sagittal hip ROM per gait cycle (GC)
Hip maximum flexion symmetry [deg]	Difference between left and right hip maximum flexion per GC
Hip maximum extension symmetry [deg]	Difference between left and right hip maximum extension per GC
Pelvis sagittal ROM [deg]	ROM of the pelvis in the sagittal plane per GC
Pelvis frontal ROM [deg]	ROM of the pelvis in the frontal plane per GC
Pelvis transversal ROM [deg]	ROM of the pelvis in the transversal plane per GC

2.2. Subjects

Twenty subjects after THA (13 females, 7 males; age 56.9 ± 8.2 years; 82.9 ± 18.9 kg and 1.74 ± 0.1 m in height) participated in the study (THA Group). All patients approximately 2 weeks after a standard cemented THA who could steadily walk at least for four minutes without support were included in the examination. All patients included in the study were allowed full weight bearing. The subjects were recruited from among the patients of the Klinik Lindenplatz (Bad Sassendorf, NRW, Germany). The study was approved by the ethical committee of the Universität Paderborn and meets the criteria of the declaration of Helsinki. After receiving all relevant study information, the participants signed an informed consent to the study including a permission to publish the data.

Additionally to the sample of 20 subjects after THA the data of 24 healthy subjects from [36] was also included (Control Group).

2.3. Data Acquisition

All measurements were recorded at the biomechanics laboratory of the institute of biomechanics of the Klinik Lindenplatz. Prior to the measurement and the subject preparation a gyroscope and accelerometer bias estimation was performed. Therefore, the IMUs were fixed in a rectangular box. The box was positioned once on each side for a few seconds. The IMU measurements during this procedure were recorded. The accelerometer bias estimation was performed using a spherical fitting, similar to a method used for magnetometers [45]. Additionally, the gyroscope biases were calculated as the sample means of the measured gyroscope values.

The subjects were instrumented by means of seven IMUs (MTw Awinda, Xsens Technologies BV, Enschede, Netherlands) and 32 retroreflective markers, positioned on anatomical landmarks according to the marker protocol described by Leardini et al. [46]. To reduce the effect of soft tissue artefacts on the difference between the OMC data and the IMU data the IMUs were inserted into rigid boxes (RB) equipped with four additional markers. Figure 1 shows a schematic model of the marker and IMU positioning. In contrast to the depicted model, the subjects in the current study had to wear shoes for hygienic reasons. Therefore, the markers on the foot had to be positioned on the shoe, approximating the underlying anatomical landmarks.

First, the subjects performed the 2-step calibration described in [36]. The 2-step calibration consists of two adapted static postures according to [47] and is used for the IMU to segment (I2S) calibration. Second, the subjects had to walk along a walkway of seven meters for a maximum of six minutes. The 3D marker positions were recorded using 12 OptiTrack Prime 13 cameras and the software Motive 1.10 (OptiTrack, NaturalPoint, Inc., Oregon, USA). The IMU data was recorded using the Xsens software MVN Biomech 4.3.7. For the further calculations, only the raw accelerometer data and raw gyroscope data were considered. All records were taken simultaneously and were hardware-synchronized using a standard 5V transistor-transistor logic signal.



Figure 1. Schematic preparation of a subject with retroreflective markers and inertial measurement units (IMUs) inserted into rigid boxes equipped with additional markers. In the actual study, the markers on the pelvis were placed directly onto the skin. Furthermore, the subjects in the present study had to wear shoes.

2.4. Data Processing

The resulting biases from Section 2.3 were subtracted prior to the processing of the raw IMU data. Based on the IMU raw data the 3D joint angle kinematics of the hip, knee and ankle as well as the 3D global pelvis rotation were calculated. However, only the hip and pelvis kinematics were considered for further procedure based on the selected features in Table 1. The same initialization and I2S calibration as reported previously in [36] were applied. Additionally, the segment lengths were scaled according to anthropometric tables and the body height. The segment coordinate systems and the joint centers were derived based on the segment lengths and a biomechanical human body model incorporating anatomical landmark positions described in [48]. For the segment orientation tracking an iterated extended Kalman filter (IEKF) approach according to [38] was used to fuse the gyroscope and accelerometer data. The same filter settings and tuning parameters as in [39] were incorporated.

The segment orientations based on the OMC data were estimated based on the RB orientations according to the recommendations of Visual 3D (C-Motion, Inc., Germantown, MD, USA). The IMU-based relative joint angle rotations as well as the OMC-based ones were calculated from the estimated segment orientations via Euler angle decomposition [49]. A detailed description of the IEKF can be found in [39]. Detailed descriptions of the IMU calibration, initialization as well as the biomechanical model building, can be found in [36]. The Euler angle decomposition was described in a supplementary file of [40].

Furthermore, the initial contact (IC) and terminal contact (TC) events were estimated according to [36] and based on that information the STP stride length, stride time, cadence and speed were calculated. The same approach for the calculation of the gait events and the STP was previously validated among the Control Group in [36], where only the validity of the STP was reported. Therefore, in the present study the joint angle kinematics of the Control Group, based on the raw IMU data from [36], were calculated in the same manner as for the THA Group.

2.5. Feature Validation—Statistical Analysis

In [39] the drift-free measurement of the IMU-based joint kinematics of the lower extremity, with the exception of the global pelvis rotation, was shown. However, in [39] it was also shown that the ROM of the global pelvis rotation was not affected by the drift. Therefore, in this study 18,000 frames of the record, of approximately 5 min, were considered for statistical analysis.

For further investigations the IMU-based joint angle waveforms were segmented into 100% gait cycle (GC) based on the IC information. Each GC of each subject was treated as an individual case. Outliers were detected based on the GC duration and removed if they were outside a boundary of the mean GC duration plus 2 times standard deviation.

The features described in Table 1 were then calculated for every GC of each subject in the THA Group as well as the Control Group. This approach resulted in a total of 1856 samples per feature (1402 labeled “healthy”, aka Control Group; 454 labeled “patient”, aka THA Group).

For comparison, the features were also calculated based on the OMC data, also segmented to 100% GC. In this case the IC was estimated based on the markers placed on the heel, toe and the pelvis and a custom written Matlab (Mathworks Inc., Natick, MA, USA) script incorporating an approach based on [50,51]. Here, feature Set 1 and 2 counted 1937 samples per feature (1404 labeled “healthy”, aka Control Group; 533 labeled “patient”, aka THA Group).

To validate the features, the following statistics were calculated based on every GC of each subject: the root mean squared error (RMSE) plus 95% confidence interval (CI), the mean absolute error (MAE) plus 95% CI and r as well as the coefficient of determination (r^2).

Additionally, the range of motion error (ROME) plus 95% CI and the coefficient of multiple correlations (CMC) were calculated for the 3D joint kinematics of the pelvis and hip. In the case of waveforms rather than single values the CMC was preferred to r according to [52].

A two-sample independent t-test was calculated to find significant differences between the THA Group and the Control Group in the RMSE of the features of Sets 1/2 and the ROME of the pelvis and hip joint kinematics. The chi square goodness of fit test was used to check for a normal distribution in the data. All statistics were conducted in Matlab 2019a and 2019b.

2.6. Classification Algorithm

Based on the information reported in Section 1, a SVM was deemed the appropriate tool for the present study. Figueiredo et al. [29] stated that SVMs are well capable of dealing with the non-linear character of human gait and represent an accurate classifier in recognition tasks concerning impaired and non-impaired gait.

First, the SVM algorithm was trained on the IMU-based features. Second, the SVM algorithm was also trained on the same features based on OMC data

Figure 2 shows the comparison of two representative features. Qualitative examination revealed that the two groups showed a non-linear relation within all features. Therefore, in this study an SVM with Gaussian RBF kernel was applied. For the model training, the Classification Learner® app from Matlab 2019b was used. In every case the Box Constrained level was set to 1.7 and the Kernel scale was set to auto. Standardize data was set to true. A 12-fold cross-validation was employed to prevent overfitting.

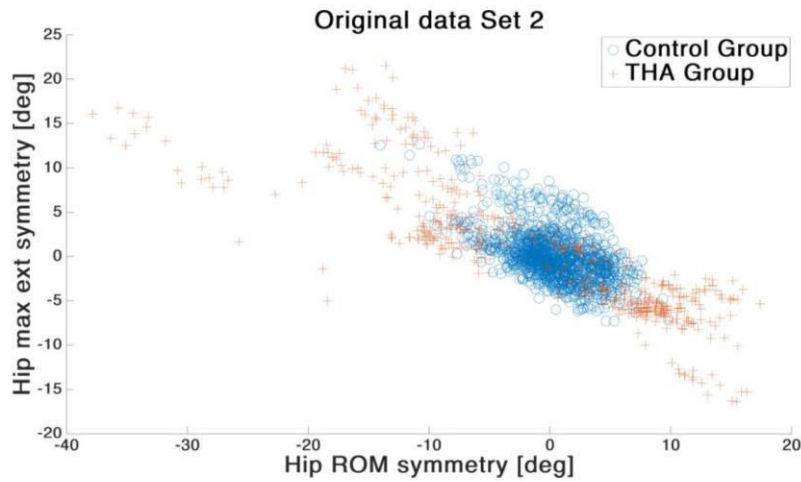


Figure 2. Exemplary data from Set 2 showing on the X-axis the hip ROM symmetry and on the Y-axis the hip maximum extension symmetry. Blue circles indicate the Control Group; red crosses indicate the total hip arthroplasty (THA) Group. The plot indicates a non-linear differentiation of the two groups.

2.7. Classification—Statistical Analysis

To compare and interpret the results of the different classifier models the following measures were calculated as reported in [53]:

The accuracy (ACC) was calculated based on the true positive rate (TP), true negative rate (TN), false positive rate (FP) and false negative rate (FN).

$$ACC (\%) = \frac{TN + TP}{TP + TN + FP + FN} * 100\% \quad (1)$$

The sensitivity (SEN) was calculated based on the TP and FN.

$$SEN (\%) = \frac{TP}{TP + FN} * 100\% \quad (2)$$

The specificity (SPEC) was calculated based on the TN and FP.

$$SPEC (\%) = \frac{TN}{TN + FP} * 100\% \quad (3)$$

Additionally, the AUC [30] was calculated.

Figure 3 summarizes the framework of the present study.

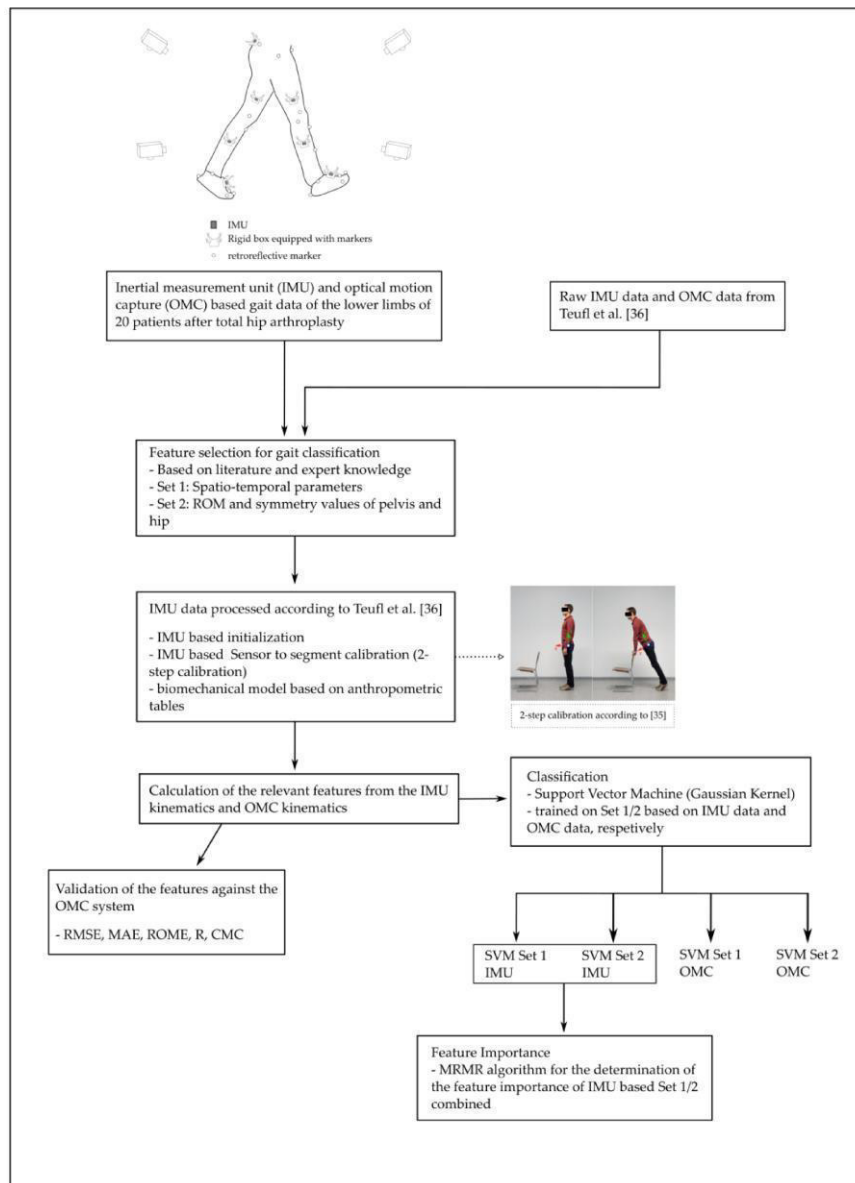


Figure 3. Workflow of the present study.

3. Results

3.1. Feature Validation

In this section the validity of the features of Set 1 and Set 2 as well as of the ROM of the pelvis and hip in three dimensions are presented for the THA Group and the Control Group, respectively. In the following, the values of the statistical measures are considered the mean over all subjects.

The validation process revealed a high accuracy of the features measured with the IMU system. The RMSE of the feature Set 2 was below 1.3° in both groups. Significant differences between the groups were found in the hip ROM symmetry and the pelvis transversal ROM. Details are shown in Tables 2 and 3.

Table 2. Validation results of the feature Set 2 within the THA Group. Shown are the root mean squared error (RMSE) \pm standard deviation (SD) (95% confidence interval (CI)), the mean absolute error (MAE) \pm SD (95% CI), the pearson correlation coefficient (r) \pm SD and the coefficient of determination (r^2). An asterisk indicates a significant difference between the THA Group and the Control Group. The corresponding p -values are given.

	RMSE \pm SD (95% CI) [deg]	p -Value	MAE \pm SD (95% CI) [deg]	$r \pm$ SD	r^2
Hip ROM symmetry	1.16 \pm 0.92 (0.32–1.23) *	0.008	0.48 \pm 0.69 (–0.15–0.54)	0.90 \pm 0.21	0.81
Hip maximum flexion symmetry	1.21 \pm 0.81 (0.39–1.20)	0.214	0.51 \pm 0.59 (–0.06–0.52)	0.48 \pm 0.56	0.23
Hip maximum extension symmetry	1.24 \pm 1.18 (0.11–1.29)	0.092	0.52 \pm 0.71 (–0.15–0.56)	0.71 \pm 0.50	0.50
Pelvis sagittal ROM	0.40 \pm 0.25 (0.14–0.39)	0.054	0.15 \pm 0.16 (–0.02–0.14)	0.94 \pm 0.18	0.88
Pelvis frontal ROM	0.39 \pm 0.32 (0.14–0.45)	0.083	0.16 \pm 0.24 (–0.06–0.18)	0.95 \pm 0.16	0.90
Pelvis transversal ROM	1.25 \pm 0.80 (0.59–1.38) *	0.000	0.47 \pm 0.50 (–0.05–0.45)	0.91 \pm 0.24	0.83

* Significant difference at p -value $<$ 0.05.

Table 3. Validation results of the feature Set 2 within the Control Group. Shown are the RMSE \pm SD (95% CI), MAE \pm SD (95% CI), $r \pm$ SD and r^2 .

	RMSE \pm SD (95 % CI) [deg]	MAE \pm SD (95% CI) [deg]	$r \pm$ SD	r^2
Hip ROM symmetry	0.52 \pm 0.39 (0.17–0.50)	0.21 \pm 0.28 (–0.04–0.20)	0.88 \pm 0.07	0.77
Hip maximum flexion symmetry	0.83 \pm 1.11 (–0.09–0.87)	0.45 \pm 0.95 (–0.31–0.51)	0.83 \pm 0.18	0.67
Hip maximum extension symmetry	0.68 \pm 0.85 (–0.02–0.71)	0.34 \pm 0.70 (–0.21–0.40)	0.74 \pm 0.20	0.55
Pelvis sagittal ROM	0.24 \pm 0.21 (0.07–0.26)	0.09 \pm 0.12 (–0.02–0.08)	0.98 \pm 0.03	0.96
Pelvis frontal ROM	0.25 \pm 0.13 (0.14–0.25)	0.09 \pm 0.10 (0.01–0.09)	0.99 \pm 0.06	0.98
Pelvis transversal ROM	0.36 \pm 0.25 (0.19–0.41)	0.12 \pm 0.15 (–0.00–0.13)	0.99 \pm 0.03	0.98

The ROME of the global pelvis and the hip joint in the sagittal, frontal and transverse plane revealed values from 0.36° to 2.70° in both groups. Significant differences between the groups in the ROME were evident in the left and right hip flexion and in the pelvis obliquity as well as pelvis rotation. Details are shown in Table 4.

The validation of the STP (feature Set 1) of the Control Group can be found to its full extend in [36]. Therefore, in Table 5 the results of the validation of feature Set 1 are shown only for the THA group. Significant differences between the RMSE in the STP of the THA Group and the corresponding results of the Control Group were found in all four parameters.

Table 4. Validation results of the 3D range of motion (ROM) of the left (LT) and right (RT) hip and pelvis in both groups. Shown are the ROM error (ROME) \pm SD (95% CI) and the coefficient of multiple correlation (CMC) \pm SD. An asterisk indicates a significant difference between the THA Group and the Control Group. The corresponding *p*-values are given.

	THA Group			Control Group	
	ROME [deg] \pm SD (95% CI)	<i>p</i> -Value	CMC \pm SD	ROME [deg] \pm SD (95% CI)	CMC \pm SD
LT Hip–Abduction	0.89 \pm 0.60 (0.46–1.13)	0.742	0.76 \pm 0.24	0.83 \pm 0.48 (0.57–0.98)	0.87 \pm 0.16
LT Hip–Rotation	0.84 \pm 0.36 (0.63–1.03)	0.226	0.69 \pm 0.24	1.05 \pm 0.62 (0.63–1.15)	0.66 \pm 0.24
LT Hip–Flexion	0.85 \pm 0.46 (0.49–1.00) *	0.000	0.73 \pm 0.20	2.70 \pm 0.97 (2.32–3.14)	0.93 \pm 0.12
RT Hip–Abduction	1.10 \pm 0.55 (0.85–1.38)	0.053	0.83 \pm 0.19	0.80 \pm 0.44 (0.45–0.83)	0.93 \pm 0.06
RT Hip–Rotation	0.98 \pm 0.60 (0.45–1.03)	0.241	0.60 \pm 0.30	1.20 \pm 0.60 (0.79–1.30)	0.71 \pm 0.23
RT Hip–Flexion	1.20 \pm 0.60 (0.92–1.50) *	0.001	0.82 \pm 0.21	2.11 \pm 1.01 (1.44–2.30)	0.93 \pm 0.11
Pelvis–Obliquity	0.36 \pm 0.24 (0.18–0.41) *	0.000	0.88 \pm 0.11	0.73 \pm 0.35 (0.49–0.79)	0.90 \pm 0.11
Pelvis–Flexion	0.51 \pm 0.17 (0.43–0.60)	0.728	0.44 \pm 0.18	0.56 \pm 0.59 (0.15–0.65)	0.52 \pm 0.25
Pelvis–Rotation	0.98 \pm 0.46 (0.66–1.10) *	0.044	0.58 \pm 0.30	0.75 \pm 0.27 (0.66–0.88)	0.65 \pm 0.22

* Significant difference at *p*-value < 0.05.

Table 5. Summary of the results of the validation of the feature Set 1 for the THA group. Shown are the RMSE \pm SD (95% CI), the MAE \pm SD (95% CI), *r* and *r*². An asterisk indicates a significant difference between the THA Group and the Control Group. The corresponding *p*-values are given.

	RMSE \pm SD (95% CI)	<i>p</i> -Value	MAE \pm SD (95% CI)	<i>r</i>	<i>r</i> ²
Stride Length [m]	0.05 \pm 0.03 (0.03–0.05) *	0.007	0.06 \pm 0.04 (0.03–0.06)	0.78	0.61
Stride Time [s]	0.04 \pm 0.02 (0.02–0.04) *	0.000	0.05 \pm 0.02 (0.02–0.05)	0.91	0.83
Cadence [steps/min]	3.85 \pm 2.50 (1.77–4.43) *	0.000	4.86 \pm 2.90 (2.27–5.36)	0.54	0.29
Speed [m/s]	0.04 \pm 0.02 (0.02–0.04) *	0.000	0.05 \pm 0.03 (0.03–0.06)	0.84	0.71

* Significant difference at *p*-value < 0.05.

3.2. Classification

The SVM classifier trained on the feature Set 1 reached an accuracy of 87.2%. In contrast, the SVM classifier trained on feature Set 2 achieved an overall accuracy of 97.0%. The same SVM model was also trained on the same features derived from optical data. In that case the classifier trained on feature Set 1 showed an accuracy of 88.6%. The classifier trained on feature Set 2 revealed an accuracy of 96.4%. See Table 6 and Figures 4–7 for detailed information on the results of the four classifier variations.

Table 6. Results of the different SVM models trained on feature Set 1 and Set 2. “OMC” indicates the support vector machine (SVM) model trained on the features calculated based on the optical motion capture system.

	SVM Set 1	SVM Set 2	SVM Set 1 OMC	SVM Set 2 OMC
Accuracy [%]	87.2	97.0	88.6	96.4
Sensitivity [%]	87.8	97.7	88.3	97.4
Specificity [%]	84.7	94.8	89.6	93.6
Area under the curve	0.84	0.98	0.87	0.99



Figure 4. Confusion matrices of the SVM trained on IMU-based feature Set 1 and 2. The numbers in the matrices indicate correctly or incorrectly classified GC.



Figure 5. Confusion matrices of the SVM trained on OMC-based feature Set 1 and 2. The numbers in the matrices indicate correctly or incorrectly classified GC.

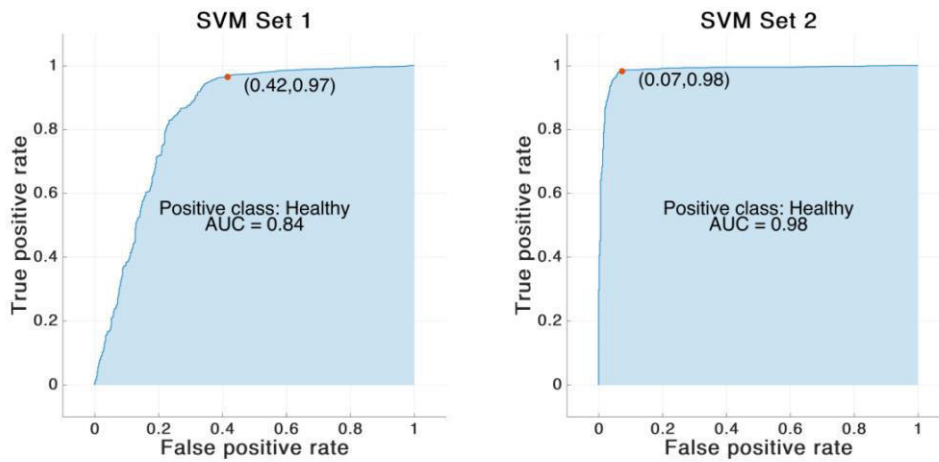


Figure 6. Receiving operating characteristic (ROC) curve for the SVM model trained on IMU-based feature Set 1 and 2. The red dot marks the performance of the corresponding model. The blue area indicates the area under the curve (AUC).

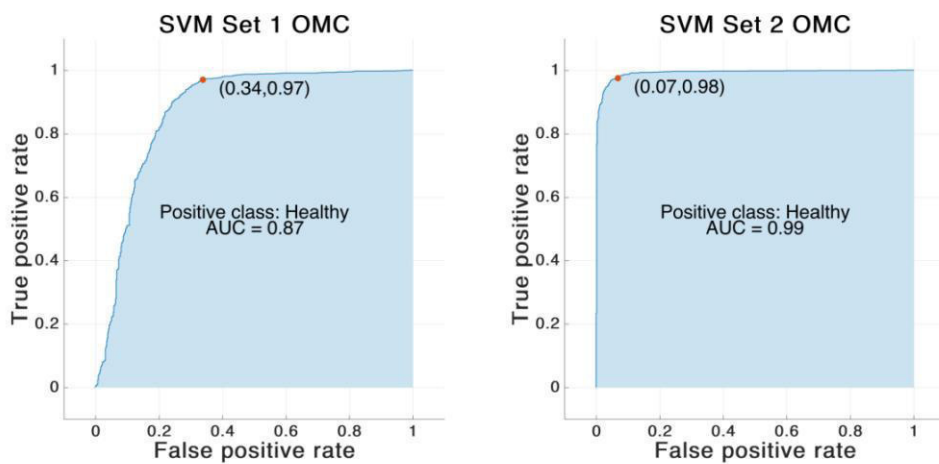


Figure 7. ROC curve for the SVM model trained on OMC-based feature Set 1 and 2. The red dot marks the performance of the corresponding model. The blue area indicates the AUC.

3.3. Feature Importance

In the case of the IMU driven SVM classifier a MRMR algorithm was employed to calculate the feature importance of the combined features of Set 1 and Set 2. Figure 8 shows the outcome of the calculation.

The ranking of the feature weights revealed that the hip ROM symmetry contributed most to the separation of the two groups. Overall, three out of the top-four ranked features belonged to the feature Set 2.

A post-examination revealed an accuracy of 95.7% of the SVM classifier trained on the four most important features.

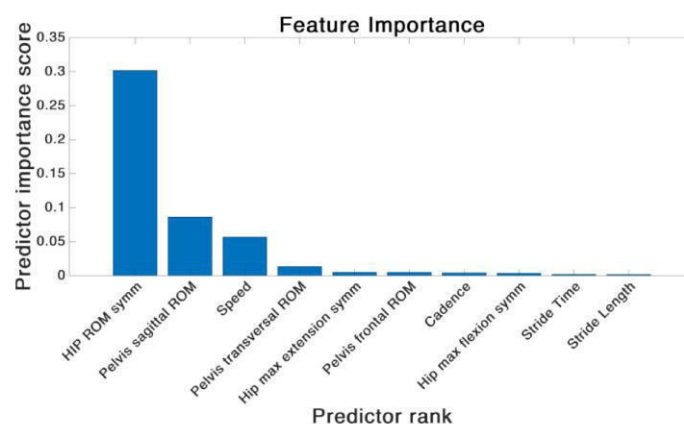


Figure 8. Ranking of the combined features from Set 1 and 2 based on IMU data after employing a minimum redundancy maximum relevance (MRMR) feature ranking algorithm.

3.4. Feature Correlation

The calculation of the correlation between the features in Set 1 and Set 2, respectively, revealed that the feature speed was correlated with stride time (-0.78) and stride length (0.80). Furthermore, in Set 2 the feature hip ROM symmetry showed correlations with hip maximum flexion symmetry (0.71) and hip maximum extension symmetry (-0.76). See Tables 7 and 8 for details.

Table 7. Correlation matrix for the features of Set 1. Shown are the values for r .

	Stride Time	Stride Length	Cadence	Speed
Stride Time	1.00	x	x	x
Stride Length	-0.33	1.00	x	x
Cadence	-0.53	0.10	1.00	x
Speed	-0.78	0.80	0.46	1.00

Table 8. Correlation matrix for the features of Set 2. Shown are the values for r .

	Hip ROM Symm.	Hip Max Extension Symm.	Hip Max Flexion Symm.	Pelvis Sagittal ROM	Pelvis Frontal ROM	Pelvis Transversal ROM
Hip ROM symm.	1.00	x	x	x	x	x
Hip max extension symm.	-0.76	1.00	x	x	x	x
Hip max flexion symm.	0.71	-0.09	1.00	x	x	x
Pelvis sagittal ROM	-0.30	0.28	-0.16	1.00	x	x
Pelvis frontal ROM	0.16	-0.08	0.16	0.02	1.00	x
Pelvis transversal ROM	-0.17	0.12	-0.14	0.26	0.29	1.00

4. Discussion

The present examination evaluated the applicability of features taken from the IMU-based 3D gait kinematics of the lower body for the discrimination of the gait of patients after THA and a healthy control. Therefore, special features were chosen according to the literature and expert knowledge. A first step was to validate the accuracy of the measured features in comparison to an OMC system. As a second step, the features were divided into two groups of features, STP and joint kinematics, due to the different kind of measurement approach to these variables. Then, an SVM model was trained on both of the feature sets, first on the IMU-derived features and second, for the sake of comparison, on the OMC derived features.

4.1. Feature Selection

Laroche et al. [1] reported that in gait analysis there is too many data recorded and it is therefore important to identify relevant features. In the present study no common feature selection algorithms were employed. As mentioned in Section 1 it was the aim to select meaningful, intelligible features from among the IMU kinematic data based on the literature and expert knowledge. It was important that the selected features are mostly independent of uncertainties in the measurement method. To date, in IMU systems one major concern is the I2S calibration. In [37] it was shown that errors in the I2S orientation were linearly transferred into the segment orientation estimation and therefore directly affect the calculated joint angles. Common IMU systems as well as the present system rely in their I2S calibration procedure on pre-defined poses, e.g., n-pose or T-pose [54]. However, in [55] it was shown that the n-pose can differ up to 15° from the assumed zero position in the joints of the lower limb. Additionally, the work revealed that in older, impaired subjects the deviations tend to increase, mainly in the frontal plane.

Considering these uncertainties in the I2S calibration process, high absolute deviations between the OMC-based joint angle waveforms and the IMU-based joint angle waveforms, i.e., static offsets, can be expected. Actually, in the present evaluation offsets in the 3D joint kinematics of the hip and pelvis up to 12.52° were found. A detailed examination and fragmentation of these errors is determined for future work.

However, differences between absolute values, expressed here as symmetry between left and right lower limb and the ROM, are considered unaffected by offsets, as long as they are static. To further prove this, the individual features as well as the ROM of the joints of interest were in this study validated against the OMC system.

4.2. Feature Validation

To the knowledge of the authors this is the first study to validate parameters from among IMU-based joint kinematics of the human gait, i.e., the features in Set 2, designed for training a classification model. It is deemed essential to prove the accuracy of features prior to its employment in a ML algorithm.

In the validation of the feature Set 2, low errors ($<1.3^\circ$) were found in both groups. However, there were significant differences between the two groups in the RMSE of the hip ROM symmetry and the pelvis transversal ROM. Also in the ROME of the 3D joint kinematics of the hip and pelvis appeared significant differences between the groups (left and right hip flexion, pelvis obliquity and rotation). Concerning the significant differences between the groups in the RMSE and ROME of some features and joint angles one has to consider a few differences in the measurement set-up of both groups. First, there were non-system related differences like the measurement location, the footwear and finally the subject's physique. The THA Group had to wear shoes due to hygienic reasons and walked on an artificial walkway incorporating force plates. The walkway exhibited a slight inclination, which was evident in the raw marker data of the OMC system. The subjects of the control group walked bare footed and on a normal floor. Further, the two groups differed, as it was intended, in their body stature. The THA group showed an average body mass index (BMI) of 27.16, whereas the control group had an average BMI of 22.49.

Zügner et al. [27], who validated the accuracy of the IMU-based pelvis, hip, knee and ankle joint angle of the sagittal plane within a group of 49 patients after THA, found a significant error in the hip sagittal ROM of about 3° . In the pelvic sagittal ROM an error of approximately 0.5° was found in their study, similar to the present findings.

Zhang et al. [17] evaluated the accuracy of an IMU system in 10 healthy subjects. They found a ROME in the 3D kinematics of the hip of 2.47° to 4.83° .

It was shown that the ROM can be measured with high accuracy in the presence of variations in the calibration or the physique of the subjects. It is considered important that the ROME showed

low values in both groups, since the ROM is regarded an essential outcome in the evaluation of the rehabilitation progress [56].

The estimation of the STP within the THA group showed valid results comparable to those results found previously within the control group [36] and to results from studies employing alternative systems for the STP estimation [26,57].

Kluge et al. [26] examined the validity of STP in subjects with Parkinson disease. Their reported mean errors of the temporal parameters were slightly higher compared to the present study. The results of the stride length revealed a smaller error (-0.001 m). They also evaluated the validity among a healthy population. Interestingly they found a higher error in the stride length concerning that group (-0.016 m). That did not apply for the current system.

Bertoli et al. [57] also examined the validity of the STP of patients with Parkinson disease, mildly cognitive impaired subjects as well as older, healthy subjects from different clinical facilities. For the stride length, they reported a mean error of -0.001 m to -0.014 m in the different clinics. Therefore, the present findings (mean error of 0.009 m) lie well within that range. The temporal parameters described by Bertoli et al. [57] show a mean error of under 0.001 s for stride time. Therefore, their results show a similar outcome compared to the current findings (mean error of 0.002 s). Note, the referenced works used a sampling frequency above 100 Hz whereas the IMUs in the present study were recording at a frequency of 60 Hz.

In feature Set 1, significant differences between the RMSEs of the THA Group and the Control Group were evident in all four parameters. That might be due to the same reasons as mentioned above concerning feature Set 2. However, the fact that the algorithm for the event detection was developed on young and healthy subjects and has not been modified for the present study might also have influenced the outcome of the STPs in the THA Group.

In summary, it can be stated that static offsets between the OMC and the IMU system were evident. These offsets might be explained by deviations from the neutral-zero calibration position or uncertainties in the segment length estimation and based on that erroneous joint center estimates. It was shown that a misalignment between joint centers and joint axes could lead to kinematic cross talk [28]. However, the selected features of Sets 1 and 2 as well as the ROM seemed unaffected by these errors. Nevertheless, these possible sources of errors should be erased in the future by employing an automated self-calibration, independent from poses, pre-defined movements as well as a strict sensor to segment assignment. A proof of concept was delivered recently [58,59].

Furthermore, a more individualized biomechanical model could improve the estimation of segment lengths and consequently the joint centers. However, an alternative approach, in regard to the scaling approach used in the current study and in [36], should support the idea of a mobile and flexibly applicable system. Therefore, the creation of a biomechanical model of the lower body based on a single-view depth camera image was recently proposed [60].

4.3. Classification

It was the aim of this part of the study to evaluate the usability of the above validated features in the classification of impaired and non-impaired gait. For this purpose the two subsets of relevant kinematic parameters were used to train an SVM model for separating the gait of patients after THA and of healthy subjects, respectively.

The classifier trained on feature Set 1, consisting of commonly used STP, showed a high accuracy (87.2%). However, the classifier trained on feature Set 2 showed an even higher accuracy (97.0%), using features based on 3D joint kinematics. Further, in the present study the same features were calculated based on the OMC data and employed to train a similar SVM model. This was done to prove the independence of the SVM model regarding the measurement approach that was used to derive the features. As expected the classifiers trained on feature Set 1/2 based on OMC data revealed a similar accuracy (Set1: 88.6° , Set 2: 96.4°) compared to the IMU-based classifier.

In summary, the model trained on feature Set 2 revealed better results. However, also the accuracy of the model trained on the feature Set 1 showed a satisfying accuracy. The post-hoc analysis of the feature importance showed the impact of the features of Set 2 on the classifier accuracy. The hip sagittal ROM proved to be the most important factor. This result supports the findings of Pietschmann et al. [41] who addressed the hip sagittal plane movement as a key parameter in their attempt to improve the gait pattern of patients after THA via acoustic feedback.

The features of Set 1 were shown to have less impact on the accuracy of the classifier despite the fact that the RMSE in all of the STP of feature Set 1 were significantly different between the two groups. Therefore, a reason could have been a high correlation between the features in Set 1. However, it was shown that only the feature speed was correlated with stride time and stride length. That was not unexpected since speed was calculated using Stride Time and Stride Length. The same goes for the features hip ROM symmetry, hip maximum flexion symmetry and hip maximum extension symmetry of Set 2. Since the Hip ROM symmetry contains information of the hip flexion and extension, these features were also correlated.

Therefore, the hip ROM symmetry and speed can be considered to contain more information compared to the remaining features. That was also proven in the feature importance calculation where the aforementioned parameters were within the top three ranked features.

There is another advantage in measuring the joint angle kinematics rather than the STP alone. Asymmetries in the STP, e.g., stride length, could be reduced by introducing compensatory mechanisms like an increased pelvic extension in late stance of the operated limb to compensate for a lack of hip extension [61]. Therefore, in an analysis a symmetry between operated and non-operated limb would be evident in the parameter stride length, whereas asymmetries could still be found in the pelvis and hip joint angle [62]. In that case, disadvantageous gait deviations can only be detected by evaluating the complete 3D gait kinematics of the lower body.

However, the examination revealed that with the kinematic information of the pelvis and the hip as well as the gait speed a classification of the gait can be achieved with an accuracy of 95.7%. In this study a full lower body set up of IMUs, i.e., seven IMUs, was initially used. The results imply that a reduced sensor set up might result in the same outcome. Employing three IMUs, mounted on the pelvis and thighs, would be sufficient to deduce the gait speed as well as the 3D global pelvis motion and the 3D joint kinematics of the hip. However, that demands an estimation of the gait events using the IMU mounted on the pelvis. In general it was shown that the gait events and the step length can be deduced from a pelvis-mounted IMU [63]. Furthermore, it has not been evaluated yet if the joint kinematics of the hip as well as the estimation of the 3D pelvis motion might suffer from a sensor reduction, using the present system. However, that is intended for future work.

It has to be stated that the results of the SVM classifier reported in this article are only valid for the specific data set used in this study. Consider that the present gait data was recorded under laboratory conditions and from a rather small sample size. However, through the extended recording time a considerable number of GCs could be regarded for the evaluation. Future work has to investigate the usability of the described IMU system as well as the utility of the proposed SVM classifier based on real-world and non-standardized recorded data.

A further limitation is the fact that the two groups were not age-matched. Strictly speaking the difference between the groups could have been due to age alone. However, Boyer et al. [64] reported that the changes in the hip kinematics due to age are rather small. Moreover, they stated that the hip ROM is slightly higher in the elderly group. That would indicate an even higher difference between subjects after THA and an age-matched control. Besides, there is no evidence that the asymmetry between the lower limbs increases at an advanced age. Nevertheless, a comparison of the THA Group with an age-matched control group would have strengthened the present outcome.

Furthermore, Ewen et al. [65] stated in their review on post-operative gait analysis after THA that the rehabilitation progress reaches a peak six months after the surgery. The patients in the present study were tested only a short time after THA, meaning they were in the midst of their stationary

rehabilitation phase. Consequently a significant progress would have been expected within the next weeks. A possible feedback system based on IMU data would take up approximately after a stationary rehabilitation. Therefore, it has to be examined if the asymmetries and gait deviations at that date are distinctive enough for successful classification using the model and features employed in the present study. On the other hand, several studies showed that significant differences between operated and non-operated side as well as a healthy control group exceed six months and more [7,11].

5. Conclusions

In summary, the present work describes an IMU system that accurately measures the ROM and special features of interest of the lower limb 3D kinematics of the human gait, in patients after THA as well as in a healthy population. Although static offsets are to be expected, it was shown that the symmetry values based on joint kinematics, the STP and, especially, the important ROM could be measured with satisfying accuracy among subjects of differing physique. However, future work will aim at the improvement of the calibration process as well as a refinement of the biomechanical model.

Furthermore, the current study proved that the described system can be successfully used to classify the gait of impaired and non-impaired subjects, employing a SVM model and elaborated features of the joint kinematics. However, this approach has to be tested for its functionality in non-standardized settings.

As mentioned in [36], it is the superior goal of the authors of the present work to design a mobile IMU system that delivers 3D gait kinematics, joint angles as well as a wide range of STP, based on which feedback on the individual gait pattern can be provided to the user independent of the location and beyond the standard rehabilitation period. In the opinion of the authors, a further step towards that goal was achieved in this work by defining valid and intelligible features from IMU-based gait kinematics that are sensitive to the subject's impairment and, therefore, seem promising as control parameters in a future feedback system.

Author Contributions: Conceptualization, W.T., B.T., T.J. and G.B.; Data curation, W.T., M.M. and M.L.; Formal analysis, W.T., B.T. and G.B.; Funding acquisition, M.F. and G.B.; Investigation, W.T., B.T. and J.P.; Methodology, W.T. and B.T.; Project administration, G.B.; Resources, J.P. and T.J.; Software, W.T., M.M., M.L. and G.B.; Supervision, M.F. and G.B.; Validation, W.T.; Visualization, W.T.; Writing—original draft, W.T.; Writing—review and editing, W.T., B.T., M.M., M.F. and G.B.

Funding: This work was performed by the Interdisciplinary Junior Research Group wearHEALTH, funded by the BMBF (16SV7115, 03IHS075B). For more information, please visit the website: www.wearhealth.org.

Acknowledgments: We would like to thank the staff of the Klinik Lindenplatz, Bad Sassendorf, Germany, for their support concerning the subject acquisition and data acquisition.

Conflicts of Interest: The authors declare no conflict of interest. The authors alone are responsible for the content and writing of this paper. The founding sponsors had no role in the design of the study; in collection, analyses, or interpretation of data; in the writing of the manuscript; and in the decision to publish the results.

References

1. Laroche, D.; Tolambiya, A.; Morisset, C.; Maillefert, J.F.; French, R.M.; Ornetti, P.; Thomas, E. A classification study of kinematic gait trajectories in hip osteoarthritis. *Comput. Biol. Med.* **2014**, *55*, 42–48. [[CrossRef](#)] [[PubMed](#)]
2. Tsai, T.-Y.; Dimitriou, D.; Li, J.-S.; Woo Nam, K.; Li, G.; Kwon, Y.-M. Asymmetric hip kinematics during gait in patients with unilateral total hip arthroplasty: In vivo 3-dimensional motion analysis. *J. Biomech.* **2015**, *48*, 555–559. [[CrossRef](#)] [[PubMed](#)]
3. Arauz, P.; Peng, Y.; MacAuliffe, J.; Kwon, Y.-M. In-vivo 3-Dimensional gait symmetry analysis in patients with bilateral total hip arthroplasty. *J. Biomech.* **2018**, *77*, 131–137. [[CrossRef](#)] [[PubMed](#)]
4. Martz, P.; Bourredjem, A.; Maillefert, J.F.; Biquet, C.; Baulot, E.; Ornetti, P.; Laroche, D. Influence of body mass index on sagittal hip range of motion and gait speed recovery six months after total hip arthroplasty. *Int. Orthop.* **2019**, *43*, 2447–2455. [[CrossRef](#)]

5. Kolk, S.; Minten, M.J.M.; van Bon, G.E.A.; Rijnen, W.H.; Geurts, A.C.H.; Verdonchot, N.; Weerdesteijn, V. Gait and gait-related activities of daily living after total hip arthroplasty: A systematic review. *Clin. Biomech.* **2014**, *29*, 705–718. [[CrossRef](#)] [[PubMed](#)]
6. Queen, R.M.; Appleton, J.S.; Butler, R.J.; Newman, E.T.; Kelley, S.S.; Attarian, D.E.; Bolognesi, M.P. Total hip arthroplasty surgical approach does not alter postoperative gait mechanics one year after surgery. *PM&R* **2014**, *6*, 221–226.
7. Bahl, J.S.; Nelson, M.J.; Taylor, M.; Solomon, L.B.; Arnold, J.B.; Thewlis, D. Biomechanical changes and recovery of gait function after total hip arthroplasty for osteoarthritis: A systematic review and meta-analysis. *Osteoarthr. Cartil.* **2018**, *26*, 847–863. [[CrossRef](#)]
8. Zomar, B.O.; Bryant, D.; Hunter, S.; Howard, J.L.; Vasarhelyi, E.M.; Lanting, B.A. A randomised trial comparing spatio-temporal gait parameters after total hip arthroplasty between the direct anterior and direct lateral surgical approaches. *HIP Int.* **2018**, *28*, 478–484. [[CrossRef](#)]
9. Thaler, M.; Lechner, R.; Putzer, D.; Mayr, E.; Huber, D.C.; Liebensteiner, M.C.; Nogler, M. Two-year gait analysis controls of the minimally invasive total hip arthroplasty by the direct anterior approach. *Clin. Biomech.* **2018**, *58*, 34–38. [[CrossRef](#)]
10. Bennett, D.; Humphreys, L.; O'Brien, S.; Kelly, C.; Orr, J.F.; Beverland, D.E. Gait kinematics of age-stratified hip replacement patients—A large scale, long-term follow-up study. *Gait Posture* **2008**, *28*, 194–200. [[CrossRef](#)]
11. Beaulieu, M.L.; Lamontagne, M.; Beaulé, P.E. Lower limb biomechanics during gait do not return to normal following total hip arthroplasty. *Gait Posture* **2010**, *32*, 269–273. [[CrossRef](#)] [[PubMed](#)]
12. Loizeau, J.; Allard, P.; Duhaime, M.; Landjerit, B. Bilateral gait patterns in subjects fitted with a total hip prosthesis. *Arch. Phys. Med. Rehabil.* **1995**, *76*, 552–557. [[CrossRef](#)]
13. Gargiulo, P.; Edmunds, K.J.; Gíslason, M.K.; Latour, C.; Hermannsson, P.; Esposito, L.; Bifulco, P.; Cesarelli, M.; Fraldi, M.; Cristofolini, L.; et al. Patient-specific mobility assessment to monitor recovery after total hip arthroplasty. *Proc. Inst. Mech. Eng. Part H J. Eng. Med.* **2018**, *232*, 1048–1059. [[CrossRef](#)] [[PubMed](#)]
14. Bolink, S.A.A.N.; Lenguerrand, E.; Brunton, L.R.; Wylde, V.; Gooberman-Hill, R.; Heyligers, I.C.; Blom, A.W.; Grimm, B. Assessment of physical function following total hip arthroplasty: Inertial sensor based gait analysis is supplementary to patient-reported outcome measures. *Clin. Biomech.* **2016**, *32*, 171–179. [[CrossRef](#)] [[PubMed](#)]
15. Zügner, R.; Tranberg, R.; Lisovskaja, V.; Shareghi, B.; Kärrholm, J. Validation of gait analysis with dynamic radiostereometric analysis (RSA) in patients operated with total hip arthroplasty: Radiostereometric validation of hip 3D-kinematic. *J. Orthop. Res.* **2017**, *35*, 1515–1522. [[CrossRef](#)]
16. Picerno, P. 25 years of lower limb joint kinematics by using inertial and magnetic sensors: A review of methodological approaches. *Gait Posture* **2017**, *51*, 239–246. [[CrossRef](#)]
17. Zhang, J.-T.; Novak, A.C.; Brouwer, B.; Li, Q. Concurrent validation of Xsens and MVN measurement of lower limb joint angular kinematics. *Physiol. Meas.* **2013**, *34*. [[CrossRef](#)]
18. Robert-Lachaine, X.; Mecheri, H.; Larue, C.; Plamondon, A. Validation of inertial measurement units with an optoelectronic system for whole-body motion analysis. *Med. Biol. Eng. Comput.* **2017**, *55*, 609–619. [[CrossRef](#)]
19. Al-Amri, M.; Nicholas, K.; Button, K.; Sparkes, V.; Sheeran, L.; Davies, J.L. Inertial measurement units for clinical movement analysis: Reliability and concurrent validity. *Sensors* **2018**, *18*, 719. [[CrossRef](#)]
20. Fasel, B.; Sporri, J.; Chardonens, J.; Kroll, J.; Muller, E.; Aminian, K. Joint inertial sensor orientation drift reduction for highly dynamic movements. *IEEE J. Biomed. Health Inform.* **2017**, *22*, 77–86. [[CrossRef](#)]
21. Fasel, B.; Spörri, J.; Schütz, P.; Lorenzetti, S.; Aminian, K. Validation of functional calibration and strap-down joint drift correction for computing 3D joint angles of knee, hip, and trunk in alpine skiing. *PLoS ONE* **2017**, *12*, e0181446. [[CrossRef](#)] [[PubMed](#)]
22. Cutti, A.G.; Ferrari, A.; Garofalo, P.; Raggi, M.; Cappello, A.; Ferrari, A. 'Outwalk': A protocol for clinical gait analysis based on inertial and magnetic sensors. *Med. Biol. Eng. Comput.* **2009**, *48*, 17–25. [[CrossRef](#)] [[PubMed](#)]
23. Donath, L.; Faude, O.; Lichtenstein, E.; Nüesch, C.; Mündermann, A. Validity and reliability of a portable gait analysis system for measuring spatiotemporal gait characteristics: Comparison to an instrumented treadmill. *J. NeuroEng. Rehabil.* **2016**, *13*, 6. [[CrossRef](#)] [[PubMed](#)]
24. Donath, L.; Faude, O.; Lichtenstein, E.; Pagenstert, G.; Nüesch, C.; Mündermann, A. Mobile inertial sensor based gait analysis: Validity and reliability of spatiotemporal gait characteristics in healthy seniors. *Gait Posture* **2016**, *49*, 371–374. [[CrossRef](#)]

25. Nüesch, C.; Roos, E.; Pagenstert, G.; Mündermann, A. Measuring joint kinematics of treadmill walking and running: Comparison between an inertial sensor based system and a camera-based system. *J. Biomech.* **2017**, *57*, 32–38. [[CrossRef](#)]
26. Kluge, F.; Gaßner, H.; Hannink, J.; Pasluosta, C.; Klucken, J.; Eskofier, B.M. Towards mobile gait analysis: Concurrent validity and test-retest reliability of an inertial measurement system for the assessment of spatio-temporal gait parameters. *Sensors* **2017**, *17*, 1522. [[CrossRef](#)]
27. Zügner, R.; Tranberg, R.; Timperley, J.; Hodgins, D.; Mohaddes, M.; Kärrholm, J. Validation of inertial measurement units with optical tracking system in patients operated with Total hip arthroplasty. *BMC Musculoskelet. Disord.* **2019**, *20*, 52. [[CrossRef](#)]
28. Horenstein, R.E.; Lewis, C.L.; Yan, S.; Halverstadt, A.; Shefelbine, S.J. Validation of magneto-inertial measuring units for measuring hip joint angles. *J. Biomech.* **2019**, *91*, 170–174. [[CrossRef](#)]
29. Figueiredo, J.; Santos, C.P.; Moreno, J.C. Automatic recognition of gait patterns in human motor disorders using machine learning: A review. *Med. Eng. Phys.* **2018**, *53*, 1–12. [[CrossRef](#)]
30. Begg, R.K.; Palaniswami, M.; Owen, B. Support vector machines for automated gait classification. *IEEE Trans. Biomed. Eng.* **2005**, *52*, 828–838. [[CrossRef](#)]
31. Mannini, A.; Trojaniello, D.; Cereatti, A.; Sabatini, A.M. A machine learning framework for gait classification using inertial sensors: Application to elderly, post-stroke and Huntington’s disease patients. *Sensors* **2016**, *16*, 134. [[CrossRef](#)] [[PubMed](#)]
32. Mulroy, S.; Gronley, J.; Weiss, W.; Newsam, C.; Perry, J. Use of cluster analysis for gait pattern classification of patients in the early and late recovery phases following stroke. *Gait Posture* **2003**, *18*, 114–125. [[CrossRef](#)]
33. Kotti, M.; Duffell, L.D.; Faisal, A.A.; McGregor, A.H. Detecting knee osteoarthritis and its discriminating parameters using random forests. *Med. Eng. Phys.* **2017**, *43*, 19–29. [[CrossRef](#)] [[PubMed](#)]
34. Steinwart, I.; Christmann, A. *Support Vector Machines*, 1st ed.; Information Science and Statistics; Springer: Berlin, Germany, 2008; ISBN 978-0-387-77241-7.
35. Lau, H.; Tong, K.; Zhu, H. Support vector machine for classification of walking conditions of persons after stroke with dropped foot. *Hum. Mov. Sci.* **2009**, *28*, 504–514. [[CrossRef](#)]
36. Teufl, W.; Lorenz, M.; Miezal, M.; Taetz, B.; Fröhlich, M.; Bleser, G. Towards inertial sensor based mobile gait analysis: Event-detection and spatio-temporal parameters. *Sensors* **2018**, *19*, 38. [[CrossRef](#)]
37. Miezal, M.; Taetz, B.; Bleser, G. On Inertial body tracking in the presence of model calibration errors. *Sensors* **2016**, *16*, 1132. [[CrossRef](#)]
38. Miezal, M.; Taetz, B.; Bleser, G. Real-time inertial lower body kinematics and ground contact estimation at anatomical foot points for agile human locomotion. In Proceedings of the International Conference on Robotics and Automation, Marina Bay Sands, Singapore, 29 May–3 June 2017.
39. Teufl, W.; Miezal, M.; Taetz, B.; Fröhlich, M.; Bleser, G. Validity, test-retest reliability and long-term stability of magnetometer free inertial sensor based 3D joint kinematics. *Sensors* **2018**, *18*, 1980. [[CrossRef](#)]
40. Teufl, W.; Miezal, M.; Taetz, B.; Fröhlich, M.; Bleser, G. Validity of inertial sensor based 3D joint kinematics of static and dynamic sport and physiotherapy specific movements. *PLoS ONE* **2019**, *14*, e0213064. [[CrossRef](#)]
41. Pietschmann, J.; Geu Flores, F.; Jöllenbeck, T. Gait training in orthopedic rehabilitation after joint replacement—Back to normal gait with sonification? *Int. J. Comput. Sci. Sport* **2019**, *18*, 34–48. [[CrossRef](#)]
42. Ferreira, L.C.V.; Rabelo, A.G.; Vieira, M.F.; Pereira, A.A.; Andrade, A.d.O. Gait variability and symmetry assessment with inertial sensors for quantitative discrimination of Trendelenburg sign in total hip arthroplasty patients: A pilot study based on convenience sampling. *Res. Biomed. Eng.* **2018**, *34*, 65–72. [[CrossRef](#)]
43. Tazawa, M.; Kurosaki, M.; Inoue, T.; Ibe, Y.; Kobayashi, H.; Kitagawa, T.; Chikuda, H.; Wada, N. Superior migration of the femoral head in patients with severe hip osteoarthritis influences the gait patterns of the coronal plane. *HIP Int.* **2019**. [[CrossRef](#)] [[PubMed](#)]
44. Hanchuan, P.; Fuhui, L.; Ding, C. Feature selection based on mutual information criteria of max-dependency, max-relevance, and min-redundancy. *IEEE Trans. Pattern Anal. Mach. Intell.* **2005**, *27*, 1226–1238. [[CrossRef](#)] [[PubMed](#)]
45. Xiaoming, H.; Yue, L.; Yongtian, W.; Yanling, H.; Dayuan, Y. Autocalibration of an electronic compass for augmented reality. In Proceedings of the Fourth IEEE and ACM International Symposium on Mixed and Augmented Reality (ISMAR’05), Vienna, Austria, 5–8 October 2005; pp. 182–183.
46. Leardini, A.; Sawacha, Z.; Paolini, G.; Inghrosso, S.; Nativo, R.; Benedetti, M.G. A new anatomically based protocol for gait analysis in children. *Gait Posture* **2007**, *26*, 560–571. [[CrossRef](#)] [[PubMed](#)]

47. Palermo, E.; Rossi, S.; Marini, F.; Patanè, F.; Cappa, P. Experimental evaluation of accuracy and repeatability of a novel body-to-sensor calibration procedure for inertial sensor-based gait analysis. *Measurement* **2014**, *52*, 145–155. [[CrossRef](#)]
48. Carbone, V.; Fluit, R.; Pellikaan, P.; van der Krogt, M.M.; Janssen, D.; Damsgaard, M.; Vigneron, L.; Feilkas, T.; Koopman, H.F.J.M.; Verdonschot, N. TLEM 2.0—A comprehensive musculoskeletal geometry dataset for subject-specific modeling of lower extremity. *J. Biomech.* **2015**, *48*, 734–741. [[CrossRef](#)] [[PubMed](#)]
49. Eie, M.; Wei, C.-S. Generalizations of Euler decomposition and their applications. *J. Number Theory* **2013**, *133*, 2475–2495. [[CrossRef](#)]
50. Banks, J.J.; Chang, W.-R.; Xu, X.; Chang, C.-C. Using horizontal heel displacement to identify heel strike instants in normal gait. *Gait Posture* **2015**, *42*, 101–103. [[CrossRef](#)]
51. Zeni, J.; Richards, J.; Higginson, J.S. Two simple methods for determining gait events during treadmill and overground walking using kinematic data. *Gait Posture* **2008**, *27*, 710–714. [[CrossRef](#)]
52. Ferrari, A.; Cutti, A.G.; Cappello, A. A new formulation of the coefficient of multiple correlation to assess the similarity of waveforms measured synchronously by different motion analysis protocols. *Gait Posture* **2010**, *31*, 540–542. [[CrossRef](#)]
53. Martins, M.; Costa, L.; Frizzera, A.; Ceres, R.; Santos, C. Hybridization between multi-objective genetic algorithm and support vector machine for feature selection in walker-assisted gait. *Comput. Methods Progr. Biomed.* **2014**, *113*, 736–748. [[CrossRef](#)]
54. Robert-Lachaine, X.; Mecheri, H.; Larue, C.; Plamondon, A. Accuracy and repeatability of single-pose calibration of inertial measurement units for whole-body motion analysis. *Gait Posture* **2017**, *54*, 80–86. [[CrossRef](#)] [[PubMed](#)]
55. Teufl, W.; Taetz, B.; Fröhlich, M.; Bleser, G. Accuracy and repeatability of the “neutral-zero position” of the lower extremity. In Proceedings of the ISB-ASB 2019 conference in Calgary, Calgary, AB, Canada, 31 July–4 August 2019.
56. Davis, K.E.; Ritter, M.A.; Berend, M.E.; Meding, J.B. The importance of range of motion after total hip arthroplasty. *Clinical Orthopaedics* **2007**, *465*, 180–184.
57. Bertoli, M.; Cereatti, A.; Trojaniello, D.; Avanzino, L.; Pelosin, E.; Del Din, S.; Rochester, L.; Ginis, P.; Bekkers, E.M.J.; Mirelman, A.; et al. Estimation of spatio-temporal parameters of gait from magneto-inertial measurement units: Multicenter validation among Parkinson, mildly cognitively impaired and healthy older adults. *Biomed. Eng. Online* **2018**, *17*, 58. [[CrossRef](#)] [[PubMed](#)]
58. Taetz, B.; Bleser, G.; Miezal, M. Towards self-calibrating inertial body motion capture. In Proceedings of the 19th International Conference on Information Fusion (FUSION), Heidelberg, Germany, 5–8 July 2016; pp. 1751–1759.
59. Zimmermann, T.; Taetz, B.; Bleser, G. IMU-to-Segment assignment and orientation alignment for the lower body using deep learning. *Sensors* **2018**, *18*, 302. [[CrossRef](#)] [[PubMed](#)]
60. Teufl, W.; Taetz, B.; Weidmann, A.; Fröhlich, M.; Bleser, G. Validity of a depth camera based approach for segment length estimation. *PLoS ONE* **2019**. [[CrossRef](#)]
61. Colgan, G.; Walsh, M.; Bennett, D.; Rice, J.; O'Brien, T. Gait analysis and hip extensor function early post total hip replacement. *J. Orthop.* **2016**, *13*, 171–176. [[CrossRef](#)]
62. Miki, H.; Sugano, N.; Hagio, K.; Nishii, T.; Kawakami, H.; Kakimoto, A.; Nakamura, N.; Yoshikawa, H. Recovery of walking speed and symmetrical movement of the pelvis and lower extremity joints after unilateral THA. *J. Biomech.* **2004**, *37*, 443–455. [[CrossRef](#)]
63. Köse, A.; Cereatti, A.; Della Croce, U. Bilateral step length estimation using a single inertial measurement unit attached to the pelvis. *J. NeuroEng. Rehabil.* **2012**, *9*, 9. [[CrossRef](#)]
64. Boyer, K.A.; Johnson, R.T.; Banks, J.J.; Jewell, C.; Hafer, J.F. Systematic review and meta-analysis of gait mechanics in young and older adults. *Exp. Gerontol.* **2017**, *95*, 63–70. [[CrossRef](#)]
65. Ewen, A.M.; Stewart, S.; St Clair Gibson, A.; Kashyap, S.N.; Caplan, N. Post-operative gait analysis in total hip replacement patients—A review of current literature and meta-analysis. *Gait Posture* **2012**, *36*, 1–6. [[CrossRef](#)]



4.2 Full Validation of the Joint Angles – Extended Results from JP 4

In this chapter the complete validation results of all joint angles and STP for both groups during the gait are shown. This part contains data not yet published. All values in the following tables are to be considered the average over all gait cycles and all subjects for each group.

The results are split into three parts according to the three different methods of the IMU data processing mentioned in Table 2. First, the joint angle estimation incorporates an OMC based I2S calibration and an OMC based biomechanical model (Procedure 1). This is shown only for the patient group. The corresponding results for the healthy group can be viewed in the JP 1.

Second, the joint angle estimation adds an IMU based I2S calibration, substituting the OMC based I2S calibration. However, the biomechanical model, e.g. the segment lengths, is still based on OMC information (Procedure 2).

Finally, the third part contains the joint angle estimation based completely on IMU information, adding a biomechanical model with incorporated AL according to [119]. The segment lengths of this model are scaled according to the gender and the body height and an anthropometric table (Procedure 3). This latter approach was also used in JP 3 and JP 4.

4.2.1 Procedure 1

In Table 4 the RMSE, ROME, CMC and BA of the patient group are shown for the joint angle estimation. The same results for the healthy group were published in JP 1.

Using the Procedure 1 approach for processing the IMU data delivered similar errors between the OMC system and the IMU system in both groups. The healthy group revealed the highest RMSE in the left knee rotation (2.34°) the patient group showed its highest RMSE in the left ankle rotation (2.88°). Further, in both groups the highest ROME were found in the frontal plane of the knee and ankle. For both groups the ROME was below 2.00°

Table 4. Validation results of the joint angles of the lower limbs for the patient group. Shown are the root mean squared error (RMSE) \pm standard deviation (SD) (95 % confidence interval (CI)), the range of motion error (ROME) \pm SD (95 % CI), the coefficient of multiple correlation (CMC) \pm SD and the Bland-Altman limits of agreement (BA).

	RMSE \pm SD (95 % CI) [deg]	ROME \pm SD (95 % CI) [deg]	CMC \pm SD	BA [deg]
LT Hip-Abduction	1.06 \pm 0.39 (0.66 – 1.10)	0.66 \pm 0.36 (0.36 – 0.76)	0.95 \pm 0.05	0.03 \pm 2.75
LT Hip-Rotation	2.38 \pm 1.33 (1.55 – 3.03)	0.77 \pm 0.43 (0.36 – 0.84)	0.80 \pm 0.19	0.90 \pm 6.08
LT Hip-Flexion	1.07 \pm 0.60 (0.53 – 1.19)	0.60 \pm 0.42 (0.26 – 0.72)	0.99 \pm 0.01	-0.07 \pm 3.60
LT Knee-Abduction	1.7 \pm 0.73 (1.19 – 2.00)	1.15 \pm 0.56 (0.65 – 1.27)	0.89 \pm 0.08	-0.32 \pm 3.84
LT Knee-Rotation	1.85 \pm 0.81 (1.28 – 2.17)	0.98 \pm 0.58 (0.51 – 1.16)	0.93 \pm 0.06	-0.44 \pm 3.83
LT Knee-Flexion	1.39 \pm 0.43 (1.13 – 1.60)	1.06 \pm 0.41 (0.78 – 1.24)	1.00 \pm 0.00	-0.28 \pm 2.63
LT Ankle-Inversion	1.68 \pm 0.58 (1.28 – 1.92)	1.66 \pm 0.97 (0.59 – 1.67)	0.92 \pm 0.04	-0.40 \pm 3.09
LT Ankle-Rotation	2.88 \pm 1.28 (1.91 – 3.33)	1.30 \pm 0.57 (1.04 – 1.67)	0.86 \pm 0.09	2.63 \pm 3.42
LT Ankle-Flexion	2.21 \pm 1.08 (1.25 – 2.44)	1.05 \pm 0.51 (0.79 – 1.36)	0.98 \pm 0.03	0.21 \pm 4.36

RT Hip-Abduction	1.46 ± 0.51 (1.24 – 1.73)	1.11 ± 0.78 (0.58 – 1.32)	0.94 ± 0.07	-0.29 ± 3.02
RT Hip-Rotation	4.01 ± 2.56 (2.95 – 5.42)	0.72 ± 0.41 (0.47 – 0.86)	0.71 ± 0.26	2.40 ± 7.52
RT Hip-Flexion	1.23 ± 0.72 (0.65 – 1.34)	0.91 ± 0.47 (0.61 – 1.06)	0.99 ± 0.01	-0.01 ± 3.14
RT Knee-Abduction	1.51 ± 0.66 (0.98 – 1.61)	1.59 ± 1.40 (0.41 – 1.76)	0.86 ± 0.08	0.75 ± 2.68
RT Knee-Rotation	2.09 ± 1.19 (0.92 – 2.06)	0.79 ± 0.43 (0.44 – 0.86)	0.93 ± 0.07	0.67 ± 4.44
RT Knee-Flexion	1.54 ± 0.63 (1.08 – 1.69)	0.86 ± 0.42 (0.66 – 1.07)	1.00 ± 0.00	0.40 ± 2.95
RT Ankle-Inversion	1.24 ± 0.43 (1.15 – 1.56)	1.09 ± 0.62 (0.77 – 1.36)	0.97 ± 0.02	0.24 ± 2.28
RT Ankle-Rotation	1.98 ± 0.80 (1.62 – 2.40)	0.85 ± 0.71 (0.24 – 0.92)	0.91 ± 0.16	-1.19 ± 3.35
RT Ankle-Flexion	1.40 ± 0.43 (1.07 – 1.48)	1.04 ± 0.41 (0.71 – 1.10)	0.99 ± 0.00	-0.20 ± 2.53
Pelvis-Obliquity	0.58 ± 0.16 (0.46 – 0.61)	0.48 ± 0.30 (0.21 – 0.50)	0.97 ± 0.02	0.10 ± 1.00
Pelvis-Flexion	0.99 ± 0.53 (0.54 – 1.05)	0.50 ± 0.17 (0.44 – 0.61)	0.91 ± 0.08	0.16 ± 2.69
Pelvis-Rotation*	x	0.76 ± 0.25 (0.61 – 0.85)	0.81 ± 0.25	x

* The RMSE and BA of the pelvis rotation are not reported since the absolute values of the pelvis rotation could not be evaluated due to the drift in the global pelvis rotation.

4.2.2 Procedure 2

In Table 5 and Table 6 the RMSE, ROME, CMC and BA of the healthy group and patient group, respectively are shown for the joint angle estimation.

Introducing an IMU based I2S calibration, in this case the 2-step calibration described in JP 3, led to an increase of the RMSE over all joint angles in both groups. The highest error increase was evident in the left and right ankle rotation of the healthy group with a mean RMSE up to 19.99°. The ROME increased only slightly, staying below 3° in all joint angles, in both groups.

Table 5. Validation results of the joint angles of the lower limbs for the healthy group. Shown are the RMSE ± SD (95 % CI), the ROME ± SD (95 % CI), the CMC ± SD and the BA.

	RMSE ± SD (95 % CI) [deg]	ROME ± SD (95 % CI) [deg]	CMC ± SD	BA [deg]
LT Hip-Abduction	2.33 ± 1.09 (1.55 – 2.41)	0.73 ± 0.30 (0.58 – 0.82)	0.93 ± 0.08	-1.27 ± 4.13
LT Hip-Rotation	5.72 ± 2.64 (3.52 – 5.61)	0.93 ± 0.59 (0.49 – 0.96)	0.77 ± 0.21	-3.25 ± 9.97
LT Hip-Flexion	2.66 ± 1.90 (1.33 – 2.83)	1.02 ± 0.41 (0.91 – 1.23)	0.98 ± 0.03	-1.94 ± 5.06
LT Knee-Abduction	3.45 ± 1.76 (2.66 – 4.05)	2.46 ± 1.63 (1.23 – 2.52)	0.75 ± 0.14	1.96 ± 6.06
LT Knee-Rotation	4.71 ± 3.79	1.69 ± 0.66	0.82 ± 0.19	-3.29 ± 9.37

	(1.69 – 4.68)	(1.30 – 1.83)		
LT Knee-Flexion	1.78 ± 0.4 (1.58 – 1.89)	0.74 ± 0.27 (0.59 – 0.81)	1.00 ± 0.00	-0.74 ± 3.02
LT Ankle-Inversion	2.92 ± 1.29 (1.96 – 2.98)	1.71 ± 0.79 (1.14 – 1.76)	0.82 ± 0.21	-1.89 ± 4.17
LT Ankle-Rotation	19.99 ± 6.81 (16.22 – 21.61)	2.01 ± 0.65 (1.66 – 2.17)	0.72 ± 0.00	19.92 ± 13.27
LT Ankle-Flexion	2.18 ± 0.88 (1.36 – 2.05)	1.03 ± 0.39 (0.78 – 1.09)	0.99 ± 0.01	-0.05 ± 4.21
RT Hip-Abduction	1.94 ± 1.11 (1.21 – 2.09)	0.86 ± 0.45 (0.60 – 0.96)	0.95 ± 0.06	0.59 ± 3.87
RT Hip-Rotation	5.21 ± 3.01 (3.37 – 5.75)	0.89 ± 0.59 (0.47 – 0.93)	0.77 ± 0.27	1.72 ± 10.38
RT Hip-Flexion	2.77 ± 2.01 (1.31 – 2.90)	0.75 ± 0.44 (0.14 – 1.12)	0.98 ± 0.03	-2.17 ± 5.02
RT Knee-Abduction	2.58 ± 1.00 (1.93 – 2.72)	2.33 ± 1.05 (1.88 – 2.71)	0.76 ± 0.22	0.14 ± 4.63
RT Knee-Rotation	5.21 ± 2.93 (3.20 – 5.51)	1.62 ± 1.17 (0.81 – 1.73)	0.81 ± 0.20	3.87 ± 7.86
RT Knee-Flexion	1.74 ± 0.56 (1.38 – 1.82)	0.92 ± 0.56 (0.44 – 0.88)	1.00 ± 0.00	-0.21 ± 3.22
RT Ankle-Inversion	2.70 ± 1.25 (1.79 – 2.78)	1.28 ± 0.54 (1.10 – 1.53)	0.86 ± 0.14	1.44 ± 4.62
RT Ankle-Rotation	18.74 ± 6.72 (16.47 – 21.78)	1.64 ± 0.57 (1.30 – 1.75)	0.96 ± 0.03	-18.67 ± 13.11
RT Ankle-Flexion	1.84 ± 0.58 (1.43 – 1.88)	1.16 ± 0.47 (0.87 – 1.24)	0.99 ± 0.01	-0.23 ± 3.29
Pelvis-Obliquity	1.37 ± 1.15 (0.42 – 1.34)	0.38 ± 0.17 (0.27 – 0.41)	0.93 ± 0.09	-0.93 ± 2.90
Pelvis-Flexion	2.99 ± 2.03 (2.07 – 3.68)	0.42 ± 0.47 (0.15 – 0.52)	0.59 ± 0.29	-2.66 ± 4.71
Pelvis-Rotation*	x	0.76 ± 0.29 (0.61 – 0.84)	0.86 ± 0.14	x

* The RMSE and BA of the pelvis rotation are not reported since the absolute values of the pelvis rotation could not be evaluated due to the drift in the global pelvis rotation.

Table 6. Validation results of the joint angles of the lower limbs for the patient group. Shown are the RMSE ± SD (95 % CI), the ROME ± SD (95 % CI), the CMC ± SD and the BA.

	RMSE ± SD (95 % CI) [deg]	ROME ± SD (95 % CI) [deg]	CMC ± SD	BA [deg]
LT Hip-Abduction	3.72 ± 0.86 (3.17 – 4.09)	0.84 ± 0.53 (0.45 – 1.02)	0.63 ± 0.18	-3.60 ± 2.11
LT Hip-Rotation	5.99 ± 3.04 (4.24 – 7.48)	0.75 ± 0.36 (0.46 – 0.84)	0.71 ± 0.20	4.27 ± 9.37
LT Hip-Flexion	4.07 ± 1.67 (2.91 – 4.69)	0.65 ± 0.31 (0.38 – 0.71)	0.94 ± 0.05	-3.83 ± 3.58
LT Knee-Abduction	4.47 ± 1.82	2.54 ± 1.15	0.61 ± 0.16	3.84 ± 5.72

	(3.09 – 5.04)	(1.74 – 2.97)		
LT Knee-Rotation	4.86 ± 2.93 (2.15 – 5.27)	1.97 ± 1.18 (1.11 – 2.37)	0.72 ± 0.24	-3.12 ± 9.37
LT Knee-Flexion	1.43 ± 0.55 (0.99 – 1.58)	1.04 ± 0.66 (0.46 – 1.16)	1.00 ± 0.00	0.29 ± 2.69
LT Ankle-Inversion	2.74 ± 2.24 (0.74 – 3.12)	1.45 ± 0.62 (0.95 – 1.61)	0.85 ± 0.15	-1.95 ± 5.25
LT Ankle-Rotation	11.44 ± 7.44 (5.89 – 13.82)	1.21 ± 0.98 (0.36 – 1.41)	0.78 ± 0.09	11.30 ± 13.87
LT Ankle-Flexion	2.08 ± 1.11 (1.27 – 2.46)	1.80 ± 0.83 (1.25 – 2.13)	0.99 ± 0.01	0.37 ± 4.22
RT Hip-Abduction	1.56 ± 0.56 (1.19 – 1.71)	1.24 ± 0.88 (0.55 – 1.38)	0.93 ± 0.06	0.60 ± 2.62
RT Hip-Rotation	4.88 ± 3.06 (3.12 – 5.99)	0.75 ± 0.32 (0.55 – 0.85)	0.67 ± 0.21	1.03 ± 9.45
RT Hip-Flexion	3.31 ± 1.67 (2.49 – 4.05)	0.88 ± 0.42 (0.69 – 1.08)	0.96 ± 0.04	-3.11 ± 3.77
RT Knee-Abduction	2.36 ± 1.40 (1.32 – 2.63)	2.60 ± 1.30 (1.98 – 3.20)	0.71 ± 0.18	-0.48 ± 4.72
RT Knee-Rotation	6.35 ± 4.51 (1.92 – 6.15)	1.47 ± 0.91 (0.85 – 1.70)	0.57 ± 0.31	5.51 ± 9.96
RT Knee-Flexion	1.74 ± 0.88 (1.12 – 1.94)	1.08 ± 0.57 (0.77 – 1.30)	1.00 ± 0.00	-0.82 ± 3.25
RT Ankle-Inversion	2.59 ± 1.59 (1.28 – 2.76)	2.07 ± 1.35 (1.29 – 2.56)	0.86 ± 0.17	1.23 ± 4.80
RT Ankle-Rotation	13.75 ± 7.14 (11.70 – 18.38)	1.10 ± 0.73 (0.64 – 1.32)	0.57 ± 0.32	-13.65 ± 13.73
RT Ankle-Flexion	1.86 ± 0.94 (1.26 – 2.14)	1.55 ± 0.71 (1.11 – 1.78)	0.99 ± 0.01	0.30 ± 3.72
Pelvis-Obliquity	0.72 ± 0.17 (0.66 – 0.82)	0.52 ± 0.26 (0.41 – 0.65)	0.95 ± 0.04	0.03 ± 1.29
Pelvis-Flexion	3.85 ± 1.22 (3.04 – 4.18)	0.55 ± 0.15 (0.46 – 0.60)	0.45 ± 0.27	-3.82 ± 2.43
Pelvis-Rotation*	x	0.93 ± 0.44 (0.73 – 1.14)	0.76 ± 0.20	x

* The RMSE and BA of the pelvis rotation are not reported since the absolute values of the pelvis rotation could not be evaluated due to the drift in the global pelvis rotation.

4.2.3 Procedure 3

In Table 7 and Table 8 the RMSE, ROME, CMC and BA of the healthy group and the patient group, respectively are shown for the joint angle estimation.

When introducing a biomechanical model based on a scaled model incorporating AL, again, the RMSE increased in the joint angles. All joint angles were affected in the healthy group, except for the left and right ankle rotation (16.86° and 15.91°) which decreased slightly.

In the patient group the RMSE in all joint angles increased except for the left hip rotation and the left knee abduction (4.35° and 3.74°).

The ROME did also increase marginally. In the healthy group all joint angles were affected except for the right hip abduction (0.80°). However, the ROME stayed below 4.10° in all joints. In the

patient group the ROME did not increase systematically. In fact, in approximately a third of the joint angles the ROME decreased. However, again all changes in the ROME were only marginal.

Table 7. Validation results of the joint angles of the lower limbs for the healthy group. Shown are the RMSE \pm SD (95 % CI), the ROME \pm SD (95 % CI), the CMC \pm SD and the BA.

	RMSE \pm SD (95 % CI) [deg]	ROME \pm SD (95 % CI) [deg]	CMC \pm SD	BA [deg]
LT Hip-Abduction	3.47 \pm 2.08 (2.59 – 4.35)	0.83 \pm 0.48 (0.57 – 0.98)	0.87 \pm 0.16	-2.78 \pm 5.23
LT Hip-Rotation	8.89 \pm 5.01 (5.61 – 9.85)	1.05 \pm 0.62 (0.63 – 1.15)	0.66 \pm 0.24	-3.88 \pm 17.50
LT Hip-Flexion	5.53 \pm 4.65 (2.95 – 6.88)	2.70 \pm 0.97 (2.32 – 3.14)	0.93 \pm 0.12	-4.78 \pm 10.12
LT Knee-Abduction	5.86 \pm 2.42 (4.37 – 6.41)	3.08 \pm 1.74 (1.57 – 3.04)	0.53 \pm 0.29	2.89 \pm 10.58
LT Knee-Rotation	10.75 \pm 7.62 (4.73 – 11.16)	1.96 \pm 1.00 (1.31 – 2.16)	0.65 \pm 0.26	-9.48 \pm 17.09
LT Knee-Flexion	4.18 \pm 2.40 (2.52 – 4.55)	2.96 \pm 0.78 (2.43 – 3.09)	0.98 \pm 0.02	-1.51 \pm 8.98
LT Ankle-Inversion	4.31 \pm 1.53 (3.75 – 5.05)	2.90 \pm 1.71 (1.52 – 2.96)	0.76 \pm 0.19	-2.30 \pm 7.19
LT Ankle-Rotation	16.86 \pm 7.22 (12.60 – 18.70)	2.45 \pm 1.15 (1.58 – 2.55)	0.56 \pm 0.31	16.85 \pm 13.90
LT Ankle-Flexion	3.49 \pm 1.16 (2.77 – 3.74)	1.51 \pm 0.51 (1.19 – 1.62)	0.96 \pm 0.03	2.25 \pm 5.17
RT Hip-Abduction	2.51 \pm 1.23 (1.63 – 2.67)	0.80 \pm 0.44 (0.45 – 0.83)	0.93 \pm 0.06	0.00 \pm 5.19
RT Hip-Rotation	7.02 \pm 5.01 (2.59 – 6.82)	1.20 \pm 0.60 (0.79 – 1.30)	0.71 \pm 0.23	-1.07 \pm 16.30
RT Hip-Flexion	5.87 \pm 4.51 (3.69 – 7.50)	2.11 \pm 1.01 (1.44 – 2.30)	0.93 \pm 0.11	-5.35 \pm 9.57
RT Knee-Abduction	4.50 \pm 2.89 (2.58 – 5.02)	2.71 \pm 2.20 (0.94 – 2.79)	0.66 \pm 0.26	-1.46 \pm 9.75
RT Knee-Rotation	16.28 \pm 6.97 (14.04 – 19.93)	2.26 \pm 2.16 (0.43 – 2.26)	0.49 \pm 0.26	16.24 \pm 13.60
RT Knee-Flexion	3.70 \pm 2.02 (2.30 – 4.00)	3.58 \pm 1.40 (3.12 – 4.30)	0.99 \pm 0.02	-0.41 \pm 8.10
RT Ankle-Inversion	3.85 \pm 1.67 (2.96 – 4.37)	4.05 \pm 1.77 (3.60 – 5.09)	0.81 \pm 0.16	1.39 \pm 7.39
RT Ankle-Rotation	15.91 \pm 6.55 (11.87 – 17.41)	1.78 \pm 0.80 (1.31 – 1.98)	0.74 \pm 0.32	-16.02 \pm 13.05
RT Ankle-Flexion	3.37 \pm 1.07 (3.05 – 3.95)	1.20 \pm 0.50 (0.86 – 1.28)	0.96 \pm 0.02	2.16 \pm 4.95
Pelvis-Obliquity	1.64 \pm 0.96 (1.02 – 1.83)	0.73 \pm 0.35 (0.49 – 0.79)	0.90 \pm 0.11	0.20 \pm 3.59
Pelvis-Flexion	10.17 \pm 5.58 (7.81 – 12.52)	0.56 \pm 0.59 (0.15 – 0.65)	0.52 \pm 0.25	-10.08 \pm 10.57

Pelvis – Rotation*	x	0.75 ± 0.27 (0.66 – 0.88)	0.65 ± 0.22	x
--------------------	---	------------------------------	-------------	---

* The RMSE and BA of the pelvis rotation are not reported since the absolute values of the pelvis rotation could not be evaluated due to the drift in the global pelvis rotation.

Table 8. Validation results of the joint angles of the lower limbs for the patient group. Shown are the RMSE ± SD (95 % CI), the ROME ± SD (95 % CI), the CMC ± SD and the BA.

	RMSE ± SD (95 % CI) [deg]	ROME ± SD (95 % CI) [deg]	CMC ± SD	BA [deg]
LT Hip-Abduction	3.72 ± 2.51 (2.37 – 5.15)	0.89 ± 0.60 (0.46 – 1.13)	0.76 ± 0.24	-2.05 ± 7.45
LT Hip-Rotation	4.35 ± 3.18 (1.74 – 5.26)	0.84 ± 0.36 (0.63 – 1.03)	0.69 ± 0.24	0.18 ± 14.33
LT Hip-Flexion	11.06 ± 6.79 (6.08 – 13.60)	0.85 ± 0.46 (0.49 – 1.00)	0.73 ± 0.20	-9.48 ± 15.80
LT Knee-Abduction	3.74 ± 2.93 (1.28 – 4.53)	3.18 ± 2.27 (1.05 – 3.57)	0.75 ± 0.15	0.74 ± 8.94
LT Knee-Rotation	15.24 ± 7.04 (13.07 – 20.87)	1.55 ± 1.49 (0.07 – 1.72)	0.45 ± 0.29	-15.30 ± 16.00
LT Knee-Flexion	7.55 ± 5.68 (2.34 – 8.63)	3.27 ± 1.30 (2.29 – 3.73)	0.94 ± 0.09	2.80 ± 16.96
LT Ankle-Inversion	4.21 ± 1.86 (2.85 – 4.91)	3.33 ± 2.18 (1.01 – 3.43)	0.70 ± 0.17	-1.45 ± 8.07
LT Ankle-Rotation	12.62 ± 7.80 (6.25 – 14.89)	1.54 ± 1.03 (0.69 – 1.84)	0.76 ± 0.16	12.55 ± 14.21
LT Ankle-Flexion	3.46 ± 1.36 (2.56 – 4.06)	1.65 ± 1.03 (0.61 – 1.75)	0.95 ± 0.04	2.56 ± 6.15
RT Hip-Abduction	2.61 ± 1.56 (1.56 – 3.07)	1.10 ± 0.55 (0.85 – 1.38)	0.83 ± 0.19	0.19 ± 7.58
RT Hip-Rotation	7.95 ± 3.70 (6.31 – 9.88)	0.98 ± 0.60 (0.45 – 1.03)	0.60 ± 0.30	2.97 ± 15.59
RT Hip-Flexion	9.86 ± 7.10 (4.66 – 11.50)	1.20 ± 0.60 (0.92 – 1.50)	0.82 ± 0.21	-8.65 ± 16.08
RT Knee-Abduction	4.85 ± 2.54 (2.51 – 4.96)	3.27 ± 1.61 (2.11 – 3.67)	0.62 ± 0.25	1.49 ± 10.55
RT Knee-Rotation	18.55 ± 8.02 (14.03 – 21.76)	1.36 ± 0.85 (0.70 – 1.52)	0.44 ± 0.22	18.41 ± 15.21
RT Knee-Flexion	6.88 ± 3.50 (5.02 – 8.39)	3.12 ± 0.60 (0.46 – 1.13)	0.95 ± 0.05	1.55 ± 14.37
RT Ankle-Inversion	4.03 ± 2.00 (2.95 – 4.87)	4.40 ± 2.46 (2.76 – 5.13)	0.79 ± 0.16	1.12 ± 7.75
RT Ankle-Rotation	13.95 ± 7.66 (11.67 – 19.05)	1.24 ± 0.63 (0.73 – 1.33)	0.65 ± 0.27	-13.66 ± 14.72
RT Ankle-Flexion	3.39 ± 1.50 (2.36 – 3.80)	2.18 ± 1.61 (0.80 – 2.35)	0.96 ± 0.03	1.37 ± 6.33
Pelvis-Obliquity	1.51 ± 1.14 (0.49 – 1.58)	0.36 ± 0.24 (0.18 – 0.41)	0.88 ± 0.11	-0.07 ± 3.94

Pelvis-Flexion	12.52 ± 5.57 (10.05 – 15.42)	0.51 ± 0.17 (0.43 – 0.60)	0.44 ± 0.18	-12.79 ± 10.64
Pelvis-Rotation*	x	0.98 ± 0.46 (0.66 – 1.10)	0.58 ± 0.30	x

* The RMSE and BA of the pelvis rotation are not reported since the absolute values of the pelvis rotation could not be evaluated due to the drift in the global pelvis rotation.

In Table 9 the complete validation of all STP, including the ones already validated in JP 4, for the patient group is shown. The equivalent validation with respect to the healthy group was published in JP 3.

Table 9. Full validation of the spatio-temporal parameters STP for the patient group. Shown are the mean absolute error (MAE) ± SD (95 % CI), the RMSE ± SD (95 % CI), the relative RMSE, the BA and the Pearson correlation coefficient (R)

	MAE ± SD (95 % CI)	RMSE ± SD (95 % CI)	Relative RMSE [%]	BA	R
Step Length [m]	0.04 ± 0.03 (0.01 – 0.04)	0.04 ± 0.03 (0.02 – 0.05)	8.41	0.001 ± 0.08	0.49
Stride Length [m]	0.05 ± 0.03 (0.03 – 0.05)	0.06 ± 0.04 (0.03 – 0.06)	5.44	0.009 ± 0.11	0.78
Step Width [m]	0.03 ± 0.01 (0.02 – 0.03)	0.03 ± 0.02 (0.02 – 0.04)	24.36	-0.004 ± 0.04	0.64
Swing Width [m]	0.03 ± 0.02 (0.02 – 0.03)	0.03 ± 0.02 (0.02 – 0.04)	22.87	-0.014 ± 0.03	0.61
Step Time [s]	0.03 ± 0.02 (0.01 – 0.03)	0.04 ± 0.02 (0.02 – 0.04)	5.22	-0.004 ± 0.07	0.50
Stride Time [s]	0.04 ± 0.02 (0.02 – 0.04)	0.05 ± 0.02 (0.02 – 0.05)	3.51	0.002 ± 0.09	0.91
Cadence [steps/min]	3.85 ± 2.50 (1.77 – 4.43)	4.86 ± 2.90 (2.27 – 5.36)	5.31	0.361 ± 9.61	0.54
Single Limb Support [s]	0.04 ± 0.02 (0.02 – 0.04)	0.04 ± 0.02 (0.03 – 0.05)	10.38	-0.027 ± 0.06	0.67
Double Limb Support [s]	0.04 ± 0.01 (0.03 – 0.05)	0.05 ± 0.02 (0.03 – 0.05)	4.88	0.026 ± 0.07	0.63
Stance Time [s]	0.04 ± 0.02 (0.03 – 0.04)	0.05 ± 0.02 (0.03 – 0.06)	5.52	0.024 ± 0.08	0.57
Swing Time [s]	0.03 ± 0.01 (0.02 – 0.04)	0.04 ± 0.02 (0.03 – 0.04)	8.87	-0.022 ± 0.05	0.48
Speed [m/s]	0.04 ± 0.02 (0.02 – 0.04)	0.05 ± 0.03 (0.03 – 0.06)	5.79	0.006 ± 0.09	0.84

4.2.4 Comparison of the three Procedures

In Figure 19 and Figure 20 the average RMSE and average ROME, respectively, over all joint angles and all subjects per approach are shown for both groups. This illustrates the different error growth of the RMSE and the ROME, respectively.

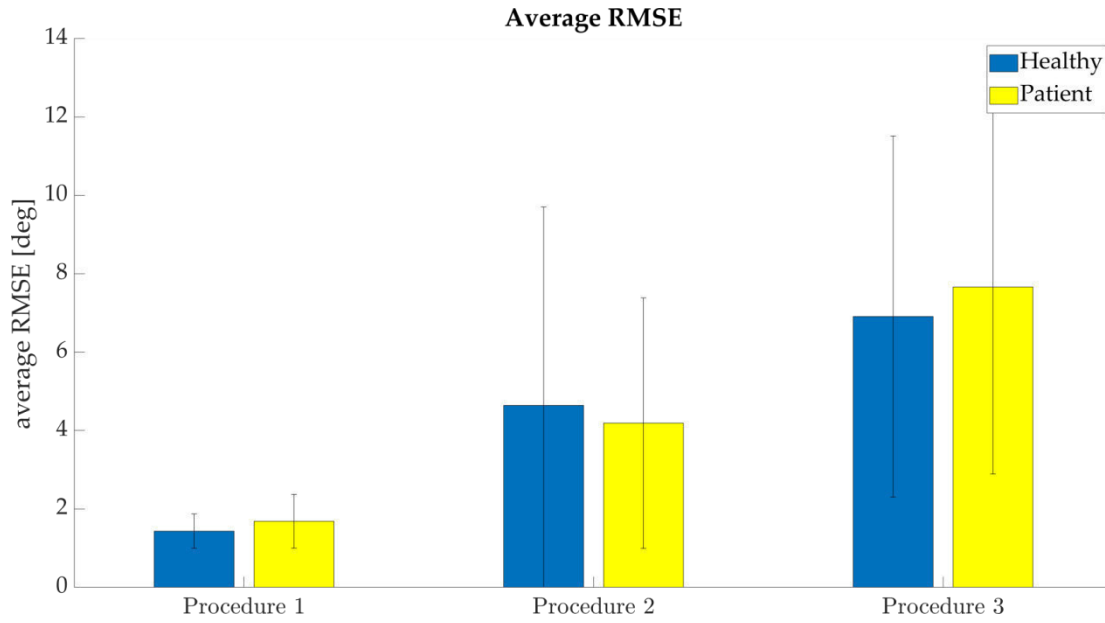


Figure 19. The RMSE averaged over all joint angles of all gait cycles and all subjects is shown for both groups and for each processing approach (Procedure 1 – 3)

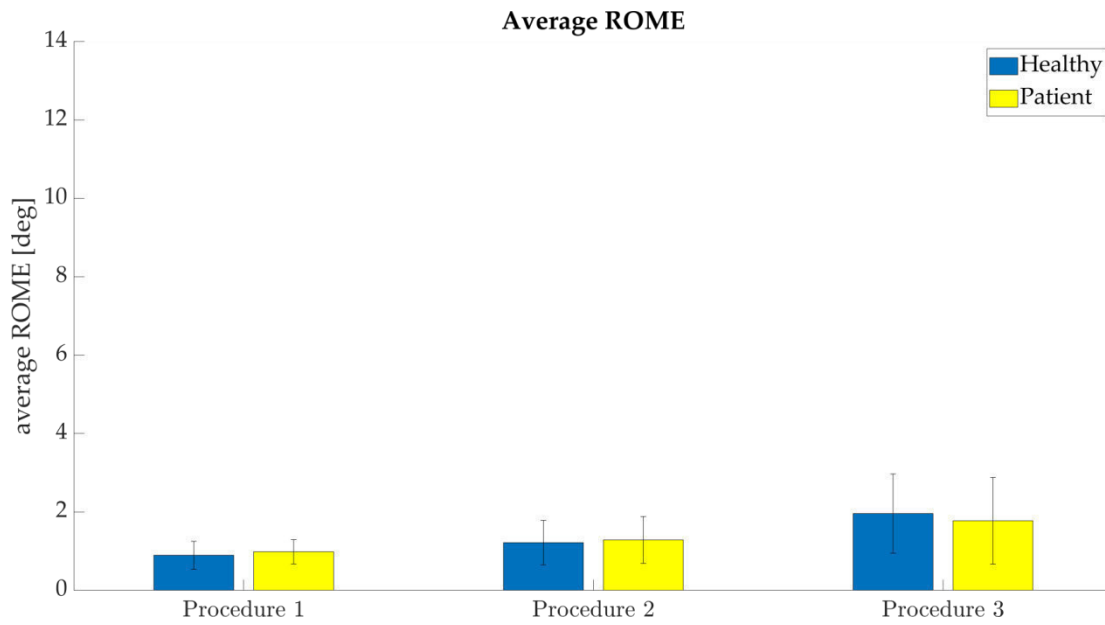


Figure 20. The ROME averaged over all joint angles of all gait cycles and all subjects is shown for both groups and for each processing approach (Procedure 1 – 3)

5 Discussion

In the present thesis a newly developed IMU system for the estimation of the 3D joint angles of the lower body was introduced. It was the aim of the four different JPs, which build the backbone of this work, to provide the research community with an extensive and careful evaluation of the performance of the mentioned system. This procedure should increase the visibility and the acceptance of the IMU system in question not only within the scientific community but rather among clinicians and physicians. Since, if the functionality and accuracy of a new system was proven it can hope for applications outside the scientific laboratory.

The evaluation of the present IMU system was thoroughly conducted throughout this thesis. Each JP contributes to that task adding step by step essential information and therefore leading to a complete overview of the possibilities and limitations of the system under consideration.

JP 1 introduced the IMU system and its fundamental technical basics. Further, it delivered a primary technical validation of the sensor-fusion algorithm used for the estimation of the relative IMU orientations and based on those the calculation of the joint angles during the essential task gait within a group of young and healthy subjects.

The JP 2 extended the technical validation of the IMU based joint angles to more specific motion tasks including movements with an increased ROM and higher accelerations.

In JP 3 the important validation of the estimation of the gait events IC and TC and the consecutively calculated STP is conducted. Further, in this article the first entity of a stand-alone version of the present IMU system was published, introducing an IMU based I2S calibration as well as a biomechanical model, independent from the OMC system.

The JP 4 transfers the approaches from JP 1 and 3 into an inhomogeneous group of subjects, patients after THA. In this article parts of the joint angles are calculated for both groups using the mentioned stand-alone version and are then employed to train a classification model to separate impaired from non-impaired gait patterns.

Finally, in this thesis additional results, not yet published, were presented, delivering a complete overview of the validation of all joint angles and STP calculated based on the purely IMU driven approach as well as on two partly IMU driven approaches.

In the following chapters, the most interesting results from chapter 4.2 are discussed. Furthermore, thoughts on the possibilities but also the restrictions of the IMU system under consideration are discussed. Moreover, limitations not yet mentioned in the single JP are addressed and, finally, an outlook and future work, yet to be accomplished, are considered.

5.1 Discussion of the Additional Results

Considering the results from chapter 4.2 it is evident that the RMSE between the OMC system and the IMU system increased when adding more IMU based information, i.e. the I2S calibration and the biomechanical model based on anthropometric tables. However, that was not unexpected. More interesting was the question of which parameters would suffer the highest decline in accuracy and what information contributed most to that decline. The latter can be analyzed considering Figure 21. Here the percentage distribution of the RMSE on the three different procedures can be viewed. Therefore the average RMSE over all subjects and all joint angles for each group was considered.

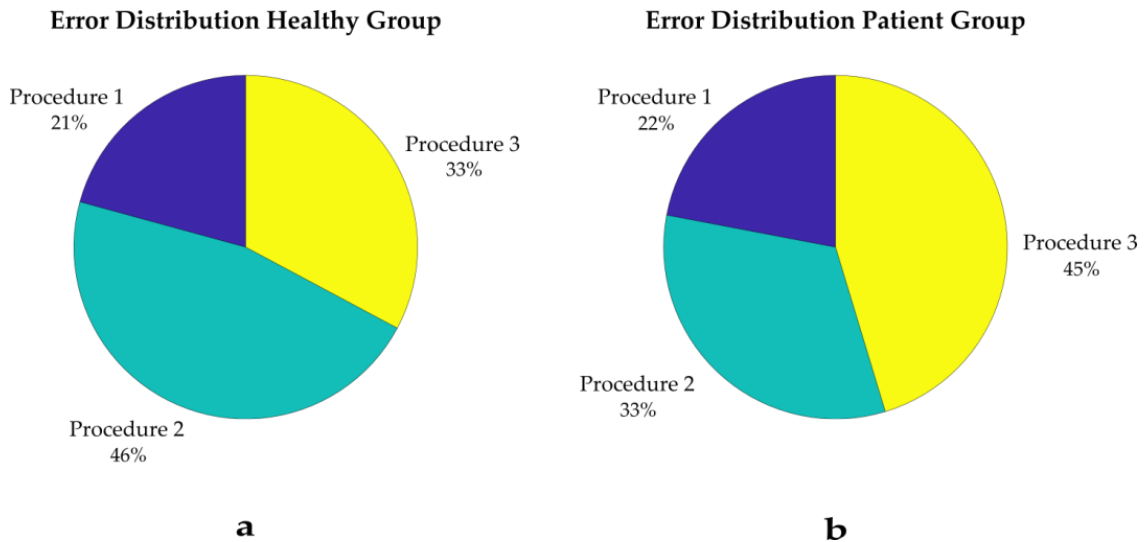


Figure 21. RMSE distribution across the three different stages of IMU data processing for the healthy group (a) and the patient group (b), respectively.

Considering Figure 21 it is evident that Procedure 1 contributed equally to the overall RMSE with respect to the two groups. However, despite the fact that Procedure 2 and 3 contributed about 80 % of the RMSE in both groups, it was shown that the distribution between the two procedures was inverted between the groups. Consequently, in the healthy group the introduction of an IMU based I2S calibration led to a higher increase of the RMSE compared to the patient group, whereas the introduction of a biomechanical model based on anthropometric tables led to a higher increase of the RMSE in the patient group compared to the healthy group. Keep in mind that in the subjects of the patient group a higher amount of soft tissue was evident. This leads to the suggestion that the markers of the OMC system were not in all cases perfectly matched with the underlying AL, despite being positioned by an experienced movement scientist. This was mainly the case considering the markers attached to the pelvis and thigh. As a consequence, when considering the higher RMSE in the patient group after introducing Procedure 3, one has to have in mind that in the presence of increased soft tissue the results of the OMC system have to be viewed very critical. However, the overall RMSE showed similar extents in both groups (healthy: 6.90° ; patient: 7.66°).

In this calculation only the RMSE averaged over all joint angles was considered. Considering the individual RMSE of each joint angle separately it becomes evident that two joint angles stand out in both groups concerning the error growth, the knee rotation and the ankle rotation. In the healthy group the RMSE in the ankle joint increased distinctively higher when introducing Procedure 2 compared to the patient group. However, when introducing Procedure 3, the RMSE in the ankle joint stayed almost the same in the patient group, whereas it even decreased in the healthy group. In contrast to these findings, the RMSE in the knee rotation increased higher in the patient group compared to the healthy group, when entering the final stage of the processing, whereas it did increase in a comparable amount to the remaining joint angles when applying Procedure 2.

An explanation for the enormous error growth in the ankle rotation concerning the healthy group when applying the IMU based I2S calibration might be found in the calibration posture. The I2S calibration procedure was described in JP 3 and consists of an upright standing neutral-zero position and a slightly forward inclined neutral-zero position (see Figure 22).

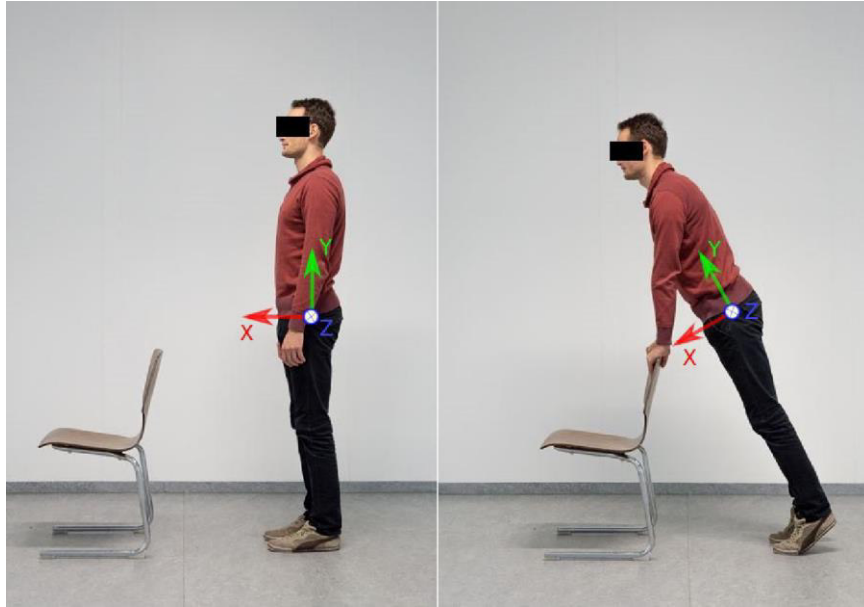


Figure 22. 2-step calibration. The first upright neutral-zero position is shown on the left. The second, slightly forward inclined neutral-zero position is shown on the right. Figure taken from JP 3 [13].

In this calibration procedure to gain satisfying results it is essential to not alter the orientation of the concerning segments in the transversal plane (around the y axis in the Figure 22). However, since one has to stand on the toes it is especially difficult to maintain the orientation of the foot in the mentioned plane. It has to be stated that in the first study, including the healthy subjects, the posture of the second pose was not sufficiently controlled. That might have led to a deviation from the zero position in the ankle joint in the transversal plane and therefore might have ended in a static offset from the OMC system (see Figure 23). Hence, in the second study involving the subjects after THA the correct execution of the second pose of the 2-step calibration was more strictly heeded. Further, the patients used a walking frame instead of the chair in Figure 22 which might have lent them more stability in maintaining the second pose despite their impaired status.

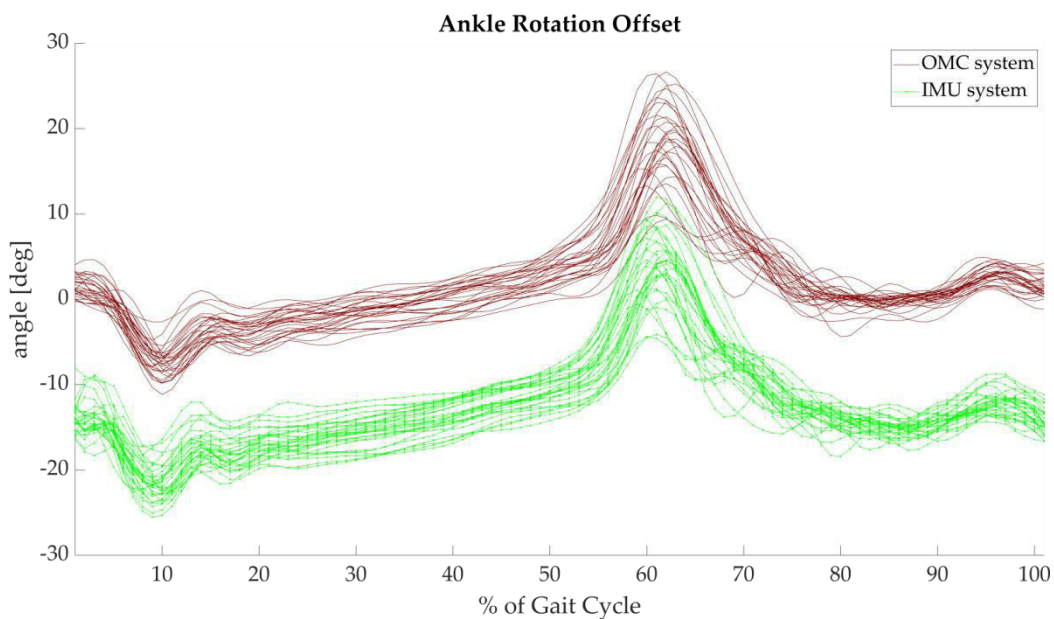


Figure 23. Shown is the right ankle rotation of an exemplary subject of the healthy group during the 6 minute walking test. The IMU based joint angle (green line with dots) was processed according to Procedure 2. The joint angle waveforms were normalized to 100 % gait cycle as it was done for all

joint angles in all cases of the evaluation. A static offset throughout the whole measurement can be observed and explains the high RMSE found in the ankle rotation.

The reason why the RMSE in the ankle joint decreased slightly when substituting the OMC based biomechanical model with the one based on anthropometric tables is not yet fully clear and needs further investigation. However, the explanation for this phenomenon might be the same that explains the high increase in the RMSE of the knee rotation in both groups in Procedure 3, the positioning of the virtual AL on the biomechanical model.

As pointed out in chapter 2.2.2 the biomechanical model used for processing in Procedure 3 was based on the so called TLEM project [119]. In this project the cadaveric pelvis and lower limb of a male individual was measured and virtual markers were attached to AL on the bones. Naturally, these virtual marker points did not exactly match the anatomical location according to Leardini et al. [21], the marker set used in the OMC approach. To overcome this discrepancy, certain marker points in the TLEM model were digitally edited in preparation of the data analysis. Especially, the position of the marker point on the Malleolus lateralis was adapted. That marker is employed to define the segment shank and the center of rotation of the ankle joint and therefore affects the knee joint as well as the ankle joint. It seems that in the case of the knee rotation the discrepancy of the marker positions, in comparison to the OMC system, worsened the results, whereas in the case of the ankle joint it accomplished an improvement. However, as mentioned above, these explanations need further investigation.

Nevertheless, consider the fact that in future applications of the present IMU system the TLEM model will not be used any more due to the restricted representativeness, only one 80-year old male cadaver, and in the presence of more accurate alternatives, e.g a biomechanical model based on a depth camera image [26].

5.2 General Discussion

In the following chapters issues concerning the application of the present IMU system and MIMU / IMU systems in general are discussed. Further, methodical limitations are considered and elaborated. Finally, some critical thoughts on the studies conducted and the systems employed as well as a prospective view on HMC in general are given.

5.2.1 Magnetometer-free Tracking and Drift

A massive advantage of the described IMU system is the omission of magnetometer information. The reason therefor is the susceptibility of the magnetic field to magnetic distortions caused by power lines, steel or electromagnetic disturbances [160], typical for the facility of a motion laboratory or clinics.

Despite there being several approaches in the literature to calculate joint angles based only on accelerometer and gyroscope data, López-Nava and Muñoz-Melendez [161] found in their review on HMC using MIMU / IMUs that 73 % of the systems included in their analysis incorporated magnetometers. Therefore, the calculation of IMU based joint angles omitting magnetometer information still seems to be a difficult and thus rare matter.

The I2S calibration of a MIMU system can be achieved by a single pose [130] and a known rough manual alignment of at least one sensor. In the case of IMU systems additional information is required to substitute the magnetometer information, used to derive the orientation in the horizontal plane, i.e. the heading direction. In the present approach a combination of two static poses, as described in JP 3 and chapter 5.1, was employed. Here the I2S orientation is estimated using accelerometers only.

However, as mentioned in chapter 2.2.1, the omission of magnetometer information leads to a drift in the heading direction estimate. Consider, the gyroscope biases, causing drift in the orientation estimates, is a fundamental concern that not only affects the present IMU system. During motion, the incorporation of biomechanical constraints in terms of connected segments, i.e. the segments stick together at the joints, into the kinematics estimation algorithm via so-called pseudo

measurement updates corrects the heading drift at the joint level even without magnetometer information [10]. Consider, global heading drift cannot be corrected in that way. However, during static phases or pure rotation around the global vertical axis, there is no corrective information, so that heading drift can appear, mostly depending on the magnitude of the gyroscope and accelerometer biases.

Therefore, another essential tool regarding this topic is the accelerometer bias estimation and its subtraction, shortly mentioned in the JP 4. However, it is not within the bounds of this thesis to elaborate that issue. Nevertheless, mentioning this phenomenon within this chapter should sensitize the user that the accelerometer and the gyroscope suffer from biases, already traced in chapter 2.2.1, and that these biases need consideration if measuring with MIMU / IMUs, in particular when omitting magnetometer information.

The present IMU system is able to perform translation estimation, e.g. estimate the distance covered by a tracked subject. However, due to the omitted magnetometer information it is not able to reliably determine the heading direction of a moving subject over a longer period of time. Actual research includes external sensors to fill this gap of information using cameras or of course GPS [162,163]. However, the latter shows restrictions in indoor applications.

Despite the advantage of being unaffected by magnetic distortions, the therefore missing global heading direction information might present a drawback in some areas of application. However, if one is considering to conduct outdoor measurements, likely in sports applications [164], sources causing magnetic disturbances might be far-off. In this case the use of magnetometers could prove beneficial. At this point it has to be stated that despite using only accelerometer and gyroscope data, the sensors used in the corresponding studies nevertheless incorporate a magnetometer. Hence, it is a legitimate suggestion to consider the temporary use of magnetometer information, if one can be sure to be out of reach of potential sources for magnetic distortions. This might improve the motion tracking in outdoor applications. Mainly, it would enable the determination of the global heading direction. However, measuring indoors the global heading drift remains an issue in applications where the global positioning over a longer time period is relevant.

It has to be stated that the missing magnetometer information, i.e. the missing global heading reference, leads to a drift in the global heading estimate on the level of each single IMU. However, in the present approach, as mentioned afore, the network of all seven sensors as well as biomechanical constraints and assumptions are used to correct for this drift and so prevent a miscalculation of the joint angles of the lower body. However, that inevitably leads to some kind of tradeoff. Consequently, it is not ad hoc possible to measure tasks that not meet the criteria described above, e.g. tasks involving a standstill over a longer time or rotating exclusively around the vertical axis, without adapting the sensor fusion algorithm.

This leads to the one parameter measured with the present system that cannot be calculated without limitations, the pelvis rotation. As described in JP 1 the pelvis is the only joint, or rather segment, that is measured globally using the information of the IMU attached to the sacrum. However, as shown in JP 1 the pelvis motion in the transversal plane, i.e. the orientation of the sacrum sensor in the transversal plane, is affected by drift. Since the segment pelvis is the root segment of the whole biomechanical model it determines the absolute heading direction of the complete model. In Figure 24 the effect of that global drift is shown on the example of the virtual marker attached to the calcaneus of the biomechanical model incorporated in the IMU system during the 6 minute waking test.

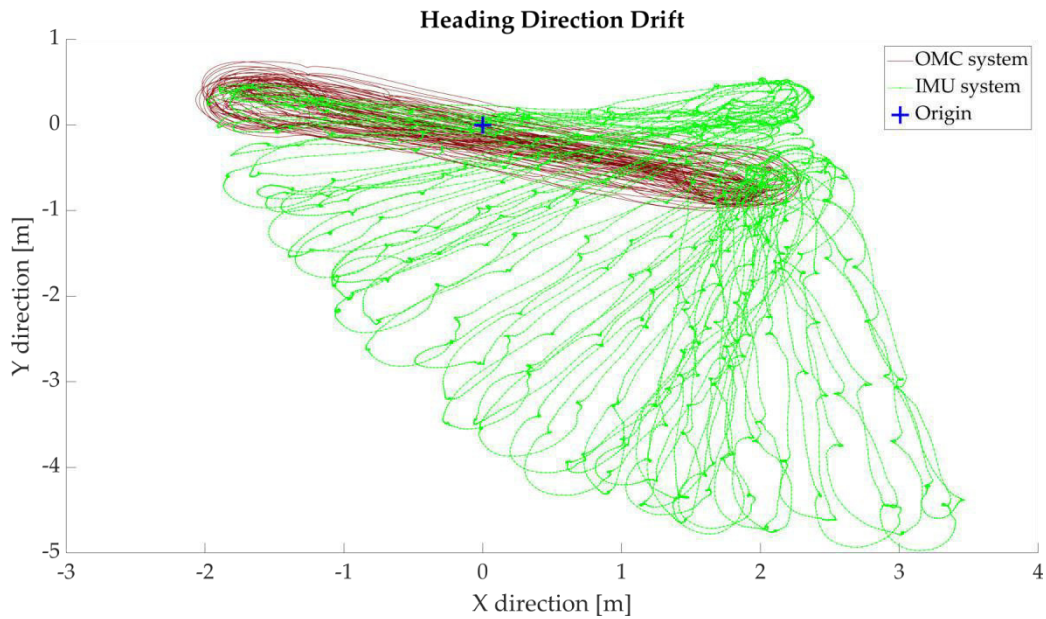


Figure 24. The red line shows the path of the left calcaneus marker, captured using the OMC system, during the 6 minute walking test. The green line with dots shows the path of the virtual left calcaneus marker of the biomechanical model used for the estimation of the IMU based gait kinematics. The blue cross indicates the origin (0/0) of the global CF, i.e. the world CF of the OMC system.

This distinctively restricts the interpretability of the pelvis rotation over a longer period of time in the actual system. That is also the reason for not reporting the RMSE of the pelvis rotation throughout the four JPs and the additional results. However, it was shown that the ROM of the pelvis rotation during each gait cycle remains valid and therefore interpretable. Consequently, despite the present drift, the pelvis rotation ROM still counted as one of the four most important features in the classification model of JP 4.

5.2.2 Biomechanical Model

The impact of the biomechanical model on the outcome of a HMC system was clearly demonstrated in the present thesis (see chapter 4.2.3). Hence, these results support the findings of Kainz et al. [165] who reported that the anatomical CFs of a segment, which are of course depending on the biomechanical model, contribute up to 57.5 % to the overall error between two HMC systems. However, they compared the Plug in gait with the OpenSim model [166].

Concerning the present comparison of biomechanical models, the model of the OMC system is assumed a reliable gold standard since the calculation of the segment's CFs, defined by Cappozzo et al. [25], are based on AL which were determined by an experienced movement scientist in the present studies. However, remember the concerns raised in chapter 5.1. The increase of the RMSE in both groups, introducing the OMC independent biomechanical model, leads to the conclusion that the segment lengths estimated based on the body height and anthropometric tables as well as a biomechanical model based on the study of one male cadaver are not fitting for the widespread use of the present IMU system. Especially the biomechanical model based on one cadaver of an 80 year old male seems not representative for the bigger part of the human population.

However, work is in progress to develop a more individualized creation of a biomechanical model based on a depth camera image [26], mentioned in chapter 2.2.2. This approach was validated against an OMC system in the referenced work. Further, it was also compared to a commercial approach which is based on segment lengths scaling according to anthropometric tables [167]. In both works, the new approach performed well concerning the estimation of the segment lengths and the position of attached AL. However, the validation of the full IMU based 3D joint angles of the lower body incorporating the depth camera based biomechanical model has not yet been conducted.

5.2.3 Sensor to Segment Calibration

As mentioned in chapter 5.1 the I2S calibration method used in the corresponding studies might have led to static offsets, e.g. in the ankle joint as well as the knee joint in the transversal plane. The calibration method, the 2-step calibration, is afflicted with a few restrictions. Like every pose based calibration method it depends strictly on the adequate execution of the required pose. In the case of the neutral-zero position, where every joint is considered to equal zero, some joints are simply anatomically restricted to fulfill this requirement. For example, the physiological alignment of the femur and the tibia in the frontal plane, i.e. the knee abduction / adduction, does not equal zero during normal standing. However, the physiological knee abduction / adduction angle in healthy subjects varies across the literature from 2° – 4° abduction [168] to about 12° abduction for males and 15° abduction for females [169]. Further, it has to be considered that the knee cannot be voluntarily moved in the frontal plane and therefore an offset from the neutral-zero position cannot be voluntarily corrected.

Other subjects might display a hyperextension in the knee joint or might suffer from a flexion contracture. Further, the parallel placement of the feet in the sagittal plane, prescribed within the present calibration procedure, is perceived as unnatural and therefore is often neglected by the subjects. A really careful active placement of the subjects by the examiner would have been necessary and might have led to improved results. However, that is only true for the subjects who are able to theoretically perform the zero position in their joints. That gets especially difficult considering older and impaired subjects, like in the patient group.

However, as mentioned in chapter 5.1 the calibration pose was given more consideration in the study including patients compared to the first study. Further, the group of patients, despite being only days after THA, included almost only subjects who displayed the full ability to sufficiently perform the neutral-zero position. It has to be stated that it was definitely a requirement to perform the neutral zero position for participating in the study. It has to be assumed that if the deviations from zero in the joints of the lower limb would have been too big, a valid evaluation of the joint angles would not have been reliable with the present calibration approach.

In contrast to the difficulty of adopting and maintaining the neutral-zero position during an upright position stands the ability to strike the same pose during a forwardly inclined position. An alternative would have been to perform the inclined calibration pose on a chair according to [111]. However, due to the additional markers and the RB of the OMC system attached to the backside of the pelvis that possibility was not realizable in the present set-up.

It can be concluded that it is definitely necessary to develop new and pose-independent I2S calibration methods considering for example subject groups like humans with cerebral palsy or patients after stroke suffering from hemiplegia. However, as mentioned throughout the JPs, work is in progress concerning the present IMU system to develop an I2S calibration independent from predefined poses or movements. A first proof of concept was already delivered 2016 [170]. The realization of that approach in combination with an individualized biomechanical model based on a depth camera image would certainly be a technological breakthrough of the human motion analysis using IMU.

5.2.4 Soft Tissue Artefacts

The varying effect of STA, common for all HMC systems that employ markers or sensors attached to the skin, was one of the reasons for conducting a second validation of the system including a heterogeneous group of subjects. However, it has to be stated that the study set-up, used in the corresponding JPs, does not allow for an interpretation of the effect of STA on the measurement results of the present IMU system. To the opinion of the author, the OMC system cannot be considered a reference system considering the evaluation of the effect of STA on the joint angles.

However, Barré et al. evaluated in their study the distribution of STA on the lower limbs [171] using an OMC system and skin markers. They attached a total of 80 markers to the thighs and shanks of the subjects. In this way they identified areas of the two segments, which were more

exposed to STA. However, the effect of the STA on the knee angle was evaluated using a bi-plane fluoroscopy in their study. Therefore, a true reference system to approximate the real movement of the underlying bones of a segment and consequently the joint angles requires technologies like MRI [172] or fluoroscopy [173].

In the JP 1 and 2 it was only shown that STA have different effects on the IMU system and the OMC system based on markers attached to AL. However, based on the data in this thesis it is not possible to state which of the two systems is more accurate in estimating the underlying bone movement. As mentioned in the JP 2 there are hints that in some cases even the IMU system's measures of the segment orientations are more trustworthy than an OMC system based on skin markers attached to AL. Nevertheless, only a validation study of the present IMU system against one of the above mentioned technologies could provide a final proof.

5.2.5 Classification Approach

In the JP 4 an SVM was used to train a classification model based on IMU data to separate gait patterns of healthy subjects and patients after THA. The choice of the machine learning algorithm was based on recommendations and experience of the literature [56]. In preparation of the JP 4 other algorithms, like decision trees, nearest neighbors or ensembles, were also tested. However, the SVM performed best and as it was neither the aim of the JP 4 nor of this thesis to compare different classification models in general, it was considered to go beyond the scope to report the outcome of alternative machine learning approaches.

A point for criticism might be the seemingly high difference between the number of samples in the patient group and the healthy group, respectively. The ratio between the two groups was approximately 1:3. If one group distinctively outnumbers the other in an SVM classifier one is at risk that the model classifies every case according to the direction of the imbalance since it is the most probable hypothesis. In more extreme cases the underrepresented group might even be treated as noise and completely ignored [174]. However, Akbani et al. [174] reported that, concerning an SVM, samples are highly imbalanced at a ratio of 1:50. Therefore, it can be assumed that the ratio between the two groups in JP 4 was well in bounds.

Another point concerning a classification problem is the selection of the features. As mentioned at various occasions it was the aim to introduce features based on expert knowledge and the literature that are comprehensible as well as interpretable rather than abstract. However, there might be other and more discriminative features among the multitude of output data from the incorporated IMUs. Therefore, it is of interest for the future to also employ automatic feature engineering, e.g. deep feature synthesis, and automatic feature selection methods [68] as well as combined feature extraction and classification methods, e.g. Auto-Kreas [175], that exploit all the parameters that are available regarding their precision in classifying gait patterns.

5.2.6 Methodical Limitations and Critical Thoughts

The studies conducted to evaluate the performance of an IMU system for the calculation of the joint angles of the lower body in comparison to an OMC system suffered from a few limitations. Some of them were already mentioned in the preceding chapters, like the neglected controlling of the neutral-zero position in the first study, and of course in the JPs themselves.

First, the author wants to draw attention to a differing joint angle designation throughout the JPs. In the JP 1 the ankle joint angle in the frontal plane was named ankle abduction. However, in the following JPs and in the chapter 4.2 this joint angle was named ankle inversion, following a more physiotherapeutic nomenclature.

An issue that might have had an influence on the joint angle calculation was the placement of the sensors assigned to the shanks. In both study groups, healthy and patient, the MIMUs were attached to the lateral side of the shank (see Figure 1 of JP 4), therefore sitting directly atop of the fibularis muscle group. This was done due to better visibility of the markers on the RBs into which the MIMUs had been inserted. However, the actual recommendation for the placement of the shank MIMUs is to place them on the anteromedial part of the shank where they would have been directly

on the bony part of the tibia (see Figure 25). It could have been that the underlying muscles had a negative effect on the accuracy of the segment orientation estimation, i.e. STA. Preceding examinations could have shown if there is indeed such an effect or if the RBs would have been visible enough for the cameras of the OMC system sitting on the anteromedial part of the tibia.



Figure 25. Sensor placement of the sensors assigned to the segment shank (green circle) according to official recommendations. Consider the difference in the positioning of the shank sensors in comparison to Figure 15.

A definite restriction of the present study, mainly concerning the measurement of the more dynamic motion in JP 2, was the reduced recording frequency. The frame rate of the MIMUs and consequently, to simplify the synchronization process, also the frame rate of the OMC system was restricted to 60 Hz. The possible effect of the limited frame rate on the quality of the kinematic results of the countermovement jump was already discussed in the JP 2.

The evaluation of the reliability of the present IMU system could still have been carried on. Only the test-retest reliability was evaluated and that was done only for the healthy group. In addition the evaluation of the inter-tester reliability would have been necessary to complete this process. Therefore, right now the IMU system can only be classified reliable if applied by an experienced tester. The evaluation of the system's reliability if used by non-experts is a step which should be concluded before its widespread use. However, therefor the IMU system would need its own user interface. Since the usage of an IMU system requires both, the application of the sensors as well as the handling of its software, which was not ready for laymen at the time of the recordings.

Another limitation concerns the estimation of the gait events and consequently the calculation of the STP. At this point it has to be stressed that the validation of the algorithm for the gait event detection was only conducted indoors during level walking. However, the present system is intended for outdoor use as well and it has to be expected that the actual algorithm for the event detection needs further refinement if it is to be considered valid during walking on uneven ground, pivoting and uphill as well as downhill walking.

Concerning the outcome of the classification approach from JP 4 it has to be stated that these results apply only to the present case. This was already mentioned in the discussion of the JP 4. However, that is an important point because it limits the significance of these findings.

Further, the present SVM model is mainly trained on symmetry values, e.g. ROM differences between left and right hip joint. Therefore, even patients with a bilateral THA might not be correctly classified, considering a similarly restricted mobility in both hip joints. Also, to achieve a more generalized classification model, able to classify different patient groups independent of their

impairment, the feature set employed in JP 4 has to be extended, consequently including features related to the remaining joints knee and ankle.

Besides, a sample of patients displaying a bigger variety of gait deviations and an age-matched control group should be examined in consecutive studies. Further, future classification approaches should employ data that was recorded in the natural environment of the subjects, rather than in the laboratory. Despite the sample size being considered high enough and well balanced for the present case, future classification models have to be trained involving more subjects and even better balanced groups.

Another, more generalized approach towards the classification of impaired gait would be the development of a one-class SVM [176], a model trained only on features from healthy subjects and therefore representing a kind of norm-group. Such a model should prove discriminative independently of the impairment of the patient group in question. Work is in progress to track this approach using the current IMU data.

There are some further thoughts on the specific subject group chosen for the evaluation in the JP 4. It has been stated several times throughout this thesis that the present findings, concerning the classification as well as the validation, cannot be generally applied to all kinds of subjects. The second evaluation of the accuracy of the IMU system within the group of patients after THA intended to extend the validation to a more heterogeneous group of subjects with respect to the gait patterns.

However, what was missing in the present examination was the evaluation of the inter-subject variability, the proof that the group of patients was indeed more heterogeneous, e.g. in the joint angles. The present statistics, e.g. standard deviation and confidence interval of the error measures, give only a hint of the inter-subject variability regarding the agreement between the two systems but do not allow for an interpretation of the inter-subject gait variability. Viewing this statistics further reveals a similar variation in the error measures compared to the healthy group. However, the fact that the group of patients included subjects operated on the left side as well as on the right side suggests that there might have been sufficient inter-subject gait variability.

In this context, another point comes to mind on which a critical view is inevitable, namely the averaging of the error measures over all subjects for the interpretation. This procedure, despite being commonly employed in the validation of HMC systems, bears a few weaknesses. For one, it does not allow to interpret possible differences between the subjects with respect to the gait patterns or anthropometrics and their influence on the error between the two HMC systems.

In retrospect, a different approach to the evaluation would have been more adequate if one wants to investigate the effect of different motion patterns or different body physiques on the error between to measurement systems. In fact, each subject should have been treated as a single case. Then the errors of each subject should have been compared regarding significant differences. Subjects with distinctively higher or smaller errors should then have been examined further, eventually allowing in-depth interpretation of the different sources that might influence a HMC system, e.g. motion pattern, STA but also sex differences, age or comorbidities.

Another approach regarding the isolated examination of different error sources uses simulated data. Concerning the present system this approach was used in [10] to investigate errors in the measurement model based on the I2S orientation, I2S translation and the segment lengths. However, the examination of the influence of different, pathological gait patterns or soft tissue artefacts requires a far more complex simulation. Nevertheless, work is in progress to simulate complex pathological gait patterns from only a few samples of real motion capture data. This approach is based on a work of Merel et al. [177].

It has to be stated that the data of the patient group was checked on individual level for extreme outliers. Consequently, one subject was excluded due to an exceeding soft tissue component caused by edema. In retrospect, exactly the measurement results of subjects like the excluded one would have been interesting. However, in this individual case it has to be stated that the OMC system would not have proved a reliable reference system since it was not possible to adequately palpate the relevant AL. Maybe that would even be a reason for preferring a MIMU / IMU system, where the AL are estimated within a biomechanical model, over a marker based OMC system.

Nevertheless, the evaluation of each subject of the patient group on an individual level might have yielded a more detailed insight regarding the difference between the systems.

Generally, HMC can be considered an individual affair, depending on many human-related factors, speaking of examiner as well as subject. And to the opinion of the author, HMC systems totally independent from non-system related factors are indeed desirable, but to date not realizable. These considerations get interesting when considering the evaluation of rehabilitation processes using HMC. It is the common approach, as it was also done in the JP 4, to compare the data of subjects undergoing rehabilitation with the data of a so called norm-group.

However, the question must be raised of what is the norm? In the present case the norm is a group of 28 subjects aged around 24 years and mainly students. It was already mentioned that at least an age-matched subject group would be desirable for comparison. However, even then, there remain a lot of factors that might be overrepresented or underrepresented in a norm-group, e.g. fitness level, profession, ethnic background.

These matters raised, there is one theoretical solution that would prove satisfying when analyzing the motion of a subject during rehabilitation, the comparison of its data with data from the same subject before the intervention, meaning injuries or the beginning of an osteoarthritis. However, from a practical point of view this is a nearly impossible endeavor. The only exception might be professional athletes. Here, the financial power and the preconditions are given to perform screening tests on a large scale. This is already standard concerning performance diagnostics, however, it is not so regarding motion analysis. For the latter, optimal HMC systems that unite a quick and easy applicability with high accuracy are still missing. To date, only simple combinations of different motion sensors, for example one MIMU / IMU and a GPS, are employed on a large scale for kinematic analysis in sports [178]. The present IMU system might be able to fill this gap if certain features of it are still improved in the future.

5.3 *Future Work*

Throughout the work on the four articles included in this thesis some issues emerged, which should be treated by future work or are already intensely treated. For example, the work on an alternative approach for the creation of an individualized biomechanical model has recently been rewarded with first publications [26,167]. However, an evaluation of the IMU based joint kinematics of the lower body relying on the information of this model is still pending.

5.3.1 Full Body Kinematics

The next logical step is the extension of the IMU based approach for the joint kinematics estimation of the lower body to the upper body, concluding a full body system. As López-Nava and Muñoz-Meléndez [161] showed in their review on MIMU / IMU based HMC systems, only 8 % of the 37 articles included in their work were concerned with both, the lower body and the upper body. Writing these lines, the data collection for the evaluation of the IMU based joint angle estimation of a full body approach is in progress.

The measurement of the joint angles of the upper body comes up with two challenges, the spine and the scapula. Both are already complicated to measure using OMC systems [179–182], due to the complexity of their anatomy and the increased influence of STA. The detailed measurement of the motion of the scapula and spine using MIMU / IMUs is therefore poorly researched, highly limited or is still dependent on additional sensors [183–186].

The modelling of the spine needs further improvement to better represent its different sections. Further, the optimal positioning of the sensors on the spine needs to be reconsidered [187]. However, simple MIMU / IMU set-ups are already a useful tool to simply measure the motion of the trunk considered as a rigid unit [188–190].

5.3.2 Automated I2S Calibration

Another important issue is the intended self-calibration [170]. This calibration method aims to be independent of certain poses or pre-defined movements. Recently, a reliable automated sensor to segment assignment was achieved [191]. This presents a major step towards a simplification of the IMU system set-up since it renders the prescribed placement of the sensor to its dedicated segment, which is common in most commercial MIMU / IMU systems, redundant.

However, both mentioned approaches towards an automated I2S calibration still require further research to provide more accurate and generalizable results.

Once the automated I2S calibration approach is ready to use it can of course be evaluated based on the data collected throughout this thesis. However, it has to be further evaluated among a group of subjects with proven limitations concerning the ROM, distinctive deviations from the neutral-zero position and a lacking mental fitness to correctly perform predefined movement tasks, like it is the case in patients with CP or patients with neurological impairments.

5.3.3 Hardware

In this thesis, as mentioned in chapter 2.2.4, the Mtw Awinda MIMUs were employed for the recording of the raw accelerometer and gyroscope data. However, as mentioned in chapter 5.2.5 and throughout the JPs, the recording frequency was restricted to 60 Hz due to technical conditions. However, the algorithm used for processing the raw accelerometer and gyroscope data is independent of a special hardware. Considering one of the intended implementations of the system, a feedback application for patients after THA, the simplicity of the sensor application as well as the performance of the hardware are key.

For example, the smart textiles shown in Figure 12 present the opportunity for a quick and easy application, which is important when working with patients. However, it has to be considered that the pants might introduce additional motion artefacts. Further, this method for sensor application might not be extendable to other patient groups like wheelchair drivers or patients who have to wear braces.

In the latter cases the methods using straps, employed in the present studies, might be preferred. In this context, new sensor-networks are developed right now at the German Research Center for Artificial Intelligence, which consist of small and light-weighted MIMUs connected with textile cables (see Figure 26.). It might be that different sets of hardware, considering the individual group of subjects, might present the optimal solution. However, future hardware set-ups should employ an increased recording frequency, especially when considering highly dynamic motions.

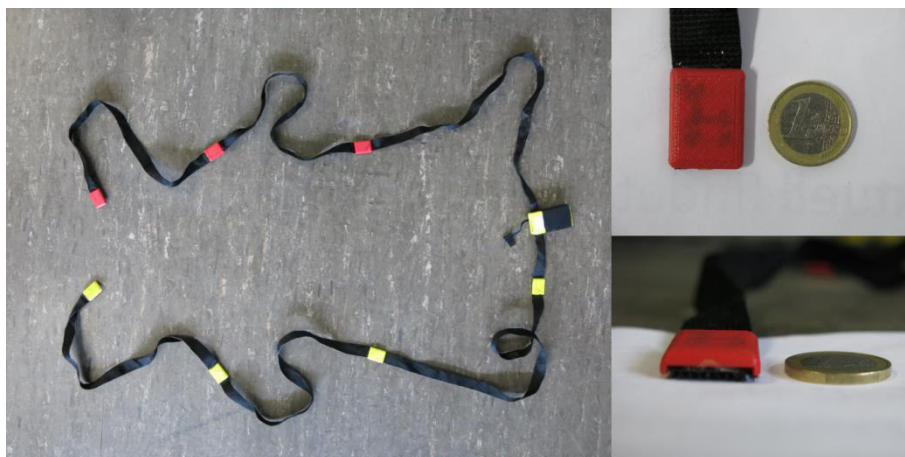


Figure 26. Example of a sensor network consisting of seven MIMUs, connected with textile cables, developed at the German Research Center for Artificial Intelligence. Smaller sub-networks of two or more sensors that can be connected among each other using Bluetooth are also in development.

5.3.4 Machine Learning

The use of MIMU / IMU systems and wearable sensors in general is rapidly increasing, as is, consequently, the amount of available data. Therefore, the importance of machine learning has increased within the society and will increase even more in the future. Hence, to the opinion of the author, the responsibility of data scientists to provide the user with high quality data is likewise growing.

Further, it is essential that professions, i.e. in the medical sector, that were not overly concerned in the past with data science and artificial intelligence, receive a fundamental knowledge concerning these issues. Researchers can play a part in this process but in the end this issue has to be heavily attended to on the level of politics. The promotion of interdisciplinary research teams and the creation of interdisciplinary courses might help to prepare society for the upcoming flood of data.

Concerning the particular gait classification example from the JP 4, this has to be considered like a sort of proof of concept. It demonstrated the theoretical possibility that the chosen features from the IMU based joint angles are able to separate impaired from non-impaired gait and can therefore be useful trigger parameters in a possible feedback application for patients after THA. However, to really employ that model or a similar model for the general classification of pathological gait further evaluations and refinements are necessary, like the mentioned development of a one-class SVM.

5.3.5 Further Validation Steps

The present IMU system is, to the opinion of the author and according to the results described in this thesis, at this point able to be applied for gait analysis within clinical settings and certain patient groups. However, the validation of the system has to be carried on.

The event detection has to be evaluated in real-life conditions, i.e. uneven terrain, obstacles or cognitive distractions, prior to the use of the IMU system in, for example, a home-based gait-training application.

Further, the performance of the IMU system should be evaluated when applied to patient groups displaying more sincere gait abnormalities compared to the patients after THA. Mainly the gait analysis in neurological patients demands highly flexible systems.

Considering ergonomics, another huge field of applications for HMC systems, other requirements are coming up to the present IMU system. These include mainly stationary tasks, or the integration of the sensors into loosely fitting work garment and thus the identification of cloth related motion artefacts as well as long-term measurements over several hours instead of minutes.

In the JP 2 the first static and moderately dynamic motion tasks were evaluated. However, in this case the joint angles were calculated according to Procedure 1, including OMC information. Therefore, the complete validation of these tasks using the stand-alone version of the IMU system is still pending. However, this thesis was focused on gait, hence the additional full validation of the static and dynamic motion tasks was considered beyond the scope of this work. This step can be conducted without recording new data and should therefore follow soon.

Nevertheless, if this system should be considered for sport specific applications, it has to be validated during the particular task, regarding the application of interest. Mainly highly dynamic motions like sprinting, cutting, etc. demand a separate evaluation.

5.4 Outlook – the Future of Human Motion Capture

In this chapter the author wants to take a prospective view at where the presently discussed IMU system might end up in a few years and what he thinks will be the next big steps in HMC.

Consider the development steps, mentioned in chapter 5.3, successfully conducted within the next years, i.e. an automated I2S calibration is established, quickly applicable sensor networks are incorporated, the joint angle estimation is extended to the upper body and, further, the sensor-fusion algorithm is able to perform real-time on small devices like smartphones or tablets, providing complete mobility. Then, the fields of application with respect to the current IMU system are almost endless.

In combination with adequate machine learning algorithms the IMU system will indeed be fit to be employed as a home-based gait-training application for patients after THA. However, for a

successful implementation, beside the easy attachment of the sensors, i.e. in the form of smart textiles mentioned in chapter 2.2.3, an intelligible user interface is key.

Also in professional sports this system will be of high interest with respect to injury screening tests, mentioned in 5.2.6. If the set-up of the IMU system lasts only a few minutes and the measurements can be conducted using wearable devices the execution of widespread standardized pre-season injury screenings becomes an imaginable scenario, consequently providing the desired norm data in the case of post-injury assessments.

Another big area of application will be the ergonomics sector. Here it is even more important that the subjects are not obstructed by the sensors. Therefore, it is of interest to integrate the MIMU / IMUs into the working garments. However, as mentioned in the preceding chapter the identification and filtering of motion artefacts due to loosely fitted clothes would be a precondition. This obstacle passed, a feedback application warning workers of disadvantageous body postures can be employed. Of course, systems using wearable sensors for the evaluation of work-related musculoskeletal disorders are already developed [192]. Here, mainly surface electromyography is used to date. However, again, present MIMU / IMU systems are not sufficiently easy to handle to be already in widespread use.

These are only a few possible fields of application for the present IMU system. However, it remains the question if there will be other alternatives to MIMU / IMU systems for the quick assessment of human motion. Another, intensely researched approach towards quickly and easily executable HMC systems, overcoming the restrictions of marker based OMC systems, are markerless OMC systems [193]. The definite advantage of markerless OMC systems is the fact that, ideally, there is absolutely no preparation of the subject necessary. Mainly in sports applications this approach is of high interest, since in this case the athlete is not disturbed by markers, sensors, etc. [194].

However, the markerless systems come along with some disadvantages, still preventing their standardized application. Markerless OMC systems require a multi-camera set up that is commonly dependent on a calibration. Therefore, their measurement volume is still spatially restricted. Further, their accuracy regarding the joint angle estimation, mainly in the frontal and transversal plane, is still lacking in comparison to marker based OMC systems [195].

On one hand markerless systems might prove useful with respect to individual sports, whereas on the other hand they face a common problem when considering team sports, occlusion [196]. There is of course research trying to tackle this problem, however, mostly including only a maximum of two subjects [196,197]. An interesting solution to the problem of occlusion in camera based systems, markerless as well as marker based systems, is the fusion of the standard camera system with alternative sensors not depending on permanent visibility, i.e. MIMU / IMUs. So called hybrid systems are already in the focus of researchers [198–200]. In such a set-up MIMU / IMUs would enable the continuous tracking of a subject's segments in the case that it leaves the measurement volume or it is partly occluded by, e.g., other persons.

Using the information of an OMC system, especially a marker based one, might solve the MIMU / IMU systems' problem of an accurate I2S calibration and biomechanical model. In this context, the results from the JP 1 and 2 as well as the additional results from the chapters 4.2.1 and 4.2.2 can be considered a kind of hybrid system since they incorporate OMC based information as well as IMU based information.

However, to date these hybrid approaches are mainly considered in the fields of computer vision and robotics, not yet sufficiently developed for applications in the areas of medicine or sports. Nevertheless, this seems a very promising approach for future HMC applications, which might even have the potential to form the new standard in motion analysis.

6 Conclusion

It was not only the aim of this thesis to present a thorough validation of the present IMU system but rather to give a compact overview about this still young technology, the possibilities it provides, the diversity of approaches for the calculation of manifold parameters and further to highlight the still unsolved technical problems and challenges it involves.

First and foremost, it has to be clarified that with the present thesis on the validation of an IMU system, that very system is not qualified for the use in all fields of application. It cannot be used without second thoughts for the gait analysis in other patient groups showing distinctively different motion patterns compared to THA patients or subjects displaying exceeding soft tissue. Further, there is no guarantee for valid results of the joint angles of the lower body if the present IMU system is applied in highly dynamic sports like running, sprinting, cutting, etc. Consider that the validation was conducted only in laboratory situations and only on level ground. Therefore, it is not yet clear if the IMU system's accuracy, mainly the gait event detection but also the joint angles, remains stable during gait in uneven terrain, including uphill and downhill walking. Consequently, as mentioned in chapter 5.3.5, further validation steps must follow. Additionally, to date the examined magnetometer-free IMU system cannot be employed in applications where the subject's global heading direction is of relevance.

However, the IMU system can be considered valid for complex gait analysis, estimation of joint angles and STP, as well as the measurement of static motion tasks incorporating moderate dynamics in young and healthy adults on level ground. Further, the gait analysis can be extended to patients after THA. The results presented in this thesis and its accompanying JPs revealed a convincing accuracy, throughout the three evaluation stages (Procedure 1 – 3), of the 3D joint angles of the lower limbs with excellent results in the sagittal plane, good results in the frontal plane and a slight decline of the accuracy in the transversal plane of the knee and ankle joint.

It turned out that the IMU based I2S calibration and the OMC-independent biomechanical model led to a static offset in the joint angles. However, as it was shown that the RMSE remains stable over the time parameters like the ROM can be considered trustworthy. The latter showed an excellent validity independent of the group of subjects or the evaluation stage. Therefore, the clinical application of the present IMU system can be highly recommended, at least in the field of orthopedics.

The evaluation of the gait event detection and the STP revealed also a highly accurate outcome in both groups, with two exceptions. The spatial parameters step width and swing width need further refinement to be of clinical relevance.

Some general thoughts were given throughout this thesis on the advantages and disadvantages of IMU systems and OMC systems, respectively, and the potential benefits of a combined application. The present work tried to sensitize potential users to the careful application of HMC systems in general and the well-considered interpretation of their results, by highlighting the technical issues, the diversity of approaches and the still remaining uncertainties in MIMU / IMU systems, despite it being a technology highly considered by researchers for the past decades.

For no matter how thoroughly a HMC system is validated the accuracy of its results can never be guaranteed throughout all possible scenarios of application. Therefore, the careful user always has to reconsider the problem one is about to solve using HMC, the application of the HMC system and, finally, in consideration of the former two, its results.

Bibliography

1. McGinley, J.L.; Baker, R.; Wolfe, R.; Morris, M.E. The reliability of three-dimensional kinematic gait measurements: A systematic review. *Gait & Posture* 2009, *29*, 360–369, doi:10.1016/j.gaitpost.2008.09.003.
2. Whittle, M.W. Clinical gait analysis: A review. *Human Movement Science* 1996, *15*, 369–387, doi:10.1016/0167-9457(96)00006-1.
3. Roberts, M.; Mongeon, D.; Prince, F. Biomechanical parameters for gait analysis: a systematic review of healthy human gait. *Physical Therapy and Rehabilitation* 2017, *4*, 6, doi:10.7243/2055-2386-4-6.
4. Boyer, K.A.; Johnson, R.T.; Banks, J.J.; Jewell, C.; Hafer, J.F. Systematic review and meta-analysis of gait mechanics in young and older adults. *Experimental Gerontology* 2017, *95*, 63–70, doi:10.1016/j.exger.2017.05.005.
5. Márquez, G.; Alegre, L.M.; Jaén, D.; Martín-Casado, L.; Aguado, X. Sex differences in kinetic and neuromuscular control during jumping and landing. *J Musculoskelet Neuronal Interact* 2017, *17*, 409–416.
6. Clarys, J.P.; Cabri, J. Electromyography and the study of sports movements: A review. *Journal of Sports Sciences* 1993, *11*, 379–448, doi:10.1080/02640419308730010.
7. Picerno, P. 25 years of lower limb joint kinematics by using inertial and magnetic sensors: A review of methodological approaches. *Gait & Posture* 2017, *51*, 239–246, doi:10.1016/j.gaitpost.2016.11.008.
8. Cappozzo, A.; Della Croce, U.; Leardini, A.; Chiari, L. Human movement analysis using stereophotogrammetry. *Gait & Posture* 2005, *21*, 186–196, doi:10.1016/j.gaitpost.2004.01.010.
9. Miezal, M.; Taetz, B.; Bleser, G. Real-time inertial lower body kinematics and ground contact estimation at anatomical foot points for agile human locomotion. In Proceedings of the 2017 IEEE International Conference on Robotics and Automation (ICRA); 2017; pp. 3256–3263.
10. Miezal, M.; Taetz, B.; Bleser, G. On Inertial Body Tracking in the Presence of Model Calibration Errors. *Sensors* 2016, *16*, 1132, doi:10.3390/s16071132.
11. Teufl, W.; Miezal, M.; Taetz, B.; Fröhlich, M.; Bleser, G. Validity, Test-Retest Reliability and Long-Term Stability of Magnetometer Free Inertial Sensor Based 3D Joint Kinematics. *Sensors* 2018, *18*, 1980, doi:10.3390/s18071980.
12. Teufl, W.; Miezal, M.; Taetz, B.; Fröhlich, M.; Bleser, G. Validity of inertial sensor based 3D joint kinematics of static and dynamic sport and physiotherapy specific movements. *PLOS ONE* 2019, *14*, e0213064, doi:10.1371/journal.pone.0213064.
13. Teufl, W.; Lorenz, M.; Miezal, M.; Taetz, B.; Fröhlich, M.; Bleser, G. Towards Inertial Sensor Based Mobile Gait Analysis: Event-Detection and Spatio-Temporal Parameters. *Sensors* 2018, *19*, 38, doi:10.3390/s19010038.
14. Teufl, W.; Taetz, B.; Miezal, M.; Lorenz, M.; Pietschmann, J.; Jöllenbeck, T.; Fröhlich, M.; Bleser, G. Towards an Inertial Sensor-Based Wearable Feedback System for Patients after Total Hip Arthroplasty: Validity and Applicability for Gait Classification with Gait Kinematics-Based Features. *Sensors* 2019, *19*, 5006, doi:10.3390/s19225006.
15. Karatsidis, A.; Bellusci, G.; Schepers, H.; Zee, M. de; Andersen, M.; Veltink, P. Estimation of Ground Reaction Forces and Moments During Gait Using Only Inertial Motion Capture. *Sensors* 2016, *17*, 75, doi:10.3390/s17010075.
16. Wouda, F.J.; Giuberti, M.; Bellusci, G.; Maartens, E.; Reenalda, J.; van Beijnum, B.-J.F.; Veltink, P.H. Estimation of Vertical Ground Reaction Forces and Sagittal Knee Kinematics During

- Running Using Three Inertial Sensors. *Frontiers in Physiology* 2018, 9, doi:10.3389/fphys.2018.00218.
17. Banks, J.J.; Chang, W.-R.; Xu, X.; Chang, C.-C. Using horizontal heel displacement to identify heel strike instants in normal gait. *Gait & Posture* 2015, 42, 101–103, doi:10.1016/j.gaitpost.2015.03.015.
 18. Veilleux, L.-N.; Raison, M.; Rauch, F.; Robert, M.; Ballaz, L. Agreement of spatio-temporal gait parameters between a vertical ground reaction force decomposition algorithm and a motion capture system. *Gait & Posture* 2016, 43, 257–264, doi:10.1016/j.gaitpost.2015.10.007.
 19. König, N.; Singh, N.B.; von Beckerath, J.; Janke, L.; Taylor, W.R. Is gait variability reliable? An assessment of spatio-temporal parameters of gait variability during continuous overground walking. *Gait & Posture* 2014, 39, 615–617, doi:10.1016/j.gaitpost.2013.06.014.
 20. Merriaux, P.; Dupuis, Y.; Boutteau, R.; Vasseur, P.; Savatier, X. A Study of Vicon System Positioning Performance. *Sensors* 2017, 17, 1591, doi:10.3390/s17071591.
 21. Leardini, A.; Sawacha, Z.; Paolini, G.; Ingrosso, S.; Nativo, R.; Benedetti, M.G. A new anatomically based protocol for gait analysis in children. *Gait & Posture* 2007, 26, 560–571, doi:10.1016/j.gaitpost.2006.12.018.
 22. Duffell, L.D.; Hope, N.; McGregor, A.H. Comparison of kinematic and kinetic parameters calculated using a cluster-based model and Vicon's plug-in gait. *Proc Inst Mech Eng H* 2014, 228, 206–210, doi:10.1177/0954411913518747.
 23. Leardini, A.; Benedetti, M.G.; Berti, L.; Bettinelli, D.; Nativo, R.; Giannini, S. Rear-foot, mid-foot and fore-foot motion during the stance phase of gait. *Gait & Posture* 2007, 25, 453–462, doi:10.1016/j.gaitpost.2006.05.017.
 24. Borhani, M.; McGregor, A.H.; Bull, A.M.J. An alternative technical marker set for the pelvis is more repeatable than the standard pelvic marker set. *Gait & Posture* 2013, 38, 1032–1037, doi:10.1016/j.gaitpost.2013.05.019.
 25. Cappozzo, A.; Catani, F.; Croce, U.D.; Leardini, A. Position and orientation in space of bones during movement: anatomical frame definition and determination. *Clinical Biomechanics* 1995, 10, 171–178, doi:10.1016/0268-0033(95)91394-t.
 26. Taetz, B.; Teufl, W.; Weidmann, A.; Pietschmann, J.; Jöllenbeck, T.; Bleser, G. Depth camera based statistical shape fitting approach for the creation of an individualized lower body biomechanical model: validity and reliability. *Computer Methods in Biomechanics and Biomedical Engineering* 2019, 1–11, doi:10.1080/10255842.2019.1688310.
 27. Leardini, A.; Chiari, L.; Croce, U.D.; Cappozzo, A. Human movement analysis using stereophotogrammetry. *Gait & Posture* 2005, 21, 212–225, doi:10.1016/j.gaitpost.2004.05.002.
 28. Geng, W.; Yu, G. Reuse of Motion Capture Data in Animation: A Review. In Proceedings of the Computational Science and Its Applications — ICCSA 2003; Berlin, Heidelberg, 2003; Vol. 2669, pp. 620–629.
 29. Bregler, C. Motion Capture Technology for Entertainment [In the Spotlight]. *IEEE Signal Processing Magazine* 2007, 24, 160–158, doi:10.1109/MSP.2007.906023.
 30. van der Kruk, E.; Reijne, M.M. Accuracy of human motion capture systems for sport applications; state-of-the-art review. *European Journal of Sport Science* 2018, 18, 806–819, doi:10.1080/17461391.2018.1463397.
 31. Valevicius, A.M.; Jun, P.Y.; Hebert, J.S.; Vette, A.H. Use of optical motion capture for the analysis of normative upper body kinematics during functional upper limb tasks: A systematic review. *Journal of Electromyography and Kinesiology* 2018, 40, 1–15, doi:10.1016/j.jelekin.2018.02.011.

32. Baker, R. The history of gait analysis before the advent of modern computers. *Gait & Posture* 2007, 26, 331–342, doi:10.1016/j.gaitpost.2006.10.014.
33. Gage, J.R. Gait analysis. An essential tool in the treatment of cerebral palsy. *Clin Orthop Relat Res* 1993, 126–134.
34. Gage, J.R. *Gait Analysis in Cerebral Palsy*; Cambridge University Press, 1991; ISBN 978-0-521-41277-3.
35. Baker, R.W. *Measuring Walking: A Handbook of Clinical Gait Analysis*; Wiley, 2013; ISBN 978-1-908316-66-0.
36. Perry, J.; Burnfield, J.; Burnfield, J.M. *Gait Analysis: Normal and Pathological Function*; SLACK, 2010; ISBN 978-1-55642-766-4.
37. Götz-Neumann, K. *Gehen verstehen: Ganganalyse in der Physiotherapie ; 18 Tabellen*; Georg Thieme Verlag, 2006; ISBN 978-3-13-132372-9.
38. Pistacchi, M.; Gioulis, M.; Sanson, F.; De Giovannini, E.; Filippi, G.; Rossetto, F.; Marsala, S.Z. Gait analysis and clinical correlations in early Parkinson's disease. *Funct Neurol* 2017, 32, 28–34, doi:10.11138/FNeur/2017.32.1.028.
39. Stolze, H. Typical features of cerebellar ataxic gait. *Journal of Neurology, Neurosurgery & Psychiatry* 2002, 73, 310–312, doi:10.1136/jnnp.73.3.310.
40. DeLuca, P.A.; Davis, R.B.; Öunpuu, S.; Rose, S.; Sirkin, R. Alterations in Surgical Decision Making in Patients with Cerebral Palsy Based on Three-Dimensional Gait Analysis. *Journal of Pediatric Orthopaedics* 1997, 17, 608–614.
41. Lofterød, B.; Terjesen, T. Results of treatment when orthopaedic surgeons follow gait-analysis recommendations in children with CP. *Developmental Medicine & Child Neurology* 2008, 50, 503–509, doi:10.1111/j.1469-8749.2008.03018.x.
42. Mayr, E.; Nogler, M.; Benedetti, M.-G.; Kessler, O.; Reinthaler, A.; Krismer, M.; Leardini, A. A prospective randomized assessment of earlier functional recovery in THA patients treated by minimally invasive direct anterior approach: A gait analysis study. *Clinical Biomechanics* 2009, 24, 812–818, doi:10.1016/j.clinbiomech.2009.07.010.
43. Lindemann, U.; Becker, C.; Muche, R.; Aminian, K.; Dejnabadi, H.; Nikolaus, T.; Puhl, W.; Huch, K.; Dreinhöfer, K.E. Gait analysis and WOMAC are complementary in assessing functional outcome in total hip replacement. *Clinical Rehabilitation* 2006, 20, 413–420, doi:10.1191/0269215506cr958oa.
44. Masani, K.; Kouzaki, M.; Fukunaga, T. Variability of ground reaction forces during treadmill walking. *Journal of Applied Physiology* 2002, 92, 1885–1890, doi:10.1152/jappphysiol.00969.2000.
45. Chao, E.Y.; Laughman, R.K.; Schneider, E.; Stauffer, R.N. Normative data of knee joint motion and ground reaction forces in adult level walking. *Journal of Biomechanics* 1983, 16, 219–233, doi:10.1016/0021-9290(83)90129-X.
46. Ewen, A.M.; Stewart, S.; St Clair Gibson, A.; Kashyap, S.N.; Caplan, N. Post-operative gait analysis in total hip replacement patients—A review of current literature and meta-analysis. *Gait & Posture* 2012, 36, 1–6, doi:10.1016/j.gaitpost.2011.12.024.
47. Bennett, D.; Humphreys, L.; O'Brien, S.; Kelly, C.; Orr, J.F.; Beverland, D.E. Gait kinematics of age-stratified hip replacement patients—A large scale, long-term follow-up study. *Gait & Posture* 2008, 28, 194–200, doi:10.1016/j.gaitpost.2007.11.010.
48. Bahl, J.S.; Nelson, M.J.; Taylor, M.; Solomon, L.B.; Arnold, J.B.; Thewlis, D. Biomechanical changes and recovery of gait function after total hip arthroplasty for osteoarthritis: a systematic review and meta-analysis. *Osteoarthritis and Cartilage* 2018, 26, 847–863, doi:10.1016/j.joca.2018.02.897.

49. Gouelle, A. Interpreting Spatiotemporal Parameters, Symmetry, and Variability in Clinical Gait Analysis. In *Handbook of Human Motion*; Springer International Publishing: Cham, 2016; pp. 1–20 ISBN 978-3-319-30808-1.
50. Zeni, J.; Richards, J.; Higginson, J.S. Two simple methods for determining gait events during treadmill and overground walking using kinematic data. *Gait Posture* 2008, *27*, 710–714, doi:10.1016/j.gaitpost.2007.07.007.
51. Braun, B.J.; Veith, N.T.; Hell, R.; Döbele, S.; Roland, M.; Rollmann, M.; Holstein, J.; Pohlemann, T. Validation and reliability testing of a new, fully integrated gait analysis insole. *Journal of Foot and Ankle Research* 2015, *8*, 54, doi:10.1186/s13047-015-0111-8.
52. Lin, F.; Wang, A.; Zhuang, Y.; Tomita, M.R.; Xu, W. Smart Insole: A Wearable Sensor Device for Unobtrusive Gait Monitoring in Daily Life. *IEEE Transactions on Industrial Informatics* 2016, *12*, 2281–2291, doi:10.1109/TII.2016.2585643.
53. Oerbekke, M.S.; Stukstette, M.J.; Schütte, K.; de Bie, R.A.; Pisters, M.F.; Vanwanseele, B. Concurrent validity and reliability of wireless instrumented insoles measuring postural balance and temporal gait parameters. *Gait & Posture* 2017, *51*, 116–124, doi:10.1016/j.gaitpost.2016.10.005.
54. Stöggl, T.; Martiner, A. Validation of Moticon’s OpenGo sensor insoles during gait, jumps, balance and cross-country skiing specific imitation movements. *Journal of Sports Sciences* 2017, *35*, 196–206, doi:10.1080/02640414.2016.1161205.
55. Eie, M.; Wei, C.-S. Generalizations of Euler decomposition and their applications. *Journal of Number Theory* 2013, *133*, 2475–2495, doi:10.1016/j.jnt.2013.01.010.
56. Figueiredo, J.; Santos, C.P.; Moreno, J.C. Automatic recognition of gait patterns in human motor disorders using machine learning: A review. *Medical Engineering & Physics* 2018, *53*, 1–12, doi:10.1016/j.medengphy.2017.12.006.
57. Dobson, F.; Morris, M.E.; Baker, R.; Graham, H.K. Gait classification in children with cerebral palsy: A systematic review. *Gait & Posture* 2007, *25*, 140–152, doi:10.1016/j.gaitpost.2006.01.003.
58. Zhang, Y.; Ma, Y. Application of supervised machine learning algorithms in the classification of sagittal gait patterns of cerebral palsy children with spastic diplegia. *Computers in Biology and Medicine* 2019, *106*, 33–39, doi:10.1016/j.combiomed.2019.01.009.
59. Wahid, F.; Begg, R.K.; Hass, C.J.; Halgamuge, S.; Ackland, D.C. Classification of Parkinson’s Disease Gait Using Spatial-Temporal Gait Features. *IEEE Journal of Biomedical and Health Informatics* 2015, *19*, 1794–1802, doi:10.1109/JBHI.2015.2450232.
60. Manap, H.H.; Md Tahir, N.; Yassin, A.I.M. Statistical analysis of parkinson disease gait classification using Artificial Neural Network. In *Proceedings of the 2011 IEEE International Symposium on Signal Processing and Information Technology (ISSPIT)*; IEEE: Bilbao, Spain, 2011; pp. 060–065.
61. Djuric-Jovicic, M.; Jovicic, N.S.; Milovanovic, I.; Radovanovic, S.; Kresojevic, N.; Popovic, M.B. Classification of walking patterns in Parkinson’s disease patients based on inertial sensor data. In *Proceedings of the 10th Symposium on Neural Network Applications in Electrical Engineering*; IEEE: Belgrade, Serbia, 2010; pp. 3–6.
62. Lau, H.; Tong, K.; Zhu, H. Support vector machine for classification of walking conditions of persons after stroke with dropped foot. *Human Movement Science* 2009, *28*, 504–514, doi:10.1016/j.humov.2008.12.003.
63. Mannini, A.; Trojaniello, D.; Cereatti, A.; Sabatini, A.M. A Machine Learning Framework for Gait Classification Using Inertial Sensors: Application to Elderly, Post-Stroke and Huntington’s Disease Patients. *Sensors* 2016, *16*, doi:10.3390/s16010134.

64. Mulroy, S.; Gronley, J.; Weiss, W.; Newsam, C.; Perry, J. Use of cluster analysis for gait pattern classification of patients in the early and late recovery phases following stroke. *Gait & Posture* 2003, *18*, 114–125, doi:10.1016/S0966-6362(02)00165-0.
65. Laroche, D.; Tolambiya, A.; Morisset, C.; Maillefert, J.F.; French, R.M.; Ornetti, P.; Thomas, E. A classification study of kinematic gait trajectories in hip osteoarthritis. *Computers in Biology and Medicine* 2014, *55*, 42–48, doi:10.1016/j.compbiomed.2014.09.012.
66. Nukala, B.T.; Nakano, T.; Rodriguez, A.; Tsay, J.; Lopez, J.; Nguyen, T.Q.; Zupancic, S.; Lie, D.Y.C. Real-Time Classification of Patients with Balance Disorders vs. Normal Subjects Using a Low-Cost Small Wireless Wearable Gait Sensor. *Biosensors* 2016, *6*, doi:10.3390/bios6040058.
67. Kotti, M.; Duffell, L.D.; Faisal, A.A.; McGregor, A.H. Detecting knee osteoarthritis and its discriminating parameters using random forests. *Medical Engineering & Physics* 2017, *43*, 19–29, doi:10.1016/j.medengphy.2017.02.004.
68. Saeys, Y.; Inza, I.; Larranaga, P. A review of feature selection techniques in bioinformatics. *Bioinformatics* 2007, *23*, 2507–2517, doi:10.1093/bioinformatics/btm344.
69. Deluzio, K.J.; Astephen, J.L. Biomechanical features of gait waveform data associated with knee osteoarthritis. *Gait & Posture* 2007, *25*, 86–93, doi:10.1016/j.gaitpost.2006.01.007.
70. Jolliffe, I.T.; Cadima, J. Principal component analysis: a review and recent developments. *Philosophical Transactions of the Royal Society A: Mathematical, Physical and Engineering Sciences* 2016, *374*, 20150202, doi:10.1098/rsta.2015.0202.
71. Hanchuan Peng; Fuhui Long; Ding, C. Feature selection based on mutual information criteria of max-dependency, max-relevance, and min-redundancy. *IEEE Transactions on Pattern Analysis and Machine Intelligence* 2005, *27*, 1226–1238, doi:10.1109/TPAMI.2005.159.
72. Hol, J. Sensor fusion and calibration of inertial sensors, vision, ultra-wideband and GPS. PhD Thesis, Department of Electrical Engineering, Linköping University: Linköping, 2011.
73. Ligorio, G.; Sabatini, A.M. A Novel Kalman Filter for Human Motion Tracking With an Inertial-Based Dynamic Inclinometer. *IEEE Transactions on Biomedical Engineering* 2015, *62*, 2033–2043, doi:10.1109/TBME.2015.2411431.
74. Ligorio, G.; Sabatini, A.M. Extended Kalman Filter-Based Methods for Pose Estimation Using Visual, Inertial and Magnetic Sensors: Comparative Analysis and Performance Evaluation. *Sensors* 2013, *13*, 1919–1941, doi:10.3390/s130201919.
75. Sabatini, A.M. Kalman-Filter-Based Orientation Determination Using Inertial/Magnetic Sensors: Observability Analysis and Performance Evaluation. *Sensors* 2011, *11*, 9182–9206, doi:10.3390/s111009182.
76. Shuster, M.D. Survey of attitude representations. *Journal of the Astronautical Sciences* 1993, *41*, 439–517.
77. Fasel, B. Drift Reduction for Inertial Sensor Based Orientation and Position Estimation in the Presence of High Dynamic Variability During Competitive Skiing and Daily-Life Walking. PhD Thesis, École Polytechnique Fédérale de Lausanne, 2017.
78. Fasel, B.; Sporri, J.; Chardonens, J.; Kroll, J.; Muller, E.; Aminian, K. Joint Inertial Sensor Orientation Drift Reduction for Highly Dynamic Movements. *IEEE Journal of Biomedical and Health Informatics* 2017, 1–1, doi:10.1109/jbhi.2017.2659758.
79. Fasel, B.; Spörri, J.; Schütz, P.; Lorenzetti, S.; Aminian, K. Validation of functional calibration and strap-down joint drift correction for computing 3D joint angles of knee, hip, and trunk in alpine skiing. *PLOS ONE* 2017, *12*, e0181446, doi:10.1371/journal.pone.0181446.

80. Takeda, R.; Lisco, G.; Fujisawa, T.; Gastaldi, L.; Tohyama, H.; Tadano, S. Drift Removal for Improving the Accuracy of Gait Parameters Using Wearable Sensor Systems. *Sensors* 2014, *14*, 23230–23247, doi:10.3390/s141223230.
81. Harada, T.; Mori, T.; Sato, T. Development of a Tiny Orientation Estimation Device to Operate under Motion and Magnetic Disturbance. *The International Journal of Robotics Research* 2007, *26*, 547–559, doi:10.1177/0278364907079272.
82. Laidig, D.; Müller, P.; Seel, T. Automatic anatomical calibration for IMU-based elbow angle measurement in disturbed magnetic fields. *Current Directions in Biomedical Engineering* 2017, *3*, doi:10.1515/cdbme-2017-0035.
83. Ligorio, G.; Sabatini, A. Dealing with Magnetic Disturbances in Human Motion Capture: A Survey of Techniques. *Micromachines* 2016, *7*, 43, doi:10.3390/mi7030043.
84. Favre, J.; Aissaoui, R.; Jolles, B.M.; de Guise, J.A.; Aminian, K. Functional calibration procedure for 3D knee joint angle description using inertial sensors. *Journal of Biomechanics* 2009, *42*, 2330–2335, doi:10.1016/j.jbiomech.2009.06.025.
85. El-Gohary, M.; McNames, J. Human Joint Angle Estimation with Inertial Sensors and Validation with a Robot Arm. *IEEE Transactions on Biomedical Engineering* 2015, *62*, 1759–1767, doi:10.1109/TBME.2015.2403368.
86. Seel, T.; Raisch, J.; Schauer, T. IMU-Based Joint Angle Measurement for Gait Analysis. *Sensors* 2014, *14*, 6891–6909, doi:10.3390/s140406891.
87. Dejnabadi, H.; Jolles, B.M.; Aminian, K. A New Approach to Accurate Measurement of Uniaxial Joint Angles Based on a Combination of Accelerometers and Gyroscopes. *IEEE Transactions on Biomedical Engineering* 2005, *52*, 1478–1484, doi:10.1109/tbme.2005.851475.
88. Dejnabadi, H.; Jolles, B.M.; Casanova, E.; Fua, P.; Aminian, K. Estimation and Visualization of Sagittal Kinematics of Lower Limbs Orientation Using Body-Fixed Sensors. *IEEE Transactions on Biomedical Engineering* 2006, *53*, 1385–1393, doi:10.1109/TBME.2006.873678.
89. Morris, J.R.W. Accelerometry—A technique for the measurement of human body movements. *Journal of Biomechanics* 1973, *6*, 729–736, doi:10.1016/0021-9290(73)90029-8.
90. Willemsen, A.Th.M.; van Alsté, J.A.; Boom, H.B.K. Real-time gait assessment utilizing a new way of accelerometry. *Journal of Biomechanics* 1990, *23*, 859–863, doi:10.1016/0021-9290(90)90033-Y.
91. Favre, J.; Jolles, B.M.; Siegrist, O.; Aminian, K. Quaternion-based fusion of gyroscopes and accelerometers to improve 3D angle measurement. *Electronics Letters* 2006, *42*, 612, doi:10.1049/el:20060124.
92. Kok, M.; Hol, J.D.; Schön, T.B. An optimization-based approach to human body motion capture using inertial sensors. *IFAC Proceedings Volumes* 2014, *47*, 79–85, doi:10.3182/20140824-6-ZA-1003.02252.
93. Weygers, I.; Kok, M.; Konings, M.; Hallez, H.; De Vroey, H.; Claeys, K. Inertial Sensor-Based Lower Limb Joint Kinematics: A Methodological Systematic Review. *Sensors* 2020, *20*, 673, doi:10.3390/s20030673.
94. van der Straaten, R.; De Baets, L.; Jonkers, I.; Timmermans, A. Mobile assessment of the lower limb kinematics in healthy persons and in persons with degenerative knee disorders: A systematic review. *Gait & Posture* 2018, *59*, 229–241, doi:10.1016/j.gaitpost.2017.10.005.
95. Shull, P.B.; Jirattigalachote, W.; Hunt, M.A.; Cutkosky, M.R.; Delp, S.L. Quantified self and human movement: A review on the clinical impact of wearable sensing and feedback for gait analysis and intervention. *Gait & Posture* 2014, *40*, 11–19, doi:10.1016/j.gaitpost.2014.03.189.

96. Caldas, R.; Mundt, M.; Potthast, W.; Buarque de Lima Neto, F.; Markert, B. A systematic review of gait analysis methods based on inertial sensors and adaptive algorithms. *Gait & Posture* 2017, *57*, 204–210, doi:10.1016/j.gaitpost.2017.06.019.
97. Chen, S.; Lach, J.; Lo, B.; Yang, G.Z. Toward Pervasive Gait Analysis With Wearable Sensors: A Systematic Review. *IEEE Journal of Biomedical and Health Informatics* 2016, *20*, 1521–1537, doi:10.1109/JBHI.2016.2608720.
98. Petraglia, F.; Scarcella, L.; Pedrazzi, G.; Brancato, L.; Puers, R.; Costantino, C. Inertial sensors versus standard systems in gait analysis: a systematic review and meta-analysis. *European Journal of Physical and Rehabilitation Medicine* 2019, *55*, doi:10.23736/S1973-9087.18.05306-6.
99. Salarian, A.; Russmann, H.; Vingerhoets, F.J.G.; Dehollain, C.; Blanc, Y.; Burkhard, P.R.; Aminian, K. Gait assessment in Parkinson's disease: toward an ambulatory system for long-term monitoring. *IEEE Transactions on Biomedical Engineering* 2004, *51*, 1434–1443, doi:10.1109/TBME.2004.827933.
100. Köse, A.; Cereatti, A.; Della Croce, U. Bilateral step length estimation using a single inertial measurement unit attached to the pelvis. *Journal of NeuroEngineering and Rehabilitation* 2012, *9*, 9, doi:10.1186/1743-0003-9-9.
101. Bertoli, M.; Cereatti, A.; Trojaniello, D.; Avanzino, L.; Pelosin, E.; Del Din, S.; Rochester, L.; Ginis, P.; Bekkers, E.M.J.; Mirelman, A.; et al. Estimation of spatio-temporal parameters of gait from magneto-inertial measurement units: multicenter validation among Parkinson, mildly cognitively impaired and healthy older adults. *Biomed Eng Online* 2018, *17*, doi:10.1186/s12938-018-0488-2.
102. Trojaniello, D.; Cereatti, A.; Pelosin, E.; Avanzino, L.; Mirelman, A.; Hausdorff, J.M.; Della Croce, U. Estimation of step-by-step spatio-temporal parameters of normal and impaired gait using shank-mounted magneto-inertial sensors: application to elderly, hemiparetic, parkinsonian and choreic gait. *J Neuroeng Rehabil* 2014, *11*, doi:10.1186/1743-0003-11-152.
103. Cimolin, V.; Capodaglio, P.; Cau, N.; Galli, M.; Santovito, C.; Patrizi, A.; Tringali, G.; Sartorio, A. Computation of spatio-temporal parameters in level walking using a single inertial system in lean and obese adolescents. *Biomedical Engineering / Biomedizinische Technik* 2017, *62*, doi:10.1515/bmt-2015-0180.
104. Donath, L.; Faude, O.; Lichtenstein, E.; Pagenstert, G.; Nüesch, C.; Mündermann, A. Mobile inertial sensor based gait analysis: Validity and reliability of spatiotemporal gait characteristics in healthy seniors. *Gait & Posture* 2016, *49*, 371–374, doi:10.1016/j.gaitpost.2016.07.269.
105. Kluge, F.; Gaßner, H.; Hannink, J.; Pasluosta, C.; Klucken, J.; Eskofier, B.M. Towards Mobile Gait Analysis: Concurrent Validity and Test-Retest Reliability of an Inertial Measurement System for the Assessment of Spatio-Temporal Gait Parameters. *Sensors* 2017, *17*, doi:10.3390/s17071522.
106. Lanovaz, J.L.; Oates, A.R.; Treen, T.T.; Unger, J.; Musselman, K.E. Validation of a commercial inertial sensor system for spatiotemporal gait measurements in children. *Gait & Posture* 2017, *51*, 14–19, doi:10.1016/j.gaitpost.2016.09.021.
107. Seel, T.; Cermeño Escobar, V.; Raisch, J.; Schauer, T. Online Gait Phase Detection with Automatic Adaption to Gait Velocity Changes Using Accelerometers and Gyroscopes. *Biomedical Engineering / Biomedizinische Technik* 2014, *59*, 795–798.
108. Hannink, J.; Kautz, T.; Pasluosta, C.F.; Galsmann, K.-G.; Klucken, J.; Eskofier, B.M. Sensor-based gait parameter extraction with deep convolutional neural networks. *IEEE journal of biomedical and health informatics* 2017, *21*, 85–93.

109. Bertuletti, S.; Cereatti, A.; Comotti, D.; Caldara, M.; Della Croce, U. Static and Dynamic Accuracy of an Innovative Miniaturized Wearable Platform for Short Range Distance Measurements for Human Movement Applications. *Sensors* 2017, *17*, doi:10.3390/s17071492.
110. Tadano, S.; Takeda, R.; Miyagawa, H. Three Dimensional Gait Analysis Using Wearable Acceleration and Gyro Sensors Based on Quaternion Calculations. *Sensors* 2013, *13*, 9321–9343, doi:10.3390/s130709321.
111. Palermo, E.; Rossi, S.; Marini, F.; Patanè, F.; Cappa, P. Experimental evaluation of accuracy and repeatability of a novel body-to-sensor calibration procedure for inertial sensor-based gait analysis. *Measurement* 2014, *52*, 145–155, doi:10.1016/j.measurement.2014.03.004.
112. Cutti, A.G.; Ferrari, A.; Garofalo, P.; Raggi, M.; Cappello, A.; Ferrari, A. 'Outwalk': a protocol for clinical gait analysis based on inertial and magnetic sensors. *Medical & Biological Engineering & Computing* 2009, *48*, 17–25, doi:10.1007/s11517-009-0545-x.
113. Picerno, P.; Cereatti, A.; Cappozzo, A. Joint kinematics estimate using wearable inertial and magnetic sensing modules. *Gait & Posture* 2008, *28*, 588–595, doi:10.1016/j.gaitpost.2008.04.003.
114. van der Straaten, R.; Bruijnes, A.; Vanwanseele, B.; Jonkers, I.; De Baets, L.; Timmermans, A. Reliability and Agreement of 3D Trunk and Lower Extremity Movement Analysis by Means of Inertial Sensor Technology for Unipodal and Bipodal Tasks. *Sensors* 2019, *19*, 141, doi:10.3390/s19010141.
115. Robert-Lachaine, X.; Mecheri, H.; Muller, A.; Larue, C.; Plamondon, A. Validation of a Low-cost Inertial Motion Capture System for Whole-Body Motion Analysis. *Journal of Biomechanics* 2019, 109520, doi:10.1016/j.jbiomech.2019.109520.
116. Dempster, W.T. The Anthropometry of Body Action. *Annals of the New York Academy of Sciences* 1955, *63*, 559–585, doi:10.1111/j.1749-6632.1955.tb32112.x.
117. Dumas, R.; Chèze, L.; Verriest, J.-P. Adjustments to McConville et al. and Young et al. body segment inertial parameters. *Journal of Biomechanics* 2007, *40*, 543–553, doi:10.1016/j.jbiomech.2006.02.013.
118. de Leva, P. Adjustments to Zatsiorsky-Seluyanov's segment inertia parameters. *J Biomech* 1996, *29*, 1223–1230.
119. Carbone, V.; Fluit, R.; Pellikaan, P.; van der Krogt, M.M.; Janssen, D.; Damsgaard, M.; Vigneron, L.; Feilkas, T.; Koopman, H.F.J.M.; Verdonshot, N. TLEM 2.0 – A comprehensive musculoskeletal geometry dataset for subject-specific modeling of lower extremity. *Journal of Biomechanics* 2015, *48*, 734–741, doi:10.1016/j.jbiomech.2014.12.034.
120. Golyanik, V.; Reis, G.; Taetz, B.; Strieker, D. A framework for an accurate point cloud based registration of full 3D human body scans. In Proceedings of the 2017 Fifteenth IAPR International Conference on Machine Vision Applications (MVA); IEEE: Nagoya, Japan, 2017; pp. 67–72.
121. Pishchulin, L.; Wuhrer, S.; Helten, T.; Theobalt, C.; Schiele, B. Building statistical shape spaces for 3D human modeling. *Pattern Recognition* 2017, *67*, 276–286, doi:10.1016/j.patcog.2017.02.018.
122. Helten, T.; Baak, A.; Bharaj, G.; Muller, M.; Seidel, H.-P.; Theobalt, C. Personalization and Evaluation of a Real-Time Depth-Based Full Body Tracker. In Proceedings of the 2013 International Conference on 3D Vision; IEEE: Seattle, WA, USA, 2013; pp. 279–286.
123. Teufl, W.; Taetz, B.; Fröhlich, M.; Bleser, G. Accuracy and repeatability of the “neutral-zero position” of the lower extremity. In Proceedings of the ISB/ASB Conference; Calgary, CAN, 2019.

124. Agostini, V.; Gastaldi, L.; Rosso, V.; Knaflitz, M.; Tadano, S. A Wearable Magneto-Inertial System for Gait Analysis (H-Gait): Validation on Normal Weight and Overweight/Obese Young Healthy Adults. *Sensors* 2017, *17*, 2406, doi:10.3390/s17102406.
125. Al-Amri, M.; Nicholas, K.; Button, K.; Sparkes, V.; Sheeran, L.; Davies, J.L. Inertial Measurement Units for Clinical Movement Analysis: Reliability and Concurrent Validity. *Sensors* 2018, *18*, 719, doi:10.3390/s18030719.
126. Cloete, T.; Scheffer, C. Repeatability of an off-the-shelf, full body inertial motion capture system during clinical gait analysis. In Proceedings of the Engineering in Medicine and Biology Society (EMBC), 2010 Annual International Conference of the IEEE; IEEE, 2010; pp. 5125–5128.
127. Ferrari, A.; Cutti, A.G.; Garofalo, P.; Raggi, M.; Heijboer, M.; Cappello, A.; Davalli, A. First in vivo assessment of “Outwalk”: a novel protocol for clinical gait analysis based on inertial and magnetic sensors. *Medical & Biological Engineering & Computing* 2010, *48*, 1–15, doi:10.1007/s11517-009-0544-y.
128. Lebel, K.; Boissy, P.; Nguyen, H.; Duval, C. Inertial measurement systems for segments and joints kinematics assessment: towards an understanding of the variations in sensors accuracy. *Biomed Eng Online* 2017, *16*, doi:10.1186/s12938-017-0347-6.
129. Nüesch, C.; Roos, E.; Pagenstert, G.; Mündermann, A. Measuring joint kinematics of treadmill walking and running: Comparison between an inertial sensor based system and a camera-based system. *Journal of Biomechanics* 2017, *57*, 32–38, doi:10.1016/j.jbiomech.2017.03.015.
130. Robert-Lachaine, X.; Mecheri, H.; Larue, C.; Plamondon, A. Validation of inertial measurement units with an optoelectronic system for whole-body motion analysis. *Med Biol Eng Comput* 2017, *55*, 609–619, doi:10.1007/s11517-016-1537-2.
131. Zhang, J.-T.; Novak, A.C.; Brouwer, B.; Li, Q. Concurrent validation of Xsens and MVN measurement of lower limb joint angular kinematics. *Physiological Measurement* 2013, *34*.
132. Cooper, G.; Sheret, I.; McMillian, L.; Siliverdis, K.; Sha, N.; Hodgins, D.; Kenney, L.; Howard, D. Inertial sensor-based knee flexion/extension angle estimation. *Journal of Biomechanics* 2009, *42*, 2678–2685, doi:10.1016/j.jbiomech.2009.08.004.
133. Kianifar, R.; Lee, A.; Raina, S.; Kulic, D. Automated Assessment of Dynamic Knee Valgus and Risk of Knee Injury During the Single Leg Squat. *IEEE Journal of Translational Engineering in Health and Medicine* 2017, *5*, 1–13, doi:10.1109/JTEHM.2017.2736559.
134. Grip, H.; Nilsson, K.G.; Häger, C.K.; Lundström, R.; Öhberg, F. Does the Femoral Head Size in Hip Arthroplasty Influence Lower Body Movements during Squats, Gait and Stair Walking? A Clinical Pilot Study Based on Wearable Motion Sensors. *Sensors* 2019, *19*, 3240, doi:10.3390/s19143240.
135. Hassan, M.; Kadone, H.; Suzuki, K.; Sankai, Y. Wearable Gait Measurement System with an Instrumented Cane for Exoskeleton Control. *Sensors* 2014, *14*, 1705–1722, doi:10.3390/s140101705.
136. Karatsidis, A.; Richards, R.E.; Konrath, J.M.; van den Noort, J.C.; Schepers, H.M.; Bellusci, G.; Harlaar, J.; Veltink, P.H. Validation of wearable visual feedback for retraining foot progression angle using inertial sensors and an augmented reality headset. *Journal of NeuroEngineering and Rehabilitation* 2018, *15*, 78, doi:10.1186/s12984-018-0419-2.
137. Seel, T.; Laidig, D.; Valtin, M.; Werner, C.; Raisch, J.; Schauer, T. Feedback control of foot eversion in the adaptive peroneal stimulator. In Proceedings of the 22nd Mediterranean Conference on Control and Automation; 2014; pp. 1482–1487.

138. Valtin, M.; Seel, T.; Raisch, J.; Schauer, T. Iterative learning control of drop foot stimulation with array electrodes for selective muscle activation. *IFAC Proceedings Volumes* 2014, *47*, 6587–6592, doi:10.3182/20140824-6-ZA-1003.01991.
139. Wang, L.; Wang, S.; Asseldonk, E.H.F. van; Kooij, H. van der Actively controlled lateral gait assistance in a lower limb exoskeleton. In Proceedings of the 2013 IEEE/RSJ International Conference on Intelligent Robots and Systems; 2013; pp. 965–970.
140. Bell, K.; Onyeukwu, C.; McClincy, M.; Allen, M.; Bechard, L.; Mukherjee, A.; Hartman, R.; Smith, C.; Lynch, A.; Irrgang, J. Verification of a Portable Motion Tracking System for Remote Management of Physical Rehabilitation of the Knee. *Sensors* 2019, *19*, 1021, doi:10.3390/s19051021.
141. Steffen, D.; Christmann, C.; Teufl, W.; Bleser, G. No Game, No Pain?: Towards a Mobile Exergame for Rehabilitation. In Proceedings of the Extended Abstracts Publication of the Annual Symposium on Computer-Human Interaction in Play; ACM: New York, NY, USA, 2017; pp. 231–237.
142. Pietschmann, J.; Geu Flores, F.; Jöllenbeck, T. Gait Training in Orthopedic Rehabilitation after Joint Replacement - Back to Normal Gait with Sonification? *International Journal of Computer Science in Sport* 2019, *18*, 34–48, doi:10.2478/ijcss-2019-0012.
143. Steffen, D.; Christmann, C.A.; Bleser, G. jumpBALL - Ein mobiles Exergame für die Thromboseprophylaxe. In Proceedings of the Mensch und Computer 2017 - Tagungsband; Burghardt, M., Wimmer, R., Wolff, C., Womser-Hacker, C., Eds.; Gesellschaft für Informatik e.V., 2017; pp. 27–36.
144. Chardonnes, J.; Favre, J.; Aminian, K. An effortless procedure to align the local frame of an inertial measurement unit to the local frame of another motion capture system. *Journal of Biomechanics* 2012, *45*, 2297–2300, doi:10.1016/j.jbiomech.2012.06.009.
145. de Vries, W.H.K.; Veeger, H.E.J.; Baten, C.T.M.; van der Helm, F.C.T. Magnetic distortion in motion labs, implications for validating inertial magnetic sensors. *Gait & Posture* 2009, *29*, 535–541, doi:10.1016/j.gaitpost.2008.12.004.
146. Bergamini, E.; Ligorio, G.; Summa, A.; Vannozzi, G.; Cappozzo, A.; Sabatini, A.M. Estimating orientation using magnetic and inertial sensors and different sensor fusion approaches: accuracy assessment in manual and locomotion tasks. *Sensors* 2014, *14*, 18625–18649, doi:10.3390/s141018625.
147. Vreede, K.; Henriksson, J.; Borg, K.; Henriksson, M. Gait characteristics and influence of fatigue during the 6-minute walk test in patients with post-polio syndrome. *Journal of Rehabilitation Medicine* 2013, *45*, 924–928, doi:10.2340/16501977-1209.
148. Yamazaki, J.; Muneta, T.; Ju, Y.J.; Sekiya, I. Differences in kinematics of single leg squatting between anterior cruciate ligament-injured patients and healthy controls. *Knee Surgery, Sports Traumatology, Arthroscopy* 2010, *18*, 56–63, doi:10.1007/s00167-009-0892-z.
149. Hatton, A.L.; Crossley, K.M.; Hug, F.; Bouma, J.; Ha, B.; Spaulding, K.L.; Tucker, K. Acute experimental hip muscle pain alters single-leg squat balance in healthy young adults. *Gait & Posture* 2015, *41*, 871–876, doi:10.1016/j.gaitpost.2015.02.013.
150. Ugalde, V.; Brockman, C.; Bailowitz, Z.; Pollard, C.D. Single Leg Squat Test and Its Relationship to Dynamic Knee Valgus and Injury Risk Screening. *PM&R* 2015, *7*, 229–235, doi:10.1016/j.pmrj.2014.08.361.
151. McMahon, J.J.; Suchomel, T.J.; Lake, J.P.; Comfort, P. Understanding the Key Phases of the Countermovement Jump Force-Time Curve: *Strength and Conditioning Journal* 2018, *1*, doi:10.1519/SSC.0000000000000375.

152. Chai, T.; Draxler, R.R. Root mean square error (RMSE) or mean absolute error (MAE)? – Arguments against avoiding RMSE in the literature. *Geoscientific Model Development* 2014, 7, 1247–1250, doi:10.5194/gmd-7-1247-2014.
153. Beaulieu, M.L.; Lamontagne, M.; Beulé, P.E. Lower limb biomechanics during gait do not return to normal following total hip arthroplasty. *Gait & Posture* 2010, 32, 269–273, doi:10.1016/j.gaitpost.2010.05.007.
154. Davis, K.E.; Ritter, M.A.; Berend, M.E.; Meding, J.B. The Importance of Range of Motion after Total Hip Arthroplasty. *Clinical Orthopaedics* 2007, 5.
155. Ferrari, A.; Cutti, A.G.; Cappello, A. A new formulation of the coefficient of multiple correlation to assess the similarity of waveforms measured synchronously by different motion analysis protocols. *Gait & Posture* 2010, 31, 540–542, doi:10.1016/j.gaitpost.2010.02.009.
156. Bland, J.M.; Altman, D.G. Measuring agreement in method comparison studies. *Statistical Methods in Medical Research* 1999, 8, 135–160, doi:10.1177/096228029900800204.
157. Donath, L.; Faude, O.; Lichtenstein, E.; Nüesch, C.; Mündermann, A. Validity and reliability of a portable gait analysis system for measuring spatiotemporal gait characteristics: comparison to an instrumented treadmill. *Journal of NeuroEngineering and Rehabilitation* 2016, 13, doi:10.1186/s12984-016-0115-z.
158. Sinclair, J.; Hebron, J.; Taylor, P.J. The Test-retest Reliability of Knee Joint Center Location Techniques. *Journal of Applied Biomechanics* 2015, 31, 117–121, doi:10.1123/JAB.2013-0312.
159. McGraw, K.O.; Wong, S.P. Forming inferences about some intraclass correlation coefficients. *Psychological Methods* 1996, 1, 30–46, doi:10.1037/1082-989X.1.1.30.
160. de Vries, W.H.K.; Veeger, H.E.J.; Baten, C.T.M.; van der Helm, F.C.T. Magnetic distortion in motion labs, implications for validating inertial magnetic sensors. *Gait & Posture* 2009, 29, 535–541, doi:10.1016/j.gaitpost.2008.12.004.
161. López-Nava, I.H.; Muñoz-Melendez, A. Wearable Inertial Sensors for Human Motion Analysis: A Review. *IEEE Sensors Journal* 2016, 16, 7821–7834, doi:10.1109/JSEN.2016.2609392.
162. Waegli, A.; Skaloud, J. Optimization of two GPS/MEMS-IMU integration strategies with application to sports. *GPS Solutions* 2009, 13, 315–326, doi:10.1007/s10291-009-0124-5.
163. Bleser, G.; Stricker, D. Advanced tracking through efficient image processing and visual-inertial sensor fusion. In Proceedings of the 2008 IEEE Virtual Reality Conference; 2008; pp. 137–144.
164. Camomilla, V.; Bergamini, E.; Fantozzi, S.; Vannozzi, G.; Camomilla, V.; Bergamini, E.; Fantozzi, S.; Vannozzi, G. Trends Supporting the In-Field Use of Wearable Inertial Sensors for Sport Performance Evaluation: A Systematic Review. *Sensors* 2018, 18, 873, doi:10.3390/s18030873.
165. Kainz, H.; Modenese, L.; Lloyd, D.G.; Maine, S.; Walsh, H.P.J.; Carty, C.P. Joint kinematic calculation based on clinical direct kinematic versus inverse kinematic gait models. *Journal of Biomechanics* 2016, 49, 1658–1669, doi:10.1016/j.jbiomech.2016.03.052.
166. Delp, S.L.; Anderson, F.C.; Arnold, A.S.; Loan, P.; Habib, A.; John, C.T.; Guendelman, E.; Thelen, D.G. OpenSim: Open-Source Software to Create and Analyze Dynamic Simulations of Movement. *IEEE Transactions on Biomedical Engineering* 2007, 54, 1940–1950, doi:10.1109/TBME.2007.901024.
167. Teufl, W.; Taetz, B.; Weidmann, A.; Fröhlich, M.; Bleser, G. Validity of a depth camera based approach for segment length estimation. In Proceedings of the ISB/ASB Conference; Calgary, CN, 2019.

168. Brouwer, G.M.; Tol, A.W.V.; Bergink, A.P.; Belo, J.N.; Bernsen, R.M.D.; Reijman, M.; Pols, H. a. P.; Bierma-Zeinstra, S.M.A. Association between valgus and varus alignment and the development and progression of radiographic osteoarthritis of the knee. *Arthritis & Rheumatism* 2007, *56*, 1204–1211, doi:10.1002/art.22515.
169. Gaskell, L. Musculoskeletal assessment. In *Tidy's Physiotherapy*; Elsevier, 2013; pp. 207–251 ISBN 978-0-7020-4344-4.
170. Taetz, B.; Bleser, G.; Miezal, M. Towards self-calibrating inertial body motion capture. In Proceedings of the Information Fusion (FUSION), 2016 19th International Conference on; IEEE, 2016; pp. 1751–1759.
171. Barré, A.; Jolles, B.M.; Theumann, N.; Aminian, K. Soft tissue artifact distribution on lower limbs during treadmill gait: Influence of skin markers\textquotesingle location on cluster design. *Journal of Biomechanics* 2015, *48*, 1965–1971, doi:10.1016/j.jbiomech.2015.04.007.
172. Noehren, B.; Barrance, P.J.; Pohl, M.P.; Davis, I.S. A comparison of tibiofemoral and patellofemoral alignment during a neutral and valgus single leg squat: an MRI study. *The Knee* 2012, *19*, 380–386, doi:10.1016/j.knee.2011.05.012.
173. Fiorentino, N.M.; Kutschke, M.J.; Atkins, P.R.; Foreman, K.B.; Kapron, A.L.; Anderson, A.E. Accuracy of Functional and Predictive Methods to Calculate the Hip Joint Center in Young Non-pathologic Asymptomatic Adults with Dual Fluoroscopy as a Reference Standard. *Ann Biomed Eng* 2016, *44*, 2168–2180, doi:10.1007/s10439-015-1522-1.
174. Akbani, R.; Kwek, S.; Japkowicz, N. Applying Support Vector Machines to Imbalanced Datasets. In Proceedings of the Machine Learning: ECML 2004; Springer: Berlin, Heidelberg, 2004; pp. 39–50.
175. Jin, H.; Song, Q.; Hu, X. Auto-Keras: An Efficient Neural Architecture Search System. In Proceedings of the Proceedings of the 25th ACM SIGKDD International Conference on Knowledge Discovery & Data Mining - KDD '19; ACM Press: Anchorage, AK, USA, 2019; pp. 1946–1956.
176. Dreiseitl, S.; Osl, M.; Scheibböck, C.; Binder, M. Outlier Detection with One-Class SVMs: An Application to Melanoma Prognosis. *AMIA Annu Symp Proc* 2010, *2010*, 172–176.
177. Merel, J.; Tassa, Y.; Dhruva, T.B.; Srinivasan, S.; Lemmon, J.; Wang, Z.; Wayne, G.; Heess, N.M.O. Learning human behaviors from motion capture by adversarial imitation. *ArXiv* 2017, *abs/1707.02201*.
178. Li, R.T.; Kling, S.R.; Salata, M.J.; Cupp, S.A.; Sheehan, J.; Voos, J.E. Wearable Performance Devices in Sports Medicine. *Sports Health* 2016, *8*, 74–78, doi:10.1177/1941738115616917.
179. Lempereur, M.; Brochard, S.; Leboeuf, F.; Rémy-Néris, O. Validity and reliability of 3D marker based scapular motion analysis: A systematic review. *Journal of Biomechanics* 2014, *47*, 2219–2230, doi:10.1016/j.jbiomech.2014.04.028.
180. Needham, R.; Stebbins, J.; Chockalingam, N. Three-dimensional kinematics of the lumbar spine during gait using marker-based systems: a systematic review. *Journal of Medical Engineering & Technology* 2016, *40*, 172–185, doi:10.3109/03091902.2016.1154616.
181. Schmid, S.; Studer, D.; Hasler, C.-C.; Romkes, J.; Taylor, W.R.; Lorenzetti, S.; Brunner, R. Quantifying spinal gait kinematics using an enhanced optical motion capture approach in adolescent idiopathic scoliosis. *Gait & Posture* 2016, *44*, 231–237, doi:10.1016/j.gaitpost.2015.12.036.
182. Brochard, S.; Lempereur, M.; Rémy-Néris, O. Double calibration: An accurate, reliable and easy-to-use method for 3D scapular motion analysis. *Journal of Biomechanics* 2011, *44*, 751–754, doi:10.1016/j.jbiomech.2010.11.017.

183. Lorussi, F.; Carbonaro, N.; Rossi, D.D.; Tognetti, A. A bi-articular model for scapular-humeral rhythm reconstruction through data from wearable sensors. *Journal of NeuroEngineering and Rehabilitation* 2016, 13, 40, doi:10.1186/s12984-016-0149-2.
184. Simpson, L.; Maharaj, M.M.; Mobbs, R.J. The role of wearables in spinal posture analysis: a systematic review. *BMC Musculoskeletal Disorders* 2019, 20, 55, doi:10.1186/s12891-019-2430-6.
185. Bauer, C.M.; Rast, F.M.; Ernst, M.J.; Kool, J.; Oetiker, S.; Rissanen, S.M.; Suni, J.H.; Kankaanpää, M. Concurrent validity and reliability of a novel wireless inertial measurement system to assess trunk movement. *Journal of Electromyography and Kinesiology* 2015, 25, 782–790, doi:10.1016/j.jelekin.2015.06.001.
186. Yan, X.; Li, H.; Li, A.R.; Zhang, H. Wearable IMU-based real-time motion warning system for construction workers' musculoskeletal disorders prevention. *Automation in Construction* 2017, 74, 2–11, doi:10.1016/j.autcon.2016.11.007.
187. Brice, S.M.; Phillips, E.J.; Millett, E.L.; Hunter, A.; Philippa, B. Comparing inertial measurement units and marker-based biomechanical models during dynamic rotation of the torso. *European Journal of Sport Science* 2019, 1–9, doi:10.1080/17461391.2019.1666167.
188. Faber, G.S.; Chang, C.-C.; Kingma, I.; Dennerlein, J.T. Lifting style and participant's sex do not affect optimal inertial sensor location for ambulatory assessment of trunk inclination. *Journal of Biomechanics* 2013, 46, 1027–1030, doi:10.1016/j.jbiomech.2012.12.007.
189. Goodvin, C.; Park, E.J.; Huang, K.; Sakaki, K. Development of a real-time three-dimensional spinal motion measurement system for clinical practice. *Medical & Biological Engineering & Computing* 2006, 44, 1061–1075, doi:10.1007/s11517-006-0132-3.
190. Morrow, M.M.B.; Lowndes, B.R.; Fortune, E.; Kaufman, K.R.; Hallbeck, M.S. Validation of Inertial Measurement Units for Upper Body Kinematics. *J Appl Biomech* 2017, 33, 227–232, doi:10.1123/jab.2016-0120.
191. Zimmermann, T.; Taetz, B.; Bleser, G. IMU-to-Segment Assignment and Orientation Alignment for the Lower Body Using Deep Learning. *Sensors* 2018, 18, 302, doi:10.3390/s18010302.
192. Alberto, R.; Draicchio, F.; Varrecchia, T.; Silvetti, A.; Iavicoli, S. Wearable Monitoring Devices for Biomechanical Risk Assessment at Work: Current Status and Future Challenges—A Systematic Review. *Int J Environ Res Public Health* 2018, 15, doi:10.3390/ijerph15092001.
193. Colyer, S.L.; Evans, M.; Cosker, D.P.; Salo, A.I.T. A Review of the Evolution of Vision-Based Motion Analysis and the Integration of Advanced Computer Vision Methods Towards Developing a Markerless System. *Sports Med Open* 2018, 4, doi:10.1186/s40798-018-0139-y.
194. Abrams, G.D.; Harris, A.H.; Andriacchi, T.P.; Safran, M.R. Biomechanical analysis of three tennis serve types using a markerless system. *British Journal of Sports Medicine* 2014, 48, 339–342, doi:10.1136/bjsports-2012-091371.
195. Harsted, S.; Holsgaard-Larsen, A.; Hestbæk, L.; Boyle, E.; Lauridsen, H.H. Concurrent validity of lower extremity kinematics and jump characteristics captured in pre-school children by a markerless 3D motion capture system. *Chiropr Man Therap* 2019, 27, doi:10.1186/s12998-019-0261-z.
196. Iwashita, Y.; Kurazume, R.; Hasegawa, T.; Hara, K. Robust motion capture system against target occlusion using fast level set method. In Proceedings of the Proceedings 2006 IEEE International Conference on Robotics and Automation, 2006. ICRA 2006.; IEEE: Orlando, FL, USA, 2006; pp. 168–174.

197. Liu, Y.; Stoll, C.; Gall, J.; Seidel, H.-P.; Theobalt, C. Markerless motion capture of interacting characters using multi-view image segmentation. In Proceedings of the CVPR; 2011; pp. 1249–1256.
198. Tao, Y.; Hu, H.; Zhou, H. Integration of Vision and Inertial Sensors for 3D Arm Motion Tracking in Home-based Rehabilitation. *The International Journal of Robotics Research* 2007, 26, 607–624, doi:10.1177/0278364907079278.
199. Pons-Moll, G.; Baak, A.; Helten, T.; Muller, M.; Seidel, H.-P.; Rosenhahn, B. Multisensor-fusion for 3D full-body human motion capture. In Proceedings of the 2010 IEEE Computer Society Conference on Computer Vision and Pattern Recognition; IEEE: San Francisco, CA, USA, 2010; pp. 663–670.
200. Glonek, G.; Wojciechowski, A. Hybrid Orientation Based Human Limbs Motion Tracking Method. *Sensors* 2017, 17, doi:10.3390/s17122857.

Scientific Curriculum Vitae

Teufl Wolfgang, M.Sc.

Scientific careere

BSc Physiotherapy

30/08/2009-03/07/2012 BSc course physiotherapy at FH Campus Wien, Austria

BSc Thesis „The effect of sEMG-feedback on asymmetries in the spatio-temporal parameters, during treadmill walking“

MSc „Biomechanics-Motor activity-Movement analysis“

10/2013 – 05/02/16 MSc course “Biomechanics-motor activity-movement analysis” at the Justus Liebig Universität Gießen / Technische Hochschule Mittelhessen, Germany

MSc Thesis „Biomechanical Quantification of the Dynamic Knee Valgus using inertial sensor system Myo Motion®“

PhD candidate and research associate at the TU Kaiserslautern, Germany

02/2017 – 09/2020 PhD candidate at the department of Sport Science at the TU Kaiserslautern

PhD Thesis “Validation and Initial Applications of a Magnetometer-free Inertial Sensor Based Motion Capture System for the Human Lower Body”

24/09/2020 Graduation: Dr. rerum naturalium (Dr. rer. nat.), summa cum laude

Academic working experience

02/2017 – 06/2018 scholarship holder at the TU Kaiserslautern, department of computer science

06/2018 – 08/2020 research associate at the TU Kaiserslautern, department of computer science

10/2020 – present Senior Scientist at the University of Salzburg, department of sport science

List of publications

Conference papers / presentations

1. Teufl, W.; Konrad, P.; Subke, J. P57: 2D video Frontal Plane Projection Angle and 3D inertial sensor based assessment of Dynamic Knee Valgus. A Comparison. *ESMAC 2017* Trondheim, doi:[10.1016/j.gaitpost.2017.06.418](https://doi.org/10.1016/j.gaitpost.2017.06.418).
2. Steffen, D.; Christmann, C.; Teufl, W.; Bleser, G. No Game, No Pain?: Towards a Mobile Exergame for Rehabilitation. In *Proceedings of the Extended Abstracts Publication of the Annual Symposium on Computer-Human Interaction in Play 2018* New York, doi: <http://doi.acm.org/10.1145/3130859.3131310>
3. Teufl, W.; Miezal, M.; Taetz, B.; Fröhlich, M.; Bleser, G. Limits of agreement between a magnetometer-independent inertial sensor system and a marker based optical motion capture system for 3D joint kinematics in gait analysis. *ECSS 2018* Dublin.
4. Teufl, W.; Miezal, M.; Taetz, B.; Fröhlich, M.; Bleser, G. Validity of spatial gait parameters based on an inertial sensor system for 3D gait analysis. 12. *Spinfortec 2018* Garching.
5. Teufl, W.; Miezal, M.; Taetz, B.; Fröhlich, M.; Bleser, G. Towards a wearable feedback system for gait training: Inertial sensor based 3D joint kinematics and spatio-temporal parameters. *GEST19 DVS Tagung 2019* Würzburg.
6. Teufl, W.; Taetz, B.; Fröhlich, M.; Bleser, G. Accuracy and repeatability of the “neutral-zero position” of the lower extremity. *ISB/ASB 2019* Calgary.
7. Teufl, W.; Taetz, B.; Weidmann, A; Fröhlich, M.; Bleser, G. Validity of a depth camera based approach for segment length estimation. *ISB/ASB 2019* Calgary.
8. Teufl, W.; Taetz, B.; Miezal, M.; Lorenz, M.; Pietschmann, J.; Jöllenbeck, T.; Fröhlich, M.; Bleser, G. Auf dem Weg zu einem mobile, inertialsensorbasierten Feedbacksystem zum Gangtraining für Patienten nach Hüft-TEP. *GAMMA Workshop 2019* Wien.
9. Dindorf, C.; Teufl, W.; Taetz, B.; Becker, S.; Bleser, G.; Fröhlich, M. Vergleichende Feature-Extraktion und Gangklassifizierung bei Hüftgelenkersatz-Patienten auf Basis kinematischer Trajektorien. *GAMMA Kongress 2020* München

Peer-reviewed journal papers

1. Teufl, W.; Miezal, M.; Taetz, B.; Fröhlich, M.; Bleser, G. Validity, Test-Retest Reliability and Long-Term Stability of Magnetometer Free Inertial Sensor Based 3D Joint Kinematics. *Sensors* **2018**, 18, 1980. doi:[10.3390/s18071980](https://doi.org/10.3390/s18071980).
2. Teufl, W.; Lorenz, M.; Miezal, M.; Taetz, B.; Fröhlich, M.; Bleser, G. Towards Inertial Sensor Based Mobile Gait Analysis: Event-Detection and Spatio-Temporal Parameters. *Sensors* **2019**, 19, 38. doi: [10.3390/s19010038](https://doi.org/10.3390/s19010038).

3. Teufl, W.; Miezal, M.; Taetz, B.; Fröhlich, M.; Bleser, G. Validity of inertial sensor based 3D joint kinematics of static and dynamic sport and physiotherapy specific movements. *PLOS ONE* **2019**, 14. doi: <https://doi.org/10.1371/journal>.
4. Taetz, B.; Teufl, W.; Weidmann, A.; Pietschmann, J.; Jöllenbeck, T.; Bleser, G. Depth camera based statistical shape fitting approach for the creation of an individualized lower body biomechanical model: validity and reliability. *Computer Methods in Biomechanics and Biomedical Engineering* **2019**, 1–11, doi:[10.1080/10255842.2019.1688310](https://doi.org/10.1080/10255842.2019.1688310).
5. Teufl, W.; Taetz, B.; Miezal, M.; Lorenz; Pietschmann, J.; Jöllenbeck, T.; Fröhlich, M.; Bleser, G. Towards an Inertial Sensor-Based Wearable Feedback System for Patients after Total Hip Arthroplasty: Validity and Applicability for Gait Classification with Gait Kinematics-Based Features. *Sensors* **2019**, 19, 5006, doi:[10.3390/s19225006](https://doi.org/10.3390/s19225006).
6. Dindorf, C.; Teufl, W.; Taetz, B.; Bleser, G.; Fröhlich, M. Interpretability of Input Representations for Gait Classification in Patients after Total Hip Arthroplasty. *Sensors* **2020**, 20, 4385, doi:[10.3390/s20164385](https://doi.org/10.3390/s20164385).

Review activity for journals

2019

ACSM Medicine & Science in Sports & Exercise